

AD-A098 727

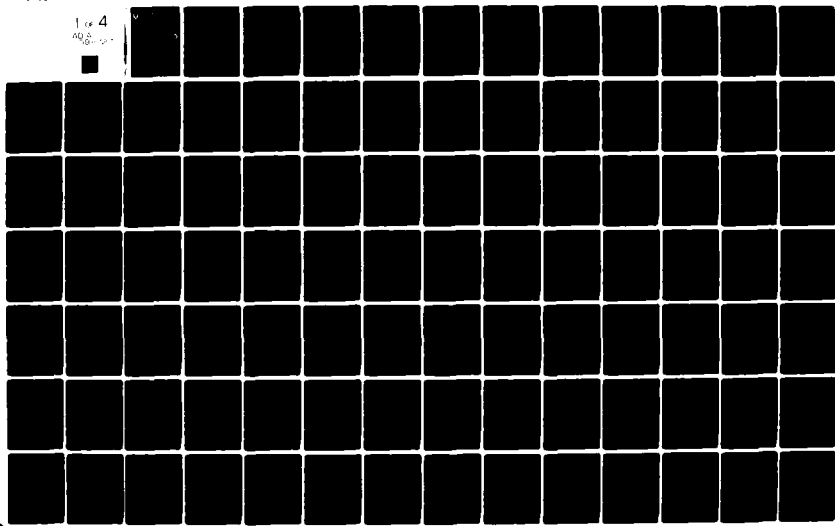
DURACELL INTERNATIONAL INC BURLINGTON MA LAB FOR PHYS--ETC F/6 10/3  
LITHIUM-THIONYL CHLORIDE BATTERY,(U)

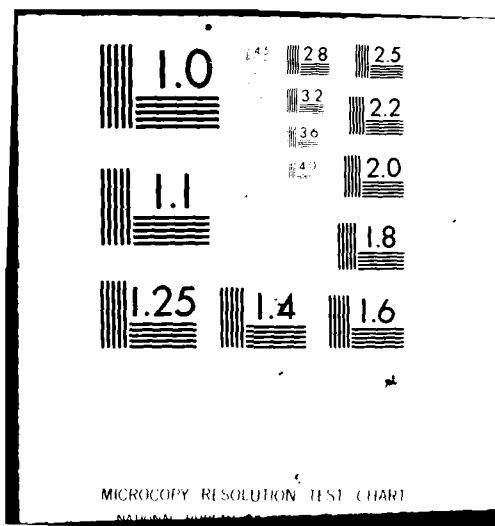
APR 81 D WONG, W BOWDEN, N HAMILTON

DAAB07-78-C-0563  
DELET-TR-78-0563-F NL

UNCLASSIFIED

1 of 4  
M03  
100%







**LEVEL**

(1)

Research and Development Technical Report

DELET - TR - 78 - 0563 - F

AD A098727

LITHIUM-THIONYL CHLORIDE BATTERY

D. WONG  
W. BOWDEN  
N. HAMILTON  
D. CUBBISON  
A. N. DEY

DURACELL INTERNATIONAL  
LABORATORY PHYSICAL SCIENCE  
BURLINGTON, MA 01803



APRIL 1981

FINAL REPORT  
FOR PERIOD 1 OCTOBER 1978 - 30 NOVEMBER 1980

DISTRIBUTION STATEMENT:  
APPROVED FOR PUBLIC RELEASE; DISTRIBUTION UNLIMITED

PREPARED FOR:  
US ARMY ELECTRONICS TECHNOLOGY AND DEVICES LABORATORY

**ERADCOM**

US ARMY ELECTRONICS RESEARCH AND DEVELOPMENT COMMAND  
FORT MONMOUTH, NEW JERSEY 07703

HISA-FM 195-78

815 11 045

## **NOTICES**

### **Disclaimers**

The citation of trade names and names of manufacturers in this report is not to be construed as official Government indorsement or approval of commercial products or services referenced herein.

### **Disposition**

Destroy this report when it is no longer needed. Do not return it to the originator.

(1) Final rept.

1 Oct 78-30 Nov 84

SECURITY CLASSIFICATION OF THIS PAGE (When Data Entered)

1 REPORT DOCUMENTATION PAGE		READ INSTRUCTIONS BEFORE COMPLETING FORM
1. REPORT NUMBER 18 DELET-TR-78-0563-F	2. GOVT ACCESSION NO. AD A098727	3. RECIPIENT'S CATALOG NUMBER
4. TITLE (and Subtitle) 6 Lithium-Thionyl Chloride Battery	5. TYPE OF REPORT & PERIOD COVERED 10/1/78 - 11/30/80	
7. AUTHOR(S) 10 D. /Wong, W. /Bowden, N. /Hamilton, D. /Cubbin- son a A. N. /Dey	6. PERFORMING ORG. REPORT NUMBER DAAB07-78-C-0563	
9. PERFORMING ORGANIZATION NAME AND ADDRESS Duracell International Inc. Laboratory for Physical Science Burlington, MA 01803	10. PROGRAM ELEMENT, PROJECT, TASK AREA & WORK UNIT NUMBERS 1L162705AH9411-219	
11. CONTROLLING OFFICE NAME AND ADDRESS U.S. Army Electronics Technology & Device Lab. ERADCOM Attn: DELET-PR Ft. Monmouth, New Jersey 07703	12. REPORT DATE 17 11	
14. MONITORING AGENCY NAME & ADDRESS (if different from Controlling Office)	13. NUMBER OF PAGES 12	
15. SECURITY CLASS. (of this report) Unclassified		
15a. DECLASSIFICATION/DOWNGRADING SCHEDULE		
16. DISTRIBUTION STATEMENT (of this Report) Approved for public release Distribution unlimited		
17. DISTRIBUTION STATEMENT (of the abstract entered in Block 20, if different from Report) 11 Apr 81		
18. SUPPLEMENTARY NOTES		
19. KEY WORDS (Continue on reverse side if necessary and identify by block number) Inorganic Electrolyte battery, Thionyl Chloride, lithium, high rate D cell, high rate flat cylindrical cell, laser designator battery. lithium-thionyl chloride		
20. ABSTRACT (Continue on reverse side if necessary and identify by block number) The main objective of this program under Contract No. DAAB07-78-C-0563 is to develop, fabricate, test, and deliver safe high rate Li/SOCl <sub>2</sub> batteries for various U.S. Army applications such as manpack ratios and GLLD Laser Designators. We have devoted our efforts in the following major areas: 1. Optimization of the spirally wound D cell for high rate applications, 2. Development of a 3 inch diameter flat cylindrical cell for the		

Unclassified

SECURITY CLASSIFICATION OF THIS PAGE (When Data Entered)

• GLLD laser designator application,  
3. Investigation of the reduction mechanism of  $\text{SOCl}_2$ .

The rate capability of the spirally wound D cell previously developed by us has been optimized for both the manpack radio (BA5590) battery and GLLD laser designator battery applications in this program. Cathode current collector design was improved and a maximum short circuit current density of up to  $\sim 200 \text{ mA/cm}^2$  has been realized. The effects of cathode additives, electrolyte concentration, and electrode length were also studied. Spirally wound D cells of the optimal design were found to deliver 11.5 Ahr/cell ( $\sim 100$  hours) on the BA5590 test load and 7.7 Ahr/cell ( $\sim 200$  bursts) on the GLLD load. The performance characteristics have been further determined under constant current discharge and voltage reversal at 0.3, 1, and 3A at room temperature and  $-30^\circ\text{C}$ . No dangerous behavior was observed during these tests and during short circuiting. One hundred D cells of such design have been constructed and delivered to the sponsor.

In this program, a flat cylindrical cell has also been developed for the GLLD laser designator application. It is 3 inches in diameter and 0.9 inch in height with extremely low internal cell impedance that minimizes cell heating and polarization on the GLLD load. Typical cell capacity was found to be 18.0-19.0 Ahr with a few cells delivering up to  $\sim 21.0$  Ahr on the GLLD test load. The performance characteristics and safety features of the flat cylindrical cell have also been experimentally determined.

The cell delivered  $\sim 20$  and 14 Ahr under constant current discharge at 20 and 100A, respectively. The short circuit current was measured to be  $\sim 1500$ A. The cells were driven into voltage reversal on GLLD test as well as at constant currents up to 20A, no dangerous behavior was noted. Finally, five GLLD laser designator batteries each containing eight such flat cylindrical cells in series have been delivered to our sponsor.

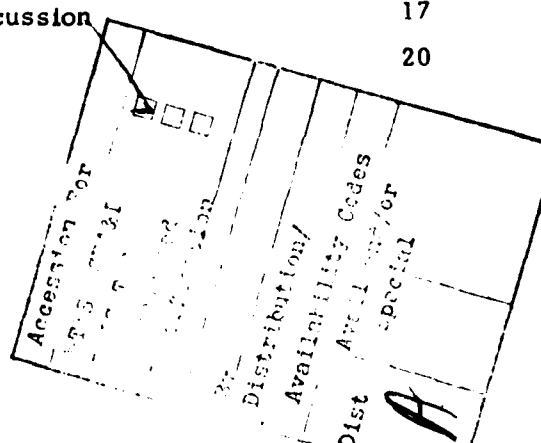
In addition to high rate Li/ $\text{SOCl}_2$  cell developmental work, study of the reduction mechanism of  $\text{SOCl}_2$  using electrochemical and spectroscopic techniques has also been carried out in this program which may be directly relevant to the intrinsic safety of the system. Cyclic voltammetry was used to investigate the electrochemical reduction of  $\text{SOCl}_2$  in various supporting electrolytes. It was established that although the  $\text{Cl}^-$  ion was formed immediately, reaction products such as S,  $\text{SO}_2$  and  $\text{S}_2\text{Cl}_2$  were not formed immediately upon  $\text{SOCl}_2$  reduction. Spectroscopic evidence obtained in our work indicated the possible formation of at least two meta-stable intermediates resulting from the discharge of  $\text{SCl}_2$  at room temperature. In addition, it was found that exhaustive electrolysis of  $\text{SCl}_2$  at a constant potential leads to the exhaustion of  $\text{SOCl}_2$  but the latter was regenerated on warming the solution. Information obtained in this work not only elucidated the Li/ $\text{SOCl}_2$  cell reaction mechanism but also provided a new approach to improve both the performance and the safety features of the system.

Unclassified

SECURITY CLASSIFICATION OF THIS PAGE (When Data Entered)

## Table of Contents

	Page No.
Abstract	i
List of Tables	ii
List of Figures	iii
I. Introduction	1
A. Background and Approach	1
B. BA5590 Battery/GLLD Laser Designator Battery	2
a. BA5590 Man Pack Radio Battery	2
b. GLLD Laser Designator Battery	3
II. Optimization of Spirally Wound D Cell for High Rate Applications	4
A. Improvement of Cathode Current Collector Design	5
a. Experimental	5
b. Results and Discussion	8
c. Conclusions	10
B. Preliminary Performance Data of D Cells with Improved Cathode Design	10
a. Experimental	10
1. BA5590 Battery	10
2. GLLD Laser Designator Battery	11
b. Results and Discussion	12
1. BA5590 Battery	12
2. GLLD Laser Designator Battery	12
c. Conclusions	16
C. Evaluation of Cathode Additives	17
a. Experimental	17
b. Results and Discussion	17
c. Conclusions	20



	Page No.
D. Effect of Electrolyte Concentration	20
a. Experimental	21
b. Results and Discussion	21
c. Conclusions	21
E. Effect of Electrode Length and Cathode Pre-treatment	21
a. Experimental	22
b. Results and Discussion	22
c. Conclusions	23
F. Design and Performance of Optimized High Rate D Cell	24
a. Experimental	24
b. Results and Discussion	25
c. Conclusions	30
G. Conclusions	30
III. Development of 1.8 inch Diameter Spirally Wound Cylindrical Cell	32
A. Experimental	32
B. Results and Discussion	33
C. Conclusion	33
IV. Development of the Three Inch Diameter Flat Cylindrical Cell.	34
A. Study of the Effect of Cathode Current Collector Design	35
a. Experimental	36
b. Results and Discussion	38
c. Conclusion	39
B. Design and Construction of Flat Cylindrical Cells	39
a. Thin Flat Cylindrical Cell (0.45")	39
b. Thick Flat Cylindrical Cells (0.90")	41

Page No.

C.	Preliminary Performance Data on Flat Cylindrical Cells	42
a.	Experimental	42
b.	Results and Discussion	43
1.	Thin Flat Cell	43
2.	Thick Flat Cell	44
c.	Conclusions	45
D.	Optimization of the Thick Flat Cylindrical Cell	45
a.	Effects of Anode Polarization Cathode Additives and Cathode Number	45
1.	Experimental	45
2.	Results and Discussion	46
3.	Conclusions	47
b.	Improvement of Electrode Stack Connection and Other Design Changes	48
c.	Performance Characteristics of the Flat Cylindrical Cells	50
1.	Experimental	50
2.	Results and Discussion	51
i.	Fresh Cell Test	51
ii.	Stored Cell Test	55
iii.	Multicell Test	58
d.	Conclusions	59
V.	Electrochemical and Spectroscopic Studies on SOCl <sub>2</sub> Reduction Mechanism	61
A.	Experimental	62
B.	Results and Discussion	62
a.	Cyclic Voltammetry	62
1.	Chloride	63
2.	Sulfur Dioxide	63
3.	Sulfur	64
4.	Sulfur and Sulfur Dioxide Mixture	64
5.	Sulfur Monochloride	65
6.	Thionyl Chloride	66

	Page No.
b. Coulometry	68
c. Reduction Mechanism of $\text{SOCl}_2$ and Its Implication on Li/ $\text{SOCl}_2$ Cell Safety	69
d. Conclusions	71
VI. Conclusions	72
VII. References	73
VIII. Acknowledgement	75

List of Tables

Table 1. Short-Circuit Currents of Hermetic D Cells with Various Cathode Designs.

Table 2. Behavior of High Rate Li/SOCl<sub>2</sub> D Cells on GLLD Modified Duty Cycle.

Table 3. Performance of High Rate Li/SOCl<sub>2</sub> D Cells on GLLD Tests Using the Old Duty Cycle at 25°C.

Table 4. Effect of Cathode Additive on the Performance of Li/SOCl<sub>2</sub> D Cells for GLLD Laser Designator Application at 25°C.

Table 5. Voltage Plateaus for the Optimized High Rate D Cells.

Table 6. Polarization Characteristics of the Flat Cells and the Circular Cathodes with Various Current Collector Designs.

Table 7. Short-Circuit Currents of the Experimental Flat Cylindrical Cells with Various Cathode Designs.

List of Figures

Figure 1. Schematic diagram of the old and new duty cycles for the GLLD battery for laser designator GLLD duty cycle.

Figure 2. Laser designator battery with thin flat cells.

Figure 3. Laser designator battery with thick flat cells.

Figure 4. Cross-sectional view of the hermetic Li/SOCl<sub>2</sub> D cell.

Figure 5. Energy density-rate curves of the medium rate and the low rate Li/SOCl<sub>2</sub> D cell.

Figure 6. Discharge characteristics of medium rate Li/SOCl<sub>2</sub> D cells at constant currents of 0.25, 1.0 and 3.0A at 25°C.

Figure 7. Discharge characteristics of low rate Li/SOCl<sub>2</sub> D cells at constant currents of 0.01, 0.03, 0.1 and 0.3A at 25°C.

Figure 8. Longitudinal reaction profiles of carbon cathode.

Figure 9. Current collector designs of the carbon cathodes of spirally wound D cells.

Figure 10. Electrical resistance of expanded Ni cathode current collector.

Figure 11. Polarization characteristics of D cells with 20 inch cathodes of various current collector designs.

Figure 12. Polarization characteristics of D cells with 25 inch long cathodes of various current collector design.

Figure 13. Performance of high rate Li/SOCl<sub>2</sub> D cell on prorated BA5590 test at 25°C.

Figure 14. Performance of high rate Li/SOCl<sub>2</sub> D cell on prorated BA5590 test at 0°C.

Figure 15. Performance of BA5590 battery of 8 Li/SOCl<sub>2</sub> D cells in series at 25°C.

Figure 16. Voltage and temperature profiles of Li/SOCl<sub>2</sub> D cell of design #2 on modified GLLD test using a 6.5A pulse at 25°C.

List of Figures (continued)

Figure 17. Voltage and temperature profiles of an insulated Li/SOCl<sub>2</sub> D cell of design #2 on modified GLLD test using an 8.0A pulse at 25°C.

Figure 18. Voltage profiles of Li/SOCl<sub>2</sub> D cell of design #2 on modified GLLD test using a 6.5A pulse at -30°C.

Figure 19. Voltage and temperature profiles of an insulated Li/SOCl<sub>2</sub> D cell of design #4 on modified GLLD test using a 6.5A pulse at 25°C.

Figure 20. Voltage and temperature profiles of Li/SOCl<sub>2</sub> D cell of design #6 on the modified GLLD test using an 8A pulse at 25°C.

Figure 21. Voltage and temperature profiles of Li/SOCl<sub>2</sub> D cells of design #7 on modified GLLD test using a 6.5A pulse at 25°C.

Figure 22. Voltage and temperature profiles of an insulated Li/SOCl<sub>2</sub> D cell of design #7 on modified GLLD test using a 6.5A pulse at 25°C.

Figure 23. Voltage and temperature profiles of a Li/SOCl<sub>2</sub> D cell of design #7 on the modified GLLD test using an 8A pulse at 25°C.

Figure 24. Voltage and temperature profiles of a Li/SOCl<sub>2</sub> D cell of design #8 on the modified GLLD test using a 6.5A pulse at 25°C.

Figure 25. Voltage and temperature profiles of a Li/SOCl<sub>2</sub> D cell of design #8 on the modified GLLD test using a 6.5A pulse at -30°C.

Figure 26. Voltage and temperature profiles of a Li/SOCl<sub>2</sub> D cell of design #8 on the modified GLLD test using a 6.5A pulse at -30°C.

Figure 27. Voltage and temperature profiles of an insulated Li/SOCl<sub>2</sub> D cell of design #8 on the modified GLLD test using a 8.75A pulse at 25°C.

Figure 28. Voltage and temperature profiles of an insulated Li/SOCl<sub>2</sub> D cell of design #9 on the modified GLLD test using a 6.5A pulse at 25°C.

List of Figures (continued)

Figure 29. Voltage and temperature profiles of an insulated Li/SOCl<sub>2</sub> D cell of design #9 on the modified GLLD test using a 8.0A pulse at 25°C.

Figure 30. Voltage and temperature profiles of two parallel connected Li/SOCl<sub>2</sub> D cells of design #2 on the GLLD test using the old duty cycle at 25°C.

Figure 31. Voltage and temperature profiles of two parallel connected Li/SOCl<sub>2</sub> D cells of design #2 on the GLLD test using the old duty cycle at 25°C.

Figure 32. Voltage and temperature profiles of two parallel connected Li/SOCl<sub>2</sub> D cells of design #8 on GLLD load using the old duty cycle at 25°C.

Figure 33. Voltage and temperature profiles of two parallel connected Li/SOCl<sub>2</sub> D cells of design #8 (with heat shrinkable jackets) on GLLD test using the old duty cycle at 25°C.

Figure 33a. Performance of two D cells with cathode additive 1, level A on old GLLD duty cycle load.

Figure 34. Performance of two D cells with cathode additive 1, level B on GLLD test using the old duty cycle.

Figure 35. Performance of two D cells with cathode additive 1, level B on GLLD test using the old duty cycle.

Figure 36. Performance of two D cells with cathode additive 1, level B on GLLD test.

Figure 37. Performance of two D cells with cathode additive 2, level A on old GLLD load.

Figure 38. Performance of two D cells with cathode additive 2 at level A the old GLLD load.

Figure 39. Performance of the two D cells with cathode additive 2, level B on old GLLD load.

List of Figures (continued)

Figure 40. Performance of two D cells with cathode additive 2 at level C on the new GLLD load.

Figure 41. Performance of two D cells with cathode additive 2 at level C on the new GLLD load.

Figure 42. Performance of two D cells with cathode additive 3 on the old GLLD load.

Figure 43. Cell wall temperature of 2 D cells with cathode additive 3 during reversal at 2A.

Figure 44. Performance of two D cells with cathode additive 3 on the old GLLD load.

Figure 45. Performance of two D cells with cathode additive 4 on the old GLLD test.

Figure 46. Performance of two D cells with cathode additive 5 on the old GLLD test.

Figure 47. Performance of two D cells with  $1.4M\ LiAlCl_4 \cdot SOCl_2$  electrolyte on the old GLLD duty cycle.

Figure 48. Performance of two D cells with  $1.4M\ LiAlCl_4 \cdot SCl_2$  electrolyte on the old GLLD duty cycle.

Figure 49. Current collector configuration of long cathodes in D cells (design #10).

Figure 50. Performance of two D cells with 25" pretreated cathodes on the old GLLD duty cycle.

Figure 51. Performance of 2 D cells with 35" cathode on the new GLLD duty cycle.

Figure 52. Li/SOCl<sub>2</sub> D cell with 35" pretreated cathode driven into voltage reversal at 2A.

Figure 53. Performance of 2 D cells with 35 inch cathode on the new GLLD duty cycle.

List of Figures (continued)

Figure 54. Voltage reversal behavior of the cell pair shown in Figure 53.

Figure 54a. Polarization curve of a D cell with 35" long pretreated cathode.

Figure 55. Performance of two D cells with 40" pretreated cathodes on the new GLLD load.

Figure 56. Performance of two D cells with 40" pretreated cathodes on the new GLLD load.

Figure 57. Performance of a D cell with 28 inch cathode on the BA5590 test.

Figure 58. Performance of a D cell with 28 inch cathode on the BA5590 test.

Figure 59. Discharge of a D cell with 28 inch cathode at 1 amp at 25°C.

Figure 60. Performance of a D cell with 28 inch cathode on 1 amp discharge at 25°C.

Figure 61. Performance of a D cell with 20 inch cathode at 1A discharge.

Figure 62. Performance of a D cell with 20 inch pretreated cathode on 1 amp discharge.

Figure 63. Performance of D cell with 26 inch cathode on BA5590 test.

Figure 64. Performance of a pair of D cells with 26 inch cathodes on the new GLLD test.

Figure 65. Polarization of an optimized high rate D cell at 25°C.

Figure 66. Performance of an optimized high rate D cell on constant current discharge at 0.3A.

Figure 67. Performance of an optimized high rate D cell on discharge at 1A.

Figure 68. Performance of an optimized high rate D cell on discharge at 3.0A.

Figure 69. Plot of cell voltage and temperature for an optimized D cell on discharge at 10A.

Figure 70. Plot of cell temperature and voltage for an optimized D cell in reversal at 0.3A at 25°C.

Figure 71. Temperature and voltage for an optimized D cell with cathode additive 2 in reversal at 1A.

List of Figures (continued)

Figure 72. Cell temperature and voltage for an optimized D cell driven into reversal at 3A.

Figure 73. Polarization of an optimized D cell at -30°C.

Figure 74. Discharge of an optimized D cell on 0.3A load at -30°C.

Figure 75. Discharge of an optimized D cell with cathode additive 2 at 1A at -30°C.

Figure 76. Discharge of an optimized D cell on 3A load at -30°C.

Figure 77. Cell temperature and voltage for an optimized D cell with cathode additive 2 in reversal at 1A at -30°C.

Figure 78. Cell temperature and voltage for an optimized D cell driven into reversal at 3A and -30°C.

Figure 79. Short circuit current of an optimized high rate D cell.

Figure 80. Performance of a high rate D cell on the BA5590 test after two weeks at 72°C.

Figure 81. Performance of a D cell at -30°C on the BA5590 test after two weeks storage at 72°C.

Figure 82. Performance of a pair of D cells on the GLLD test after two weeks storage at 72°C.

Figure 83. Performance of a pair of D cells on the GLLD test at -30°C after two weeks of storage at 72°C.

Figure 83a. Performance of a 16 cell GLLD battery on the new GLLD load at 25°C after six months on storage.

Figure 84. Schematic drawing of the completed 1.8 inch diameter cell top with fill port, vent and G/M feedthrough.

Figure 85. Photograph of the finished 1.8 inch diameter cylindrical cell.

Figure 86. Performance of a 1.8 inch diameter cylindrical cell on the old GLLD test cycle.

List of Figures (continued)

Figure 87. Performance of a 1.8 inch diameter cylindrical cell on the new GLLD test cycle.

Figure 88. Schematic view of the experimental demountable flat cylindrical cell.

Figure 89. Current collector designs for the 2.8 inch diameter disc cathodes.

Figure 90. Polarization characteristics of disc shaped cathodes with various current collector designs.

Figure 91. Polarization characteristics of disc shaped cathodes with various current collector designs.

Figure 92. Flat cylindrical cell container.

Figure 93. Flat cylindrical cell top with G/M seal and the electrolyte fill port.

Figure 94. Cross-section of the hermetic flat cylindrical cell.

Figure 95. Photograph of a hermetic thin flat cylindrical cell.

Figure 96. Top of hermetically sealed flat cell with G/M seal and fill tube.

Figure 97. The anode and cathodes for a flat cell.

Figure 98. Assembly stacking sequence for the flat cell.

Figure 98a. Top view of an assembled flat cell.

Figure 99. Lithium anode contact detail.

Figure 100. Photograph of finished flat cell.

Figure 101. Performance of the thin flat cylindrical cell on the old GLLD test.

Figure 102. Performance of a thick flat cell with 40 cathodes and 41 anodes on the old GLLD load.

Figure 103. Performance of a thick flat cell with 35 cathodes and 36 anodes on the old GLLD duty cycle.

Figure 104. Performance of a flat cell with thick anodes on the new GLLD load.

List of Figures (continued)

Figure 105. Performance of a flat cell with 32 cathodes on the old GLLD test at 25°C.

Figure 106. Performance of a flat cell with 32 cathodes on the new GLLD test cycle at 25°C.

Figure 107. Performance of a flat cell with 40 cathodes on the old GLLD load at 25°C.

Figure 108. Performance of a flat cell with 36 cathodes on the new GLLD load at 25°C.

Figure 109. Performance of a flat cell with 36 cathodes on the new GLLD load at 25°C.

Figure 110. Voltage-current curve of a flat cell with 36 cathodes.

Figure 111. Performance of a flat cell with cathode additive 1 at level A on the new GLLD test.

Figure 112. Lithium anode contact detail of finalized version of the flat cell.

Figure 113. Assembly stacking sequence for the flat cell.

Figure 114. Top of hermetically sealed flat cell showing G/M seal, nickel tab and fill tube.

Figure 115. Performance of a fresh flat cell with new electrode design on the GLLD test at room temperature.

Figure 116. Performance of a fresh flat cell with new electrode design on the new GLLD test at room temperature.

Figure 117. Performance of a fresh flat cell with old electrode design on the new GLLD test at room temperature.

Figure 118. Schematic outline for the GLLD battery using 8 3" O.D., 0.90" thick flat cells.

Figure 119. Performance of a fresh flat cell on the new GLLD test at 25°C.

Figure 120. Performance of a fresh flat cell on the new GLLD test at 25°C.

List of Figures (continued)

Figure 121. Performance of a fresh flat cylindrical cell on the new GLLD test at 0°C.

Figure 122. Performance of a fresh flat cell on the new GLLD load at -30°C.

Figure 123. Performance of a fresh flat cell on 20A constant current discharge.

Figure 124. Voltage, temperature and internal pressure profiles of a fresh flat cylindrical cell on 100A at 25°C.

Figure 125. Short circuit performance of a flat cylindrical cell.

Figure 126. Photograph of a fresh and a shorted flat cell.

Figure 127. Voltage and temperature profiles of a flat cell on force-discharge at a constant current of 3.0A at 25°C.

Figure 128. Behavior of a flat cell during voltage reversal on the new GLLD cycle.

Figure 129. Behavior of a flat cell during voltage reversal at 3.2A and 20A on the new GLLD cycle.

Figure 130. Behavior of a flat cell during voltage reversal at 3.2A and 20A on the new GLLD cycle.

Figure 131. Behavior of a flat cell during voltage reversal on the new GLLD cycle.

Figure 132. Behavior of a flat cell during voltage reversal on the new GLLD cycle.

Figure 133. Behavior of a flat cell during voltage reversal on the new GLLD cycle.

Figure 134. Behavior of a lithium excess flat cell during voltage reversal on the new GLLD load.

Figure 135. Performance of a lithium excess flat cell during voltage reversal at the new GLLD load.

List of Figures (continued)

Figure 136. Performance of a lithium excess flat cell during voltage reversal on the new GLLD load.

Figure 137. Performance of a lithium excess flat cell on voltage reversal at 20A.

Figure 138. Performance of a flat cell on the new GLLD test at room temperature after three days at room temperature.

Figure 139. Performance of a flat cell on the new GLLD test at room temperature after one week at room temperature.

Figure 140. Performance of a flat cell on the new GLLD test at room temperature after one week at room temperature.

Figure 141. Performance of a flat cell on the GLLD test at room temperature after two weeks at room temperature.

Figure 142. Performance of a flat cell on the GLLD test at room temperature after three weeks at room temperature.

Figure 143. Performance of a flat cell on the GLLD test at room temperature after six weeks at room temperature.

Figure 144. Plot of capacity on GLLD test vs. storage time for flat cylindrical cells.

Figure 145. Performance of a flat cell on the new GLLD test at 0°C after three weeks at room temperature.

Figure 146. Performance of a flat cell on GLLD test at room temperature after two days at 50°C and two days at 72°C.

Figure 147. Performance of a flat cell with cathode additive 1 on the new GLLD test at room temperature after 2 days at 72°C and 3-1/2 days at room temperature.

Figure 148. Performance of a cell with vacuum dried cathodes on the new GLLD test at room temperature after 1 day at 72°C and 3-1/2 days at room temperature.

Figure 149. Performance of a flat cell tested on the new GLLD test at 48°C after three weeks at room temperature.

List of Figures (continued)

Figure 150. Performance of a flat cell with new design on GLLD test after 2.5 days at 72°C.

Figure 151. Performance of a flat cell on the new GLLD test at room temperature after 5 days at 72°C.

Figure 152. Performance of a flat cell on the new GLLD test at room temperature after 5 days at 72°C.

Figure 153. Performance of a flat cell on the new GLLD test at room temperature after 5 days at 72°C.

Figure 154. Performance of a three cell stack on the new GLLD cycle at 25°C.

Figure 155. Performance of an 8 cell GLLD battery on the new GLLD duty cycle at 25°C.

Figure 156. Performance of a 7 cell battery on the GLLD test at 25°C.

Figure 157. Performance of a GLLD battery on the GLLD test load at 25°C.

Figure 158. Schematic drawing of the jacketed cell used for cyclic voltammetry at various temperatures.

Figure 159. Cyclic voltammograms of tetrabutyl ammonium hexafluorophosphate solution in acetonitrile on Pt electrode, background, scan rate 200 mv/sec.

Figure 160. Cyclic voltammogram of tetramethyl ammonium chloride in acetonitrile/tetrabutyl ammonium hexafluorophosphate, scan rate 200 mv/sec.

Figure 161. Cyclic voltammogram of SO<sub>2</sub> in acetonitrile/tetrabutyl ammonium hexafluorophosphate, scan rate 1v/sec.

Figure 162. Cyclic voltammogram of SO<sub>2</sub> in dimethyl formamide (DMF)/tetrabutyl ammonium hexafluorophosphate; scan rate 200 mv/sec.

Figure 163. Cyclic voltammogram of SO<sub>2</sub> in methylene chloride/tetrabutyl ammonium hexafluorophosphate (TBAPF<sub>6</sub>). scan rate 100 mv/sec.

List of Figures (continued)

**Figure 164.** Cyclic voltammogram of S in methylene chloride/TBAPF<sub>6</sub>, scan rate 200 mv/sec.

**Figure 165.** Cyclic voltammogram of S in DMF/TBAPF<sub>6</sub>, scan rate 500 mv/sec.

**Figure 166.** Cyclic voltammograms of (a) S trace SO<sub>2</sub> in DMF/TBAPF<sub>6</sub>, (b) S more SO<sub>2</sub> in DMF/TBAPF<sub>6</sub>, scan rate 200 mv/sec.

**Figure 167.** Cyclic voltammogram of S<sub>2</sub>Cl<sub>2</sub> in acetonitrile/TBAPF<sub>6</sub>, scan rate 500 mv/sec.

**Figure 168.** Cyclic voltammograms of SOCl<sub>2</sub> in DMF/TBAPF<sub>6</sub> (a) before th electrolysis, (b) immediately after the exhaustive electrolysis at -0.25V vs Ag wire reference, (c) after warming the electrolyzed solution; scan rate 200 mv/sec.

**Figure 169.** Plot of the peak currents versus the square root of the scan rate (V) of the two reduction waves of SOCl<sub>2</sub> in the DMF/TBAPF<sub>6</sub>.

**Figure 170.** Cyclic voltammogram of SOCl<sub>2</sub> in CH<sub>3</sub>CH/0.1N N(C<sub>4</sub>H<sub>9</sub>)<sub>4</sub>PF<sub>6</sub> showing the effect of sweep rate at a Pt wire electrode.  
a) 0.20 V/sec, b) 0.50 V/sec, c) 1.0 V/sec, d) 2.0 V/sec.

**Figure 171.** Cyclic voltammograms of SOCl<sub>2</sub> in CH<sub>3</sub>CN/N(C<sub>4</sub>H<sub>9</sub>)<sub>4</sub>PF<sub>6</sub> at various concentrations. a) 25μl SOCl<sub>2</sub>/75 ml (V 0.50 V/sec., b) 50μl SOCl<sub>2</sub>/75 ml (V 0.050 V/sec), c) 100μl SOCl<sub>2</sub>/75 ml (V 0.20 V/sec., d) 200μl SC<sub>2</sub>Cl<sub>2</sub>/75 ml (V 0.20 V/sec).

**Figure 172.** Cyclic voltammograms of SOCl<sub>2</sub> in CH<sub>3</sub>CN/0.1N N(C<sub>4</sub>H<sub>9</sub>)<sub>4</sub>PF<sub>6</sub>.  
a) Ni wire electrode, b) Ir wire electrode, c) Au·Hg wire electrode (V = .20V/sec in all)

**Figure 173.** Cyclic voltammogram of SOCl<sub>2</sub> in CH<sub>3</sub>CN/0.1N N(C<sub>4</sub>H<sub>9</sub>)<sub>4</sub>PF<sub>6</sub> at a silver wire electrode (0.05V/sec).

**Figure 174.** Cyclic voltammogram of SOCl<sub>2</sub> in DMSO/0.1N N(C<sub>4</sub>H<sub>9</sub>)<sub>4</sub>PF<sub>6</sub> at a platinum wire electrode (0.05 V/sec).

List of Figures (continued)

Figure 175. UV-VIS spectrum of 2mM SO<sub>2</sub> in CH<sub>3</sub>CN vs CH<sub>3</sub>CN (pathlength 1 cm).

Figure 176. UV-VIS spectrum of 2mM S in CH<sub>3</sub>CN vs CH<sub>3</sub>CN (pathlength 1 cm).

Figure 177. UV-VIS spectrum of 1.8 mM SOCl<sub>2</sub> in CH<sub>3</sub>CN/0.1N N(C<sub>4</sub>H<sub>9</sub>)<sub>4</sub> PF<sub>6</sub> vs CH<sub>3</sub>CN/0.1N N(C<sub>4</sub>H<sub>9</sub>)<sub>4</sub> PF<sub>6</sub> in a 1 cm pathlength cell.

Figure 178. Cyclic voltammogram of 1.8 mM SOCl<sub>2</sub> in CH<sub>3</sub>CN/0.1N N(C<sub>4</sub>H<sub>9</sub>)<sub>4</sub> PF<sub>6</sub>. a) n = 0.00, b) n = 0.300, c) n= 0.84, d) n = 1.33, e) n = 1.76, f) n = 2.0 after one week stand.

Figure 179. Absorbance spectra of 1.8 mM solution of SOCl<sub>2</sub> CH<sub>3</sub>CN/0.1N N(C<sub>4</sub>H<sub>9</sub>)<sub>4</sub> PF<sub>6</sub>. a) n = 0.00 (start of electrolysis), b) n = 0.30, c) n = 0.84, d) n = 1.33, e) n = 1.33 after 16 hour stand, f) n = 1.76, g) n = 2.0 after one week stand.

Figure 180. Variation of max and absorbance of SOCl<sub>2</sub> solution as a function of charge passed during electrolysis.

## I. Introduction

### A. Background and Approach

The Li/SOCl<sub>2</sub> inorganic electrolyte system (1-4) is the highest energy density system known to date. Energy densities as high as 20 Wh/in<sup>3</sup> and 300 Wh/lb have actually been realized in practical cells (4). The system consists of a Li anode, a porous carbon cathode, and SOCl<sub>2</sub> which acts both as a solvent and as a cathode depolarizer. As for the electrolyte salt, LiAlCl<sub>4</sub> has been widely used. Compounds such as Li<sub>2</sub>B<sub>10</sub>Cl<sub>10</sub> (5) and Li<sub>2</sub>O (AlCl<sub>3</sub>)<sub>2</sub> (6) have also been successfully used in this system for longer shelf life.

The main objective of this program is to develop high rate Li/SOCl<sub>2</sub> cells and batteries for portable applications of the U.S. Army. The cells and batteries must deliver higher capacities than the ones presently available especially at high discharge rates. Perhaps more importantly, these batteries must also be safe to handle under a wide range of field conditions.

We have carried out a research and development program (7) previously for the U.S. Army on the spirally wound high rate D cell. Substantial progress was made to correct performance limitations and to improve safety features. The performance characteristics and the abuse resistance of the spirally wound D cell developed in that program has been well established and this cell was found to approach the high rate requirements of the various U.S. Army applications more closely than does any other cell design known at the time this program began. Accordingly, we used this spirally-wound D cell as a starting point and attempted to improve its rate capability in order to meet the requirements of two specific applications, viz. the BA5590 Battery for Man Pack Radio and the battery for the GLLD Laser Designator. The specifications and load requirements of these two batteries are described in detail in the next section.

In addition, we have begun the development of a 3 inch diameter flat cylindrical cell for the GLLD Laser Designator application because such a design offers better heat generation and dissipation characteristics than the

cylindrical spirally wound design due to the higher outer surface area to volume ratio and low internal cell impedance. A 1.8 inch diameter spirally wound cylindrical cell design for the GLLD Laser Designator application was also developed during the course of this program.

A parallel research effort was made in order to gain further understanding of the cell discharge reaction mechanism, particularly with respect to the unstable intermediates using both electrochemical and spectroscopic techniques. We believe this knowledge is directly relevant to the improvement of the safety features of the Li/SOCl<sub>2</sub> system in general.

This report summarizes all the activities carried out and the progress made during the two year period.

B. BA5590 Battery/GLLD Laser Designator Battery

a. BA5590 Man Pack Radio Battery

The specifications of the above battery are as follows:

Dimension: 4.4" x 2.45" x 5.00"

Voltage: Nominal 12 or 24V

Maximum (OCV) 15 or 30V

Average 12.5 or 25V

End Voltage 10 or 20V

Capacity (at 70°F): 10A.hr (30 hour rate)

Maximum Rate: 2 hour rate

Duty Cycle for  
30 Volt Operation: 8<sub>n</sub> load for 100 msec followed by 39<sub>n</sub> load for 1 minute followed by 560<sub>n</sub> load for 9 minutes.

The above is repeated.

The presently used battery contains 10 Li/SO<sub>2</sub> D cells (OCV 3.0 volt) in series and parallel to meet the 15 and 30 volt requirements. It weighs 940 grams with a service life of 80 hours on the above duty cycle. In view of the higher OCV of the Li/SOCl<sub>2</sub> D cell only 8 spirally wound D cells are needed to satisfy the voltage requirement. Therefore, it has been envisioned that the 8 Li/SOCl<sub>2</sub>

D cell package should provide both longer service life and significant weight reduction.

b. GLLD Laser Designator Battery

The specifications for the GLLD Laser Designator Battery are as follows:

Dimension: 2.82" x 3.75" x 9.30"

Voltage: Nominal 24V

Maximum (OCV) 32V

Average 24V

End Voltage 20V

Old Duty Cycle: 17.5A for 35.5 msec followed by 1.8A for 14.5 msec and the cycle continues for 3 minutes. This constitutes one burst (0.647 Ahr/burst). The three minute cycle occurs every 30 minutes.

New Duty Cycle: 20A for 29 msec followed by 3.2A for 21 msec and the cycle continues for 20 sec. This constitutes one burst (0.072 Ahr/burst). The 20 sec cycle occurs every 3 minutes.

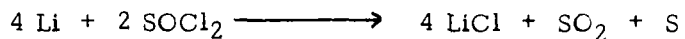
Both duty cycles are shown schematically in Figure 1. The presently used Ni/Cd batteries provide ~1.95 A.hr per charge.

The voltage requirements necessitates the use of at least 8 Li/SOCl<sub>2</sub> cells in series. We have considered the following types of individual cells based on dimensional concerns:

1. 16 spirally wound D cells; 8 in series with the two series stacks in parallel.
2. 8 cylindrical 1.8 inch diameter spirally wound cells in series.
3. 16 thin flat cells (3 in. O.D., 0.45" high); 8 in series with the two series stack in parallel. (Figure 2).
4. 8 thick flat cells (3 in. O.D. 0.90" high) in series. (Figure 3).

## II. Optimization of Spirally Wound D Cell for High Rate Applications

The cross-sectional view of a typical spirally wound hermetic Li/SOCl<sub>2</sub> D cell is schematically shown in Figure 4. We have developed two types of spirally wound D cells, one for low rates using 10-15 inch long electrodes and 0.5M LiAlCl<sub>4</sub>/SOCl<sub>2</sub> electrolyte and the other for medium rates having 20 inch long electrodes and 1.0M LiAlCl<sub>4</sub>/SOCl<sub>2</sub> electrolyte. The design details were discussed elsewhere (7, 8). The energy density versus discharge current curves for these two types of cells are shown in Figure 5. Typical discharge curves of the low and medium rate cells are shown in Figures 6 and 7, respectively. Note that the low rate cells were capable of delivering capacities of 18-19 A.hr corresponding to energy densities of 20 Whr/in<sup>3</sup> and 300 Whr/lb. The SOCl<sub>2</sub> utilization efficiency was estimated at 95-98% based on the following cell reaction stoichiometry



Therefore, these energy density levels represented the upper limits available from this low rate spirally wound D cell package and we do not anticipate any significant gain by additional effort to further improve the cell. The medium rate cell, on the other hand, delivered constant energy densities of only 13 Whr/in<sup>3</sup> and 190 Whr/lb at drain rates up to 1.0A. The energy densities dropped sharply at discharge rate above 2.0A. The SOCl<sub>2</sub> utilization efficiency was only 70-75%. These energy density penalties at moderate discharge rates stem from (a) lower operating voltage and (b) lower capacity or lower utilization efficiency. The former is dependent upon the electrical conductivity of the current collector (anode and cathode) and the electrolyte and the latter is dependent upon the mass transfer (diffusion of active material) in the porous carbon cathode which was the capacity limiting electrode.

We have experimentally determined the longitudinal reaction profile in these cathodes by monitoring the LiCl content of the discharged cathodes as a

function of length from the cathode tab onward. The results for 2A discharge, at three different depths of discharge, are shown in Figure 8. Note that at the early stages of discharge, (2.5 Ahr and 5.4 Ahr), most of the reaction occurs near the tab. This demonstrates that at 2A and higher currents, the electrical conductivity of the cathode grid controls the current distribution. The higher the current, the greater the non-uniformity of the current distribution. Therefore, our first task was to optimize the current collector design of the cathode of the spirally-wound D cell. The choice of a proper electrolyte composition which provides the highest electrical conductivity across the range of operating conditions would also improve the energy density levels somewhat. Finally, efforts were focused on the optimization of the porous cathode structure to maximize the utilization efficiency of the active cell materials.

#### A. Improvement of the Cathode Current Collector Design

For this study, we kept the cathode mix composition and the cathode fabrication process invariant in order to keep the porosity of the carbon cathodes identical for all the cathode collector designs. The carbon cathode consists of an expanded Ni grid covered with Shawinigan Black + 10% Teflon mixture on both sides of the grid. The selection of the above was made from the optimization of the carbon mixture and the carbon types, carried out in our previous work (9, 10).

##### a. Experimental

We chose to investigate two sizes of the cathodes, viz., 20" x 1.75" x 0.025" and 25" x 1.75" x 0.015". The various collector designs studied are discussed below.

Design #1. One Tab on End Standard Design: This cathode design consists of one tab welded vertically at one end of the 20" x 1.75" cathode strip as shown in Figure 9 (1). This is the standard design used in all the D cells studied so far. The longitudinal reaction profiles shown in Figure 8 refers to this design.

Design #2. One Tab in Middle Design: In this design the one vertical tab is located at the center of the 20" x 1.75" electrode as shown in Figure 9 (2).

Design #3. Two Tab Design: In this design the two tabs are placed in such a manner that the farthest points from both the tabs are identical and are 5 inches away from the 20" x 1.75" cathode. A schematic view of the cathode design is shown in Figure 9 (3). The total current is distributed evenly between the two tabs.

Design #4. Horizontal Tab with Single Vertical Tab Design: In this design one horizontal tab is welded on one side of the cathode along its length and a vertical tab is welded at one end for connecting the cathode to the cell terminal as shown in Figure 9 (4). In this design the maximum distance from the tab is the width of the cathode and as such the current collection should be most efficient.

Design #5. Horizontal Tab with Double Vertical Tab Design: In this design, two vertical tabs, located 5 inches from either ends of the cathode, were used in addition to the horizontal tab as above. The schematic view is shown in Figure 9 (5).

Design #6. One Tab-Long Cathode Design: This design is identical to the design 1, above, except that the cathode is 25" long (Figure 9 (6)) instead of 20" long.

Design #7. Horizontal Tab-Long Cathode Design: This design (Figure 9 (7)) is identical to the design 4, above, except that the cathode is 25" long.

Design #8. Triple Tab-Long Cathode Design: In this design three tabs were used, one located at the center and the other two were located at either ends of the 25" long cathode. The schematic view is shown in Figure 9 (8).

Hermetic D cells were made by winding the cathode, Li anode and glass filter paper separator in Ni cans for evaluating the efficacy of the

cathode on the rate capability of the cells. All the cells were filled with 1.8M LiAlCl<sub>4</sub>-SOCl<sub>2</sub> electrolyte.

The tabs were 0.002" thick and 0.25" wide and were folded over the expanded Ni grid which was exposed by removing the carbon mix from the grid area where the tabs were welded. Thus each tab consists of a double layer of 0.002" Ni foil.

Some other specific construction details of the D cells with the various cathode designs are described below.

Design 1. Li anode dimension was 21" x 2" x 0.015"; one tab was attached at one end of the anode.

Design #2. Li anode was identical to design 1.

Design #3. Li anode was made by sandwiching expanded Ni current collector with a 0.25" wide tab welded horizontally lengthwise between two layers of 0.005" thick Li foil. Overall Li anode dimension was 21"x 2" x 0.010".

Design #4. Li anode was identical to design 1. The horizontal tab on the cathode was attached by welding two layers of the 0.25 inch wide tab on either side of the expanded Ni grid which was stripped of the carbon mix. The edge of the thin horizontal tab was very sharp and it cut through the separator to cause the cells to short during assembly. In order to prevent this, a thin Teflon film was folded over the horizontal tab of the cathode. This made the fabrication of these cells quite cumbersome.

Design #5. The Li anodes were similar to those of design 3 and the fabrication of these cells was as difficult as in design 4.

Design #6. The Li anode dimensions were 26" x 2" x 0.01", and it had one set of vertical tabs at one end of the anode as in design 1.

Design #7. The Li anode dimensions were 26" x 2" x 0.01" and it had expanded Ni current collector with 0.25" wide Ni tab welded horizontally, similar to that used in design 3. The cathode was covered with Teflon film over the horizontal and vertical tab areas.

Design #8. The Li anode was identical in construction to that of design 7. The construction of these cells was considerably easier than that of cells of design 7 because of the absence of the horizontal tab.

The polarization characteristics at currents below 17.5A were determined using a constant current discharge method and all the short circuit currents were measured through a 1milliohm shunt at 25°C for hermetic D cells made according to the above designs. The results will be used to select the promising cell designs for detailed performance evaluation according to the requirements of the BA5590 and the GLLD Laser Designator Batteries.

b. Results and Discussion

The electrical resistance of the 2" wide Li anode was calculated to be 0.113 and 0.169 milliohm/inch for 0.015" and 0.01" thick foils respectively, using the  $8.6 \times 10^{-6}$  ohm-cm as the resistivity of Li metal. The electrical resistance of two layers of the 0.25 inch wide and 0.002 inch thick Ni foil was calculated to be 2.677 milliohm/inch using  $6.8 \times 10^{-6}$  ohm-cm as the resistivity of Ni. The electrical resistance of the 1.75 inch wide expanded Ni was experimentally determined (Figure 10) to be approximately 14.4 millibhm/inch. In Figure 10 the electrical resistance at zero length represents the resistance of the tab. The cathode grid resistance was two orders of magnitude higher than the electrical resistance of the Li anode. Once again, it is demonstrated that the cathode current collector design is a controlling factor in the discharge of the cells at high rates. The Li anode current collector is relatively less important insofar as the short circuit current and the current distribution at high currents are concerned but it becomes more important insofar as the efficiency and uniformity of Li utilization are concerned.

The polarization characteristics of the hermetic D cells with 20" long cathodes of various current collector designs are shown in Figure 11. Note that significant improvements in the polarization characteristics of the cells have been achieved over the standard cathode designs by designs #2 to #5. While the best performance was obtained with design #3, there was no

significant difference between designs #2, #4 and #5. Note that design #2 is the simplest of all the designs and consists of a vertical tab located at the middle of the cathode strip as opposed to the end of the cathode strip. The cumbersome construction of cells with cathodes having horizontal tabs as in design #4 and #5 as well as the lack of any substantial improvement in performance over the simpler design #2, lead us to eliminate designs #4 and #5 from further consideration. The cells of design #3 consisting of two horizontal tabs performed best among the cells with 20" long cathodes. Accordingly, both design #2 and #3 were selected for further studies.

The polarization characteristics of hermetic cells with 25" long cathodes are shown in Figure 12. Note that significant improvements were realized with three tab designs over the single tab designs. The horizontal tabs (design #7) showed some improvement, but the difficulty in cell construction leads us to reject it from further consideration. The three tab design was found to be easier to construct and the cells performed the best. Therefore, we chose design #8 for further evaluation.

The maximum short circuit currents of the hermetic D cells made with the various types of cathodes are shown in Table 1. The short circuit current densities were calculated using the apparent geometric areas of both sides of the cathodes. The short circuit current increased by a factor of three from design #1 to design #2 by placing the tab at the middle instead of at the end. Use of two tabs as in design #3 led to a four-fold increase in the short circuit current over that of the standard design #1. The use of a horizontal tab (design #4) only led to a modest increase in the short circuit current which may be due to the reduction (by 14%) of the active area of the cathode. The short circuit current of cathode with both horizontal and two vertical tabs (design #5) was found to be similar to that of the cathodes with only two vertical tabs (design #3), indicative of the lack of any significant contribution of the horizontal tabs. Therefore, designs #2 and #3 for the 20" long cathodes were chosen for further studies in BA5590 and GLLD laser designator applications.

The short circuit currents of spirally wound D cells with 25" long cathodes increased by a factor of two with a horizontal tab (design #7).

It was also found that the short circuit current was further improved to 104 ampere with a vertical three tab design. Again, the three tab design (design #8) was chosen for further studies.

c. Conclusions

An analysis of the impedance of the various cell components and an analysis of the longitudinal cathode reaction profiles showed that the impedance of the cathode current collector is a major contributor to the cell impedance which leads to non-uniform current distribution and low current carrying capability. Eight different cathode current collector designs were investigated using hermetic D cells with wound electrode assembly. Based on the polarization characteristics and the short circuit currents, three designs were found to be promising and were selected for further evaluation. Short circuit currents approaching 100A and current densities of  $200 \text{ mA/cm}^2$  were realized by the above approach.

B. Preliminary Performance Data of D Cells with Various Improved Cathode Designs

We have demonstrated the importance of cathode current collector design to the rate capability of the spirally wound D cells especially at high discharge rates. It was noted that by simply placing the cathode tab in the middle (referred to as design #2 in Figure 9) rather than at one end (design #1), the short circuit current was found to increase from  $53 \text{ mA/cm}^2$  to  $168 \text{ mA/cm}^2$  (Table 1). In view of the simplicity of this cathode design and the substantial improvement in performance, we chose this particular design for the spirally wound D cells to be tested for BA5590 manpack radio battery as well as GLLD Laser Designator Battery applications in order to obtain some preliminary performance data to serve as a baseline.

a. Experimental

1. BA5590 Test

The specifications and duty cycles of the BA5590 battery have been described in Section IBa. The presently used battery contains

10 Li/SO<sub>2</sub> D cells. It is envisioned that only 8 Li/SOCl<sub>2</sub> D cells are needed because of the higher OCV (3.6V) of the Li/SOCl<sub>2</sub> system.

Hermetically sealed D cells with 20 inch long cathodes having one tab in the middle (design #2) were constructed and tested under BA5590 load. Initially, single D cells were evaluated instead of the 8 cell battery under a continuous prorated duty cycle; each cycle consists of a 1  $\mu$  load for 100 msec. followed by a 5  $\mu$  load for 1 min. and then followed by a 70  $\mu$  load for 9 min. For an 8 cell battery, the 30 volt duty cycle as stated in Section IBa was used as the load. A mechanical timer and relay device was used to provide both duty cycles in our tests.

## 2. GLLD Laser Designator Battery

The specifications and duty cycles (both old and new) have been described in Section IBb. The voltage requirement necessitates the use of at least 8 Li/SOCl<sub>2</sub> D cells in series. The available volume is sufficient to hold 16 D cells, two parallel stacks each consisting of 8 D cells in series. A single D cell only experiences half the constant current loads listed in the specifications.

Initially, a modified duty cycle was used to test D cells on GLLD load. It involved the discharge of cells at an average current of 6.5A/cell (or 8A in some cases) for 3 minutes. This cycle was repeated every 30 minutes. This modified test consumes almost the same cell capacity ( $\sim 0.65$  A.hr) per 3 minute burst as the specified "old" duty cycle.

The test equipment was specifically designed and constructed to conduct testing on the GLLD Laser Designator duty cycles specified earlier. This test equipment was capable of drawing constant currents from the cells at different levels for the desired time intervals down to a voltage of approximately 0.8 volt through a microprocessor control method. At that point the test automatically terminated thus preventing any force discharge on the cells. This test is usually performed using two D cells in parallel instead of the entire 16 cell package.

b. Results and Discussion

1. BA5590 Battery

One Li/SOCl<sub>2</sub> D cell of design #2 was tested under the BA5590 load at 25°C. The cell voltage versus time curves under the 70, 5, and 1 $\Omega$  loads are shown in Figure 13. This cell ran for 95 hours delivering approximately 10 Ahr in cell capacity.

Another D cell with identical cathode design was tested at 0°C under the same duty cycle. The voltage versus time curves under the 70, 5, and 1 $\Omega$  loads are shown in Figure 14. This cell ran for 93 hours to a 2.5 volt cutoff (on 1 $\Omega$  load) delivering approximately 9.8 Ahr.

A BA5590 battery was assembled using 8 Li/SOCl<sub>2</sub> D cells in series with cathodes of design #2. The test was performed at 25°C on duty cycle mentioned earlier. The battery voltage on the 8, 39, and 560  $\Omega$  loads as well as the battery temperature were monitored as a function of time. The results are shown in Figure 15. The average battery voltages were measured to be 25.5, 27.0 and 28.5 volts under the 8, 39, and 560  $\Omega$  loads, respectively. The battery ran for approximately 100 hours to the 20 volt cutoff, delivering approximately 11 Ahr in capacity. The temperature of the battery remained unchanged during the test cycles as shown in Figure 15.

The above BA5590 battery weighed 840 gms and contained 8 D Li/SOCl<sub>2</sub> cells. The present BA5590 battery, on the other hand, contains 10 Li/SO<sub>2</sub> D cells and weighs 940 gms with a service life of 80 hours on the same duty cycle. This corresponds to a 12% weight reduction and a 25% increase in service life. Thus, the improvement in performance of the Li/SOCl<sub>2</sub> BA5590 battery over that of the Li/SO<sub>2</sub> BA5590 battery was significant at the temperatures of these tests.

2. GLLD Laser Designator Battery

1. Modified Duty Cycle

The modified duty cycle as specified earlier was used to screen the efficacy of the various current collector designs for the

GLLD laser designator application while the GLLD test equipment was still under development.

One Li/SOCl<sub>2</sub> D cell with a cathode of design #2 (having the tab located at the center of the 20 inch long electrode) was tested under the modified GLLD duty cycle using a 6.5A current at 25°C. The voltage and the temperature of the cell were monitored during the three minute burst and are plotted as a function of burst numbers in Figure 16. During each three minute, 6.5A burst, the cell voltage showed a slight recovery during the early stages of the discharge and a slight decline towards the end of the discharge. The cell temperature showed a sharp rise during the three minute burst and declined to almost the original level during the 27 minute open circuit stand. The cell delivered 16 bursts at a voltage above 2.5 volt, corresponding to a capacity of 5.2 Ahr. The cell temperature during the burst periods rose to a maximum of 30°C which is well within the safe limits of temperature excursion.

A second D cell of similar construction was tested under the modified duty cycle using 8A and the cell was thermally insulated using glass filter paper. The test results are shown in Figure 17. Note that the cell temperature rose to a maximum of 40°C towards the end of the discharge during the three minute 8A bursts. The cell delivered 12 bursts corresponding to a capacity of 4.8 Ahr.

Another D cell of the same design was tested on the modified duty cycle using 6.5A bursts at -30°C. The results are shown in Figure 18. Although the cell delivered 11 bursts, the cell voltage remained around and most of the time below 2.0 volt during most of the bursts. A serious voltage delay problem was observed in the initial stage of the test.

One D cell with a 20 inch long cathode having both a horizontal and a vertical tab (design #4) was tested on the modified duty cycle using 6.5A bursts at room temperature. This cell was also thermally insulated with glass filter paper separator. The results are shown in Figure 19. The cell delivered 10 bursts corresponding to a cell capacity of only 3.25 Ahr. This low cell capacity is most likely due to the lower effective cathode area because of the presence of the horizontal tab.

One D cell with a 25 inch long cathode having one tab at one end (design #6) was tested on the modified duty cycle using an 8A pulse at 25°C. The results are shown in Figure 20. The cell showed unusually high polarization as well as a sharp rise in the cell temperature during the 3 minute bursts. The cell temperature reached a maximum of 55°C during the last burst. The cell only delivered 4 bursts above 2.0 volt. This poor performance may be attributed to the non-uniform current density distribution as a result of the poor current collection.

Two D cells with the 25 inch long cathode having both a horizontal and a vertical tab (design #7) were tested on the modified duty cycle using 6.5A bursts at room temperature. The results from these two cells are shown in Figure 21 and 22 respectively. The cells delivered 10 and 12 bursts corresponding to capacities of 3.25 and 3.9 Ahr, respectively. The maximum cell temperature remained below 40°C.

Another D cell of the same design was tested using 8A bursts at 25°C. The results are shown in Figure 23. The cell delivered only 7 bursts corresponding to a capacity of only 2.8 Ahr. Although the use of the horizontal tab did lead to some improvement over the single vertical tab design, the improvement was slight due to the decrease in the active cathode area caused by the horizontal tab.

Several D cells were made with 25 inch long cathodes having three tabs as in design #8. One cell was tested at room temperature on the modified duty cycle using 6.5A. The results are shown in Figure 24. The average cell voltage on load remained only slightly below 3 volts and was found to be rather stable. The cell temperature rose to a maximum of only 36°C during the 6.5A burst. The cell delivered 16 bursts above 2.5 volt, corresponding to a cell capacity of 5.2 Ahr.

Two D cells of the same design were tested at -30°C on the modified duty cycle using 6.5A current. The results are shown in Figure 25 and 26, respectively. Note, that the average cell voltage on load was above 2.0 volt. The two cells delivered 10 and 8 bursts, corresponding to the cell capacities of 3.25 and 2.6 Ahr, respectively. The performance of these cells was

somewhat better than the cells of design #2 at -30°C.

Another D cell of the same design was tested at room temperature on a modified duty cycle using 8.75A. The results are shown in Figure 27. The cell delivered 11 bursts and went into reversal during the 12th burst. The capacity delivered was 4.8 Ahr.

A new cathode current collector design (#9) was also evaluated by making two D cells with 25 inch cathodes having two vertical tabs located equidistant from the cathode ends and the middle (see Figure 28). One cell was tested on the modified duty cycle using 6.5A and the other one was tested using 8A at 25°C. The results are shown in Figure 28 and 29, respectively. The two cells delivered 16 bursts (at 6.5A) and 12 bursts (at 8A), corresponding to cell capacities of 5.2 and 4.8 Ahr, respectively. This represents a significant improvement over the cells of design #2, #4, #6 and #7. Also, its performance is comparable to that of the cell design #8.

All the above results are summarized in Table 2 for comparison.

### ii. Old GLLD Duty Cycle

The old GLLD duty cycle is schematically shown in Figure 1. The design and construction of a piece of test equipment capable of testing 8 batteries simultaneously on the GLLD Laser Designator duty cycle has been completed. This test equipment was designed to draw constant currents of 17.5A and 1.8A for the old duty cycle for the desired time intervals from the battery down to a voltage of approximately 0.8 volt at which point the test is automatically terminated thus preventing any force-discharge on the cells. Since the GLLD battery will contain two D cells in parallel, we carried out the initial test using two D cells in parallel instead of using the full 16 cell battery.

D cells made with cathodes of design #2 were tested at 25°C using the old duty cycle. The results are shown in Figure 30. The cell voltages on both the 17.5A and 1.8A loads are shown as a function of number of

bursts. The two D cells delivered 9 bursts above 2.0 volts delivering 2.9 Ahr/cell in capacity. On the 10th burst, the cell voltage on 17.5A dipped to 1.0 volt at which point the cell temperature rose sharply to 50°C. The test results of a second pair of D cells of the same design are shown in Figure 31. In this case, the cells delivered 12 bursts corresponding to 3.9Ahr/cell. These results are approximately similar to the previous test results on the modified duty cycle (see Table 2).

Two cells made with design #8 were tested at room temperature on the old duty cycle. The results are shown in Figure 32. The voltages on the first two bursts were not obtained because of recorder malfunction. Note that the cell voltage on 17.5A was substantially above 2.5 volt and that the voltage remained quite stable during the 3 minute bursts. The two cells (in parallel) delivered 17 bursts corresponding to a total capacity of 11 Ahr or 5.5 Ahr/cell. This is approximately the same as the results obtained using the modified duty cycle.

The above tests were repeated with another pair of D cells of the same design. The results are shown in Figure 33. In this test, the individual cells were covered with a heat shrinkable plastic jacket. The cell wall temperature was monitored during the test and it rose to a maximum of 40°C toward the end of the test. The cell delivered 18 bursts above 2.0 volt corresponding to a capacity of approximately 5.8 Ahr/cell. This is approximately 50% of the total available cell capacity of 12 Ahr. These results are summarized in Table 3 and are extremely encouraging particularly in view of the fact that the presently used Ni/Cd batteries deliver only 3 bursts per charge.

### c. Conclusions

The rate capability of the Li/SOCl<sub>2</sub> D cells was increased substantially by improving the cathode design. The cells with the improved cathodes (design #2) were used to fabricate a BA5590 manpack radio battery containing 8 cells in series. The battery had a service life of 100 hrs delivering 11 Ahr at room temperature. This represents a 20% increase in service life with an associated weight reduction of 11% relative to the presently used BA5590 batteries which use 10 Li/SO<sub>2</sub> D cells.

The GLLD Laser Designator battery can accommodate 16 D cells which will be connected 8 in series and two in parallel. Li/SOCl<sub>2</sub> D cells of various cathode designs were tested on a prorated basis using single cells and two cells in parallel. Designs #8 and #9 appeared to be most promising. The results showed that these batteries are capable of providing at least six times longer service life than do the currently used Ni/Cd batteries. The temperature of a single cell remained below 40°C during these tests.

#### C. Evaluation of Cathode Additive

Since the cathode configuration of the spirally wound D cell has already been optimized for high rate applications, our efforts were shifted to the study of the effects of cathode additives (catalytic and/or conductive) on the performance and abuse resistance of these Li/SOCl<sub>2</sub> D cells. We selected six catalytic additives after a preliminary screening for compatibility with cell components.

##### a. Experimental

Spirally wound D cells with cathodes of design #8 were used as the test vehicle in this work. Additive 1 was evaluated at two concentration levels and additive 2 was examined at three levels while the remaining additives were studied at one level. A pair of D-cells in parallel was tested on the GLLD load using either the old or the new duty cycle as specified earlier. Cell voltage on load and temperature was recorded during each test. All tests were conducted at 25°C.

##### b. Results and Discussion

###### i. Additive 1 (Ni)

Two pairs of spirally wound D cells with additive 1 at level A were tested on the old GLLD duty cycle. In the first pair of cells (Figure 33a) the load voltage for the first 17.5A pulse was 2.6V, with an increase to 2.9V through the 3 minute pulse regime. The 1.8A pulse voltage began at 3.1V and increased to 3.3V. For the remainder of the test the voltage at 17.5A was quite steady in the range 2.70-2.90V. The two cells delivered 19 bursts,

corresponding to 6.1 Ahr/cell. These two cells polarized during the 20th burst, with voltage on both pulse loads dropping, precipitously. The second pair of cells using additive 1 at level B delivered 21 bursts (6.8 Ahr/cell), and polarized during the 22nd duty cycle as shown in Figure 34. One of these pairs of D cells was then driven into reversal at 1A for 19 hours. During this reversal some cell heating was observed as the cells entered reversal, but no venting or other misbehavior occurred as the cells cooled to room temperature during the reversal.

Two more pairs of D cells with additive 1 level B were also examined on the GLLD duty cycle. The first pair initially had a very low 17.5A load voltage of 0.25 volt which rose to 2.5 volt during the first three minute burst as shown in Figure 35. This pair of cells gave a pulse voltage above 2.5V for 17 bursts (5.5 Ahr/cell) and polarized badly during the 19th cycle. This pair of cells was then driven into reversal at 1A for 21 hours. The temperature of the cell rose to 54°C as the cell entered voltage reversal, then declined to near room temperature at the end of the discharge. The second pair of cells delivered 14 bursts (4.5 Ahr/cell) and became badly polarized during the 15th burst as shown in Figure 36.

### ii. Additive 2 (Cu)

Two pairs of cells with additive 2 at level A were tested on the GLLD test cycle. One pair delivered 7 bursts above 2.5V, 16 bursts above 2.0V and did not polarize until the 21st burst as shown in Figure 37. The pair of cells then ran smoothly in reversal for 19.5 hours. The second pair of cells had load voltage rise from 1.1V to 2.45 in the first burst as shown in Figure 38. This pair of cells never had a voltage above 2.5V at 17.5A but delivered 19 bursts above 2.0V and polarized during the 24th pulse. This pair of cells was driven 8 hours into reversal at 1A without incident. Maximum measured cell wall temperature was 43°C.

The performance of a pair of D cells with cathode additive "2" at level B is shown in Figure 39. The cell capacity of 17 bursts or 5.6 Ahr/cell is very similar to that for a cell without additive and the additive appears ineffective at this level.

We tested two further pairs of cells with cathode additive 2 at level C. These cells were tested on the new GLLD test cycle. The results are shown in Figures 40 and 41, respectively. The cell capacity was found to be approximately between 7.4-7.6 Ahr/cell . (22 bursts under the old GLLD test cycle). This is about 25% better than the standard cell. The load voltages at high current were also near 2.5-2.6V, which is higher than observed earlier with additive 2 at level A (see Figures 37 and 38). For cathode additive 2 at level C, the additive gave increased cell capacity without a penalty in discharge voltage and thus seems most satisfactory.

iii. Additive 3 (Cr)

Two pairs of cells fabricated with cathode additive 3 were tested on the old GLLD duty cycle. In one case the initial load voltage was 2.5V, rising to 2.85V during the burst. The cell pair delivered 17 bursts (5.5 Ahr/cell) over 2.5V and was polarized to below 2V during the 19th burst as shown in Figure 42. This cell pair was then driven into reversal for 21 hours at 2A. The cell wall temperature rose as the cells entered reversal as shown schematically in Figure 43, but later cooled during the reversal with no venting or other misbehavior. The second pair of cells with additive 3 gave an initial load voltage of 1.20V rising to 2.75V during the burst. This pair delivered 19 bursts corresponding to 6.1 Ahr/cell. These cells were polarized during the 20th burst as shown in Figure 44. These cells were also driven into reversal at 2A for 21 hr. with no misbehavior.

iv. Additive 4 (Co)

One pair of D cells using cathode additive 4 was tested on the old GLLD test. The voltage on the initial 17.5A pulse was 0.6, rising to 2.1V in the first burst. The cell polarized during the 21st burst, but load voltage never reached 2.5V and was below 2V after the 12th pulse, as shown in Figure 45.

v. Additive 5 (Mn)

One pair of cells using cathode additive 5 was discharged. The initial pulse voltage of 2.60V rose to 2.85V through the first burst. This cell delivered 16 bursts with a load voltage above 2.5V (which corresponds to

5.2 Ahr/cell) as shown in Figure 46 before polarizing very quickly in the 17th pulse.

The above results are further summarized in Table 4 for easy comparison.

#### c. Conclusions

It is apparent based on Table 4 that catalytic additive 1 at level A and 2 at level C both improved the performance of the cells, for example, these cells delivered 20-23 bursts on the old GLLD duty cycle compared to 17-18 bursts realized from cells without any catalytic additive. In view of the fact that the cathodes were unoptimized both with respect to the amount of additive and the manner of impregnation, the 22% increase in performance was rather significant. The abuse resistance of the cells on force discharge was also significantly improved. Although we did not measure the internal pressure of the cells during the test and the abuse, the fact that the low pressure (130 PSI) vents of these cells remained unopened during both the test and the abuse of the cells, indicate that there was no pressure build-up problem. Therefore, we believe that the approach involving use of catalytic materials in the cathode to improve performance and safety is efficacious. For the GLLD application, cathode additive 2 at level C seemed to be the best choice so far.

#### D. Effect of Electrolyte Concentration

The 1.8M LiAlCl<sub>4</sub> electrolyte used in the hermetically sealed spirally wound D cell may not be the optimal concentration to use for high rate applications. Since 1.8M LiAlCl<sub>4</sub> in SOCl<sub>2</sub> is very near the electrical conductivity maximum for LiAlCl<sub>4</sub> in SOCl<sub>2</sub>, partial discharge of the cell would increase the LiAlCl<sub>4</sub> content which leads to a reduction in electrolyte conductivity and, perhaps, even premature cathode passivation due to LiAlCl<sub>4</sub> precipitation. Therefore, the effect of electrolyte concentration on the cell performance under the old GLLD load was briefly investigated.

a. Experimental

The effect of electrolyte concentration was evaluated using spirally wound D cells of cathode design #8 as illustrated in Figure 9. A pair of such cells were connected in parallel and then tested on the old GLLD duty cycle. We chose 1.4M LiAlCl<sub>4</sub>-SOCl<sub>2</sub> to study because electrical conductivity changes relatively slowly with concentration in the high concentration region.

b. Results and Discussion

The performance characteristics of two pairs of D cells filled with 1.4M LiAlCl<sub>4</sub>-SOCl<sub>2</sub> electrolyte on the old GLLD duty cycle are shown in Figures 47 and 48, respectively. Both cell pairs delivered only 12 bursts, or 4 Ahr/cell compared to 18 bursts of 6 Ahr/cell for an identical cell filled with 1.8M LiAlCl<sub>4</sub> electrolyte. The 1.4M LiAlCl<sub>4</sub> cells also showed a voltage penalty, with a load voltage of less than 2.5V at 17.5A compared to 2.75-2.85V for cells with 1.8M LiAlCl<sub>4</sub>. This 10% voltage penalty coupled with a 30% capacity loss indicates there is little benefit to be gained from a reduction in LiAlCl<sub>4</sub> concentration for the GLLD Laser Designator battery.

c. Conclusion

The use of more dilute concentration of electrolyte than the presently used 1.8M LiAlCl<sub>4</sub>-SOCl<sub>2</sub> did not improve the cell performance on the GLLD test. Instead, a 10% penalty in load voltage and a 30% loss in capacity have been observed. Therefore, we decided to stay with the 1.8M LiAlCl<sub>4</sub>-SOCl<sub>2</sub> electrolyte throughout the remainder of this program.

E. Effect of Electrode Length and Cathode Pretreatment

We suspected that cathode passivation was the limiting factor in D cell performance on the GLLD test and examined the effect of greatly increasing electrode area within the D cell. This, of course, will increase the resistive loss in the cathode because of the greater length but it will also increase the amount of cathode material while decreasing the current density at the cathode.

A cathode pretreatment process has been developed to enable us to place longer cathodes (than 25") into a D cell. The effect of this cathode pretreatment process was examined experimentally.

a. Experimental

Spirally wound D cells with 25" long pretreated cathodes were made using current collector design #8. A pair of cells in parallel was tested on the old GLLD duty cycle to provide baseline data. Several D cells were made with 25" and 40" long pretreated cathodes using a new current collector configuration (design #10) shown in Figure 49. These cells were parallel connected in pairs and tested on the new GLLD load at 25°C. In some cases, the cell pairs were driven into voltage reversal at constant current to determine their abuse resistance. In addition, the polarization curve of a single cell was also obtained.

b. Results and Discussion

A pair of D cells with 25" pretreated cathodes was tested on the old GLLD load at 25°C. The performance characteristics of this cell pair are shown in Figure 50. This cell pair delivered 19 bursts on the old GLLD duty cycle corresponding to 6.2 Ahr/cell in capacity which is very similar to that of a cell with the same length of cathode without the pretreatment step. The load voltage at 17.5A was ~ 2.7 volt which is also near that of a standard cell. This cathode pretreatment process incorporated in the fabrication procedures did not appear to affect the performance of these D cells on the GLLD load.

A pair of D cells with 35" pretreated cathode of design #10 (Figure 49) was tested on the new GLLD duty cycle and the results are shown in Figure 51. The cells delivered 230 pulses, corresponding to 8.2 Ahr/cell in capacity which is about 1/3 more than that of the standard cell (~ 6 Ahr/cell). The load voltage at 20A stayed above 2.5 volt for more than 90% of the entire test period. This pair of cells was driven into voltage reversal at 2A with one cell venting quietly 16 hours into reversal at a cell voltage near -1.0V and a cell wall temperature of 45°C (Figure 52).

A second pair of D cells of identical electrode configuration was also tested on the new GLLD load. This cell pair also delivered 230 pulses with each cell contributing 8.2 Ahr in capacity with the load voltage at 20A above 2.5 volt for nearly all the 230 cycles as shown in Figure 53. This pair was first resistively discharged to 0V and then driven into voltage reversal at 2A. Cell wall temperature rose first to 42°C and then dropped back and stayed at ~25°C for about 60 hours (well beyond Li exhaustion) without venting.

Additionally, the polarization curve of a single D cell was also obtained as shown in Figure 54. The high rate capability of this type of cell was fully demonstrated by a cell voltage of 3.0 volt at 5A.

To test the practical limits of electrode length in a conventional spirally wound D cell, we prepared some cells using the cathode pretreatment and 40" electrodes. These cells were also filled with 1.8M LiAlCl<sub>4</sub> electrolyte and examined on the new GLLD test. The performance of these cells, shown in Figure 55 and 56, was somewhat disappointing. The cell pairs delivered 220 and 243 bursts, corresponding to capacities of 7.8 Ahr/cell and 8.7 Ahr/cell, respectively. The load voltage at 20A was found to be 2.70-2.75, but there was no significant increase in cell capacity. One problem with the use of such extremely long electrode stacks is that the portion of the cell volume occupied by the separator increases very substantially. For example, with 40" electrodes and .005" separators, about 34% of the available electrode volume is taken up by separator. This, combined with our test results on the 35 and 40 inch cathodes suggests that 35 inch cathodes are near the optimum for a spirally wound high rate D cell.

### c. Conclusions

The cathode pretreatment process developed in our laboratory made it possible to use longer electrodes in a spirally wound D cell. We evaluated the effect of 35 and 40 inch electrodes and found that a substantial capacity increase (from ~ 6.0 Ahr/cell with a 25" electrode design to ~ 8.5 Ahr/cell with 35-40" cathodes) could be obtained without any penalty in load voltage. However, the 35 inch design appears to be the optimal one for high rate D cells.

F. Design and Performance of Optimized High Rate D Cells

It has been established that a Li/SOCl<sub>2</sub> D cell made with cathodes of design #2 (20" cathode with tab in the middle) capable of delivering 10 Ahr on the BA5590 test cycle. However, a D cell of identical design only gives ~ 5.0 Ahr on the GLLD test cycle. A D cell made with 25" cathode with three tabs (design #8) can deliver ~ 6.0 Ahr on the GLLD load with the proper level and type of catalytic cathode additive present. The same cell will deliver up to 7.6 Ahr on the GLLD test cycle. The use of cathode pretreatment and extremely long electrode enables a D cell to provide ~ 8.5 Ahr on the GLLD test. However, the performance of such a cell on the BA5590 load is reduced due to the presence of glass fiber separator material. The above facts led to the conclusion that the optimal high rate D cells suitable for both BA5590 man pack radio and GLLD Laser Designator applications most probably should be made with 26-28" long cathodes. This length would also allow a substantial excess of lithium capacity for improved abuse resistance during voltage reversal.

a. Experimental

The improved electrode configurations for the optimized high rate D cell were evaluated in D cells of standard hermetic construction. These cells incorporate a hermetic G/M seal feedthrough and G/M seal low pressure vent which is hermetic until opened on short circuit or other abusive treatment. The electrode stack, consisting of catalytic carbon cathode, lithium foil anode and glass fiber separator paper is wound about a mandrel and inserted into the can. The anode tab is welded to the centerpost in the G/M feedthrough while the cathode tabs are welded to the can during welding of cell top to can. The cells are filled using a special piece of apparatus which allows us to evacuate the welded cell through the fill port and then add electrolyte to the evacuated cell. The fill tube is then closed, first by crimping, then by resistance welding to create a hermetic cell. D cells with both 26" and 28" cathodes were made and evaluated in this work.

We tested the D cells on the specified BA5590 and GLLD loads using a mechanical timer and relay for the BA5590 test and a specially built

microprocessor controlled pulse discharger for the GLLD test. We also discharged cells at three current levels: 0.3A, 1A and 3A using conventional DC power supplies and load resistors to assure constant current behavior throughout the test. The short circuit current was measured through a shunt. The effect of abusive storage at 72°C was also studied. Cell discharges at -30°C were done in a Blue-M Versa-Range test chamber after the cells were allowed to equilibrate at -30°C, usually overnight. Cell wall temperatures were measured by attaching an OMEGA iron-constantan thermocouple to the side of the cell with tape. Data were recorded on a variety of conventional stripchart recorders as well as Linseis LD-12 12-channel recorder and Gould 220 high speed recorders.

b. Results and Discussion

We first developed a new D cell design using the cathode pretreatment process with a 28" cathode. These cells were first tested on BA5590 load. The performance of two typical cells of this design is shown in Figures 57 and 58. The cell life was found to be 120-130 hours which is superior to that of the earlier cell type (Figure 13) by some 25-30%. The operating voltage on the 1  $\Omega$  load was also increased from near 2.8 to above 3.0V for most of the cells life. A typical cell of this design was found to deliver  $\sim$  12.5Ahr on the BA5590 test.

With this improvement in performance we evaluated these cells for constant current performance at moderate rates, as a quick check of cell capacity and abuse resistance. Two cells were discharged at 1A, as shown in Figures 59 and 60. The cell capacity of 11.5 Ahr was somewhat less than the 11.8 Ahr delivered by a cell with 20" electrodes as shown in Figure 61. The cathode pretreatment process was suspected as the cause of the reduction in cell capacity at 1A constant current discharge. This was confirmed when a cell with 20" pretreated cathode gave only 8.6 Ahr at 1A as shown in Figure 62. This is contrary to what we observed when we put cells with pretreated cathodes on the GLLD test as described in the previous section.

While the 1A capacity of 11 Ahr was still reasonably good, we

decided to modify the cathode pretreatment process, reducing the cathode length to 26", giving a cell which will give good performance on BA5590, GLLD and constant current discharges. On the BA5590 test this type of D cell ran for 103 hours as shown in Figure 63, giving a capacity of some 11 Ahr. The same cell type was tested on the GLLD test, where it delivered over 220 bursts, or 7.7 Ahr/cell as shown in Figure 64.

This optimized cell design was selected for the D cells for delivery to the sponsor at the end of the present contract. Accordingly, we further characterized the performance and the abuse resistance of this cell in some detail. The polarization characteristics of this optimized D cell at 25°C are shown in Figure 65. Note that the cell voltage remains above 3.0 volt up to a discharge current of 7.0A. The cells were discharged at currents of 0.3, 1.0, 3.0 and 10A at 25°C. In addition to cell voltage, the wall temperature was also monitored during the test. The results are shown in Figure 66 through 69. At 0.3A the cell delivered approximately 10.8 Ahr to 3.0 volt cutoff. The operating cell voltage was 3.5 volt during most of the discharge. The cell wall temperature remained below 24°C during the entire discharge. At 1.0A, the cell delivered 9.4 Ahr (Figure 67), the cell operating voltage remained above 3.25 volt during most of the discharge. At 3.0A, (Figure 68) the cell delivered approximately 9.2 Ahr. The cell operating voltage was 3.2 volt during most of the discharge. The cell wall temperature increased during the test up to 37°C. At 10A (Figure 69) the cell ran for 28 minutes, delivering a capacity of approximately 4.8 Ahr prior to a mild venting. The cell operating voltage was approximately 2.7 volt, while cell wall temperature increased substantially during the test, reaching 95°C towards the end of the test. The cell did not exhibit any unsafe behavior during the test. Li/SOCl<sub>2</sub> D cells of earlier designs (7) exploded on 10A test.

We determined the abuse resistance of the above cells by driving them into reversal at 25°C at constant currents of 0.3, 1.0 and 3.0A. We monitored both the cell voltage and the wall temperature of the cells during this abuse test. Voltage and the temperature profiles of the D cell on 0.3A reversal at 25°C is shown in Figure 70. The cell voltage stabilized near zero after the initial drop on 0.3A reversal, and remained at near zero volts all throughout the 35 hr duration of the reversal. The cell wall temperature increased

only slightly at the beginning of the reversal but remained below 30°C. There was no cell venting or explosion, in contrast to the D cells of earlier designs (7). The above cell was discharged to 10.8 Ahr before being reversed for 10.5 Ahr worth of capacity, to a total capacity of 21.3 Ahr which was well over the stoichiometric lithium capacity of 18 Ahr.

The voltage and the temperature profile of another cell of similar construction but with cathode additive 2 on 1.0A reversal at 25°C is shown in Figure 71. Note that the cell wall temperature increased initially to 45°C but then declined to 25°C and remained there for the duration of the reversal. The cell voltage remained locked at virtually zero volt all throughout the reversal lasting for 18 hrs. This is a typical demonstration of the "voltage clamp" mechanism that makes these cells safe on reversal. There was no cell venting or explosion.

The voltage and the wall temperature profile of another D cell on 3.0A reversal at 25°C are shown in Figure 72. The cell temperature increased sharply at the start of the reversal to approximately 100°C and then declined to 28°C on continued reversal. The cell voltage clamped at -0.3 volt during the reversal which was continued for 3.3 hours. The cell exhibited only mild venting. There was no cell bulging or explosion. The operation of the "voltage clamp" to achieve safety on reversal was further demonstrated by this experiment.

The performance and the abuse resistance of the standard high rate D cell is now reasonably well defined at room temperature. We then examined the performance of these cells at -30°C to determine the performance penalty associated with low temperature discharge.

A polarization curve for a standard D cell at -30°C is shown in Figure 73. The drop in voltage at a given load is far more pronounced than that at 25°C (Figure 65) even at low current drains. An optimized high rate D cell was discharged at -30°C on 0.3A load. The cells delivered 7 Ahr to a 2V cutoff with only a very moderate rise in temperature as shown in Figure 74. This represents approximately 65% of the capacity available at room temperature. An optimized high rate D cell with cathode additive 2 was discharged at 1A at -30°C. This cell gave 5.15 Ahr as shown in Figure 75 with a greater increase in cell temperature.

This corresponds to 55% of the capacity delivered at room temperature. As a final high rate test at -30°C, we discharged an optimized high rate D cell at -30°C on 3A load shown in Figure 76. The temperature rise during discharge was somewhat greater than noted at the low currents while the capacity of 4.8 Ahr was quite comparable to the 1A capacity and 52% of the room temperature capacity. Beside the capacity loss at -30°C, there is a power loss as well due to the lower voltage plateaus as shown in Table 5.

These cells discharged at -30°C were also driven in voltage reversal at constant currents of 0.3 and 3A. There was no venting or other mis-behavior after 23 hours of reversal at 0.3A at -30°C. Again, the cell voltage remained at zero volt showing the excellent voltage clamping characteristics. The standard D cell with cathode additive 2 was driven into reversal at 1A for 13 hours at -30°C as shown in Figure 77. There is some cell heating as the cell enters reversal, but not enough to raise cell temperature above 0°C. There was no venting during this test. Again the cell voltage clamped at zero volt with concurrent lowering of cell temperature on prolonged reversal. The final voltage reversal test was of an optimized high rate D cell in 3A reversal at -30°C. The temperature (measured at the cell wall) and voltage are shown in Figure 78. There was a very large rise in temperature as the cell entered reversal, followed by a return of cell voltage to small positive voltages. This cell behavior may be due to thermal decomposition of the intermediate species generated by the reduction of  $\text{SOCl}_2$ , giving a reversal of the cathode passivation. Thereafter the cell voltage declined and clamped at -0.3 volt as before without any cell explosion. There was evidence of mild cell venting.

Additionally, we shorted a standard D cell with additive 2 in the cathode through a shunt and monitored the cell voltage, the short circuit current and the wall temperature of the cell. The results are shown in Figure 79. Note that the cell delivered a short circuit current of 200A at a cell operating voltage of 1.0 volt. Both the current and the voltage remained at a high level for 0.68 sec when the cell vented. There was no rupture of the cell. The cell wall temperature remained unchanged because the duration of the shorting was so brief.

We investigated the performance of this optimized high rate D cell after storage. We stored a D cell at 72°C for two weeks, followed by

one week at room temperature, then tested it on the BA5590 duty cycle as shown in Figure 80. The cell delivered 110 hours of service to a 2.5V cutoff, a capacity of over 12 Ahr. The well known voltage delay phenomenon was observed only on the 1  $\Omega$  load, and even at 1  $\Omega$ , load voltage is over 3V after  $\sim$  2 hours. The load voltage is always over 2.5V and thus there should be little or no start-up problem. This test also showed very good capacity retention for the cells on the BA5590 loads after high temperature storage. A second D cell was stored at 72°C for two weeks and discharged on the BA5590 load test at -30°C after 6 weeks at room temperature, as shown in Figure 81. This cell delivered 8.8 Ahr to 2.0V, or over 70% of the fresh cell capacity on the same test at room temperature, once more demonstrating the good capacity retention of this design.

We stored a pair of D cells at 72°C for two weeks and then tested the cells on the GLLD duty cycle at room temperature as shown in Figure 82. The capacity realized on this high rate test was 6.8 Ahr/cell to a 2.5V cutoff, over 90% of the fresh cell capacity. Some voltage delay was observed early in the test, but a load voltage of 2.0V at 20A was reached in 12 minutes and 2.5V in 2-1/2 hours. The capacity at 20A above 2.0V was higher, 8.6 Ahr/cell, which is very comparable to capacities above 2.0V at 20A for unstored cells, showing once more the very good capacity retention of the high rate D cell on abusive storage.

We stored a further pair of D cells at 72°C for two weeks, followed by six weeks at room temperature. These cells were then equilibrated at -30°C and discharged on the GLLD duty cycle at -30°C as shown in Figure 83. The cell capacity on the GLLD test was very low, with the 20A load voltage never reaching 2.5V and the capacity above 2.0V only 1.8 Ahr. At lower currents and voltages the cells showed higher capacity. There was also some delay in the cells reaching their running voltage at 20A, although there was much less delay at 3.2A.

Finally, we assembled 16 high rate D cells into two parallel, 8 series connected cell stacks after storage at room temperature for approximately nine months. These cells were tested as a GLLD battery on the new GLLD load. The battery delivered 180 pulses at above 20 volt equivalent to 12.8 Ahr in total

capacity output. The temperature of the cells remained at around 30-35°C. Towards the end of the discharge, the test equipment malfunctioned leading to multiple pulsing without the 3 minute rest intervals. This caused a sharp increase in temperature to 50°C as shown in Figure 83a. An initial voltage delay was observed. The load voltage at 20A went above 20 volt after 1 hour on the new GLLD test cycle. These results indicate that these high rate D cells are capable of retaining their capacity and rate capability even after storage over extended periods of time after filling.

c. Conclusions

We have refined our several high rate D cell designs to produce a cell with good performance on both GLLD and BA5590 tests, while maintaining abuse resistant design features. We verified the good performance of this cell on both GLLD and BA5590 tests and selected this design as a new standard high rate D cell design with significant performance advantage over previous Li/SCCl<sub>2</sub> D cells.

This high rate D cell design has been characterized further by determining its capacity at currents ranging from 0.3A up to 10A at 25°C and -30°C. The cells showed excellent abuse resistance on voltage reversal. There were no cell explosions on either shorting or reversal. The cells vented on short circuiting and on prolonged reversal, the cells exhibited "voltage clamping" and the concurrent safe behavior. The good capacity retention properties after abusive storage at 72°C on both BA5590 and GLLD test loads were also experimentally demonstrated.

G. Conclusions

The use of spirally wound Li/SOCl<sub>2</sub> D cells for the BA5590 Battery Man Pack Radio and the GLLD Laser Designator Battery applications is attractive because similar manufacturing technology has been well developed for the Li/SO<sub>2</sub> D cells. We have successfully developed such a high rate D cell with an optimal design which is suitable for both BA5590 and GLLD applications.

This new design was reached through careful and systematical studies of the effects of cathode current collector configuration, electrolyte

concentration, electrode length, cathode additive, and cathode pretreatment process. Finally, a spirally wound D cell with 26" electrode was proven to be the optimal design for both high rate applications (i.e. BA5590 and GLLD laser designator) considered in this work. The cathodes were pretreated and a three tab design was adopted in this final version of D cells to minimize electrical resistance of the cathode. The cells were filled with the conventional 1.8M LiAlCl<sub>4</sub>·SOCl<sub>2</sub> electrolyte system.

At 25°C, a typical fresh D cell can deliver 11 and 7.7 Ahr/cell on BA5590 and GLLD tests, respectively. The constant current discharge characteristics were also obtained at current levels ranging from 0.3 up to 10A at 25 and -30°C. At 1A the cell capacities were found to be 9.4 and 5.5 Ahr at 25 and -30°C, respectively. After abusive storage at 72°C for two weeks, the cells were found to have good capacity retention properties on both BA5590 and GLLD loads at 25°C. Furthermore, a sixteen cell GLLD battery can safely deliver 12.8 Ahr in capacity after a nine month storage period. Excellent retention of both capacity and rate capability in the D cell configuration has once again been demonstrated.

The short circuit current of this optimized D cell was found to be about 200A. Upon accidental shorting and during deep voltage reversal, the cell usually vents quietly through its G/M seal without any incident.

One hundred Li/SOCl<sub>2</sub> D cells of this optimized high rate design have been fabricated and delivered.

### III. Development of the 1.8 Inch Diameter Cylindrical Cell

We chose to develop the 1.8 inch diameter cylindrical cell for the GILD Laser Designator Battery to reduce the number of cells required from 16 to 8. The construction of this cell uses the technology already developed for the spirally wound D cell, including wound electrode geometry, low pressure glass-to-metal seal hermetic vent, glass-to-metal seal feedthrough and fill port in the cell top. The details of the development are presented here.

#### A. Experimental

Cell Can: The stainless steel cans with dimensions of:

O.D.: 1.812"  $\pm$  0.010"  
Ht.: 2.609"  $\pm$  0.015"  
Wall: 0.031"  $\pm$  0.003"

Cell Top: The cell top is made of Kovar and has the following dimensions:

O.D.: 1.750"  $\pm$  0.010"  
Ht.: 0.188"  $\pm$  0.010"

G/M Seal: The glass-to-metal seal with the hermetic feedthrough for the center post was fabricated using the seal technology developed for the Li/SOCl<sub>2</sub> D cell.

Vent: The cell top has a G/M seal vent similar to that developed for the D cell. A schematic diagram of the completed cell top with electrolyte fill port, vent and G/M seal feedthrough is shown in Figure 84.

Welding Fixture: The necessary heat sinking fixtured for TIG welding the cell top and can were designed and built. The welding step was perfected using empty cans. No unusual difficulties were encountered in this operation. The efficiency of the heat sinking was determined by checking the temperature of the can wall after welding. The temperature was found to remain within safe limits.

**Cell Construction:** Cells were made by winding two layers of 2" x 20" cathodes and two layers of 2" x 21" anodes arranged alternately and separated by layers of glass filter paper. The cathodes each have two tabs located 5" from the ends while the anodes have two tabs located at the ends. Thus, both anode and cathode have four tabs each for current collection.

The cells were filled with about 90 grams of 1.8M LiAlCl<sub>4</sub> in SOCl<sub>2</sub> through the fill port, which was then closed. A photograph of the finished cell is shown in Figure 85.

B. Results and Discussion

One cell was tested at room temperature on the old GLLD test cycle of alternating 17.5A and 1.8A pulses. The results are shown in Figure 86. The cell delivered 19 bursts above 2.0V which corresponds to a capacity of 12.5 Ahr. Another cell was tested on the new GLLD test cycle with the results shown in Figure 87. The cell delivered 179 bursts to give a capacity of 12.9 Ahr.

C. Conclusion

Considering the fact that 1.8" diameter cylindrical cell has twice the internal volume of the D cell, the performance on GLLD test was inferior to that of a pair of D cells in parallel. Particularly, the voltage on the high current pulse was only around 2.0V, which is below the required cutoff voltage of 2.5V. For this reason we decided to discontinue the development of the 1.8" diameter cell and to concentrate our efforts on the development of flat cells to fulfill the GLLD Laser Designator application requirements.

#### IV. Development of the Three Inch Diameter Flat Cylindrical Cell

The safety of the Li/SOCl<sub>2</sub> cells was demonstrated (7, 11) to depend on the internal temperature of the cells. DTA studies of the cell constituents showed that Li + S exothermic reactions taking place at temperatures of approximately 150°C may be responsible for the thermal runaway of the Li/SOCl<sub>2</sub> batteries. Therefore, it is important that the internal temperatures of the cells be kept below 150°C under all conditions of use and abuse. For low rate applications the safety of the cells was successfully achieved by controlling the heat generation of the cells by lowering their intrinsic rate capability. However, for high rate applications, such as the GLLD laser designator which requires pulse currents of 20A at 24 volts involving a power drain of 480 watts, the heat generation of the cells can no longer be easily controlled. Therefore, in order to maintain the internal cell temperature below 150°C, heat dissipation of the cells must be enhanced. Cell configurations with a maximum surface area to volume ratio become more preferable. Considering only the cylindrical shape, in view of its advantage in terms of containing high internal pressures with minimal distortion, the surface to volume ratio, R is expressed as:

$$R = \frac{\text{Surface Area}}{\text{Volume}} = \frac{2\pi r^2 + 2\pi rL}{\pi r^2 L} = \frac{2}{L} + \frac{2}{r}$$

where r is the radius and the L is the length of the cylinder.

The surface/volume ratio can be increased either by decreasing the length of the cylinder while increasing the radius to maintain the internal volume, or by decreasing the radius of the cell and correspondingly increasing the length. Considering the difficulties involved in the construction of narrow cylindrical cells, we opted in favor of the former shape, viz., the flat cylindrical cell.

The high surface area to volume ratio of the flat cylindrical cell enhances the heat dissipation of the cell from its surface to the environment and as such is a better configuration from the safety standpoint. However, this is true in the case of single cells only. In the case of multicell battery, the individual cells may be potted in such a manner that they may be thermally insulated from the environment and the heat dissipation may be rather insignificant.

Therefore, reliance on heat dissipation of cells for safety is unsound. For this reason, we have attempted to achieve,

- (a) low heat generation
- (b) high internal thermal equilibration

in the design of our flat cells. In this manner, the cells will be safe when used either as single cells or as multicell batteries. The design objective is to balance the total heat generation during the high current pulses with the total thermal mass of the battery such that the internal temperature of the cells does not exceed the upper limit of the safe temperature. We determined this temperature (7) by doing DTA of the cell constituents and found that the lowest temperature of initiation of an exothermic reaction is 150°C for the Li + S combination. S is a reaction product of the cell. This exothermic reaction may initiate a thermal runaway. Therefore, the internal temperature of the cell should be kept below that. Arbitrarily, we chose an upper limit of the safe temperature of 130°C.

The electrode designs chosen for this cell consisted of stacked circular discs instead of the commonly used spirally wound electrodes. In addition, a safety vent was incorporated so that the internal pressure and temperature buildups can be relieved on accidental short circuiting or force discharge.

#### A. Study of the Effect of Cathode Current Collector Design

Since it has been demonstrated in our D cell optimization work that the impedance of the current collector is a major contributor to the cell impedance leading to non-uniform current distribution and low current carrying capability, it is apparent that an optimal current collector design must be obtained for the disc shaped cathodes used in the flat cylindrical cells specially developed for high rate applications. We designed and built a demountable flat cylindrical cell for the purpose of evaluating the effect of the current collector design on the performance of the disc shaped carbon cathodes. Such a cell enabled us to screen a variety of current collector designs swiftly.

a. Experimental

The cell made of two thick stainless steel plates which act as heat sinks to prevent any significant temperature rise in the cell which may affect the polarization measurements. The disc shaped Li anode and carbon cathode are welded on the stainless steel plates by means of tabs of various designs. The schematic view of the experimental cell is shown in Figure 88. The two plates are insulated by means of viton rubber gaskets and the sealing of the cell was accomplished by compressing the plates with polypropylene nuts and bolts. The cell contained a Li reference electrode connected to a nickel tab which is placed between the two layers of the viton rubber gaskets. The two stainless steel plates acted as cell terminals. The cell was filled with 1.8M  $\text{LiAlCl}_4\text{SOCl}_2$  electrolyte through an electrolyte fill port located in one of the plates.

The disc electrodes were 2.8 inch in diameter. The Li anode was made by punching out 2.8 inch discs of 15 mil thick Li and pressing it on the expanded Ni current collector which was welded to one of the stainless steel plates.

The carbon cathode was similar in composition and thickness (0.025 in) as used in D size cells and comprise porous carbon on expanded Ni current collector. Carbon cathodes were made by punching out 2.8 inch diameter discs from a sheet of carbon cathode. The details of the various current collector designs are shown in Figure 89. A total number of eight different designs were studied. The details of the various current collector designs are described below:

Design #1. In this design the expanded Ni grid of the carbon was welded to the stainless steel plate at four different spots as shown in Figure 89 (1). There was no separate tab for the current collection. There was no significant reduction of the active carbon area in this design, since weld areas were very small and the amount of carbon removed from the grid was negligible.

Design #2. In this design two layers of 0.20 inch wide Ni ring was welded all around the carbon cathode. The thickness of each layer of the ring was 0.01 inch. The Ni ring was then welded to the stainless steel block at four different spots as shown in Figure 89 (2), without any tab. This design leads to a reduction of the active carbon area of approximately 27%.

Design #3. This design was identical to design #2 in all respects except that the Ni ring was 0.005 inch thick.

Design #4. In this design, the cathode with the metal ring as in design #3, was welded to the stainless steel block by means of two layers of 0.25 inch wide, 0.002 inch thick Ni tab. The length of the tab was approximately 0.25 inch. The cathode was otherwise insulated from the stainless steel block by a layer of separator.

Design #5. In this design two layers of 0.25 inch wide Ni tab was connected to one edge of the cathode disc and then welded to the stainless steel block of the cell. There was virtually no loss of the active cathode area by this design. The cathode was otherwise insulated from the block by means of a layer of glass filter paper separator.

Design #6. In this design, two layers of 0.25 inch wide Ni tab were welded from the center to the edge of the cathode disc, as shown in Figure 89 (6). This tab was then welded to the stainless steel block. There was also a layer of separator between the cathode and the cell block. The reduction in active cathode area was approximately 9%.

Design #7. In this design two layers of 0.125 inch wide tab were welded across the diameter of the cathode disc as shown in Figure 89 (7). The cathode was also separated from the block as before. The reduction in active area as a result of the tab was approximately 6%.

Design #8. In this design two 0.125 inch wide tabs (two layers) were welded at 90 degrees along the diameter of the cathode disc as shown in Figure 89 (8). The two tabs were welded to the stainless steel cell block and the cathode

was separated from the block by glass filter paper separator. The reduction of the active area was approximately 12%.

The cell was made with the above cathodes and Li anode with glass filter paper separator. Only one side of the electrodes was used. Both the short circuit current and the polarization characteristics were measured. During the polarization measurements, both the cell voltage and the cathode potential against the Li reference electrode were measured. All the measurements were made at room temperature. The wall temperature of the cells were also monitored during the above measurements.

b. Results and Discussion

The polarization characteristics of circular cathodes of various current collector designs are summarized in Table 6. The difference between the cathode and the cell polarization represents the internal cell impedance which varied from 0.01 to 0.1 ohm and was affected significantly by the current collector design as well as the current level. This relatively high cell impedance stems from the relatively large space between the anode and the cathode as necessitated by the particular stainless steel block cell design. Therefore, we chose to use the cathode polarization data as measured against the Li reference electrode as the basis for the evaluation of various current collector designs.

The results of the first four designs are shown in Figure 90. Note that the polarization characteristics of the four types of cathodes are virtually identical in spite of the fact that the cathodes of designs 2, 3 and 4 has 27% less active area than the cathodes of design 1. This indicates that the detrimental effect of loosing electrode area has been successfully compensated by the beneficial effect of the improved current collection as in designs 2, 3 and 4. The results of the designs 5, 6, 7 and 8, as shown in Figure 91, also show the lack of significant differences in the polarization characteristics of the various cathode designs. Therefore, we conclude that for the 2.8 inch diameter disc cathodes, the current collector design does not have any dramatic effect on the polarization characteristics of the cathodes. Any design which is convenient to fabricate can be adopted in the flat cell design.

The short circuit currents of the experimental flat cells with the cathodes of eight different designs are shown in Table 7. The lowest short circuit was obtained with design #5 having one tab connected at one point at the edge of the disc, indicating the poor current collection of this design. The higher short circuit currents of the other designs indicate the relative compensatory effects between the mass transport and the current collection. Based on the short circuit current, the designs 6 and 7 emerge as the preferable designs for the high rate cathodes. The highest short circuit current density realized from these cathode designs was  $200\text{-}230 \text{ mA/cm}^2$ , very similar to that realized from the spirally wound D cells indicating the adequacy of the current collection.

c. Conclusions

The effect of the cathode current collector design on the polarization and the short circuit current of the flat cells did not appear to be as significant as in the case of spirally wound D cells, for eight different current collector designs investigated. Two designs both with a current collector tab located along the radius and along the diameter of the circular disc shaped carbon cathode appeared to be most attractive. The maximum short circuit current densities were  $200\text{-}230 \text{ mA/cm}^2$ , very similar to that realized in spirally wound D cells having improved cathode current collectors.

B. Design and Construction of Flat Cylindrical Cells

We have developed two types of flat cells, both are 3 inch in diameter. One is 0.45 inch thick. Sixteen of these cells, connected two in parallel and 8 in series, are required for one GLLD laser designator battery. A sketch of the battery pack with sixteen 0.45 inch flat cells is shown in Figure 2. The other flat cell is approximately 0.90 inch thick and it requires eight cells per battery as shown in Figure 3.

a. Thin Flat Cylindrical Cell (0.45")

Cell Can: The specifications of the stainless steel can which is 3 inch in diameter and 0.45 inch high are shown in Figure 92.

Cell Top: The design of the cover of the cell is shown schematically in Figure 93. The glass-to-metal seal located on the cell top consists of an outer metallic ring and a central post both of which were custom made. A graphite boat with multiple cavity was designed and fabricated to make the glass-to-metal seals. A multi-zoned quartz tube furnace was used for the firing and annealing of the glass-to-metal seals.

The glass-to-metal seal was resistance welded to the cover. The welding step was found to be quite critical in obtaining hermetic welds. The design of the metal seal body, the location and the contour of the projection on the seal body, all played an important role in accomplishing rugged hermetic welds. This process has finally been developed.

The resistance welding of the electrolyte fill tube to the cell top was found to be fairly straight forward.

Welding of Cell Top to Can: We designed and fabricated elaborate heat sinking fixtures for TIG welding the top to the can. The elaborate heat-sinking was needed to prevent excessive internal heating of the cell which may have undesirable effects on the electrode materials. The welding process was developed and perfected in this program.

The Cell: Circular donut shaped anodes, cathodes and glass filter paper separators were used to make this cell. The cross-sectional view of the cell and the electrode stack is schematically represented in Figure 94.

The current collector design chosen for the cathode was design 5 as shown in Figure 89. This had the highest short circuit current density of all the designs based on the results from the demountable cell experiments described in the previous section.

The electrical conductivity of the lithium anode was sufficiently high so that no current collector was needed. Disc shaped Li anodes were welded directly to the feed through.

The glass filter paper separators used to make the cell was found to be rather fragile. The successful assembly of the electrode stack required extensive fixturing and special handling procedures to prevent internal shorting. The cell contained eight cathodes and nine anodes. The diameter of the cathode was approximately 2.8 inch. Therefore, the total effective cathode area, using both sides, was approximately  $70 \text{ cm}^2$  per cathode with a total of  $560 \text{ cm}^2$ . This corresponds to a current density of  $31 \text{ mA/cm}^2$  on 17.5 A load. The carbon cathode was approximately 0.015 inch thick and the Li anode was 0.010 inch thick. The glass filter paper separator was nominally 0.005 inch thick. Two layers of the separators were used to prevent shorting.

The cell was evacuated through the fill port and then filled with 1.8M  $\text{LiAlCl}_4\text{-SOCl}_2$  electrolyte and the fill port was closed by welding. The electrolyte weight was approximately 44 gms. A photograph of the finished thin flat cylindrical cell is shown in Figure 95.

b. Thick Flat Cylindrical Cell (0.90 inch)

In this design, the flat cell is not only twice as thick as the previous one, but the welding lip is located halfway between the two faces of the cell. Essentially, the cell can comes in two halves of equal thickness. The volume not utilized by the active ingredients because of the welding projection is significantly less than that in the previous design. Also, the space wasted due to intercell connections is minimized by reducing the number of cells, although the thickness of the stainless steel wall of the can was increased from 0.019 inch to 0.032 inch in this design in order to make the cell more rugged and capable of withstanding high pressures without bulging or rupturing.

**Cell Can:** The flat cell can is of two piece construction, consisting of a cell top and bottom. Both parts are constructed of 0.032" stainless steel. The details of the cell top is shown in Figure 96. It incorporates a fill tube which is internally welded and a G/M seal which is joined to the top by resistance welding. The G/M seal also serves as a low pressure vent which opens upon misuse and abuse. The bottom piece of the can is a solid piece of stainless steel identical in shape to the top piece without the G/M seal.

Cathode: The flat cell cathode is made up of a carbon-PTFE blend (90 - 10%) which is pasted on an expanded metal grid, rolled to the desired thickness and cured. The cathodes are then cut to shape as shown in Figure 97 with a die.

Anode: The flat cell anode is a circular disc of 0.005" Li foil, cut to size with a die.

Electrode Stack: The electrode stack is assembled in a specially designed fixture which indexes the anode, cathode and separator with proper offset for the cathode current collector. The assembly order incorporates an expanded metal washer above and below each anode disc, as shown in Figure 98. The electrode stack is terminated by a double anode and separator at each end to give better heat transmission. The assembled electrode stack is tested for short circuits to the can. A hollow threaded bolt is inserted on the center of the stack and a nut is screwed down on the exmet washers to assure good anode contact. The finished cell stack is schematically shown in Figure 98a.

The hollow bolt is then topped with a plug of Li and pressed onto the anode center post as shown in Figure 99. The cell top and bottom are now fitted together with the ends of the cathode current collector tabs protruding. The tabs are trimmed with scissors and the cell is closed by TIG welding the rim. A photograph of a finished thick flat cylindrical cell is shown as Figure 100.

The cell is tested for internal short circuits using an ohmmeter and evacuated to 0.2 mm Hg. The cell is then filled with 1.8M  $\text{LiAlCl}_4/\text{SOCl}_2$  electrolyte using a vacuum filling technique. The cell resistance is monitored during evacuation and voltage is monitored during filling as precautionary measures. Each cell weighs approximately 225g.

C. Preliminary Performance Data on Flat Cylindrical Cells

a. Experimental

A thin flat cylindrical cell was constructed using 2.8 inch diameter

disc electrode stack consisting of eight cathodes and nine anodes. This cell was tested at 25°C under the old GLLD duty cycle as specified in Section IBb using the microprocessor controlled test equipment mentioned previously in this report. Since it was originally designed to use two parallel stacks of 8 series connected cells in an actual battery, a single cell should experience only half of the old GLLD load.

Due to the inflexibility of the test equipment, however, we tested the single cell on the full load in order to obtain some preliminary performance data.

Two thick flat cylindrical cells were also built for preliminary testing on the old GLLD test load at 25°C. One cell contained 40 cathodes and 41 anodes and the other one was packed with 35 cathodes and 36 anodes. One of the cells was driven into voltage reversal in order to obtain information on the safety feature of this new cell design.

b. Results and Discussion

1. Thin Flat Cell

The cell was tested at 25°C under the GLLD laser designator duty cycle. The cell voltage on the two loads, viz 17.5A for 35.5msec and 1.8A for 14.5 msec were monitored during the three minute duty cycle. The results are shown in Figure 101. The voltage profiles are shown for each three minute bursts and the results are plotted as a function of the number of bursts instead of as a function of time. Each burst occurs every 27 minutes.

The cell showed some voltage-delay on the first cycle. The cell polarization on 17.5A load was found to be rather severe, although the operating voltage at 17.5A remained above 2.5 volt most of the time. In order to meet the end voltage of 20 volt for the whole battery, the single cell voltage must be 2.5 volt. Considering the fact that the cell was subjected to twice the required load, the operating cell voltage was considered to be quite satisfactory. The cell delivered 8 bursts above 2.0 volt. With two cells in parallel, one may expect at least 16 bursts or possible more. With two D cells

in parallel, we realized about 17 bursts above 2.5 volt. Therefore, this flat cell did not appear to provide any significant improvement over the D cells.

## 2. Thick Flat Cell

The voltage of the cell containing 41 anodes and 40 cathodes on both the 17.5A load and on the 1.8A load (as per the duty cycle) are shown in Figure 102. Note that on increasing the load from 1.8A to 17.5A, the cell voltage drops from 3.4V to 3.35 volt, a polarization of only 50 mV. This is a major accomplishment in the design of the high rate cell. This demonstrates the efficacy of the electrode designs in terms of the current collector design and the electrode separation on the rate capability of the cells. Cells delivered 18 bursts, at which point the cell voltage on 17.5A was still above 3.0 volt. The test was terminated prematurely due to the malfunctioning of the test equipment. In spite of this, the results was very impressive. The maximum temperature of the cell was found to be less than 29°C. This low temperature rise is expected in view of the low cell polarization. The low heat generation during the high current pulse is one of our major design objectives that we have accomplished by this flat cell.

The other flat cell with 35 cathodes and 36 anodes was also tested under the old GIID laser designator duty cycle. The voltage profiles on the three minute bursts are shown in Figure 103. Exceedingly low cell polarization on high current pulse is again noted. The maximum cell temperature was again less than 29°C. The cell delivered 26 bursts (correspond to 16.9 Ahr) at which point, the cell voltage on 17.5A pulse was still 3.0 volt. The cell was automatically shut off at this stage. This represents a 44% improvement in terms of the number of bursts obtained over that obtained from optimized high rate D cells in parallel at the same cut-off voltage.

The cell was abused after the above test by force-discharging at 2A. The cell delivered another 2.2A hr to 2.0 volt. One cell reversal, the cell temperature rose to 49°C at which point the cell vented.

c. Conclusions

We have designed and built two different prototype flat cylindrical cells for preliminary testing on the GLLD duty cycle. Based on data obtained, the thin flat cell did not show any significant advantage over the spirally wound D cell design. The thick flat cell, on the other hand, performed well above our design objectives. Therefore, this particular design was chosen to be optimized in both performance and safety characteristics for the GIID Laser Designator application.

D. Optimization of the Thick Flat Cylindrical Cell

The 3" diameter 0.90" thick high rate flat cylindrical cell developed in this program has shown significant advantages over the optimized spirally wound D cell design in both load voltage and capacity for the high rate GLLD Laser Designator application. Accordingly, this cell design was selected for further optimization.

a. Effects of Anode Polarization Number of Cathode and Cathode Additives

Flat cells discharged in our preliminary tests showed a high utilization of lithium which led us to suspect that anode polarization might be limiting the cell capacity. We planned to place thicker anodes into the cell for evaluation. It was also decided to optimize the design of this flat cell package with respect to the number of cathodes needed in the cell. In addition, since the use of cathode additives has been demonstrated to improve the performance of spirally wound D cells, the effect of similar additives on the performance of a flat cell was also briefly investigated.

1. Experimental

The design and construction of the 3 inch diameter, 0.90" thick high rate flat cell have been discussed in detail in Section IV B b. One cell with lithium anodes of twice the usual thickness (0.010") was built and tested on the new GIID load at room temperature to determine the effect of anode thickness on cell capacity. As for the study of cathode number, a flat cell was

made with 32 cathodes and 33 standard anodes (0.005" thick) and discharged on the old GLID test. An identically built cell was tested on the new GLID duty cycle for comparison. Cells were also made with 36 and 40 cathodes and tested on both the old and new GLLD test loads. The polarization curve at high current levels was also obtained using a DC constant current discharge method.

## 2. Results and Discussion

### (i) Anode Polarization

A thick flat cylindrical cell was constructed with 0.010" thick lithium anodes and tested on the new GLLD duty cycle. It contained thirty (30) cathodes and delivered 190 bursts above the 2.5 volt cutoff voltage which corresponds to a cell capacity of 13.5 Ahr as shown in Figure 104. The cell capacity of this thick anode cell is much less than the 16.9 Ahr delivered by a cell containing 35 cathodes and 26 standard anodes as previously rejected in Section IV C b 2. Therefore, we reached the conclusion that anode polarization does not appear to be a performance limiting factor of the flat cylindrical cell.

### (ii) Number of Cathodes

A flat cylindrical cell was constructed with 32 cathodes and 33 anodes and discharged on the old GLLD duty cycle at 25°C. The results are illustrated in Figure 105 which shows that the cell delivered 25 bursts corresponding to an equivalent of 16.2 Ahrs of capacity above the 2.5 volt cutoff. The load voltage at 17.5A remained above 2.9 volt during the entire service life. An identically built cell was tested on the new GLID test load. This cell provided 230 pulses above 2.5 volt delivering 16.3 Ahr in capacity (see Figure 106). The cell's load voltage at 20A remained around 3.0 volt during most of its service life. The duplication of the above two performance tests proves that the old and new GLLD loads do not noticeably affect cell capacity.

A cell with 40 cathodes was made and tested on the old GLLD load. The performance of this cell, as shown in Figure 107, was not as good as one would predict. The cell gave 25 bursts delivering 16.8 Ahr in cell capacity which showed no improvement over the 32 cathode cell despite a 25% increase in electrode area.

Finally, a 36 cathode cell was assembled and tested on the new GLLD test. This cell provided 290 pulses, which corresponds to a cell capacity of 20.3 Ahr. The load voltage at 20A stayed near 3.2 volt during most of the discharge and it remained above 2.5 volt at the 290th pulse which is remarkably good at this high rate. The performance of this cell is also illustrated in Figure 108. The high performance of this 36 cathode design was further confirmed by repeating the same test using a cell of identical design. The cell gave 287 bursts which is equivalent to 20.1 Ahr in terms of cell capacity as shown in Figure 109. This cell also showed a load voltage of around 3.0 volt at 20A which indicates that the internal impedance is remarkably low. Therefore, heat generation due to iR heating was minimized as indicated by the temperature data included in Figure 109.

The polarization curve of this cell design was also obtained experimentally and it is shown in Figure 110. The load voltage at 50A was found to be 2.95 volt, corresponding to an impressive power density of around 330 W/lb.

Based on these results, 36 cathodes seemed to be near the optimal number of cathodes to use in a flat cylindrical cell for the GLLD Laser Designator application.

### (iii) Cathode Additive

A flat cylindrical cell was made with 36 cathodes. These cathodes were treated with additive 1 at level A as described previously in Section II Ca. The cell was discharged on the new GLLD load at 25°C and the results are plotted in Figure 111. The cell provided 302 bursts equivalent to 21.1 Ahr in capacity before polarizing. The cell voltage on the 20A load was found to be ~3.3 volts during most of its service life. The presence of this cathode additive provided a 5% improvement on cell capacity and at 10% increase in load voltage.

### 3. Conclusions

The performance of the 3 inch diameter 0.90 inch high flat cell was further improved. An optimal cathode number of 36 was experimentally determined for this package. Cell performance can be futher improved, although not by much, with the addition of cathode additive 1 at level A. Anode polarization does

not appear to be a performance limiting factor in this flat cell design.

A flat cell can deliver more than 20 Ahr on the GLLD load. The volumetric energy density approaches 10 Whr/in<sup>3</sup>. The gravimetric energy density is approximately 145 Whr/lb despite the fact that the weight of the can is 40% of the total weight of a finished cell.

b. Improvement of Electrode Stack Connection and Other Design Changes

We have made several design changes to the electrode stack of the flat cylindrical cell in order to improve the anode connection. The original design has been described in detail in section IV B b. This final version differs from the "old" design in several ways. The anodes are now clamped against a solid stainless steel centerpost which has a solid stainless steel washer at the top and is threaded at the bottom. A tantalum tab is welded to this post. An exmet washer located at the top of the electrode stack is then welded to this tantalum tab. This exmet washer, as has been described in our previous reports, is buried in the top anode of the cell to complete the electrical contact between the anode and the centerpost. This arrangement is further illustrated in Figure 112. An identical piece of tantalum tab is also welded to the centerpost on the opposite side with the same exmet washer welded to it.

The sequence adopted to stack the electrodes in the flat cell is shown in Figure 113. In this final version an additional lithium washer is placed under each exmet washer to act as a spacer. Without these spacers, the electrode stack tended to become distorted during the assembly process.

Another design change involves the can itself. Originally, the center-post of the can protruded approximately 1/8" above the glass-to-metal seal in the top half of the can. This post is now flush with the top of the G/M seal as shown in Figure 114. A nickel tab welded to the end of the post is used as the negative terminal. This change was made to better utilize the space available in the eight cell battery package.

### 1. Experimental

Three inch diameter, flat cylindrical cells were made with the new electrode connection design and discharged on the new GLLD duty cycle using procedures described previously. Cell temperature was also monitored during the tests. A transducer was attached to the fillport of the cell to measure the internal pressure of the cell during GLLD discharge. All tests were performed at room temperature.

### 2. Results and Discussion

The voltage-time curve of two fresh flat cells built with the newly developed anode connections on GLLD duty cycles are shown in Figures 115 and 116. These cells were filled with 1.8M LiAlCl<sub>4</sub>/SCCl<sub>2</sub>. They were found to be capable of delivering 12.4 and 10.8 Ahrs to a 2.5V cutoff, respectively. Cell pressure rose to 40-50 psig during the discharge. Temperature of the cell was found to rise to 40°C. The second cell (Figure 116) did not perform as well as the first one (Figure 115) due to internal self-discharge, (the cell became warm during filling). Both cells showed a voltage plateau at 20A in contrast to a sharp voltage drop, characteristic of Li/SOCl<sub>2</sub> cells.

The rate capabilities of the two cells tested were found to be significantly lower than the ones reported in section IV C of this report using cells made with the old electrode design. Some of those cells were capable of delivering up to 21 A.hrs on the GLLD load. Therefore, we constructed and tested another cell of the old electrode design and the results are shown in Figure 117. This cell delivered 13.2 A.hrs on GLLD which is not too different from the performance of the two cells reported above. Based on these results, we concluded that the new design changes most probably did not cause the flat cell to lose its rate capability. We are reasonably confident that the new anode connections are superior to the original design. The decrease in rate capability must be caused by a source other than the design changes.

### 3. Conclusions

Several design changes were made to improve the anode connections to the negative terminal post inside the cell. Modifications were also made to

the can itself for safety and packaging considerations.

Unfortunately, we discovered that the rate capability of the flat cells was lower than that of the cells we built earlier in this program. It has also been established that this loss in cell capacity is most probably not caused by these design changes. This new electrode connection design and other changes were incorporated into the final design of the flat cylindrical cells to be delivered to the sponsor.

#### C. Performance Characteristics of the Flat Cylindrical Cell

The performance of the 3 inch diameter, 0.90 inch thick flat cylindrical cell specifically designed for high rate applications has been determined not only on the GLID test load but also under constant current discharge conditions. In addition, its behaviors under short circuit and force overdischarge conditions were also obtained. These tests were first performed with freshly filled single cells and then followed by using cells stored for a period of time in order to quantitatively determine the extent of voltage delay and capacity retention as a function of storage time and temperature. Finally, multicell batteries were assembled and evaluated on the GLID test load.

##### 1. Experimental

In general test procedures for the flat cell were identical to those for the D cell, with some exceptions. Pressure measurements in flat cells were made with a pressure transducer attached to the cell by a Swagelock fitting and second fill tube specially incorporated into this cell. Because of the high short circuit current for the flat cylindrical cell, we designed and built a special fixture for short circuit testing. This fixture incorporates a 500 amp shunt for current measurement and is manually actuated through a 300 amp knife switch by a manual control rod extending through the wall of our abusive testing area. Electrical connection from the knife switch to the anode is made via a compression collet on the center post and a 1/16" x 4" x 8" copper strip forming a flexible connection. There is an electrically isolated voltage probe at the centerpost to allow voltage measurement unaffected by iR drop through the leads. Cathode connection to

the cell is made via a 1/16" copper sheet bolted to the 500 amp shunt. This design features large areas for electrical contact and short electrical paths to keep external resistance to a minimum. From the current and cell voltage measured during shorting, we estimate the resistance of this fixture to be  $5 \times 10^{-4}$  ohm.

As for the multicell battery tests, a battery made with 3 series connected flat cylindrical cells and two 8 cell GLLD batteries were assembled and evaluated on the new GLLD duty cycle. The latter is schematically shown in Figure 118. A 25A fuse was placed in the battery package to prevent cell venting due to accidental shorting or other abusive conditions.

## 2. Results and Discussion

### (i) Fresh cells

The voltage-time behavior of two typical flat cylindrical cells at 25°C on the GLLD test are shown in Figures 119 and 120. These cells were both discharged shortly after filling with 1.8M LiAlCl<sub>4</sub> in SOCl<sub>2</sub>. The cell capacities of 18.0 and 19.0 Ahr are typical of test results for flat cylindrical cells although some cells have given as much as 21.3 Ahr on this test. Both cells show the very flat voltages at high currents typical of the very high rate flat cell design.

One fresh flat cell was soaked at 0°C for 6 hours prior to initiating the test on the new GLLD load. Both the cell voltage and the wall temperature was monitored during the test. The results are shown in Figure 121. The average cell voltage on 3.2 A load was 3.2 volt while on the 20A load it was 2.75 volt. The cell delivered 11.4 Ahr to 2.5 volt and 14 Ahr to 2.0 volt. The cell wall temperature rose up to 10°C toward the end of the test. The cell delivered approximately 70% of its room temperature capacity of 20 Ahr at 0°C up to a 2.0 volt cutoff. This is quite satisfactory, considering the high rate pulsing requirements.

A fresh flat cell was soaked at -30°C for three days and then it was tested on the new GLLD load. The voltage profile of the cell on 3.2A and 20A pulse are shown in Figure 122. The voltage regulation on 3.2A pulse was found to be significantly better than on 20A pulse. The cell delivered approximately 7.1 Ahr to 2.5 volt and 9.9 Ahr to 2.0 volt cutoff. This corresponds to a 50% reduction in cell performance up to 1.0 volt cutoff. Again, considering the high rate requirements of the GLLD application, the performance at -30°C was found to be quite satisfactory.

A fresh flat cell was discharged at a constant current of 20A on a continuous basis, instead of pulse discharge as in GLLD application. The discharge curve is shown in Figure 123. The cell operated at 3.2 volt and ran for 40 minutes above 3.0 volt corresponding to a capacity of 13 Ahr. The cell showed a voltage recovery towards the end of the discharge. The total cell capacity realized above 2.0 volt was approximately 19.8 Ahr. On GLLD pulse mode we realized 20 Ahr, thus indicating that the cell performs equally well in pulse as well as in continuous mode.

We discharged a flat cell on a continuous current of 100A at 25°C. In this case we monitored the cell wall temperature, the cell internal pressure, along with the cell voltage. Since, the discharge was done through a variable resistor, the cell current was not controlled very precisely and therefore, we monitored the cell current as well. The results are shown in Figure 124. The cell voltage was above 3.0 volt during most of its operation. The cell ran for 8.5 minutes to a voltage of 2.7 volt, corresponding to a capacity of 13.6 Ahr. The cell internal pressure began to increase after one minute into the test and reached 280 PSI after 6 minutes. The cell vented after 8.5 minutes. The high rate performance of the cell was found to be exceptional. The cell venting is intrinsically preventable by proper cell cooling.

We short circuited several flat cells using the short circuiting device described in the experimental section. In one experiment we shorted the cell in short duration installments in order to measure the short circuit current

without allowing the cell to vent. The current and voltage profiles on the first shorting pulse are shown in Figure 125. The cell delivered a short circuit current of 1,700A at a cell voltage of 0.8V. This corresponds to a power output of 1.36 KW. The short circuit current remained virtually constant at around 1,500A for the duration of the short which was 0.12 second. The cell voltage remained constant at approximately 0.8 volt. It is interesting to note that the above short circuit characteristics of the cell represents a power density of approximately 2.7 KW/lb or 0.21 KW/in<sup>3</sup>. This is the highest power density capability of any primary or reserve cell known today. The temperature rise during this pulse was found to be rather modest. The cell is capable of delivering the above pulse power every half and hour without any cell heating or venting.

We repeated the shorting tests several times over several days, and we found that the cell consistently delivered short circuit currents in excess of 1,500A at a cell voltage of 1.0 volt. The internal impedance of the cell turned out to be 0.17 milliohm, which is the lowest ever achieved in lithium batteries to date. This is truly a super high rate cell.

On continuous shorting lasting for about a second, the cell vented. There was no rupture of the can, it only bulged. A photograph showing a fresh and a shorted cell is shown in Figure 126. It appears that the high rate design of the cell also imparts additional safety in that the super high rate flat cells do not explode on either shorting or forced-discharge.

Several flat cells were force discharged at a constant current of 3A to voltage reversal for a period of from 20-30 hours after the regular discharge on the GLLD loads. None of the cells tested showed any undesirable behavior on this type of abuse. There was no cell venting or explosion. A typical voltage and temperature profile on reversal at 3.0A are shown in Figure 127. Note that the cell temperature became constant after the initial rise to 38°C. The cell voltage clamped itself at zero volt within one hour of reversal and remained there for 20-30 hours. Again, the voltage clamping mechanism was found to be operable in those flat cells thus making these safe on forced discharge.

We have been particularly concerned with the safety of the flat cell during voltage reversal, especially during overdischarge on the GLLD test. We used a 12V automobile battery to drive a flat cell into reversal on the GLID test. A flat cell was discharged and driven into reversal on the modified GLLD test using two bursts every three minutes, delivering 16.3 Ahr to 2.5V. The behavior of the cell on voltage reversal is shown in Figure 128. The voltage at 3.2 A stays near 0V while the 20A voltage becomes more negative before the cell vents at -3.25V after ~1.4 hours into reversal. The cell temperature peaked at 75°C during the first hour of reversal and then declined to ~60°C when venting occurred. This venting occurred through a hole in the can which developed opposite the G/M seal and centerpost.

We further investigated the safety of the flat cylindrical cell during GLLD voltage reversal. It has been established that a proper excess of lithium in the cell will greatly enhance the safety of the cell during voltage reversal. Figures 129 and 130 showed the voltage-time curves of two flat cells (each originally contained 25 Ahrs of lithium). Both cells vented through the G/M seal with pressures exceeding 170 psig during voltage reversal on the new GLLD load. The voltage was near 0.0V at 3.2 and -0.75V at 20A when venting occurred. During reversal a vented can showed a 0.2 inch increase in can thickness due to bulging.

Three other cells originally containing 25-27 Ahrs of lithium did not vent during GLLD voltage reversal tests. The results are shown in Figures 131 - 133. They all show the characteristic voltage clamping of the flat cell during reversal. Cell temperatures peaked at ~65°C and then equilibrated at ~30°C. Cell pressures were found to go as high as 125 psig under voltage reversal and decrease to the 20-30 psig range.

The voltage reversal test was also carried out using a cell with a large excess of lithium (41 Ahrs) and the result is shown in Figure 134. The cell was driven deep into voltage reversal and only a very temporary and modest pressure build-up and temperature increase were recorded. Voltage was found to be clamped at 0.0V at 3.2A and -0.25V at 20A, respectively, for up to 17

hours. The large excess of lithium seemed to insure a safe, uneventful voltage reversal over an indefinite period.

Two more flat cells were also driven into reversal at the GLLD rate, as shown in Figures 135 and 136. Both of these cells passed through a temperature maximum about 1 hour into reversal with a pressure maximum near 215 psi. In both of these cells the voltages in reversal stabilized near -0.2V at 20A and 0.0V at 3.2A. The cells continued in reversal with no evidence of venting for 16 and 40 hours respectively before the tests were terminated. The cells appear to form an internal short circuit by electrodeposited Li in the cathode. This process results in the cell showing an OCV of 0.0 and a very low resistance. With the voltage thus clamped and internal heating negated the cell can run in reversal for an indefinite period of time. Both of these cells contained some 45 Ahr of lithium, a substantial amount in excess of the cell capacity for  $\text{SOCl}_2$ .

We also drove a flat cell into reversal at a steady current of 20A, after it was discharged on the GLLD test, as shown in Figure 137. During the reversal voltage clamped near -0.3V as temperature rose to 68°C in the course of the 35 minute cell reversal at 20A. Once more the lithium excess design (32 Ahr) prevented cell venting or explosion during the voltage reversal.

#### (ii) Stored Cells

A flat cell was discharged on the GLLD test at room temperature after three days of room temperature storage as shown in Figure 138. This cell delivered 16 Ahr to a 2.5V cutoff and 19.8 Ahr to 2V. There is an apparent plateau near the end of the cell's diacharge. Another flat cell was tested on the GLLD duty cycle after one week of storage at room temperature as shown in Figure 139. This cell gave 14.2 Ahr to 2.5V and 16.1 Ahr to 2.0V with the apparent plateau in cell voltage at 20A occurring somewhat earlier. A third flat cell was stored for one week after filling and then discharged on the GLLD rate at room temperature as shown in Figure 140. This cell delivered 20.8Ahr to a 2.5V cutoff and showed no evidence of any voltage plateau at 20A. This cell was then driven into voltage reversal at the conclusion of the GLLD test. After 4 hours in reversal the cell vented. We continued storage of flat cells at room temperature and found that the behavior of this cell was exceptional.

Cells were stored at room temperature for 2, 3 and 6 weeks, then discharged on the GLLD test as shown in Figures 141, 142 and 143 respectively. In each case a decreased cell capacity was observed with the cells giving 11.4, 14.2 and 16.3 Ahr to 2.5V, respectively. The capacity decline is clearly not a simple function of storage time as indicated by Figure 144. Capacities to a 2.0V cutoff were much more reproducible at 16.8, 17.5 and 17.5 Ahr, indicating the storage phenomenon is more of a decline in rate performance of the cell than a loss in coulombic capacity per se.

We have further explored the performance of these cells on storage by discharging on GLLD test at 0°C a cell which had been stored at room temperature for three weeks. This cell delivered 7.8 Ahr to 2.5V and 12.8 Ahr to 2.0V as shown in Figure 145 with the lower voltage plateau at 20A being quite marked. We stored another flat cell for two days at 50°C and then two days at 72°C to simulate abusive storage, we discharged the cell on the GLLD test regime at room temperature. During storage there was no can bulging, while pressure inside the cell never exceeded 50 psi. The cell capacity, as shown in Figure 146, was 16.8 Ahr to 2.5V and 18.5 Ahr to 2.0V. The cell shows no greater deterioration in performance on high temperature storage. The cell required less than 15 minutes to reach load voltage of 2.5 at 20A. Internal pressure and wall temperature were monitored during the discharge. Note, that the cell internal pressure rose very rapidly towards the end of the discharge, remaining below 100 psi up to the 2.0 volt cutoff point.

We stored a flat cell with cathode additive 1 for two days at 72°C and 3-1/2 days at room temperature. This cell gave a capacity of 10.5 Ahr to 2.5V on the GLLD test and 14.7 Ahr to 2.0V as shown in Figure 147. While the use of cathode additives gave improved performance in the D cell on the GLLD test, the flat cell is not cathode limited in the sense of the D cell design, and no performance improvement was expected. The lower voltage plateaus were quite apparent in this cell.

We constructed a flat cell in which the cathodes were scrupulously dried in a vacuum oven. This cell was stored for 1 day at 72°C and 3-1/2 days at 25°C before being discharged on the GLLD test. This cell delivered 14.6 Ahr to 2.5V and 17.8 Ahr to 2.0V as shown in Figure 148. The loss of rate performance vis-a-vis a fresh cell shows that the possible water contamination is not the source for flat cell rate deterioration on storage.

We stored a flat cell for three weeks at room temperature and then discharged the cell at an elevated temperature of 48°C as shown in Figure 149. This cell demonstrated quite good performance, delivering 19.9 Ahr to 2.5V and over 21 Ahr to 2.0V on the new GLLD test. The cell temperature rose to 55°C during the course of the test, while capacity was equal to that of a fresh cell.

A number of cells were placed on abusive storage at 72°C. These cells were then tested at room temperature on GLLD duty cycles. Once again, they all showed a decrease in capacity to 2.5V and an increased capacity between 2.5V and 2.0V when compared to the performance of the fresh cells. Figure 150 shows a voltage-time curve of a cell stored at 72°C for 2-1/2 days. It delivered 8.5 Ahrs to 2.5 and 14.6 Ahrs to 2.0V. Once again, a voltage "tail" similar to the one observed in fresh tests is present at the 20A rate. The temperature of this cell reached 50°C during discharge which is 10°C higher than what we observed with a fresh cell (Figure 115).

Three other cells stored at 72°C for 5 days were found to deliver 7.4, 6.2 and 9.9 Ahrs, respectively, to a 2.5V cutoff voltage (Figures 151 - 153). These cells were also capable of delivering large capacities between 2.5 to 2.0V with apparent voltage tails. The capacities of these cells to 0 V is almost the same as that of a fresh cell. This indicates that the coulombic capacity remained unchanged after abusive storage at 72°C.

At this point it is clear that there exists a problem with the 3 inch diameter flat cylindrical cell in that the rate performance of the cell appears to drop significantly on storage. The extend of this decline is not a simple function of temperature, nor is cell performance degraded to the level of the D cell.

We have determined that water in the electrolyte or in the porous cathode matrix is not the cause of the problem. More research and development efforts should be invested in this aspect of the flat cell program in the future.

(iii) Multicell Tests

The performance of battery packages containing multiples of flat cylindrical cells on the new GLLD test load has been determined. A battery consisting of three series connected flat cells was assembled to simulate the two three cell stacks used in the eight cell GLLD battery as shown schematically in Figure 118. The temperature of the center cell and the internal pressure of the top cell were monitored during discharge on the new GLLD cycle. This battery delivered 54 pulses on the 3.2A and 20A cycles before the malfunction of our test equipment took place. Instead of the 3.2A and 20A pulse, the test equipment provided 1.5A and 16A pulses. The test continued on these cycles and the battery delivered an additional 326 pulses above 7.5 volt. This corresponds to a capacity of 21.7 Ahr above the cutoff voltage of 7.5V which is very impressive. The middle cell ran at about 30°C during most of the normal discharge. It rose to a maximum of 75°C towards the end of the discharge. The internal pressure of the cell stayed below 50 psi during the normal discharge period and increased to 145 psi at the end of the test without venting. These results are also illustrated in Figure 154.

An eight cell GLLD battery was assembled and tested on the new GLLD test cycle. The battery initially delivered 15 pulses before the leakage of one of the cells was detected. The leaky cell was located and removed from the package and the test was resumed as a seven cell battery. This battery provided an additional 88 pulses above the cutoff voltage of 17.5 volt delivering a total capacity of 13.4 Ahr. The cell temperature kept on rising to 80°C without ever equilibrating. Four cells vented at the end of the discharge. The results are also shown graphically in Figures 155 and 156. The performance of this battery is quite unsatisfactory.

A second GLLD battery containing 8 series connected flat cylindrical cells was assembled and tested at 25°C. The performance characteristics of this battery on the new GLLD duty cycle were determined and the results are shown in Figure 157. The battery delivered 255 pulses corresponding to 18.1 Ahr in capacity above the 20V cutoff. On the 256th pulse, one cell vented which led to the termination of the test. The wall temperature of the middle cell in the center stack of the package remained at about 55°C during the entire normal discharge period. The behavior of this GLLD battery demonstrated the superiority of the 8 flat cell design over the 16 D cell design for the GLLD Laser Designator application.

D. Conclusions

The performance and safety characteristics of the 3 inch diameter, 0.9 inch thick flat cylindrical cell have been further improved specifically for high rate applications. Cathode additives and anode thickness did not appear as major influencing factors. A design using 36 disc cathodes was adopted in the final version because it provided the longest service life during our tests. Anode contacts have been improved to ensure proper electrical connection to the negative terminal of the cell throughout the entire discharge period. About 100 flat cells have been assembled for characterization and delivery to the sponsor. The delivery has been made in the form of five 8 cell GLLD batteries.

The optimized flat cell can deliver up to 21 Ahr on the GLLD duty cycle when tested as a single cell. At 0 and -30°C, the cell can still provide 11.4 and 7.1 Ahr to a 2.5 volt cutoff, respectively. At 100A constant current discharge, the cell runs at above 2.7 volt for over 8 minutes. Its short circuit is approximately 1,500A. These are quite impressive results demonstrating the superiority of this flat cell design over other existing systems.

The low pressure vent incorporated into the structure works very reliably under extreme abusive conditions such as force discharge and short circuiting. Upon being driven into voltage reversal, the cells do not necessarily vent.

A lithium excess design has been developed to prevent cell venting on voltage reversal either on the GLLD load or at constant current.

The entire eight cell (connected in series) GLLD battery behaves satisfactorily. It is capable of delivering approximately 19 Ahr on the GLLD test cycle. The temperature of the cells never exceeds 35°C during most of the discharge process.

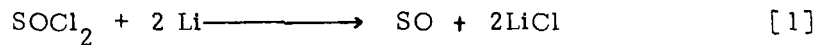
The retention of rate capability after storage over any period of time does present a major problem. The capacity retention after storage, however, is excellent. Water contamination has been ruled out as the possible source causing this problem. More efforts should be addressed to this effect in the follow-on work.

In summary, we have successfully designed and constructed a super high rate Li/SOCl<sub>2</sub> cell whose performance has yet to be surpassed by any other design. It will become a more practical primary cell once the storage problem is resolved.

V. Electrochemical and Spectroscopic Studies on the  
 $\text{SOCl}_2$  Reduction Mechanism

A parallel research effort was made in this program to gain increased understanding of the reduction mechanisms of  $\text{SOCl}_2$  with the hope that such information will be useful in finding ways to improve the performance characteristics as well as the abuse resistance of the Li/ $\text{SOCl}_2$  system.

Calorimetric (12) and DTA studies (7, 11) of Li/ $\text{SOCl}_2$  D cells showed that chemical reactions continue to occur liberating heat after the discharge of the cell. Since these reactions do not occur in an undischarged cell, it is reasonable to assume that the reduction products of  $\text{SOCl}_2$  are responsible, at least in part, for these spontaneous exothermal reactions. The reported spontaneous explosions of partially discharged Li/ $\text{SOCl}_2$  cell on casual storage may also be initiated by the above unknown reactions involving the  $\text{SOCl}_2$  reduction intermediates. Thus, knowledge regarding the nature of the unstable intermediates of  $\text{SOCl}_2$  reduction may be useful as a guide for the improvement of the safety of the Li/ $\text{SOCl}_2$  cells. We postulated (9, 13) the overall cell reaction to be



where SO may dimerize and then decompose to S and  $\text{SO}_2$  or may form polymers. There is substantial evidence (5, 14) in favor of cell stoichiometry [1]. The quantitative formation of LiCl and qualitative formation of S and  $\text{SO}_2$  are known. Very little has been known regarding intermediate species formed during the reduction of  $\text{SOCl}_2$ . Attempts to use cyclic voltammetry (15, 16) in neat  $\text{SOCl}_2$ - $\text{LiAlCl}_4$  solutions to study the discharge reaction were complicated by electrode passivation due to the precipitation of LiCl, insoluble in  $\text{SOCl}_2$ . We have circumvented this electrode passivation problem by using a supporting electrolyte consisting of tetrabutylammonium hexafluorophosphate ( $(\text{C}_4\text{H}_9)_4\text{N}^+\text{PF}_6^-$ ) in organic solvents such as dimethyl formamide (DMF) acetonitrile (AN), methylene chloride and dimethyl sulfoxide since both tetrabutylammonium chloride and S

are soluble in the solvents studied. We carried out both cyclic voltammetry and coulometry in the above electrolytes to study the reduction of  $\text{SOCl}_2$ . The formation and evaluation of the intermediate species were examined using a number of techniques, including high rate cyclic voltammetry and UV-VIS spectroscopy.

A. Experimental

Electrochemical experiments were performed using a PAR 173 potentiostat and PAR 175 function generator with associated ancillary equipment. Pulse polarograms were performed with a PAR 174A polarographic analyzer. The data were collected using conventional x-y and strip chart recorders. The data for fast sweep experiments were taken on a Tektronix model 5115 storage oscilloscope or a PAR 4101 scan recorder. Platinum working electrodes were pretreated by chromic acid followed by a wash with distilled water and air drying. Experimental solutions were routinely degassed with argon before the substrates were added. A silver chlroide coated silver wire was used as a reference electrode. This electrode has a potential of 3.30V vs. Li in  $\text{PF}_6^-$  - DMF solutions.

The cyclic voltammetric experiments were performed in cells of conventional design. The coulometric experiments were carried out in a two compartment H-cell using a glass frit to prevent passage of material from the working and auxiliary electrode compartments. A jacketed cell, as shown in Figure 158, was used to study the reduction of  $\text{SOCl}_2$ .

The organic solvents were either Burdick & Jackson "Distilled in Glass" DMF, and  $\text{CH}_2\text{Cl}_2$  or Eastman Spectro Grade acetonitrile or Aldrich "Gold Seal" Dimethyl Sulfoxide. The supporting electrolyte was prepared by metathesis of tetrabutylammonium chlroide (TBACl) and lithium hexafluorophosphate in acetone/water and purified by multiple recrystallizations in hot ethanol.

B. Results and Discussion

a. Cyclic Voltammetry

The electrochemical characteristics of some of the impurities and proposed reduction products of  $\text{SOCl}_2$  were examined by cyclic voltammetry in the organic

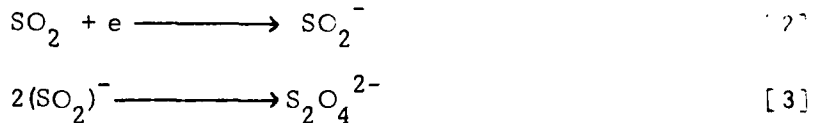
supporting electrolyte solutions. In particular, sulfur, sulfur monochloride, and sulfur dioxide are materials of interest, while chloride ion is generally accepted as a reduction product.

### 1. Chloride

A cyclic voltammogram on Pt electrode in  $TBAPF_6$  in AN is shown in Figure 159 which demonstrates the clean background. A suitable chloride source was found in tetramethylammonium chloride (TMACl) which is both soluble and ionized in acetonitrile solution. A cyclic voltammogram obtained with a platinum wire electrode of a solution of TMACl and  $TBAPF_6$  in AN is shown in Figure 160. The oxidation of free chloride to chlorine and the associated reduction to chloride are clearly located about 1.1V positive of the reference potential.

### 2. Sulfur Dioxide

The electrochemical reduction of sulfur dioxide is itself of considerable practical importance and reasonably stable solutions of sulfur dioxide in organic solvents are easily obtained. The reduction of  $SO_2$  in DMF, acetonitrile and methylene chloride has been examined. In acetonitrile,  $SO_2$  is reduced in a diffusion controlled process at  $E_{1/2} = -1.15V$  vs. the silver reference as shown in Figure 161. The oxidation wave with  $E_p$  near + 0.35V is much diminished at lower sweep rates and represents the oxidation of a product of the  $SO_2$  reduction, viz.  $S_2O_4^{2-}$  according to the reaction



Even at the relatively high sweep rate of 1V/sec there is little evidence for any other oxidation peaks corresponding to the oxidation of species such as  $SO_2^-$ . A similar voltammogram of  $SO_2$  in dimethylformamide solution is shown in Figure 162 under similar circumstances. Once more  $E_{1/2}$  is near -1.15 V and there is a kinetic oxidation wave due to  $SO_2$  reduction products, but there is also a small wave near -0.13V which is due to a new product species. Finally,  $SO_2$  was also examined in methylene chloride solution, where two oxidation peaks

corresponding to the oxidation of  $\text{SO}_2^-$  and  $\text{S}_2\text{O}_4^{2-}$  are more apparent, as shown in Figure 163. In general the initial reduction behavior of the  $\text{SO}_2$  in organic solvents was quite consistent with the established mechanisms (20) but the oxidation of the reduction products was substantially affected by the solvent, probably due to varying degrees of saturation of the two reduced species,  $\text{SO}_2^-$  and  $\text{S}_2\text{O}_4^{2-}$ .

### 3. Sulfur

The cyclic voltammetry of sulfur was examined in dimethyl-formamide and methylene chloride because of the difficulty of dissolving sulfur in acetonitrile. In both methylene chloride and DMF, the reduction of sulfur is a rather complex phenomenon. The reduction of sulfur in  $\text{CH}_2\text{Cl}_2$  as shown in Figure 164, consists of two successive reduction waves whose relative heights are sweep rate dependent (as V increases the second wave becomes less prominent) at ca. -1.1V and -1.5V with oxidation near -0.2V which is also sweep rate dependent and becomes more prominent as the sweep rate increases. Both of these reduction processes appear to be quite irreversible. The reduction of sulfur in DMF, as shown in Figure 165 again consists of two irreversible, but more widely spaced waves near -0.6V and -1.15V. The shape of this second reduction wave is dependent on sweep rate. Finally there is an oxidation wave, also irreversible at +0.25V. The species responsible for this oxidation has been shown by other voltammograms to be the product of the first reduction wave. The height of this oxidation wave is also a function of the sweep rate and becomes much more obvious at high sweep rates. In acetonitrile the cyclic voltammogram for sulfur is somewhat similar to that for DMF, although the second wave is much less well defined and the oxidation wave is near 0V.

### 4. Mixture of Sulfur and Sulfur Dioxide

Since both S and  $\text{SO}_2$  are known to form in the cell, the cyclic voltammogram of a mixture of S with trace amounts of  $\text{SO}_2$  in  $\text{TBAPF}_6^- \text{DMF}$  electrolyte was obtained, and, as shown in Figure 166 (a), it contained only the two peaks corresponding to the reduction of S. Cyclic voltammograms of the same solution with slightly higher concentrations of  $\text{SO}_2$ , as shown in Figure 166 (b),

contain three reduction peaks, the middle one represents the  $\text{SO}_2$  reduction. There was no noticeable interaction between S and  $\text{SO}_2$  that could be detected by the cyclic voltammetry.

#### 5. Sulfur Monochloride

In contrast to the other products examined,  $\text{S}_2\text{Cl}_2$  showed a complicated electrochemical behavior in organic solvents. As shown in Figure 167, the voltammogram of  $\text{S}_2\text{Cl}_2$  in acetonitrile is dominated by an adsorption wave near -1.15V. This wave is followed by an apparently reversible reduction near -1.75V. On the return sweep we see peculiar behavior suggesting absorption of  $\text{S}_2\text{Cl}_2$  or its products on the electrode surface. At +1.1V we see the oxidation of chloride generated during the reduction of  $\text{S}_2\text{Cl}_2$ .

#### 6. Thionyl Chloride

A cyclic voltammogram for  $50\mu\text{l}$   $\text{SOCl}_2$  in approximately 75 ml DMF with  $0.1\text{ M N}(\text{C}_4\text{H}_9)_4\text{PF}_6$  at a platinum wire electrode is presented in Figure 168 (a). The reduction of thionyl chloride shows two successive reduction waves with  $E_{1/2}$  at -0.20V for the first wave, (17) with a peak potential which is sweep rate dependent, but near -0.37V, while the peak potential for the second reduction is near -0.65V. In addition to these reduction processes, there is an irreversible and broad oxidation on the return sweep near 0.0V. This oxidation wave is absent at lower sweep rates and more prominent at higher sweep rates of 200 mV/sec or more. The small reduction wave near -1.25V is present in the background and presumably due to a trace impurity in the DMF. Both of the reduction peaks due to thionyl chloride are due to diffusion controlled processes as shown by the linear relationship of the peak cathodic current  $i_{pc}$  and  $\sqrt{V}$ , where V is the sweep rate, as shown in Figure 169. Under similar circumstances an adsorption controlled process would show  $i_{pc}$  linear with V and a kinetic controlled process is not a simple function of V (17).

This solution of DMF and thionyl chloride is sufficiently stable that an exhaustive electrolysis of the thionyl chloride can be performed at a platinum foil electrode. It is somewhat difficult to get completely reproducible

n values from coulometry because of the closely spaced second reduction wave, but reduction at -0.25V gives an apparent n of 1.71-1.9 e per  $\text{SOCl}_2$ . A cyclic voltammogram of this reduced  $\text{SOCl}_2$  solution is shown in Figure 168. This reduced product is characterized by a reduction wave near -0.63V with little clear evidence for any oxidation processes. If this reduced solution is either allowed to stand or is slightly warmed with a water bath, some thionyl chloride is regenerated, as shown in Figure 168. If this material is then further reduced at -0.25V, n is 2.04 or very nearly 2.0, while a shoulder appears near -0.9V.

A series of voltammograms for 10 mM  $\text{SOCl}_2$  in  $\text{CH}_3\text{CN}/0.1 \text{ N TBAPF}_6$  are shown in Figure 170. In these voltammograms on a constant current scale of  $25\mu\text{A}/\text{cm}^2$ , the sweep rate, V, was varied from 0.20V/sec to 2.0V/sec. As the sweep rate increases, the peak current increases, but an oxidation process near 0.0V appears at 500 mV/sec and becomes more prominent at 1.0 and 2.0V/sec. The chemical entity which is being oxidized at this potential is not present in the solution originally since there is no anodic current at this potential until some of the thionyl chloride has been reduced. The sweep rate dependence of this oxidation wave shows that the species responsible for the oxidation is reacting fairly rapidly in solution. The oxidation and coupled reduction near + 1.0V is due to oxidation of chloride ion to chlorine. The chloride itself is generated by reduction of thionyl chloride.

The effect of concentration of the  $\text{SOCl}_2$  reduction has been examined. Cyclic voltammograms of  $\text{SOCl}_2$  at various concentrations at a Pt electrode are shown in Figure 171. For a given sweep rate of 500 mV/sec the oxidation near 0.0V becomes less prominent as concentration increases. From the sweep rate dependence of this oxidation, we can conclude that the species responsible for this oxidation wave is reacting with thionyl chloride in solution or with itself. Change in the reduction behavior was also noted as the wave near -0.65V became less prominent and the one near -1.0V more prominent as the concentration increased.

We have also examined the effect of substrate changes on the thionyl chloride reduction. Ordinary graphite or porous carbon electrodes displayed too high a background current to usable in these experiments. We have, however, examined the use of nickel, iridium, gold, amalgamated gold, copper and silver as electrode materials for observing the  $\text{SOCl}_2$  reduction. Cyclic voltammograms on nickel, iridium and gold electrodes were quite similar to those observed with Pt as shown in Figure 172. The copper electrode showed a very limited area of usable voltage while the results with silver electrode are anomalous and reproduced in Figure 173.

We have continued our work on the thionyl chloride reduction in DMF (and in AN) and the reduction appears to take place by the same mechanism. The better separation of the two reduction waves in DMF makes it a more attractive solvent for use in strictly electrochemical studies on this system. Experiments in which sweep rate and concentration were systematically varied in DMF/TBAPF<sub>6</sub> gave similar results for the reduction of  $\text{SOCl}_2$  to those found in acetonitrile. The second reduction wave remained more prominent in DMF, suggesting that coordination with DMF was stabilizing the species responsible for the reduction process.

To examine the formation of the intermediate species more closely we also examined the reduction at higher sweep rates than usual, recording the current/voltage trace on a storage oscilloscope. At sweep rates as high as 100V/sec no qualitative change in the voltammogram could be observed. Except for uncompensated iR losses the voltammogram was similar to those generated at lower sweep rates. We were also able to use the storage oscilloscope with multiple sweeps of the same voltage range to examine the relationships of the two reduction waves and the oxidation near 0V. Using this method we were able to generate a "steady state" voltammogram of reduced thionyl chloride species. This voltammogram showed that the first thionyl chloride reduction wave was absent while the second reduction wave and the oxidation near 0V were still present. This result indicates that the oxidation near 0.0+ does not regenerate thionyl chloride since the first reduction wave corresponding to the reduction of  $\text{SOCl}_2$  is absent and as such the reduction of thionyl chloride is irreversible.

For further comparison we ran cyclic voltammograms in dimethylsulfoxide (DMSO), a solvent which is regarded as very good for reduced species because of its ability to stabilize reactive materials by complexation. DMSO is also known to have a rather low activity of residual water because of the sulfoxide's coordinating ability. A cyclic voltammogram for  $\text{SOCl}_2$  in DMSO/TBAPF<sub>6</sub> is shown in Figure 174. The pattern of two successive reduction waves and an oxidation near 0.0V are very similar to that observed in DMF. The oxidation near 0.0V is quite prominent even at 0.05V/sec sweep rate, indicating that the reaction species involved is greatly stabilized by the DMSO solvent. The definition of the two reduction waves is very clear and there is little evidence for the appearance of the third wave near -1.0V which we noted in other solvents.

b. Coulometry

We have examined the coulometric reduction of  $\text{SOCl}_2$  in DMF, acetonitrile, and methylene chloride. In all three solvents we have observed the regeneration of thionyl chloride by destruction of an intermediate species and have confirmed the Faradaic current of 2 equivalents of charge for each equivalent of  $\text{SOCl}_2$  reduced. In particular, the reduction in acetonitrile is of interest since the UV-VIS solvent cutoff of 190 nm gives a much better spectral window than DMSO (268 nm), DMF (270 nm), or methylene chloride (230 nm). We were able to monitor the course of a coulometric reduction by using both cyclic voltammetry and UV-VIS spectroscopy to monitor changes in the solution. For comparative purposes, spectra of  $\text{SO}_2$  and S in acetonitrile are reproduced in Figures 175 and 176, respectively. The wave lengths of maximum absorbance, 279 nm for  $\text{SO}_2$  and 277 for S are very similar to that of  $\text{SOCl}_2$ , 277 nm as shown in Figure 177, however, there is a second band in the spectrum near 234 nm which is not present in the spectra of  $\text{SO}_2$  and S. In this particular experiment 10 $\mu$ l of  $\text{SOCl}_2$  was used in 75 ml of  $\text{CH}_3\text{CN}$  to give a concentration of 1.82 mM  $\text{SOCl}_2$  in  $\text{CH}_3\text{CN}$ . This concentration was experimentally determined to be usable for both cyclic voltammetry and UV-VIS spectroscopy. Changes in the cyclic voltammograms and spectra as a function of charge passed are displayed in Figures 178 and 179. As the electrolysis proceeds, the absorbance maximum

in the UV-VIS spectrum shifts from 277 to 291 nm corresponding to a lower energy. The absorbance also increases gradually with the electrolysis and reaches a maximum of 1.94 from 0.63. The absorbance then declines drastically to 0.79 at n = 1.76 (Figure 180). The absorption peak at 290 nm disappears on storing the electrolyzed solution (n = 2) for one week at room temperature. At the same time, the first reduction wave in the cyclic voltammogram is destroyed and the second reduction wave becomes much more prominent. The UV-VIS spectra of the solutions after the electrolysis did not show the presence of S or SO<sub>2</sub>. When the solution was allowed to stand overnight the first wave became somewhat more noticeable and some poorly defined waves at more negative potentials also appeared. The final voltammograms showed two very poorly defined reduction waves with no SOCl<sub>2</sub> present, while the final spectra showed a substantial decline in absorbance.

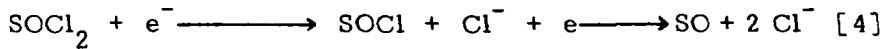
c. Reduction Mechanism of SOCl<sub>2</sub> and Its Implications on Li/SOCl<sub>2</sub> Cell Safety

The cyclic voltammograms of sulfur, sulfur dioxide and sulfur monochloride and that of the reduced SOCl<sub>2</sub> solution lead to the conclusion that none of these three materials are immediately formed after the reduction of SOCl<sub>2</sub>. The coulometric data demonstrate an overall n value of 2.0 for the reduction of thionyl chloride. Reductions for extended times have given green, air-sensitive solutions possibly including polysulfides, but there is no evidence to suggest that this reflects any process occurring in SOCl<sub>2</sub> reduction since the cyclic voltammograms show that no further unreduced SOCl<sub>2</sub> is present.

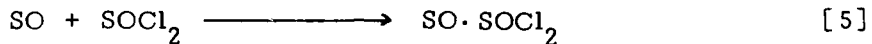
The spectroscopic evidence also shows that S and SO<sub>2</sub> are not formed during the reduction process itself. Instead a different species is formed with an absorption band near 291 nm. This is confirmed by the cyclic voltammograms which show only a slow formation of species reducing at potentials near those for S and SO<sub>2</sub>. This intermediate species is reasonably stable and only slowly decomposes to generate more SOCl<sub>2</sub>.

We can now present a reasonable reduction mechanism for SOCl<sub>2</sub> which

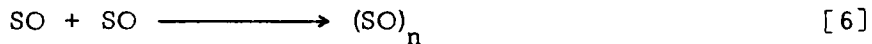
gives the large waves in DMF and DMSO, there are two successive one electron processes to generate SO by a net two electron transfer.



For reactions such as this, it is not unusual for  $E^\circ_\text{o}$  for the second reduction process to be positive of  $E^\circ_\text{o}$  of the first. Early in the reduction process  $\text{SOCl}_2$  is present in large concentration compared to SO and reaction with  $\text{SOCl}_2$  is favored.



This species can slowly dissociate to regenerate  $\text{SOCl}_2$ . As the electrolysis progresses the concentration of SO increases compared to  $\text{SOCl}_2$  as reaction with SO is favored (18).



The product  $(\text{SO})_n$  is characterized by the absorbance near 291 nm and is reduced near  $\sim 0.65\text{V}$  and the reduced product oxidized near  $+ 0.3\text{V}$  while the  $\text{SO} \cdot \text{SOCl}_2$  product is oxidized near  $0.0\text{V}$  as shown by the potential shift in this wave as the electrolysis continues. This species  $(\text{SO})_n$  appears to be reasonably inert kinetically and only slowly decomposes to S and  $\text{SO}_2$ , perhaps by loss of  $\text{SO}_2$  to form successively oxygen deficient polymers. Observations of delayed pressure rise (19) and thermal activity (12) in discharged thionyl chloride cells are quite consistent with this hypothesis.

Based on the above reaction mechanism it occurred to us that a lot of the instability and sudden pressure build-up and explosions associated with the discharged and force-discharge Li/ $\text{SOCl}_2$  batteries may be due to the formation of the kinetically stable but thermodynamically unstable intermediates such as  $(\text{SO})_n$ . The decomposition of  $(\text{SO})_n$  to form  $\text{SO}_2$  may be triggered by various means such as shock, or local heating during a force-discharge, etc. and this could lead to a rapid pressure build-up. This decomposition process may also

produce sufficient heat to trigger the explosive Li + S reaction. Therefore, one approach towards improved safety involves the use of a catalytic material in the carbon cathode which will catalyze the decomposition of the unstable species such as  $(SO)_n$  so that during cell discharge, the cell reaction will result in the formation of stable reaction products S and  $SO_2$  according to



In this manner the pressure build-up and the heat evolution (if any) during the cell discharge will be gradual and predictable instead of being sudden and unpredictable. Also, the addition of catalyst may prevent the formation of species such as  $\text{SO} \cdot \text{SOCl}_2$ , and thus increase the efficiency of  $\text{SOCl}_2$  reduction at high rates. The formation of  $\text{SO} \cdot \text{SOCl}_2$  does not affect the efficiency at low rates as demonstrated earlier (10) where we discharged  $\text{SOCl}_2$  with 98% efficiency based on 2 electrons per mole of  $\text{SOCl}_2$ .

d. Conclusions

Experimental evidence obtained to date strongly suggests that there are at least two intermediate species formed in the reduction of  $\text{SOCl}_2$  in a Li/ $\text{SOCl}_2$  cell to form LiCl, S and  $SO_2$ . The formation of these species  $\text{SO} \cdot \text{SOCl}_2$  and  $(SO)_n$  have been postulated. The decomposition of these intermediates are probably responsible for the delayed  $SO_2$  generation and thermal activities noted in discharge Li/ $\text{SOCl}_2$  cells.

#### VI. Conclusions

The significant technical accomplishments we have achieved in this program can be summarized as follows:

1. We have successfully improved the cathode current collector design for a spirally wound D cell for high rate applications.
2. We have optimized the spirally wound D cell with excellent performance characteristics and abuse resistance for both BA5590 and GLID Laser Designator applications.
3. We have designed, constructed and evaluated a flat cylindrical cell design for super high rate applications.
4. We have further improved the performance and demonstrated the safety features of the flat cylindrical cell.
5. We have assembled and evaluated several GLID batteries using both the 16 D cell and the 8 flat cell designs. The performance and safety features of the multicell batteries have been established.
6. We have gained further understanding regarding the reduction mechanism of  $\text{SOCl}_2$  which may be useful in improving the performance and the safety of the  $\text{Li}/\text{SOCl}_2$  cells even further.

### VII. References

1. W.K. Behl, J. A. Cristopoulos, M. Ramirez and S. Gilman, *J. Electrochem. Soc.*, 120, 1619 (1973).
2. J. J. Auborn, K. W. French, S. I. Lieberman, V. K. Shah and A. Heller, *ibid*, 120, 1613 (1973).
3. D. L. Maricle et al, U.S. Pat. 3, 567, 515 (1971); G. E. Blomgren and M. L. Kornenberg, German Pat. 2, 262, 256 (1973).
4. A. N. Dey and C. R. Schlaikjer, Proc. 26th Power Sources Symposium, Atlantic City, April 1974.
5. C. R. Schlaikjer, U.S. Pat. 4, 020, 240 (1977), Proc. 28th Power Sources Symposium, Atlantic City, June 1978.
6. J. P. Gabano and P. Lenfant, Abstract No. 27, Electrochemical Society Meeting, Pittsburgh, PA, October 1978.
7. A. N. Dey, "Sealed Primary Lithium Inorganic Electrolyte Cell" Final Report, DELET-TR-74-0109-F, P. R. Mallory & Co., Inc., July 1978.
8. A. N. Dey and P. Bro., Proc. Brighton Power Sources Symposium (1976), p. 508.
9. A. N. Dey, *J. Electrochem. Soc.*, 123, 1262 (1976).
10. A. N. Dey, *J. Electrochem. Soc.*, 126, 2052 (1979).
11. A. N. Dey, Proc. 28th Power Sources Symposium, Atlantic City, June 1978.
12. P. Bro, *J. Electrochem. Soc.*, 125, 674 (1978).
13. A. N. Dey, *Thin Solid Films*, 43, 131 (1977).

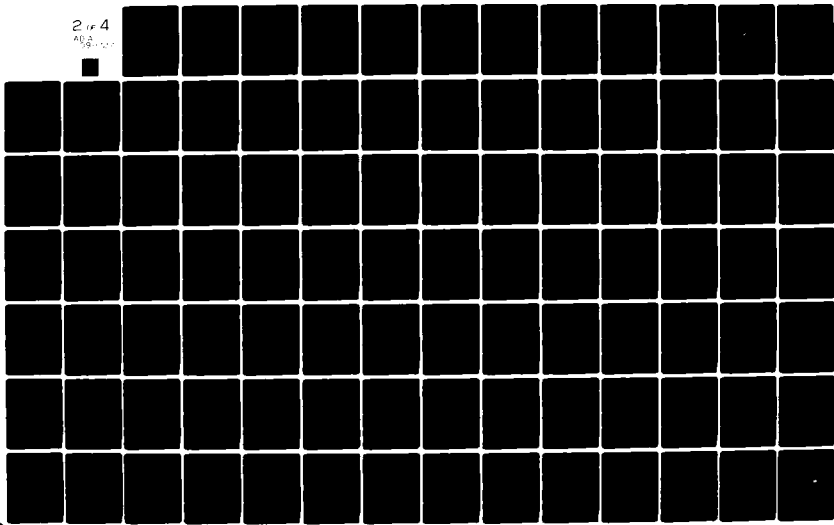
14. D. R. Cogley and M. J. Turchan, "Lithium-Inorganic Electrolyte Batteries," Second Quarterly Report; ECOM-74-0030; AD 779477 EIC Inc., May 1974.
15. W. K. Behl, in "Proceedings of the 27th Power Sources Symposium," Atlantic City, NJ, June 1976.
16. G. E. Blomgren, V.Z. Leger, M. L. Kronenberg, T. Kalnoki-Kis and R. J. Brodd, in "Proceedings 11th International Power Sources Symposium," Brighton, England, 1978.
17. R. N. Adams "Electrochemistry at Solid Electrodes," Dekker (1969).
18. P. W. Schenk and R. Steudel, Angew. Chem. Internat. Edit. 4, 402 (1965).
19. M. Domeniconi, K. Klinedinst, N. Marincic, C. Schlaikjer, R. Staniewicz and L. Swette, "Inorganic Electrolytes," Office of Naval Research; Interim Report, Contract #N00014-76-C-0524; GTE Laboratories; Jan. 1976 to Oct. 1977.
20. R. P. Martin, Thesis "The electrochemical Reduction of Sulfur Dioxide and of Elemental Sulfur in Nonaqueous Solvents," University of California, March 1973.

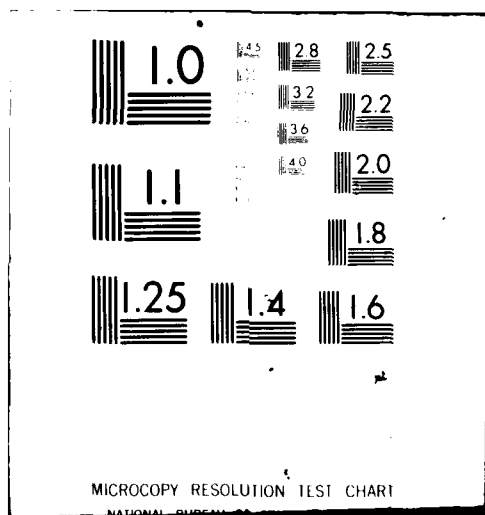
AD-A098 727 DURACELL INTERNATIONAL INC BURLINGTON MA LAB FOR PHYS--ETC F/G 10/3  
LITHIUM-THIONYL CHLORIDE BATTERY, (U)  
APR 81 D WONG, W BOWDEN, N HAMILTON

DAAB07-78-C-0563  
DELET-TR-78-0563-F NL

UNCLASSIFIED

2 IF 4  
AD-A098-727





VIII. Acknowledgement

Helpful suggestions from Dr. Sol Gilman and experimental assistance of John Miller, Paul Witalis, Robin Granelli and Jean Haggerty are gratefully acknowledged.

TABLE 1  
Short-Circuit Currents of Hermetic D Cells  
With Various Cathode Designs

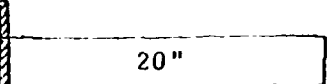
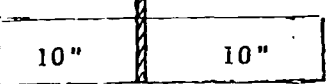
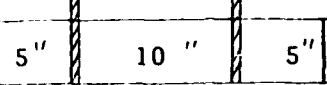
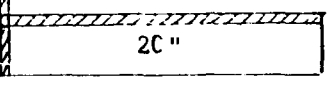
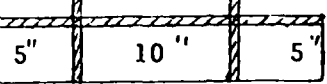
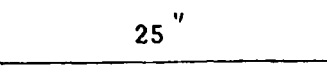
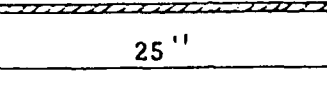
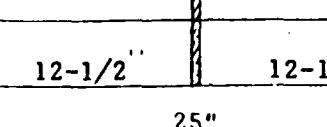
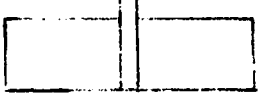
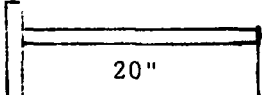
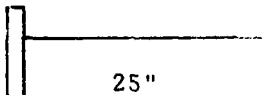
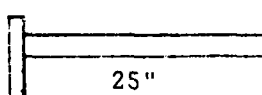
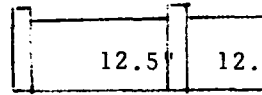
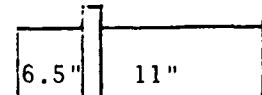
No.	Cathode Designs	Maximum Short Circuit Current (A)	Current Density ( $\text{mA/cm}^2$ )
1.		24	53
2.		76	168
3.		94	208
4.		58	128
5.		98	217
6.		35	62
7.		65	115
8.		104	184

TABLE 2

Behavior of High Rate Li/SOCl<sub>2</sub> D Cells on GLLD Modified Duty Cycle

No.	Cathode Designs	Current (A)	Number of Modified Duty Cycles Above 2.0 Volt	Cell Capacity (Ahr/cell)	Temperature (°C)
2		20"	6.5	16	5.2
		8.0	11	4.4	25
		6.5	0 <sup>+</sup> (11)*	(3.6)*	-30
4		20"	6.5	10	3.3
6		25"	8.0	4	1.6
7		25"	6.5	10	3.3
		8.0	7	2.8	25
		6.5	12	3.9	25
8		12.5" 12.5"	6.5	8 (11)*	(3.6)*
			6.5	10 (13)*	(4.2)*
			6.5	16	5.2
			8.75	11	4.8
9		6.5" 11" 6.5"	6.5	16	5.2
			8	12	4.8

\* Number of cycles before the cell entered voltage reversal.

+ Cell voltage below 2 volt under load.

TABLE 3

**Performance of High Rate Li/SOCl<sub>2</sub> D Cells on GLLD Tests  
Using the Old Duty Cycle at 25°C**

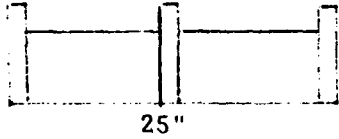
No.	Cathode Configuration	Above 2.5V on 17.5A		Above 2.0V or 17.5A	
		Bursts	Capacity (Ahr/cell)	Bursts	Capacity (Ahr/cell)
2		9	2.9	11	3.6
8		17	5.5	17	5.5

TABLE 4

**Effect of Cathode Additive on the Performance of Li/SOCl<sub>2</sub> D Cells  
For GLLD Laser Designator Application at 25°C**

Additive	Level	Bursts*	Capacity (Ahr/cell)	Max. Cell Temp/°C
1	A	19	6.1	40
	B	14-21	4.5-6.8	40-55
2	A	16-19 (2V cutoff)	5.2-6.1	43-55
	B	17	5.5	38
	C	22-23 (208-214 pulses on the new load)	7.4-7.6	30-35
3	--	17-18	5.5-5.8	38-45
4	--	19 (2V cutoff)	6.1	--
5	--	16	5.2	--

\* Old GLLD duty cycle 2.5 volt cutoff on 17.5A load unless otherwise specified.

TABLE 5  
Voltage Plateaus for the Optimized High Rate D Cells

Current (A)	Voltage at	
	+25°C	-30°C
0.3A	3.5V	3.1V
1.0A	3.30V	3.1V
3.0A	3.25V	2.9V
4.0A	3.2V	--
10.0A	2.7V	--

TABLE 6  
Polarization Characteristics of the Flat Cells and the Circular Cathodes with Various Current Collector Designs

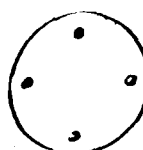
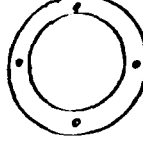
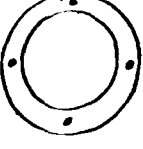
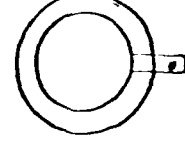
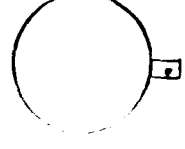
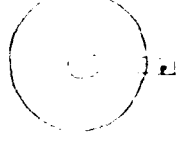
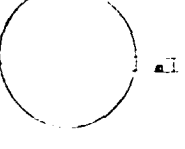
Current (A)	Design 1		Design 2		Design 3		Design 4		Design 5		Design 6		Design 7		Design 8	
	Cell Volt	Cath. Pot														
0.1	3.39	3.40	3.30	3.40	3.33	3.36	3.35	3.38	3.37	3.39	3.33	3.38	3.35	3.40	3.34	3.37
0.3	3.20	3.27	3.15	3.28	3.15	3.21	3.19	3.23	3.18	3.23	3.18	3.26	3.22	3.30	3.16	3.22
0.5	3.10	3.15	-	-	-	-	-	-	-	-	-	-	-	3.14	3.16	3.06
1.0	2.80	2.87	2.80	2.96	2.70	2.89	2.85	2.91	2.80	2.90	2.84	2.87	2.96	2.99	2.81	2.94
2.0	2.35	2.41	2.35	2.59	2.30	2.50	-	-	-	-	2.50	2.55	2.69	2.74	-	-
3.0	1.95	2.10	-	-	-	-	-	-	-	-	-	-	-	-	-	-

\* Projected Values; the Reference Electrode was Disconnected.

TABLE 7

82.

Short-Circuit Currents of the Experimental Flat Cylindrical Cells  
with Various Cathode Designs

Cathode Current Collector Design	Short Circuit Current (A)	Short Circuit Current Densities (mA/cm <sup>2</sup> )
1. 	7.0	176
2.  (10 mil)	8.0	201
3.  (5 mil)	7.4	186
4. 	8.6	216
5. 	6.2	156
6. 	9.2	231
7. 	8.8	221
8. 	7.2	181

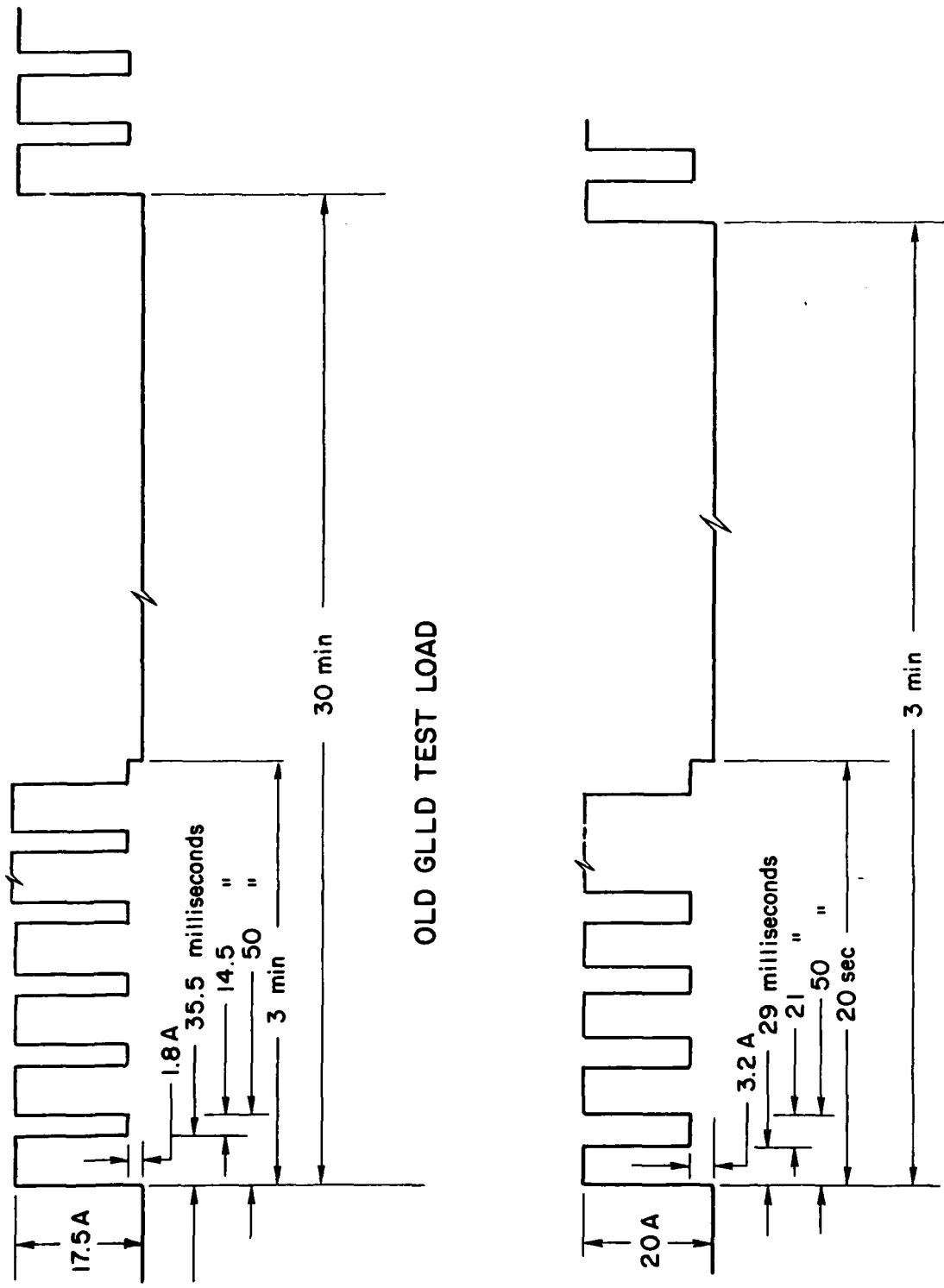


Figure 1. Schematic diagram of the old and new duty cycles for the GLLD battery for laser designator GLLD duty cycle.

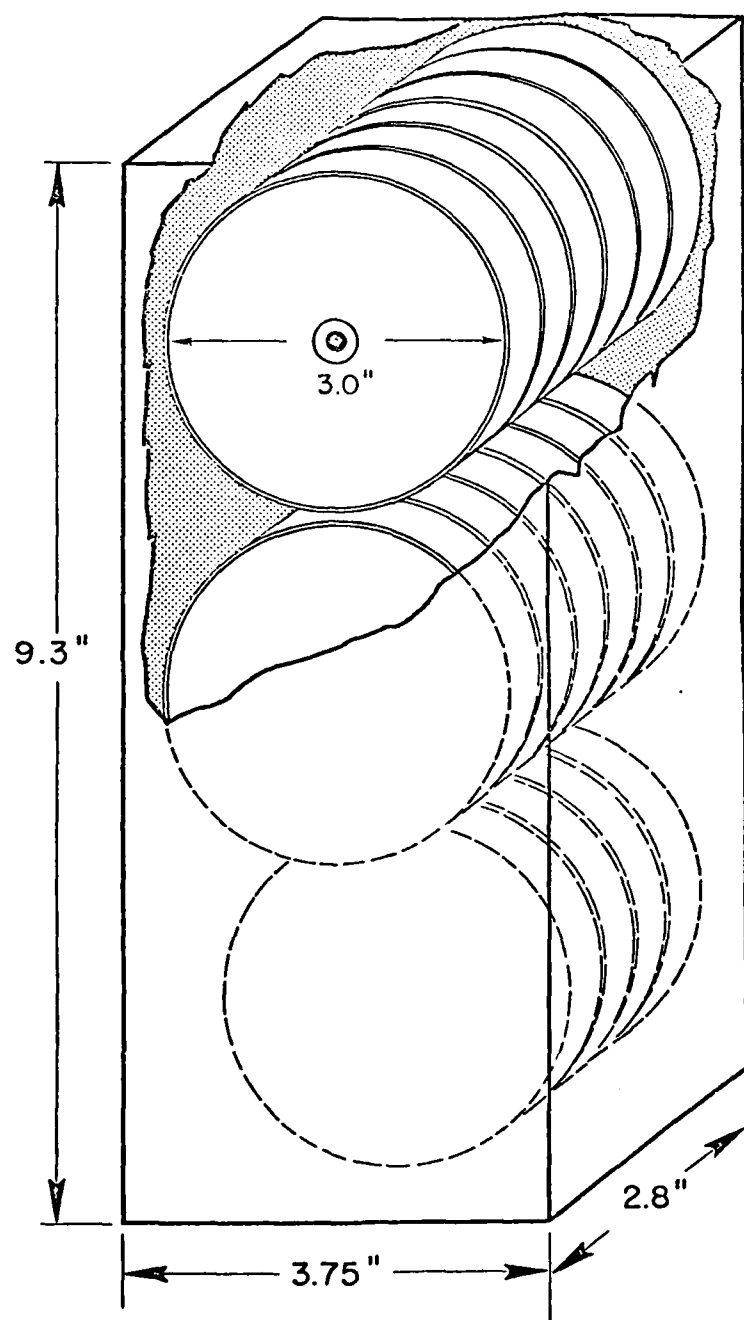


Figure 2. Laser designator battery with thin flat cells

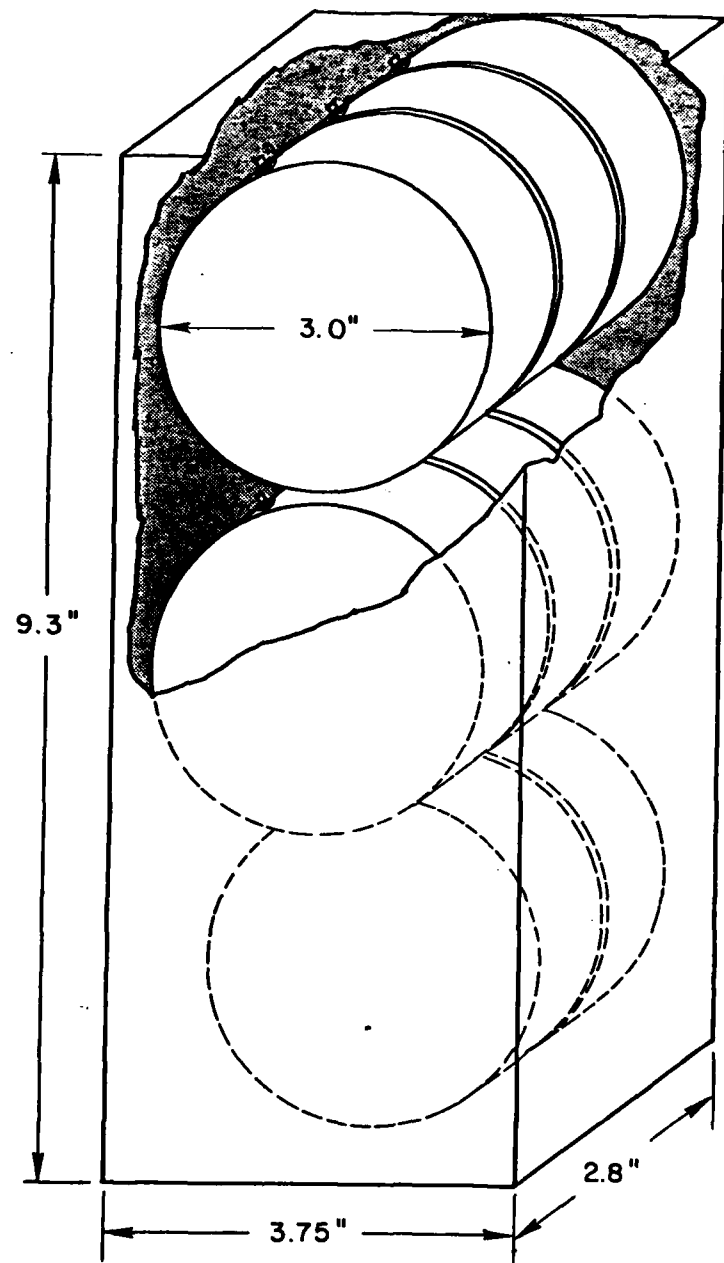


Fig. 3 Laser designator battery with thick flat cells

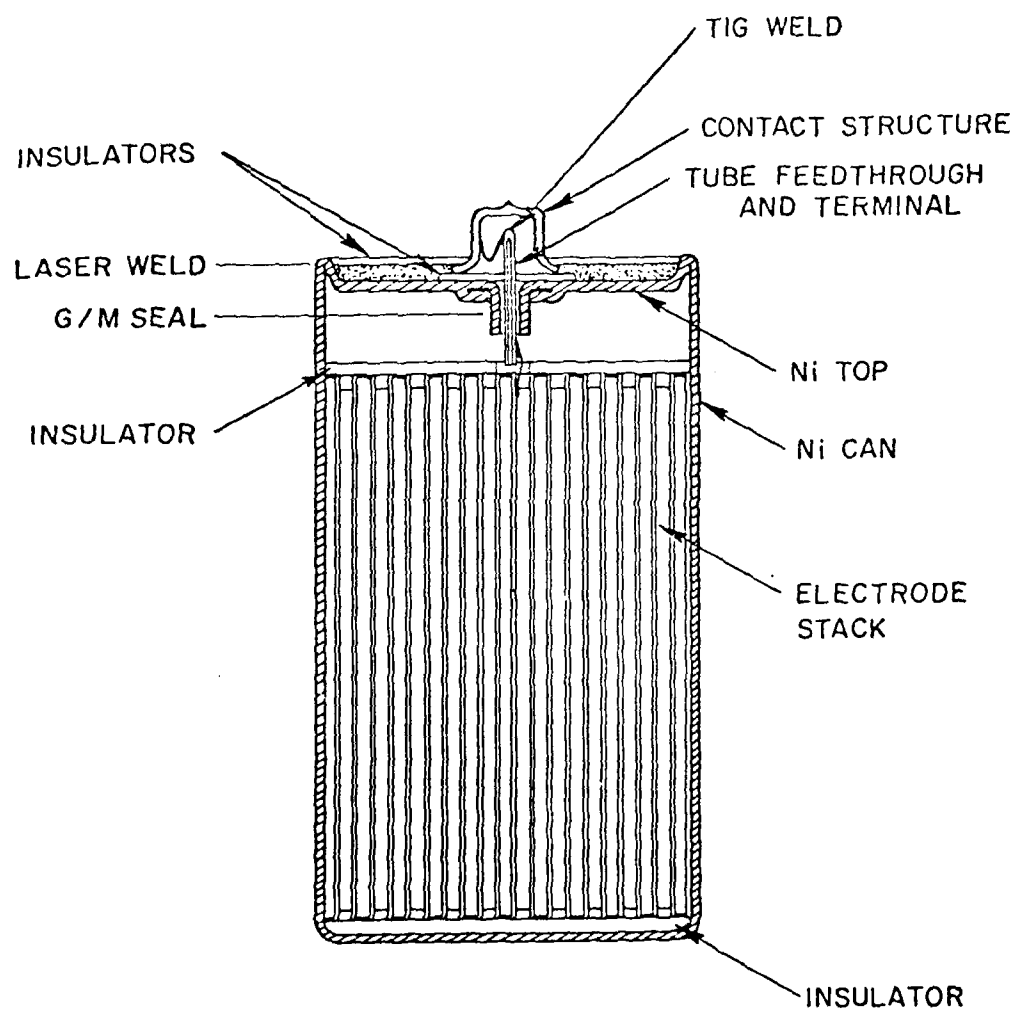


Figure 4. Cross-Sectional view of the hermetic Li/SOCl<sub>2</sub> D cell.

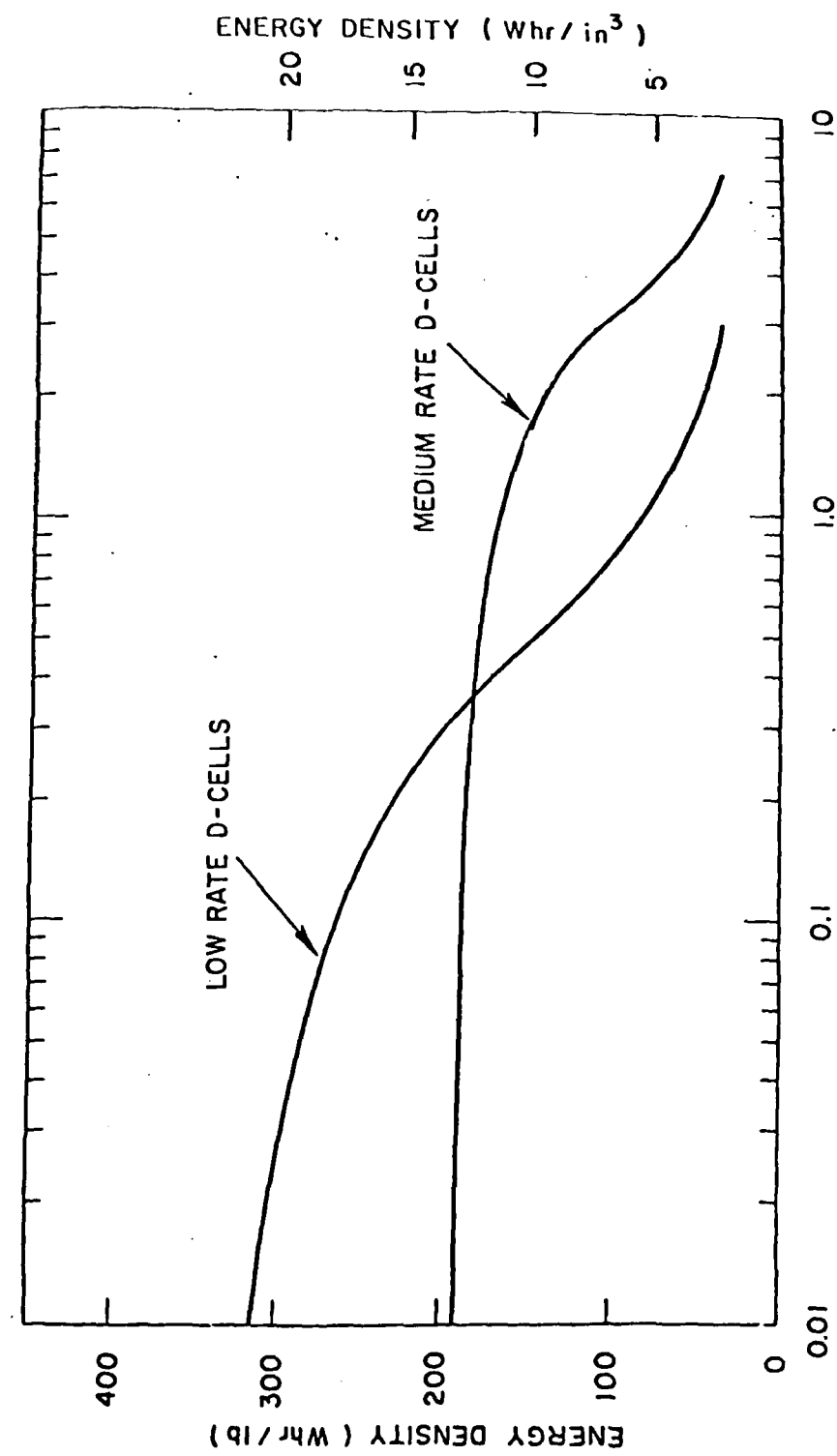


Figure 5. Energy density-rate curves of the medium rate and the low rate Li/SOCl<sub>2</sub> D cell.

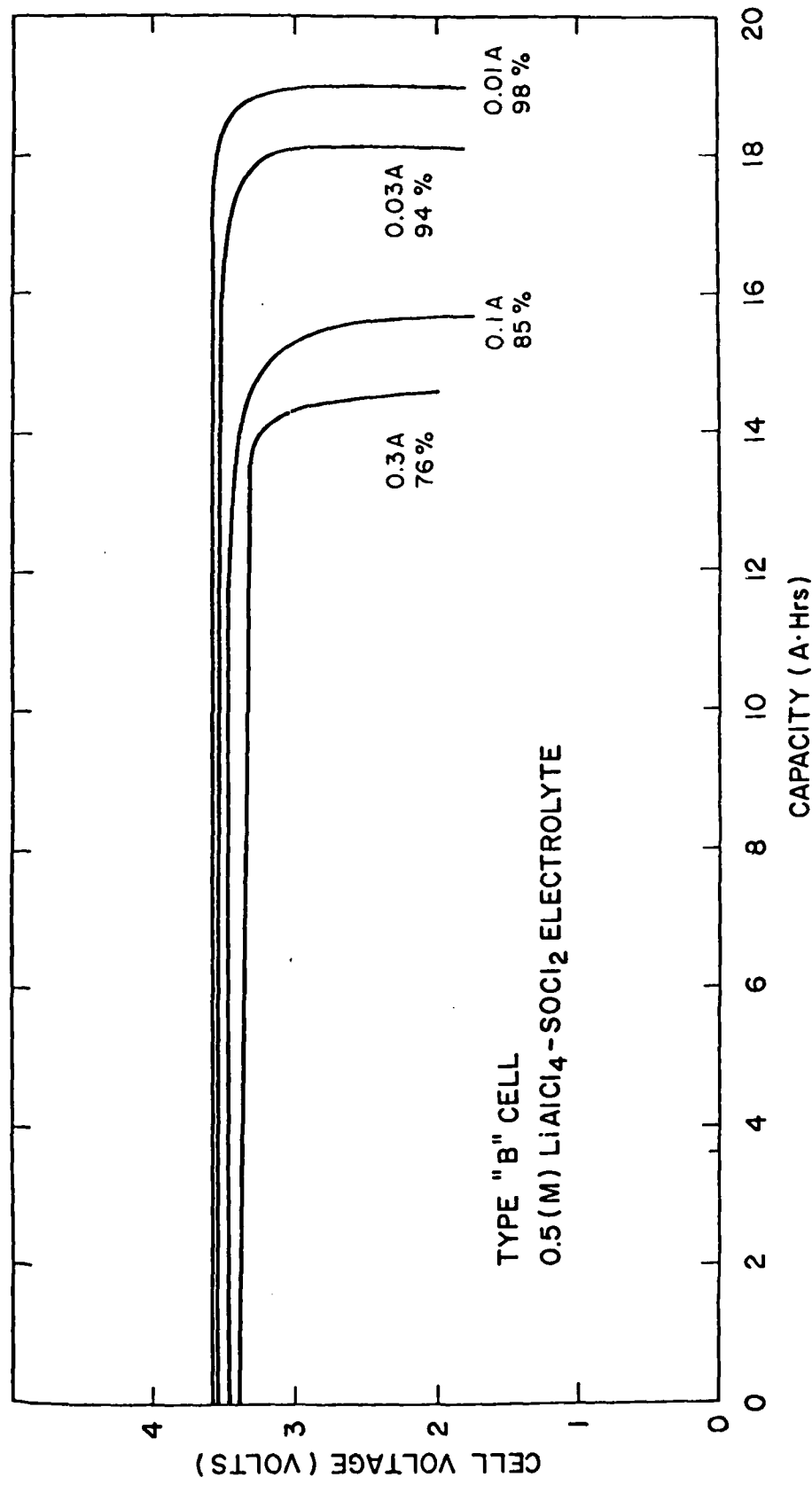


Figure 6. Discharge characteristics of low rate Li/SOCl<sub>2</sub> D cells at constant currents of 0.01, 0.03, 0.1 and 0.3A at 25°C.

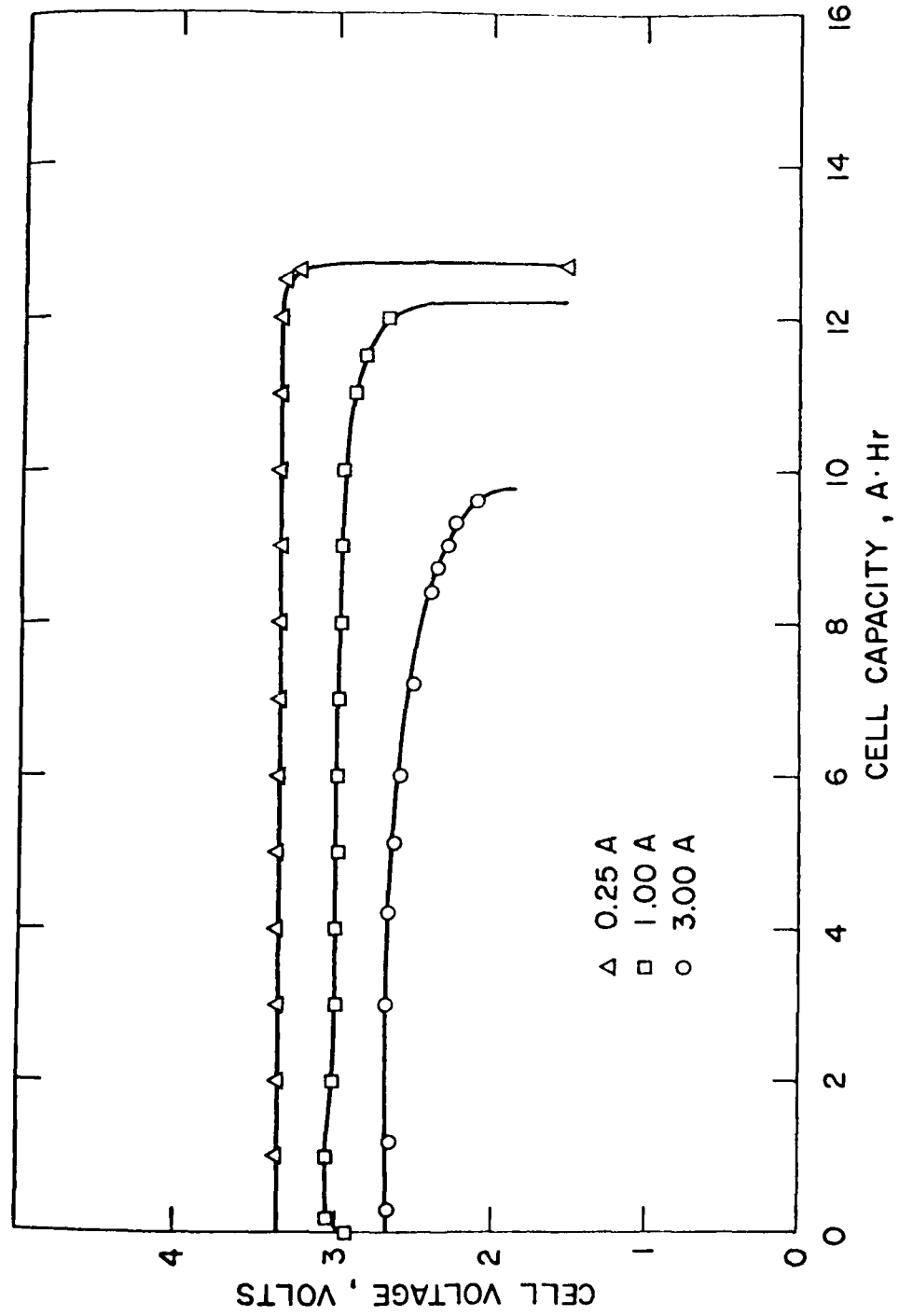


Figure 7. Discharge characteristics of medium rate Li/SOCl<sub>2</sub> D cells at constant currents of 0.25, 1.0 and 3.0A at 25 °C.

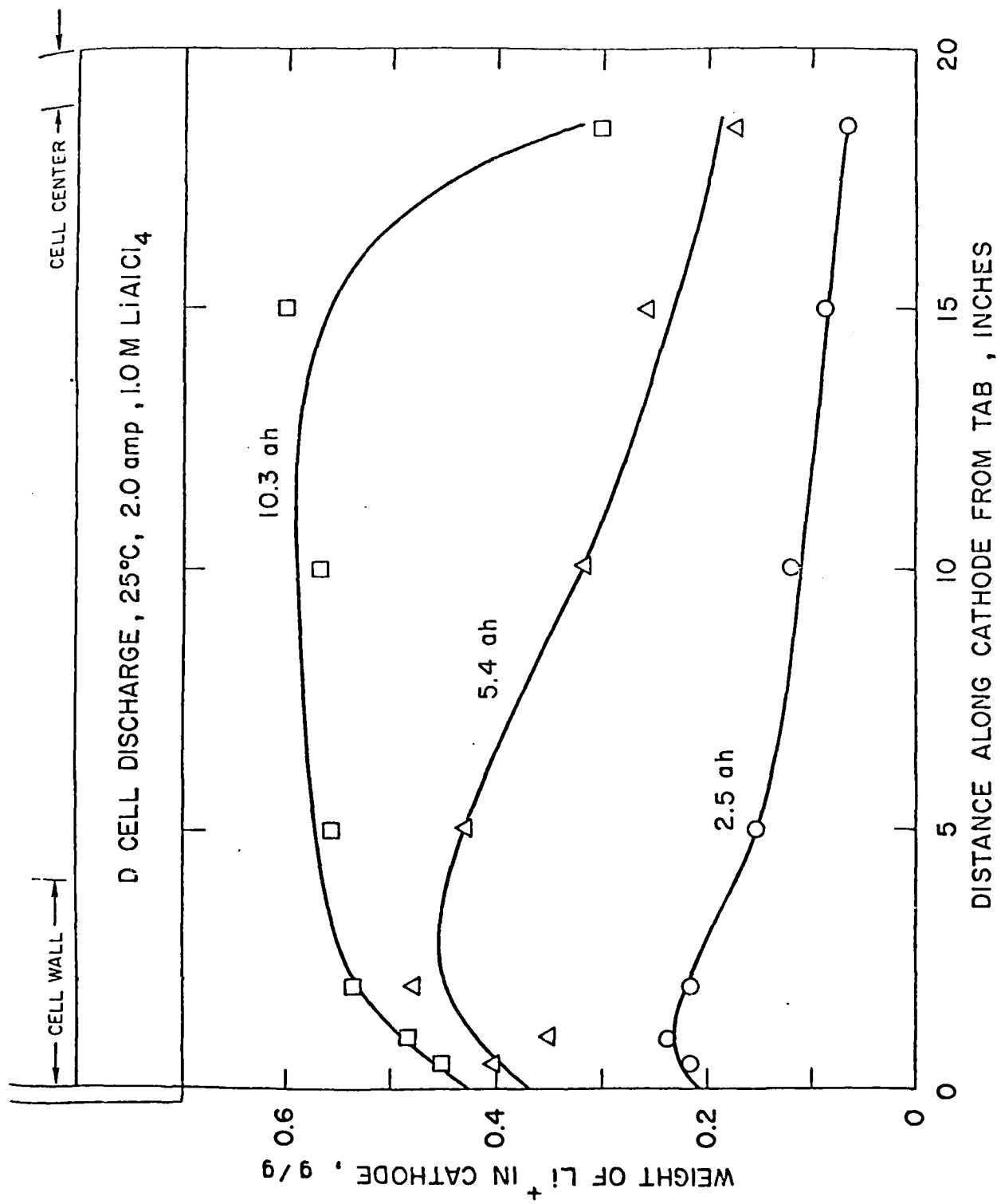


Figure 8. Longitudinal reaction profiles of carbon cathode.

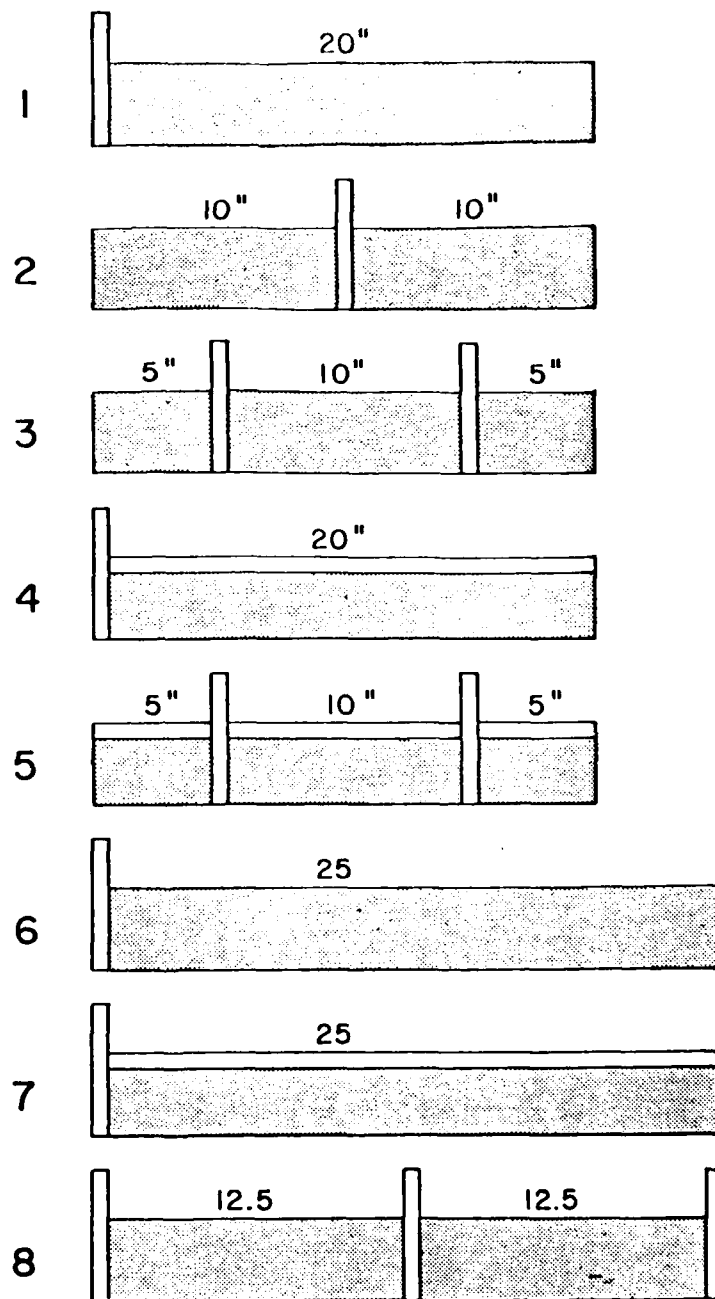


Figure 9. Current collector designs of the carbon cathodes of spirally wound D cells.

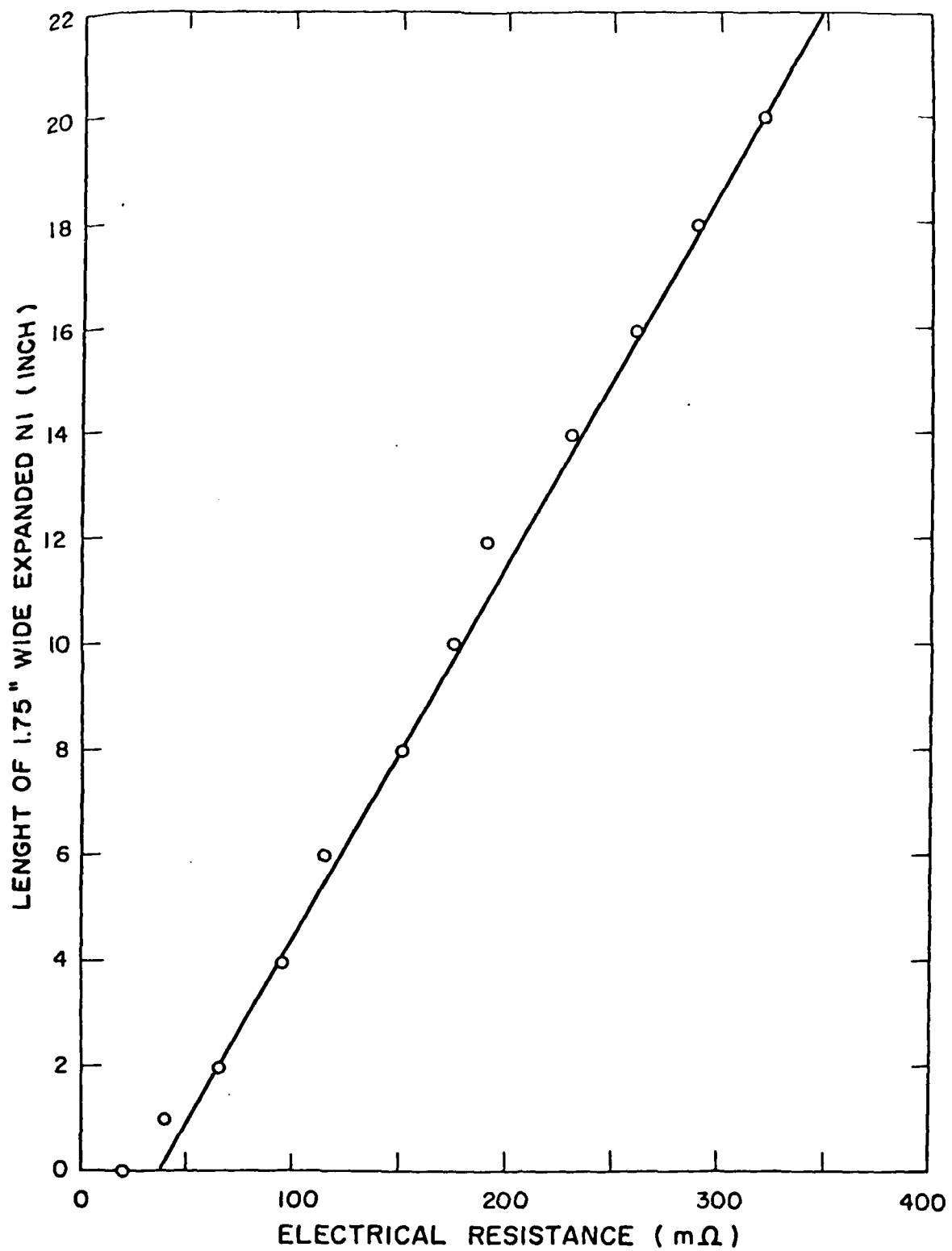


Figure 10. Electrical resistance of expanded Ni cathode current collector.

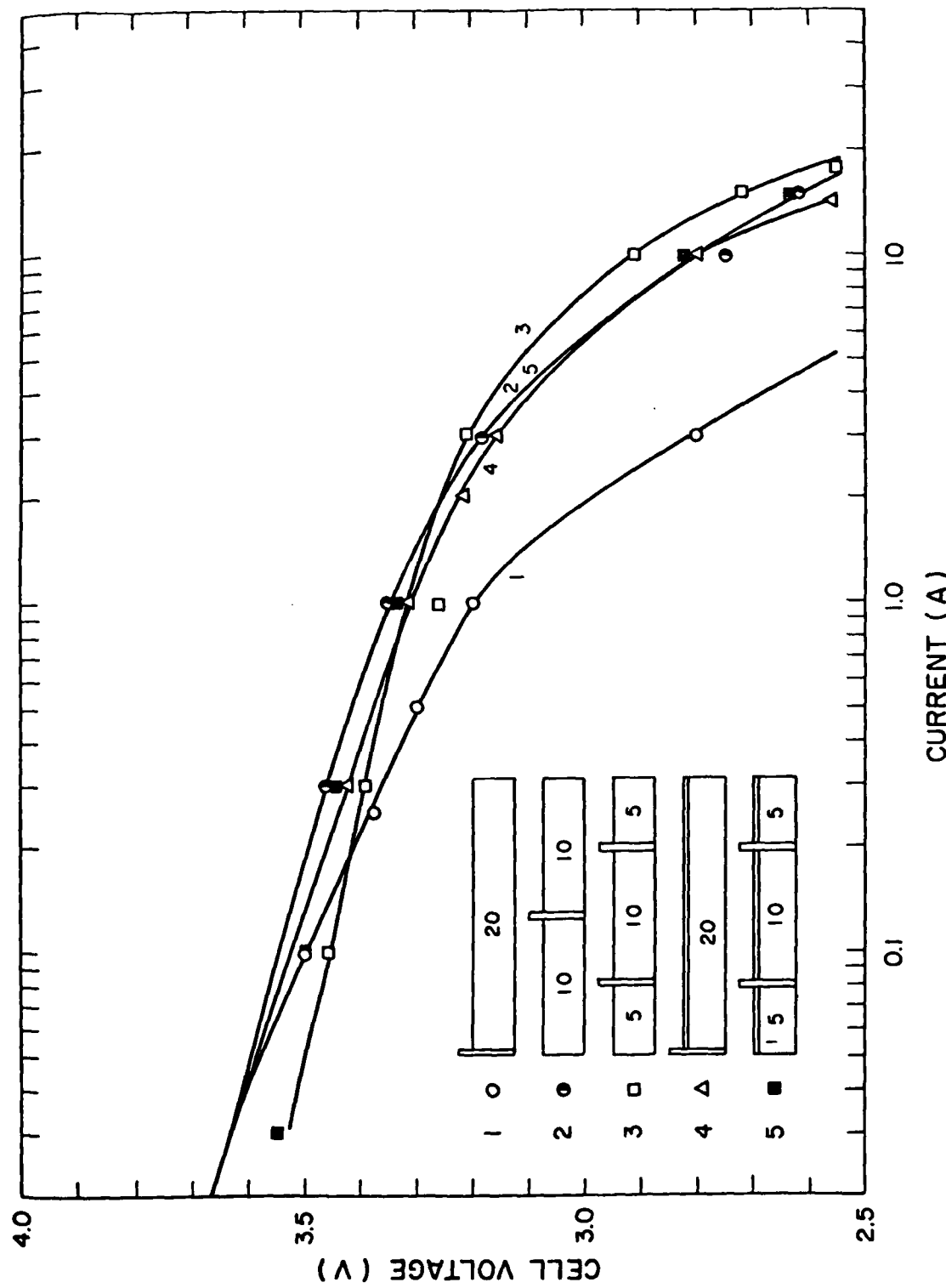


Figure 11. Polarization characteristics of D cells with 20 inch cathodes of various current collector designs.

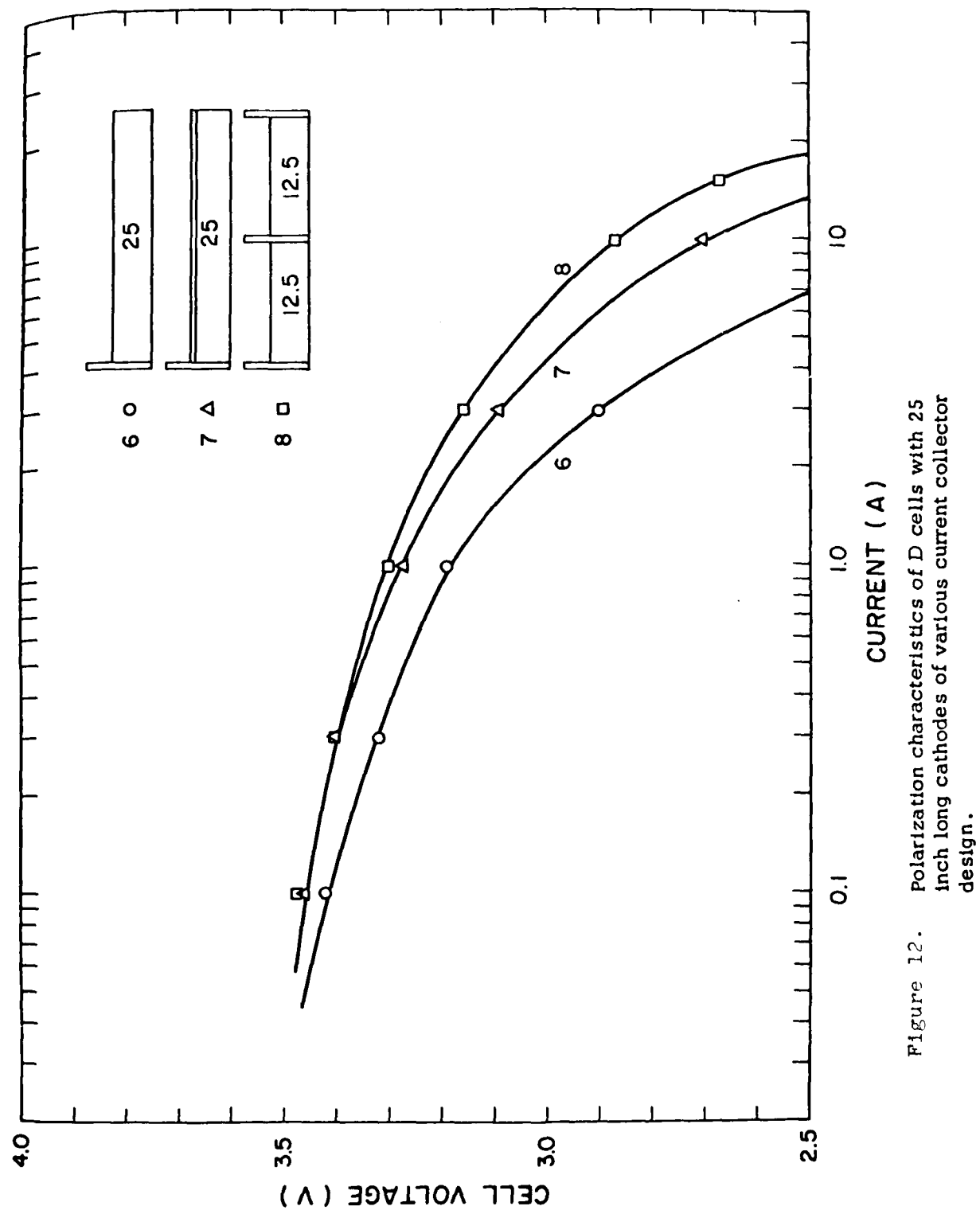


Figure 12. Polarization characteristics of D cells with 25 inch long cathodes of various current collector designs.

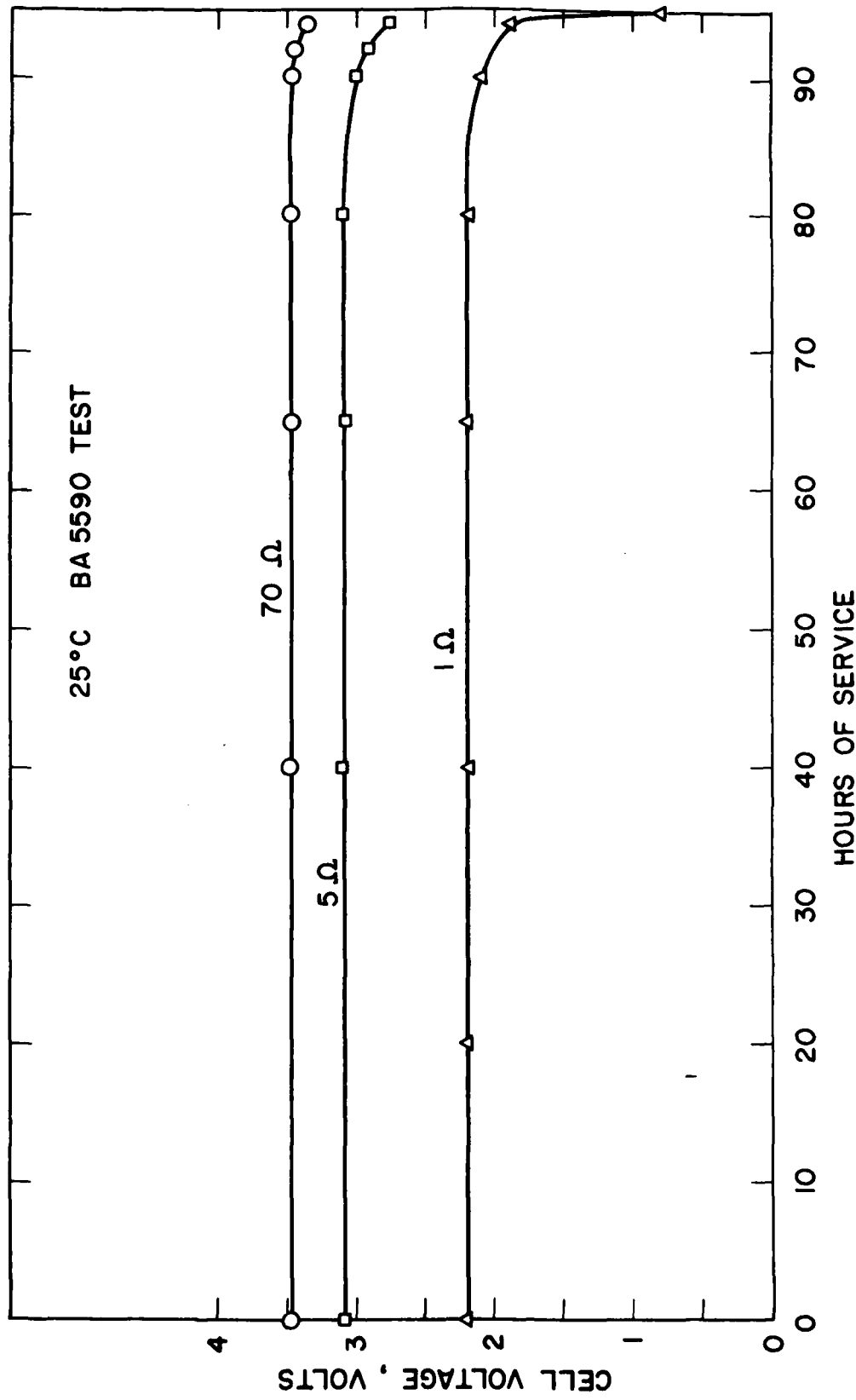


Figure 13. Performance of high rate Li/SOCl<sub>2</sub> D cell on prorated BA5590 test at 25°C

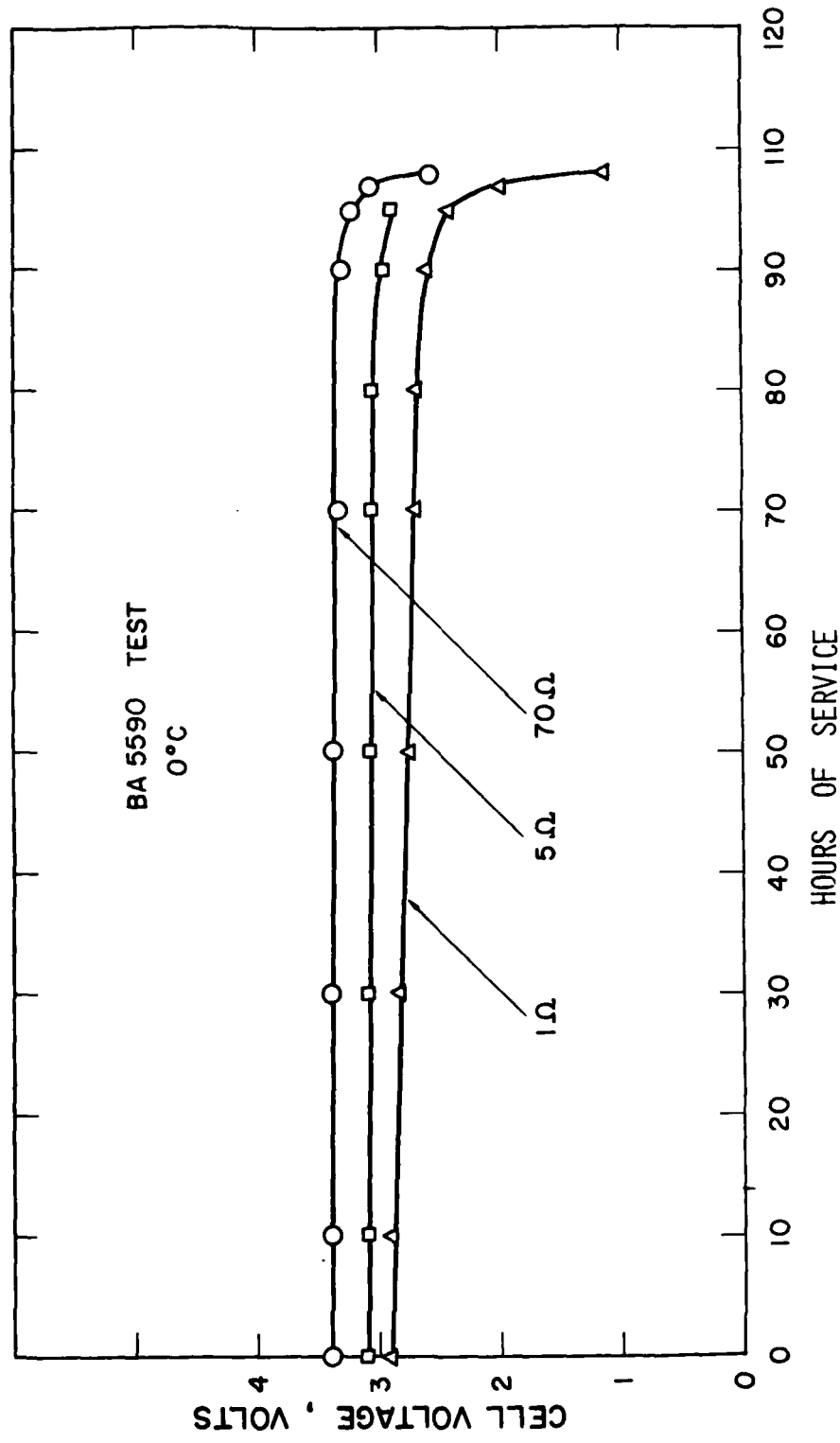


Figure 14. Performance of high rate Li/SOCl<sub>2</sub> D cell on prorated BA5590 test at 0°C

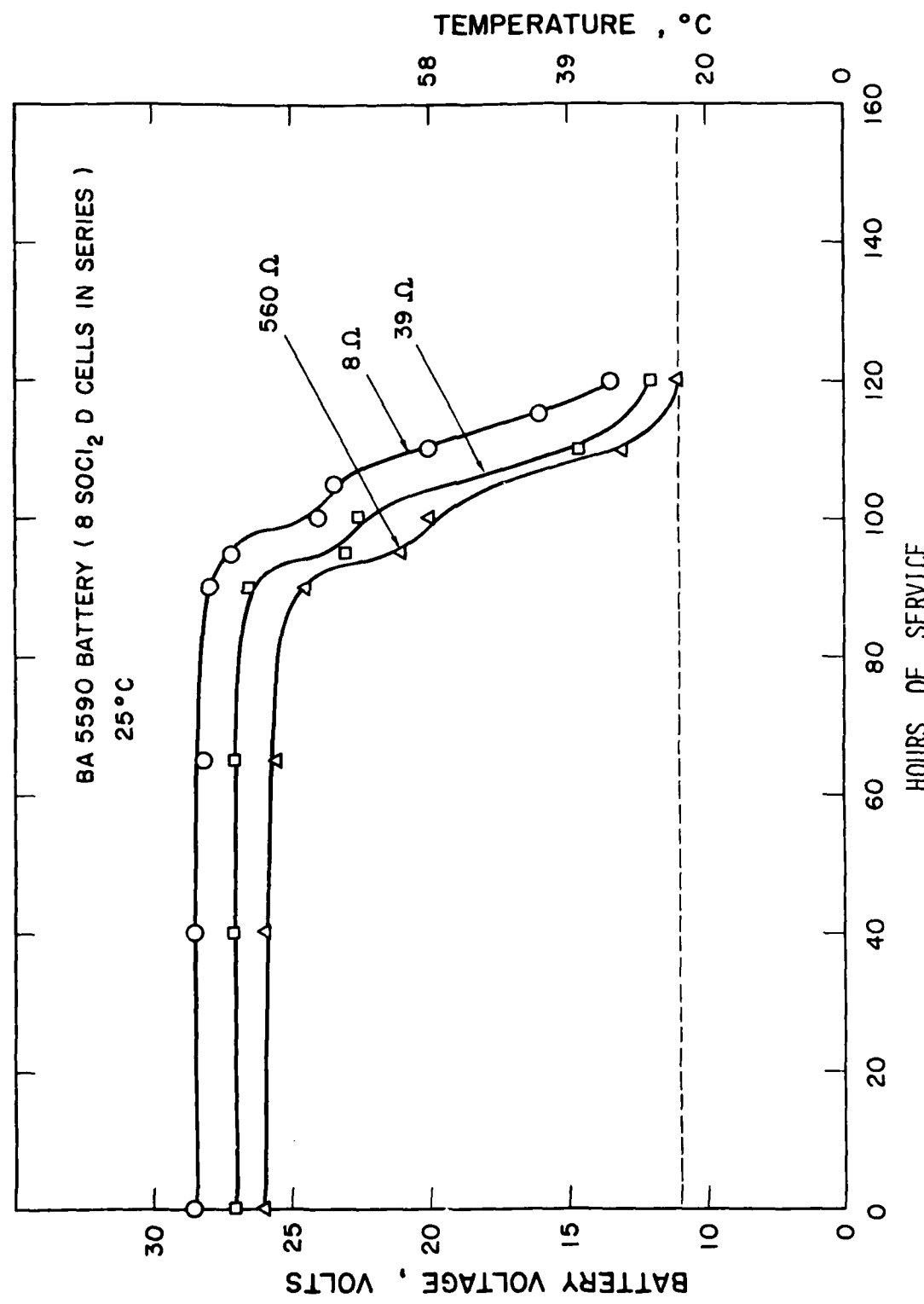


Figure 1c. Performance of BA 5590 battery of  $\text{SOCl}_2$ -D cells in series at  $25^{\circ}\text{C}$

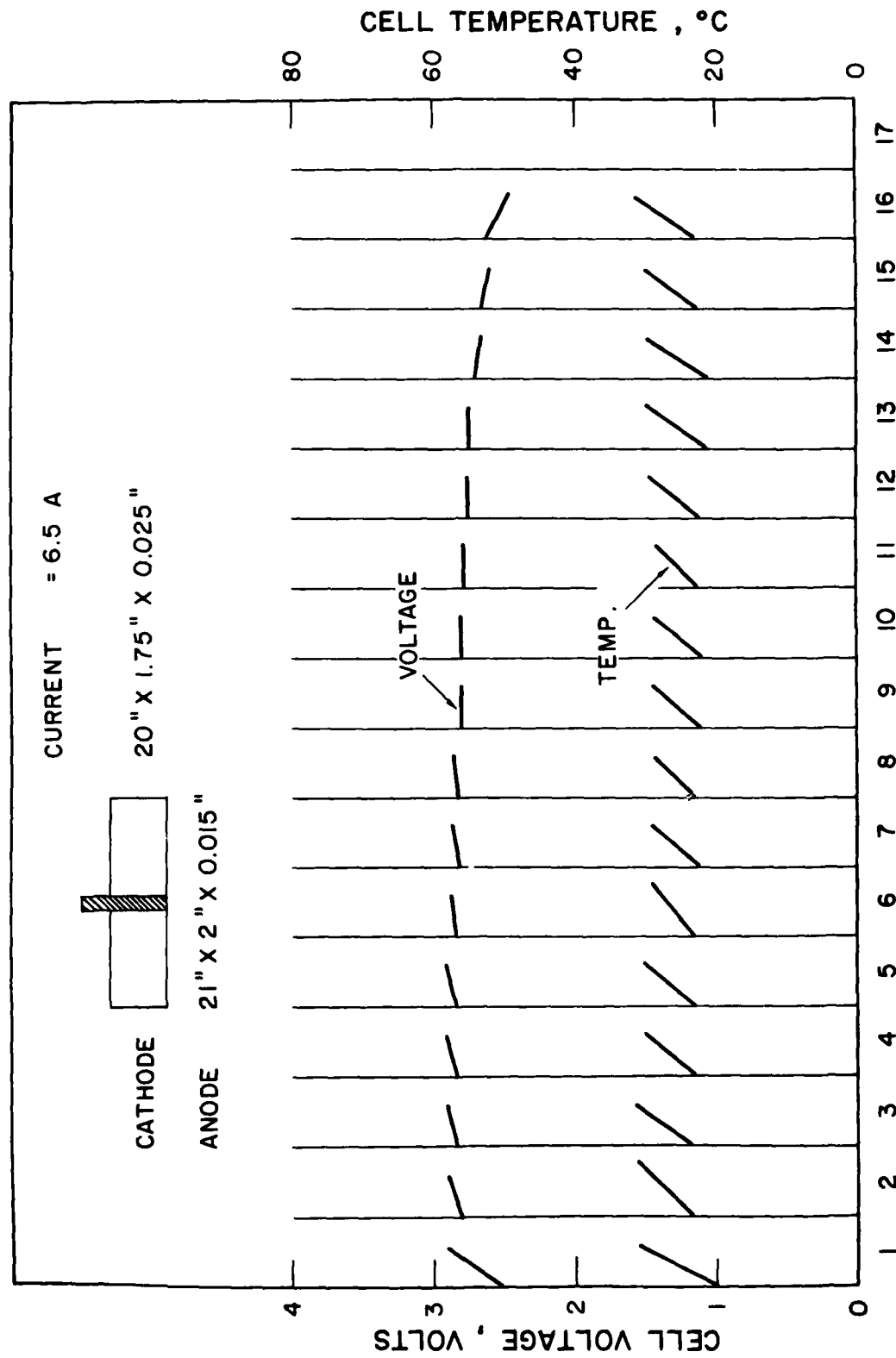


Figure 16. Voltage and temperature profiles of  $\text{Li}/\text{SOCl}_2$  cell of design #2 on modified GLLD test using a 6.5A pulse at 25°C

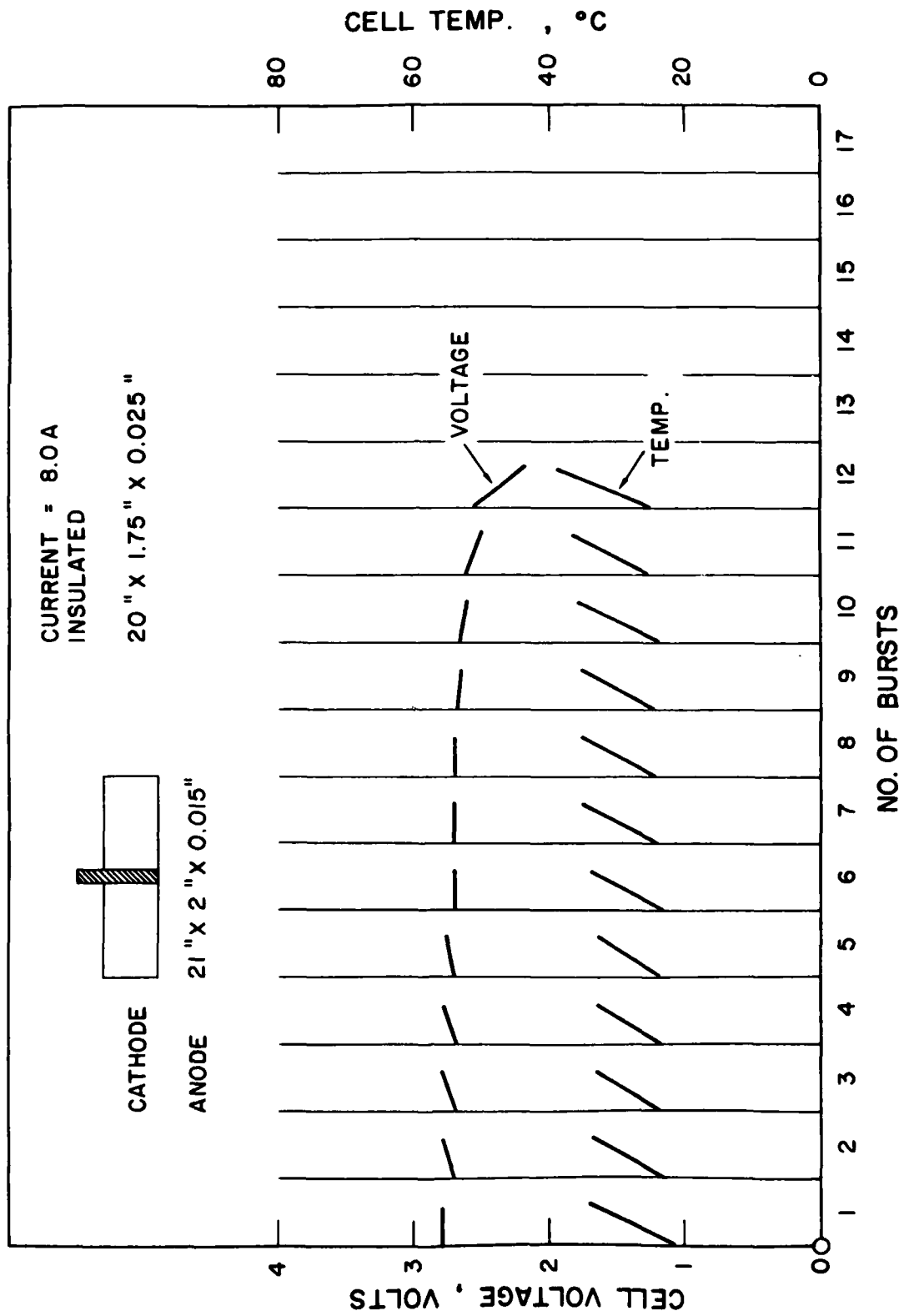


Figure 17. Voltage and temperature profiles of an insulated Li/SOCl<sub>2</sub> cell of design #2 on modified GLLP test using an 8.0A pulse at 25°C

100.

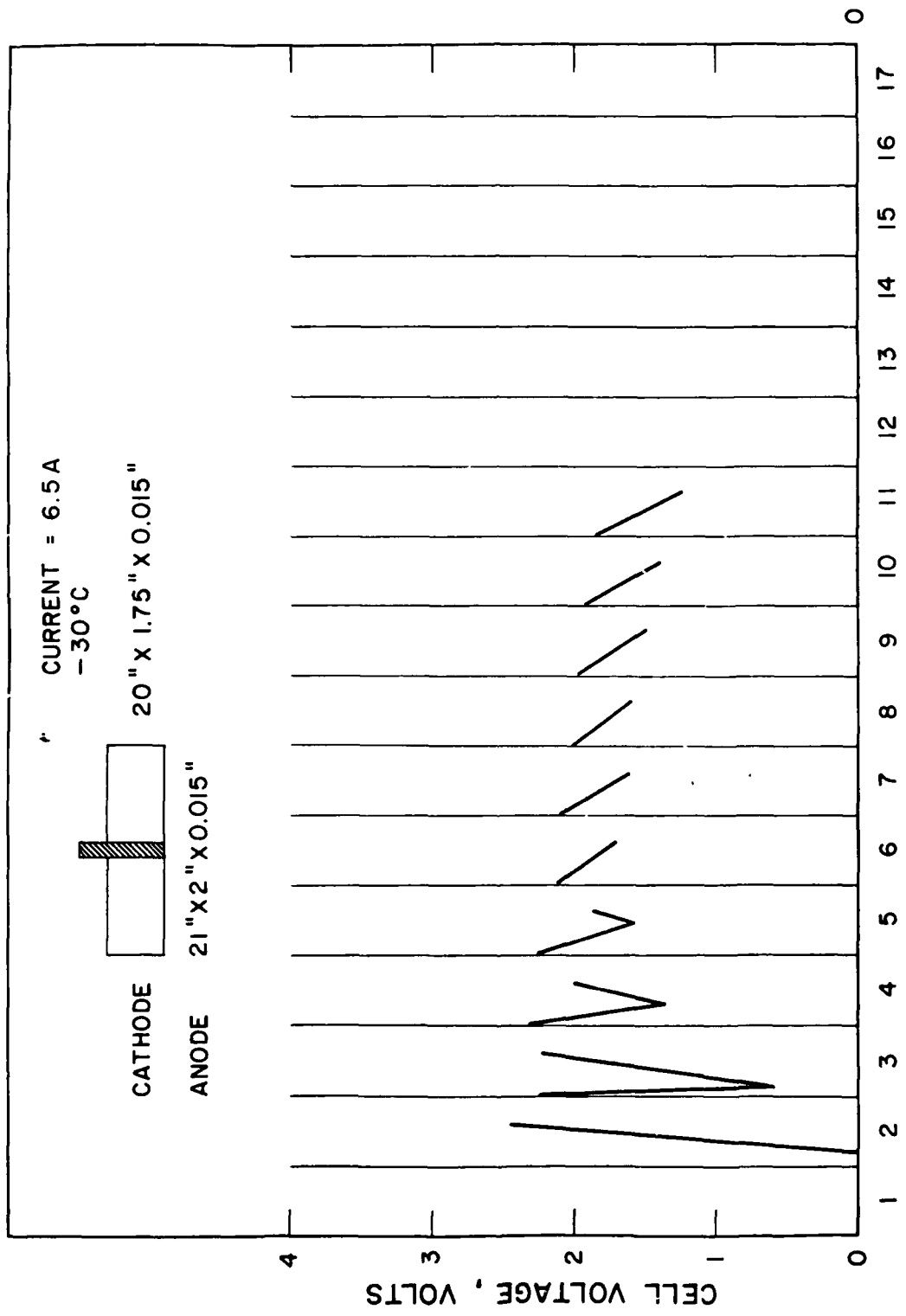
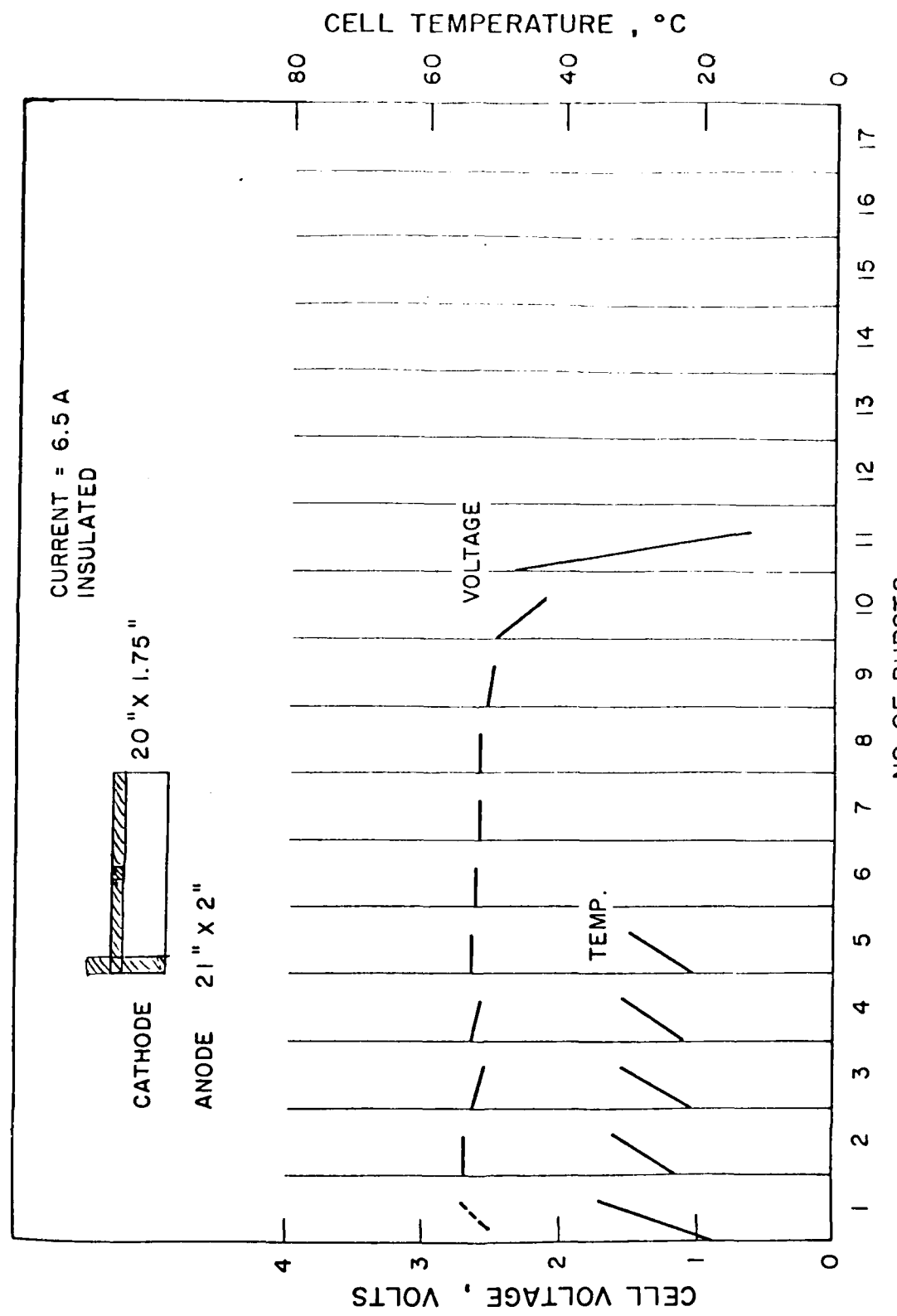


Figure 1a. Voltage profiles of Li/SOCl<sub>2</sub> cell of design #2 on modified Gurn test using a 6.5A pulse at -30°C.

101.



102.

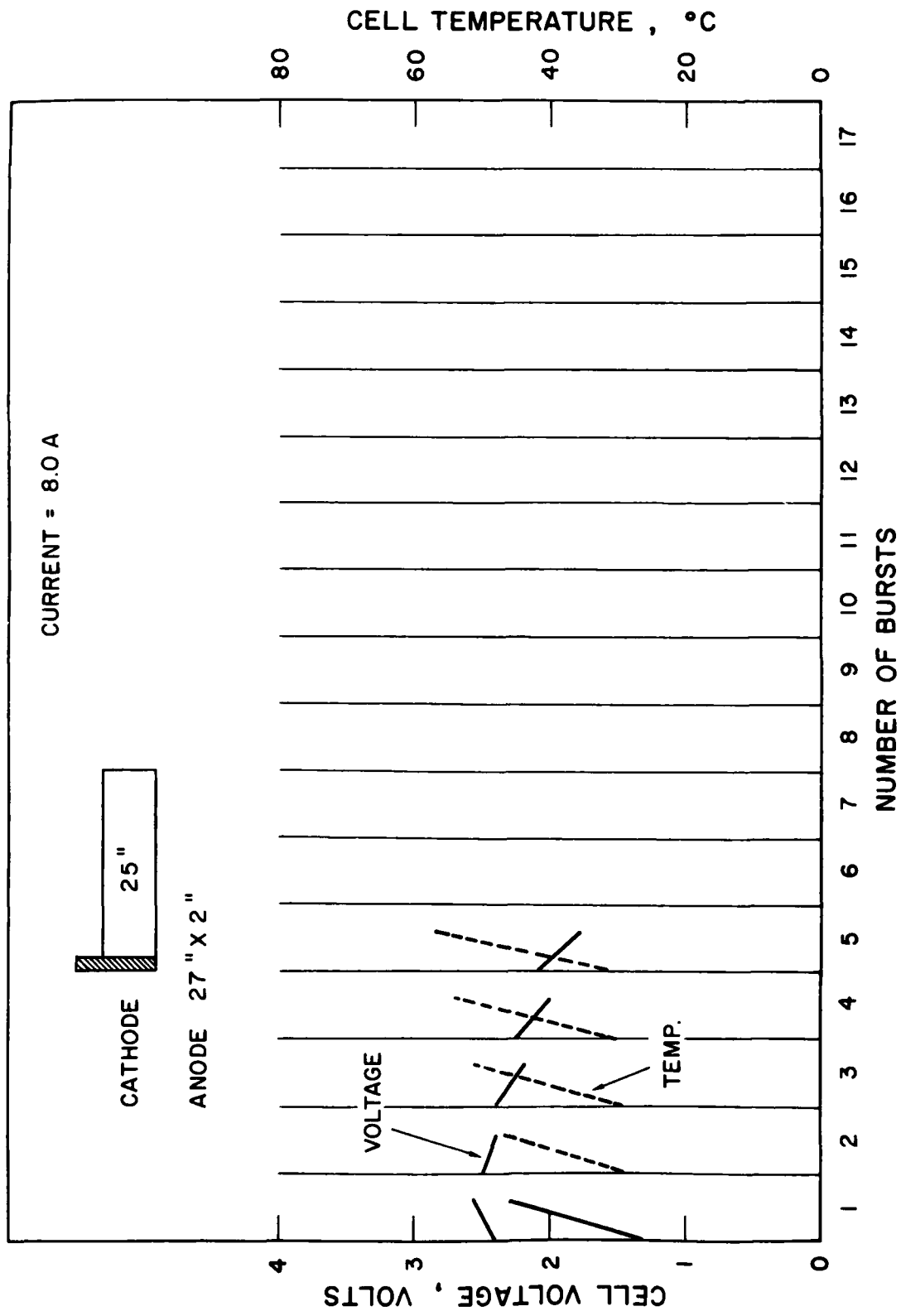


Figure 20. Voltage and temperature profiles of Li/SOCl<sub>2</sub> D cell of design #6 on the modified GLLD test using an 8A pulse at 25°C.

103.

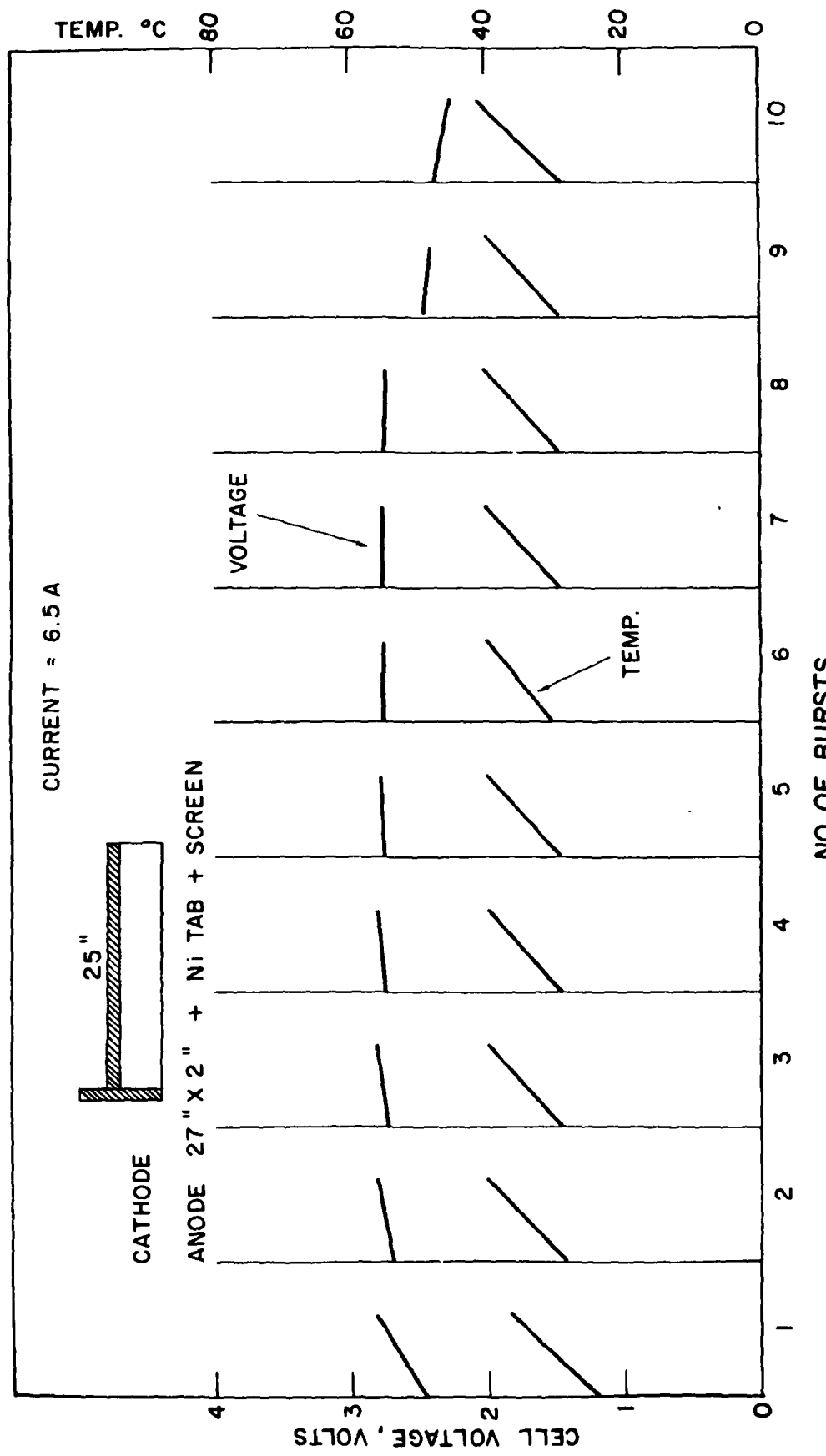


Figure 21. Voltage and temperature profiles of Li/SOCl<sub>2</sub> cells of design #7 on modulated SLD test using a 6.5A pulse at 25°C.

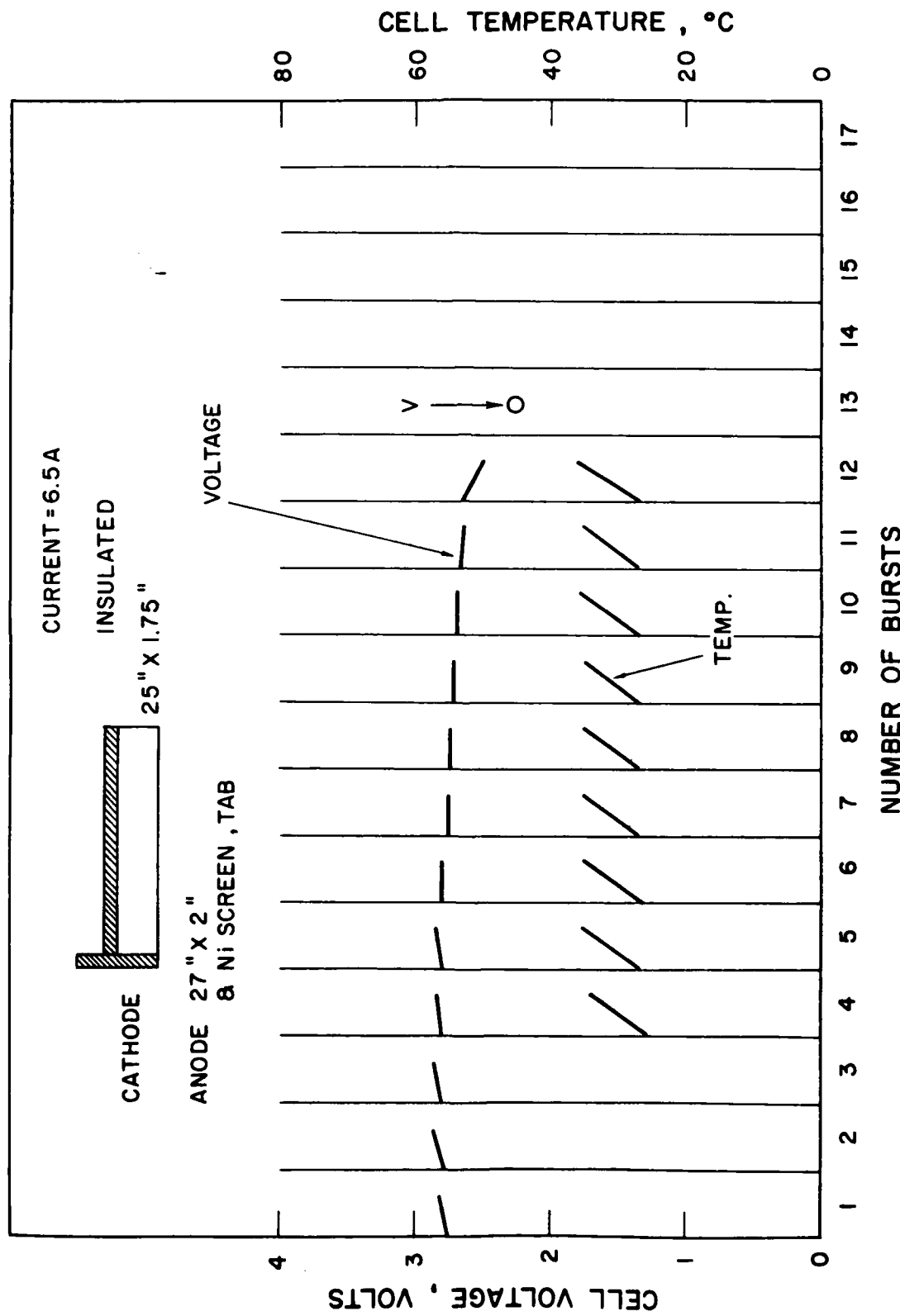
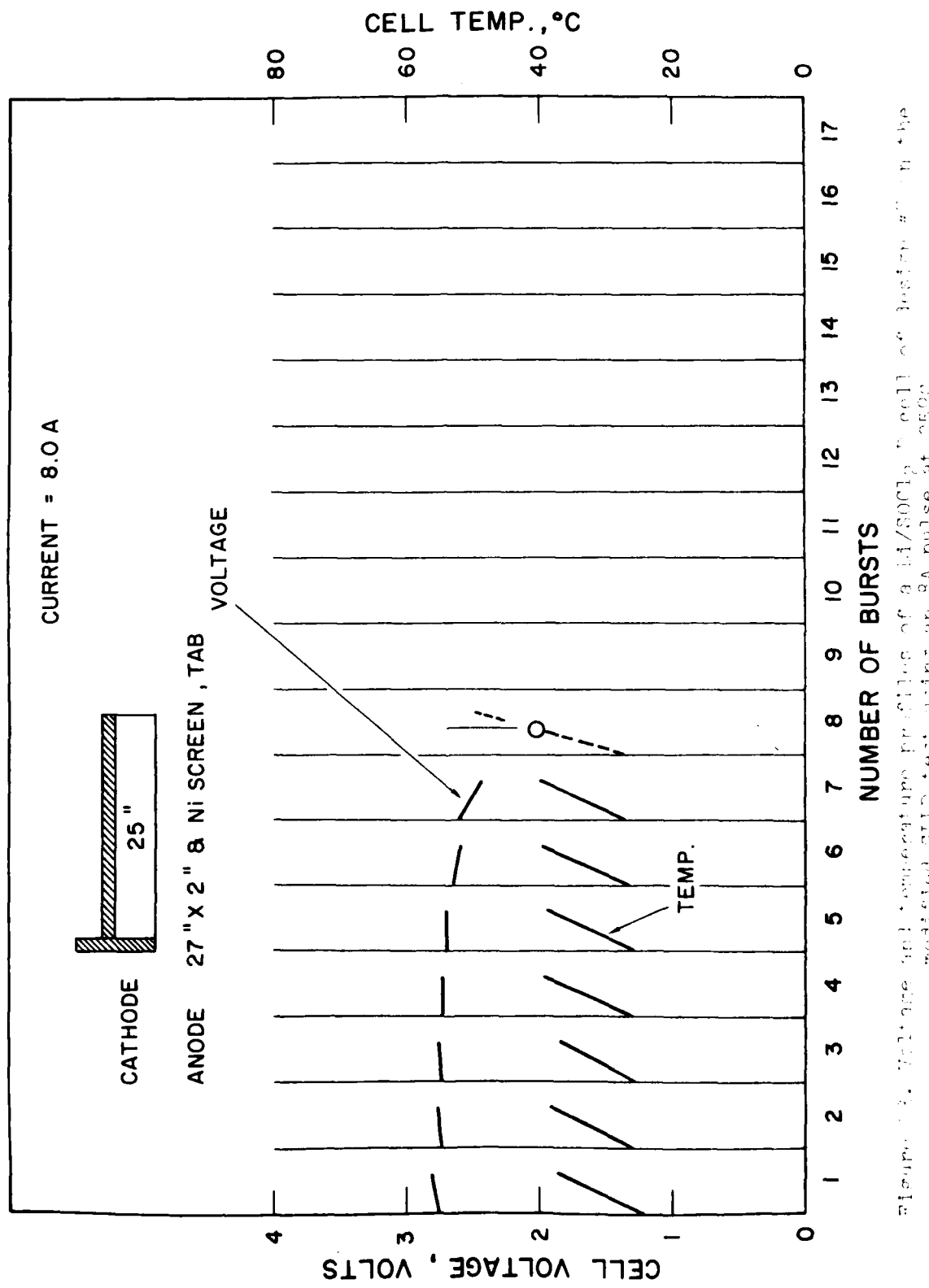


Figure 22. Voltage and temperature profiles of an insulated Li/SOCl<sub>2</sub> D cell of design #7 on modified GLLD test using a 6.5A pulse at 25°C.

105.



106.

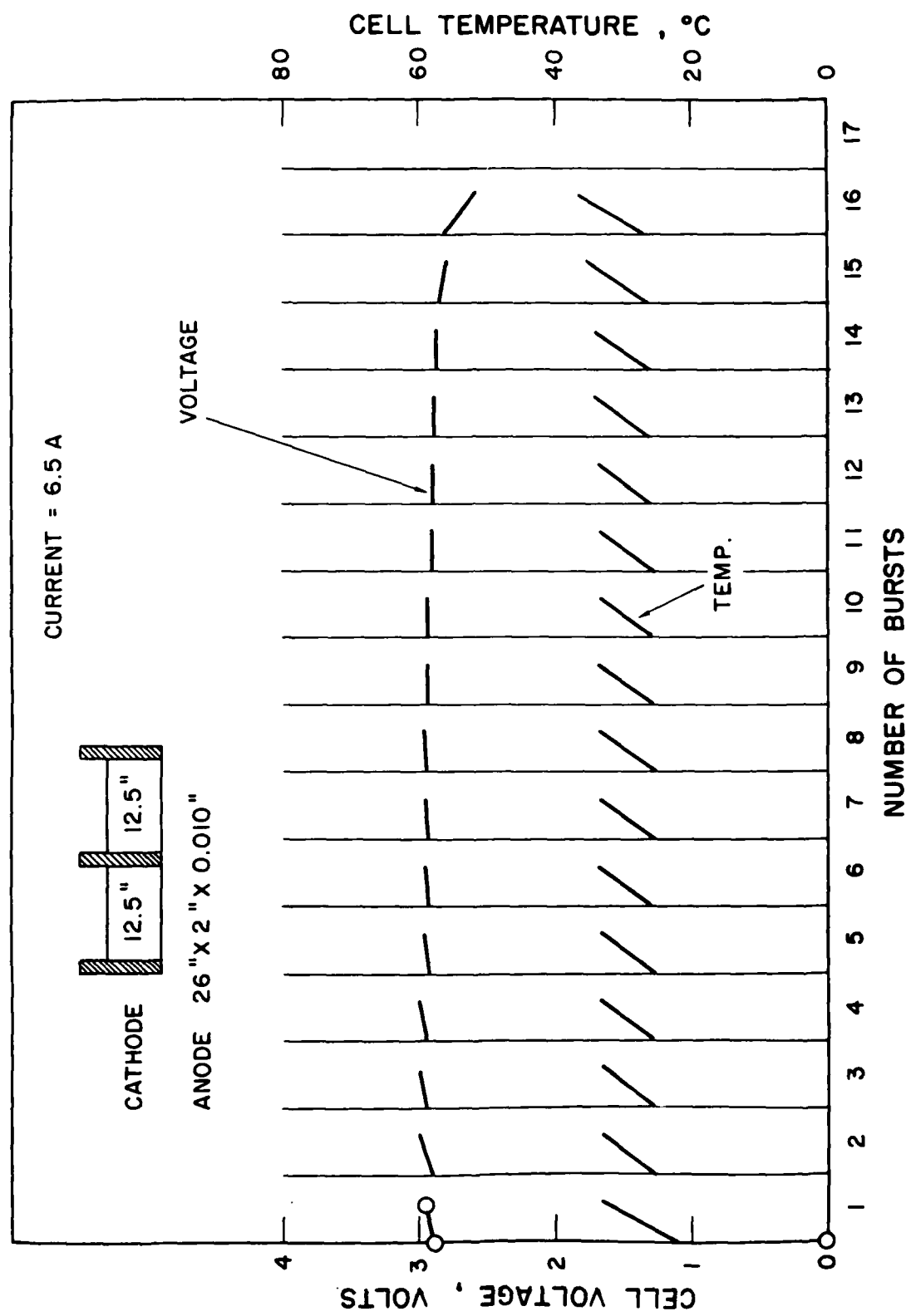


Figure 2h. Voltage and temperature profiles of a Li/SOCl<sub>2</sub> D cell of design #2 on the modified GLLD test using a 6.5A pulse at 25°C

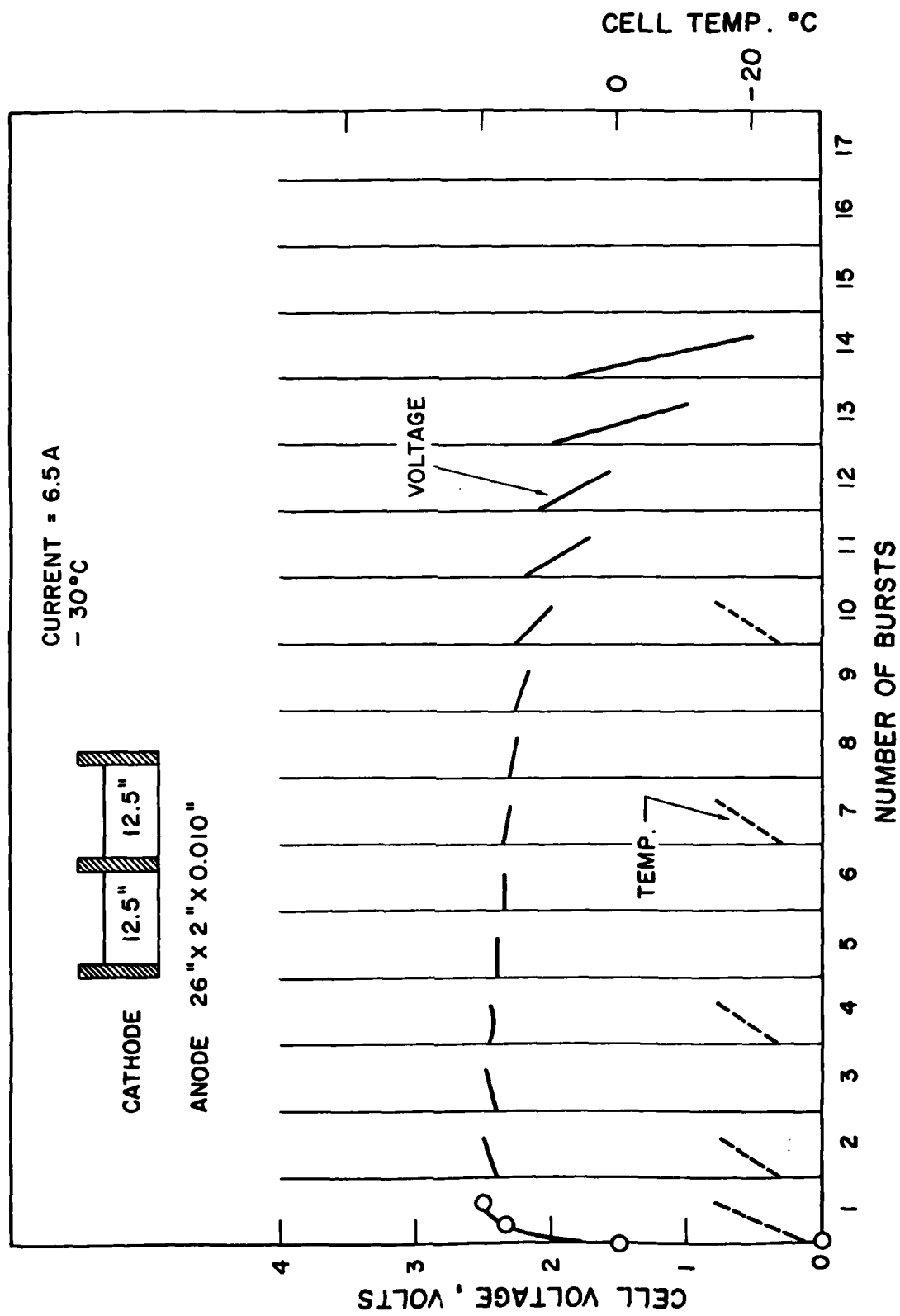


Figure 25. Voltage and temperature profiles of a Li/SOCl<sub>2</sub> D cell of design #8 on the modified GLID test using a 6.5A pulse at -30°C.

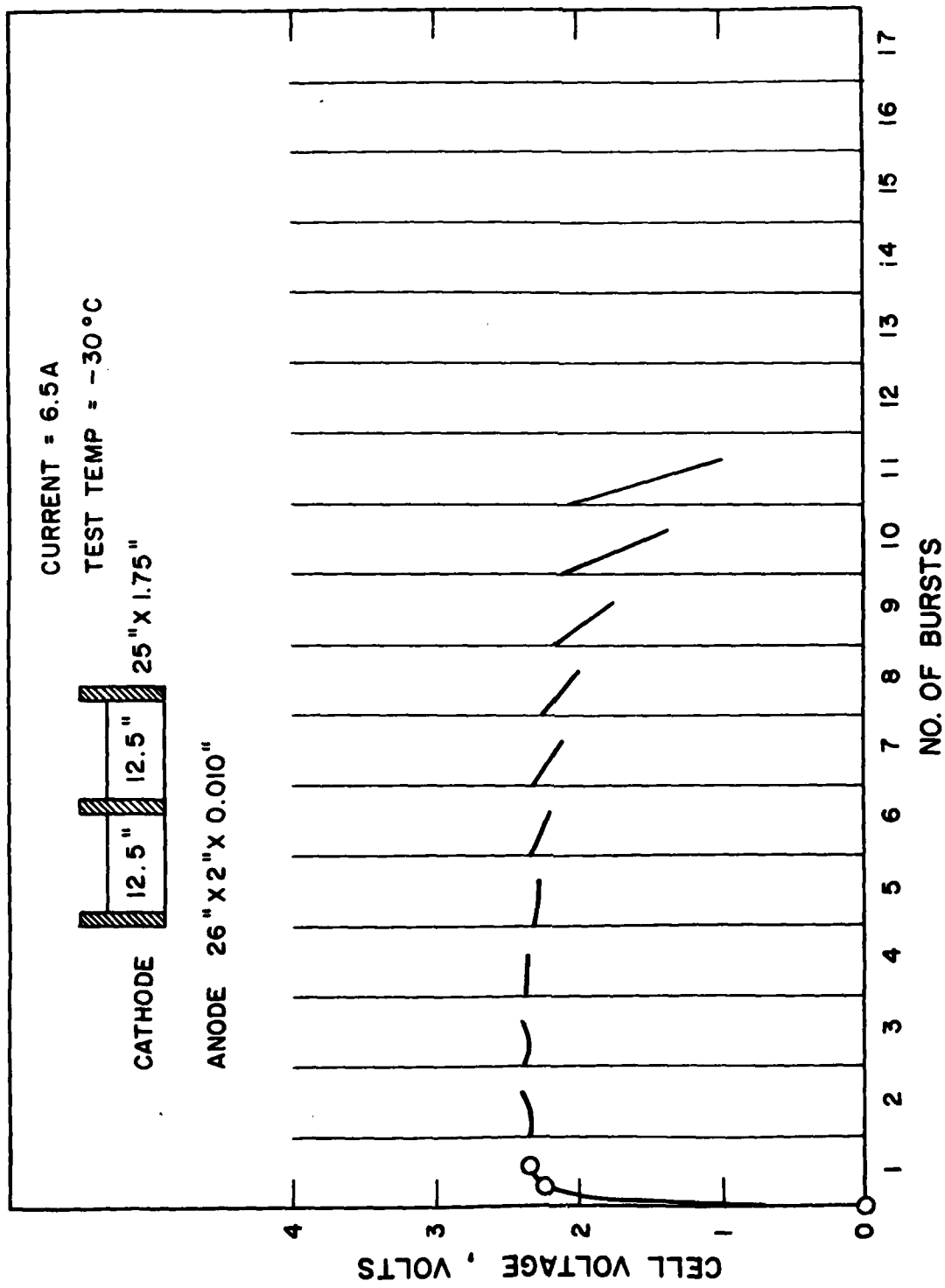


Figure 26. Voltage and temperature profiles of a Li/SOCl<sub>2</sub> D cell of design #8 on the modified GLID test using a 6.5A pulse at -30°C.

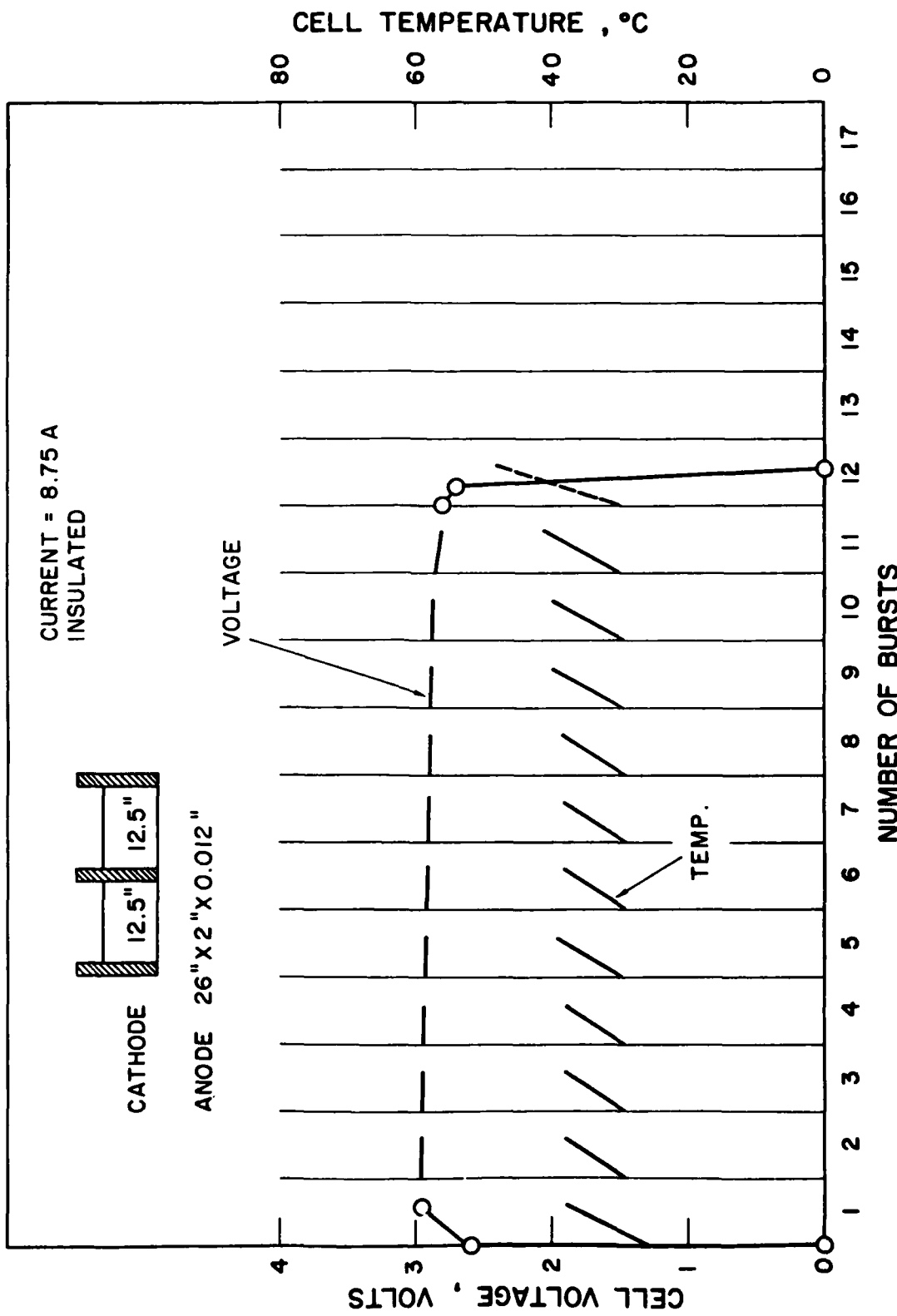


Figure 27. Voltage and temperature profiles of an insulated Li/SOCl<sub>2</sub> D cell of design #8 on the modified GLLD test using a 8.75A pulse at 25°C.

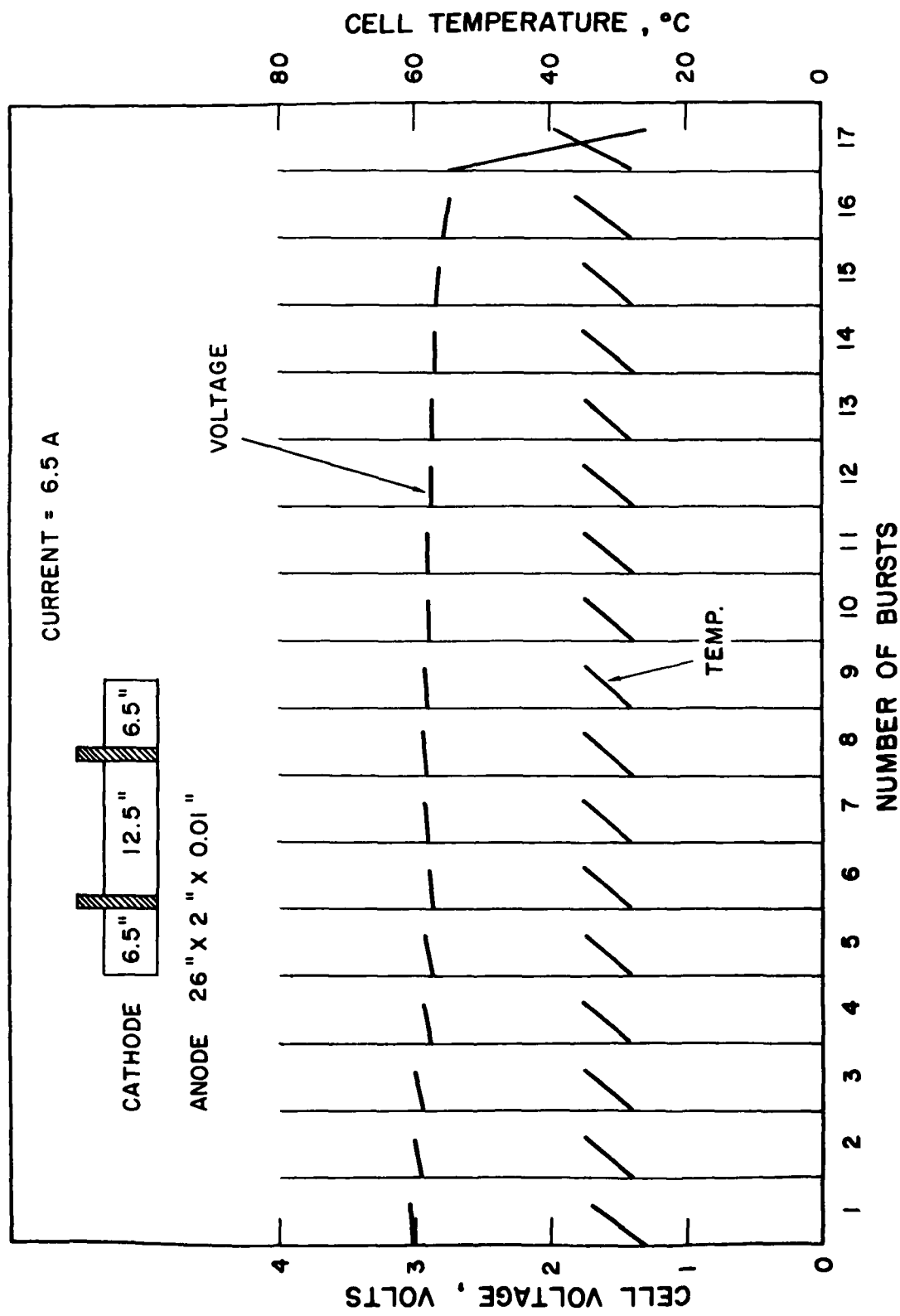


Figure 28. Voltage and temperature profiles of an insulated Li/SOCl<sub>2</sub> D cell of design #9 on the modified GLLD test using a 6.5A pulse at 25°C.

111.

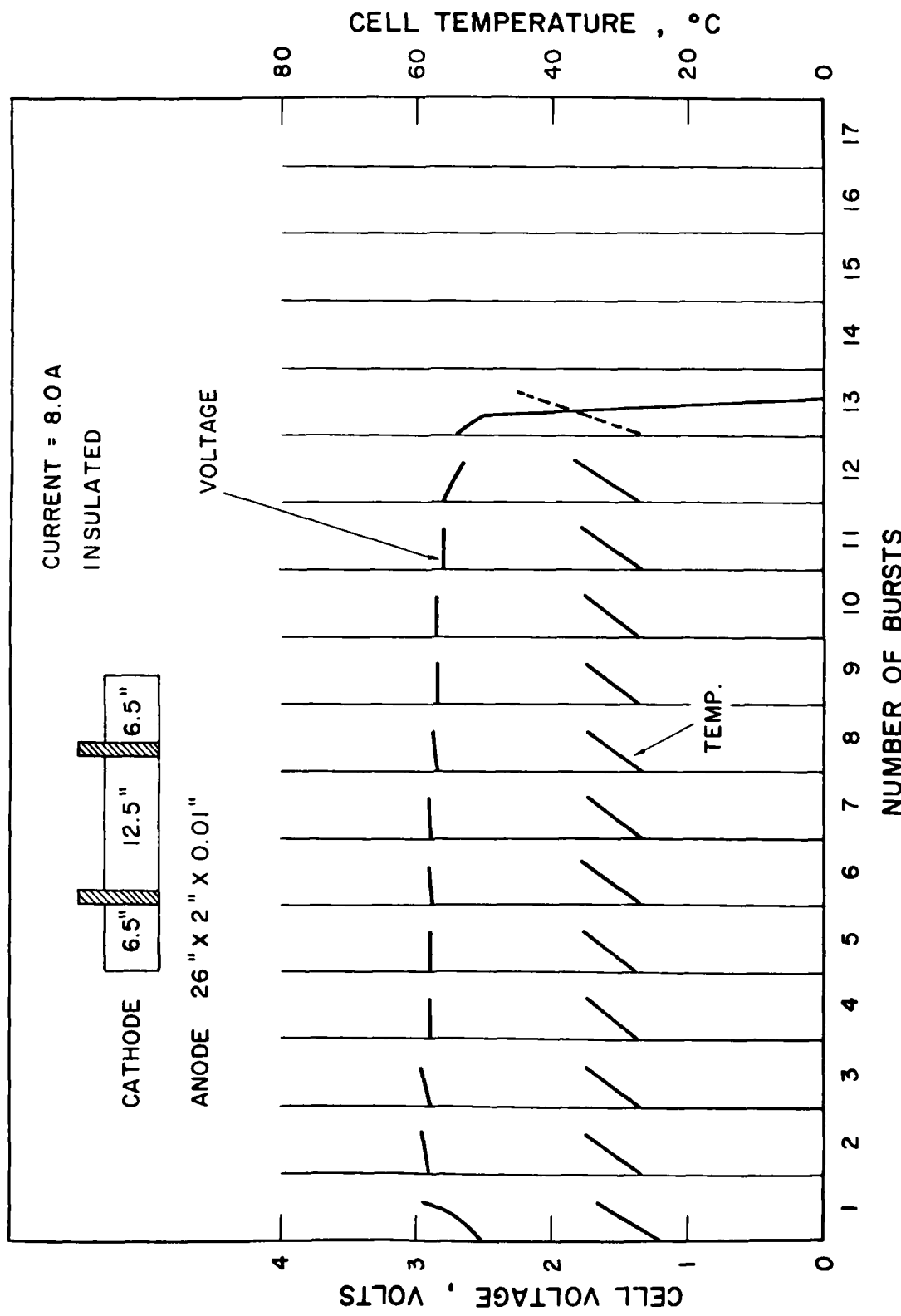


Fig. 111. Voltage and temperature profiles of an insulated Li/SOCl<sub>2</sub> cell at 8.0A  
#3 on the modified G.I.R. test using a 8.0A pulse at 30°.

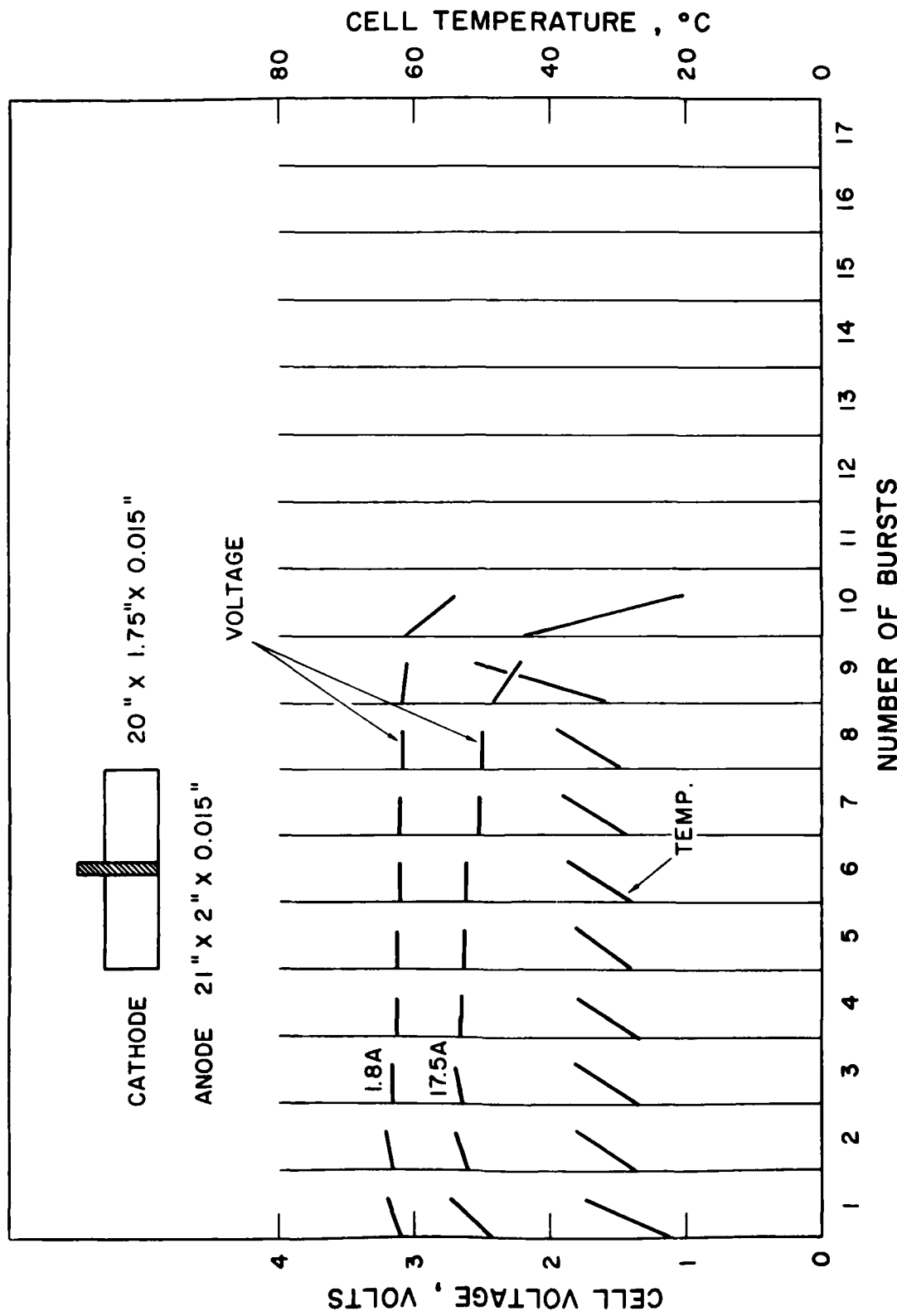


Figure 20. Voltage and temperature profiles of two parallel connected Li/SOCl<sub>2</sub> cells of design #7 on the GLLD test using the old duty cycle at 25°C.

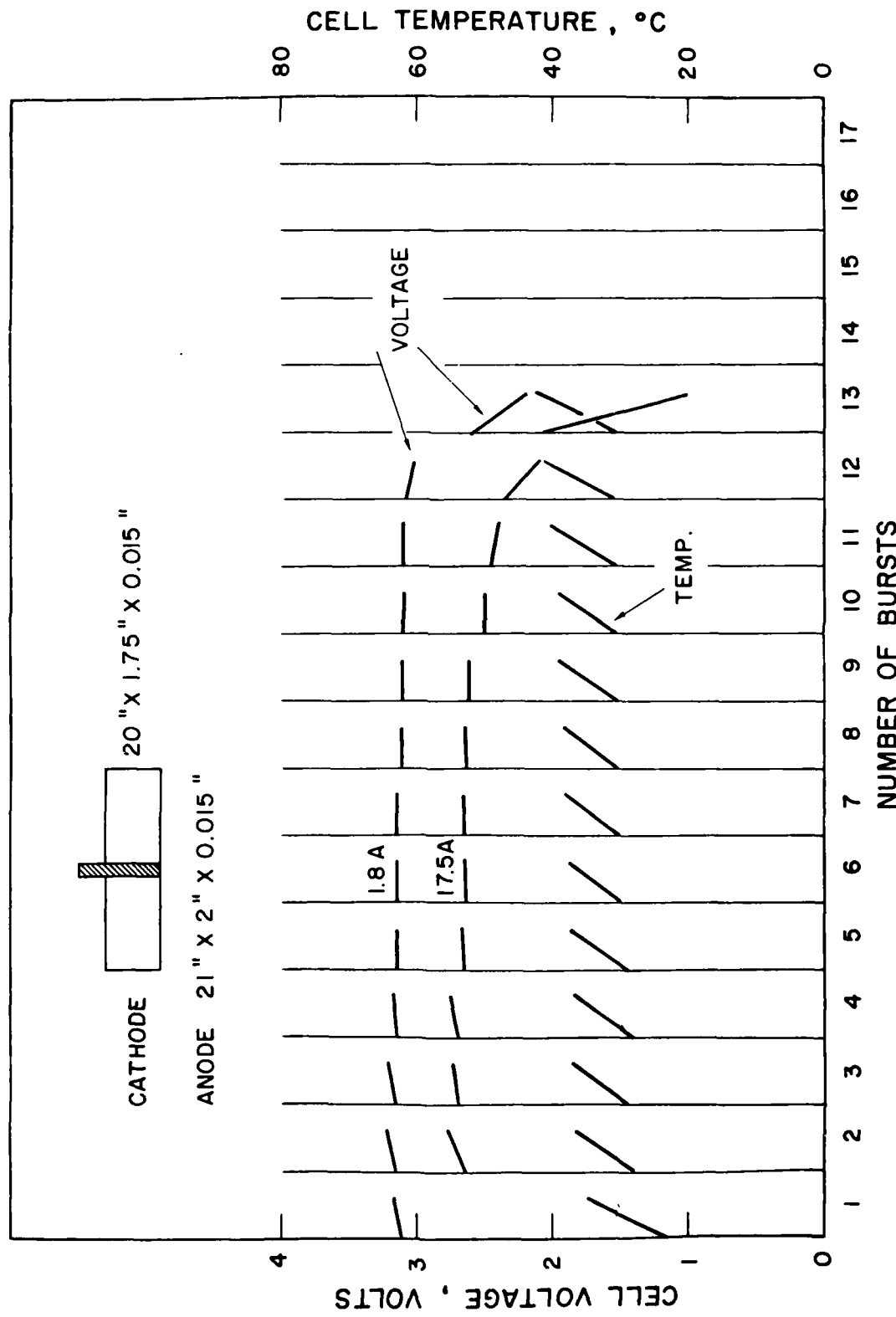


Figure 31. Voltage and temperature profiles of two parallel connected Li/SOCl<sub>2</sub> cells of design #2 on the CIND test using the old duty cycle at 25°C.

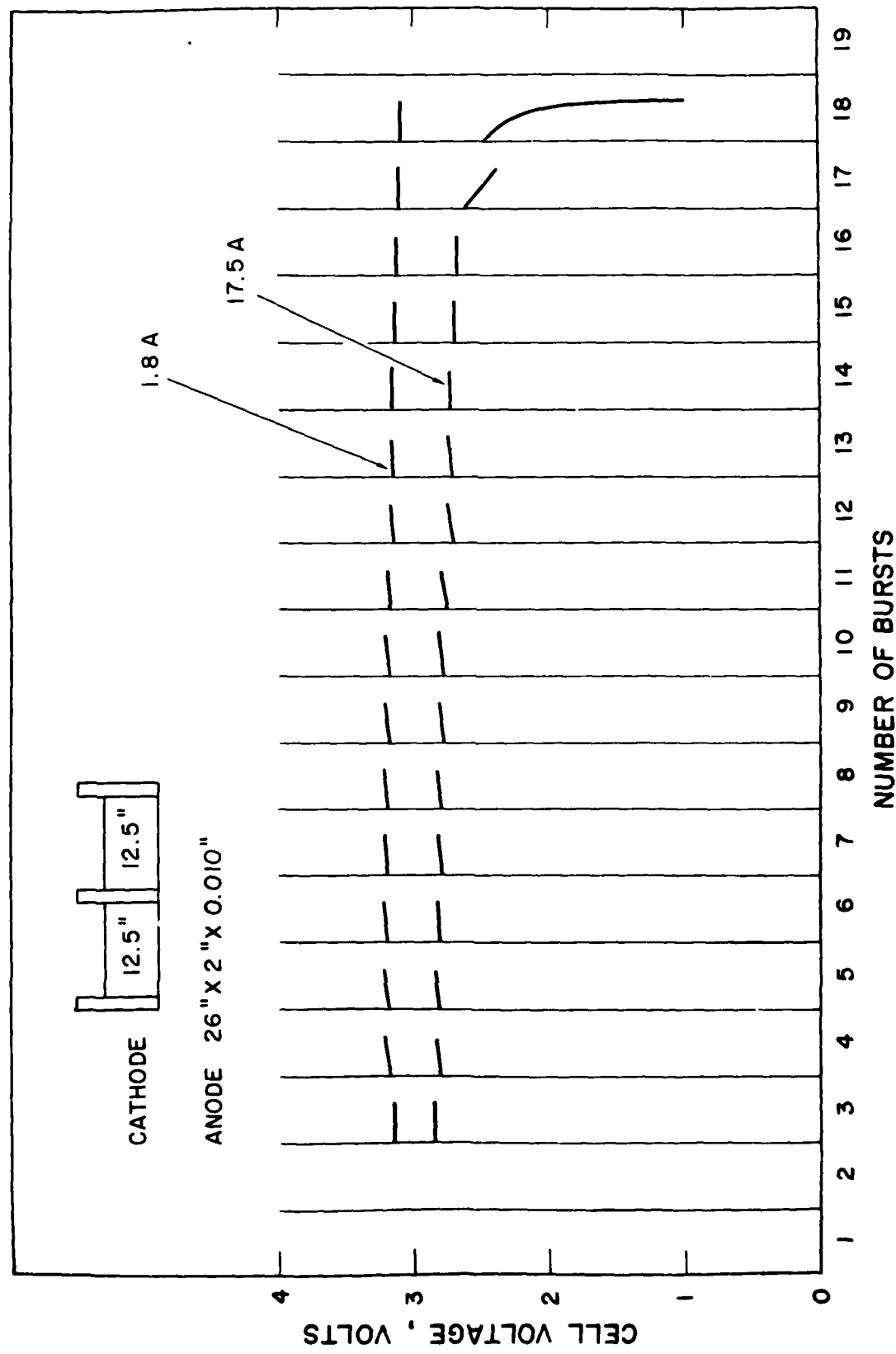


Figure 32. Voltage and temperature profiles of two parallel connected Li/SOCl<sub>2</sub> cells of design #2 on G.M.D load using the old duty cycle at 25°C.

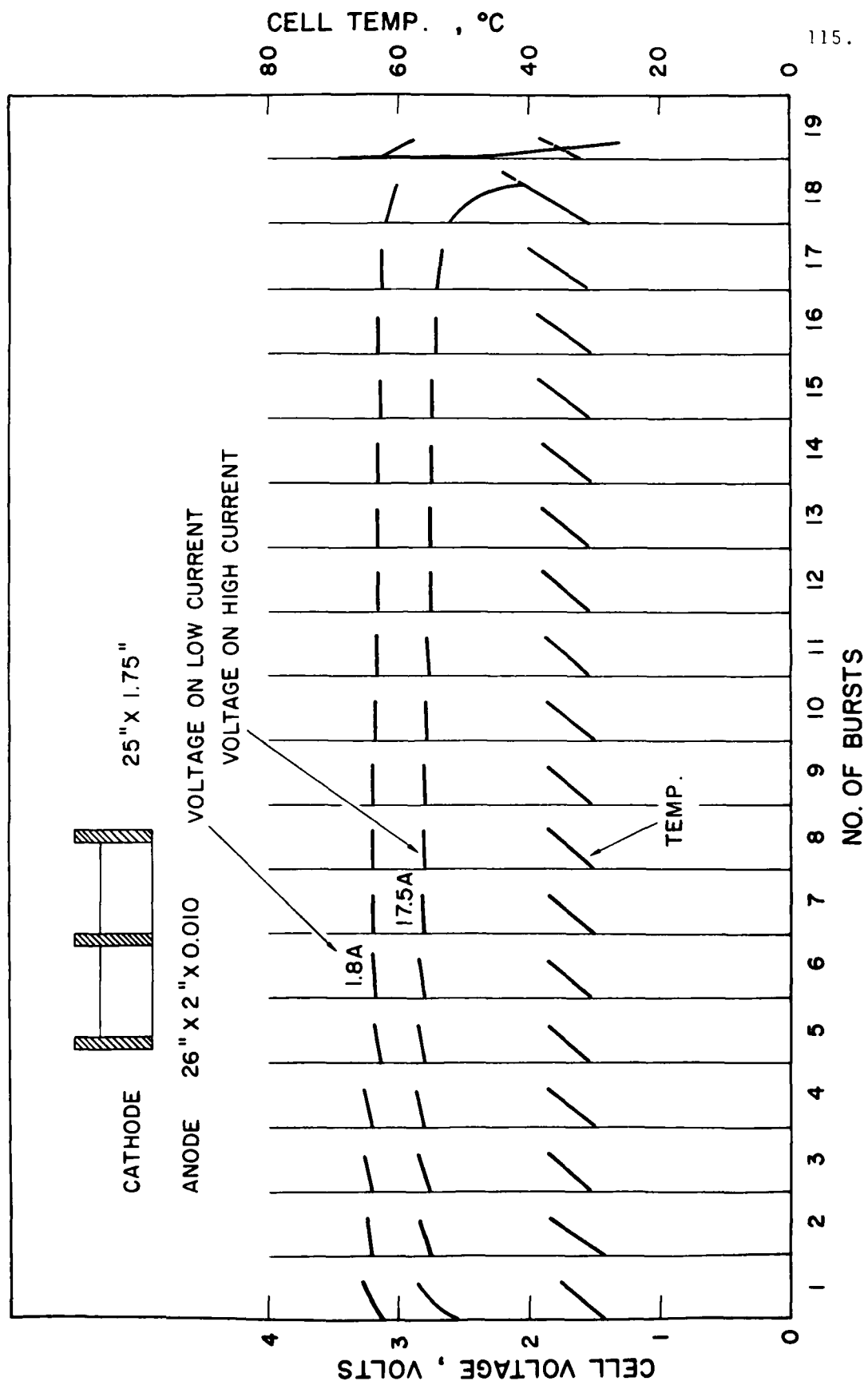


Figure 2. Voltage and temperature profiles of two parallel connected Li/SOCl<sub>2</sub> cells of section #2 (with heat shrinkable jackets) on GALT test using the old duty cycle at 100%.

115.

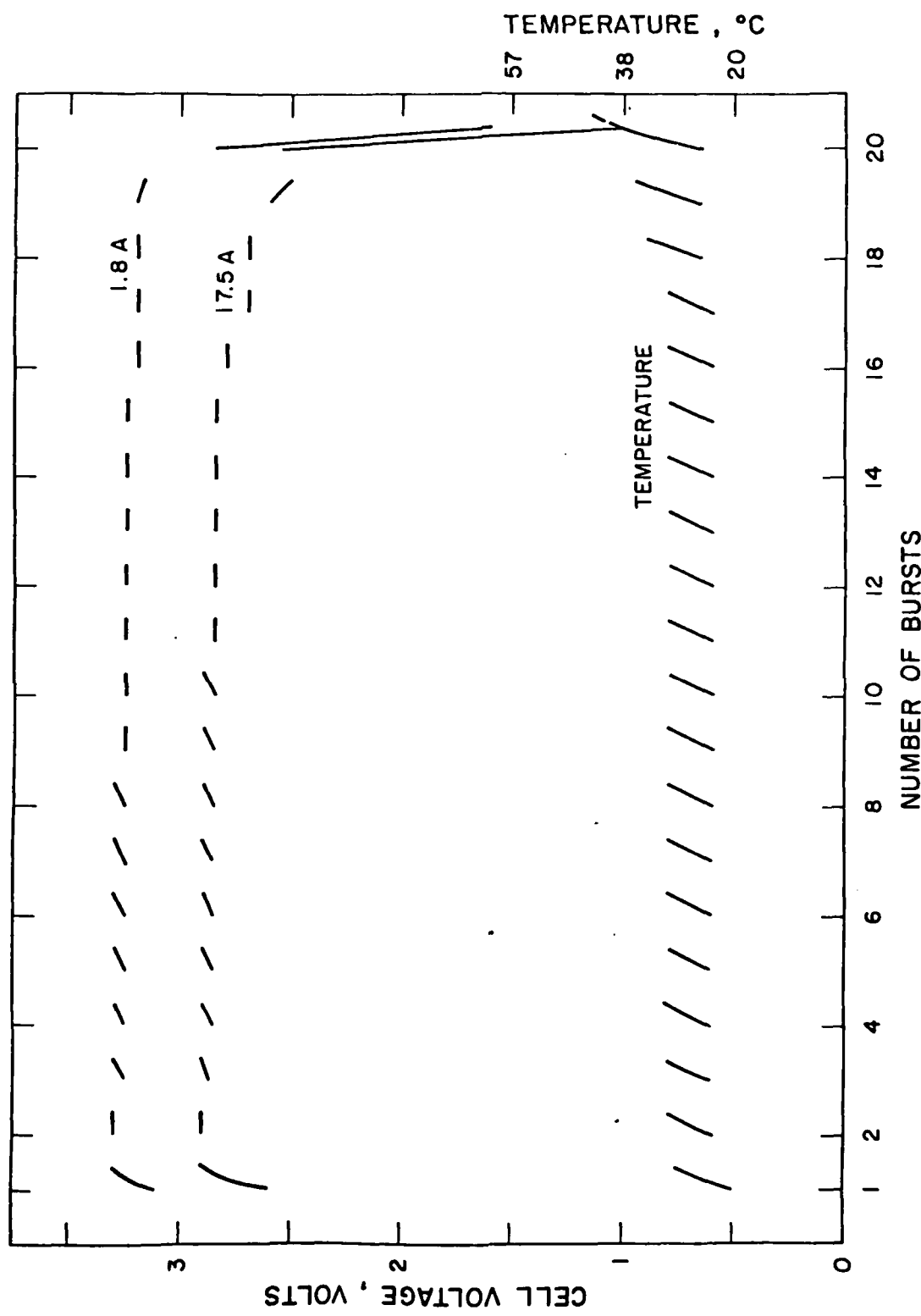


Figure 33a. Performance of two D cells with cathode additive 1, level A on old GLID duty cycle load

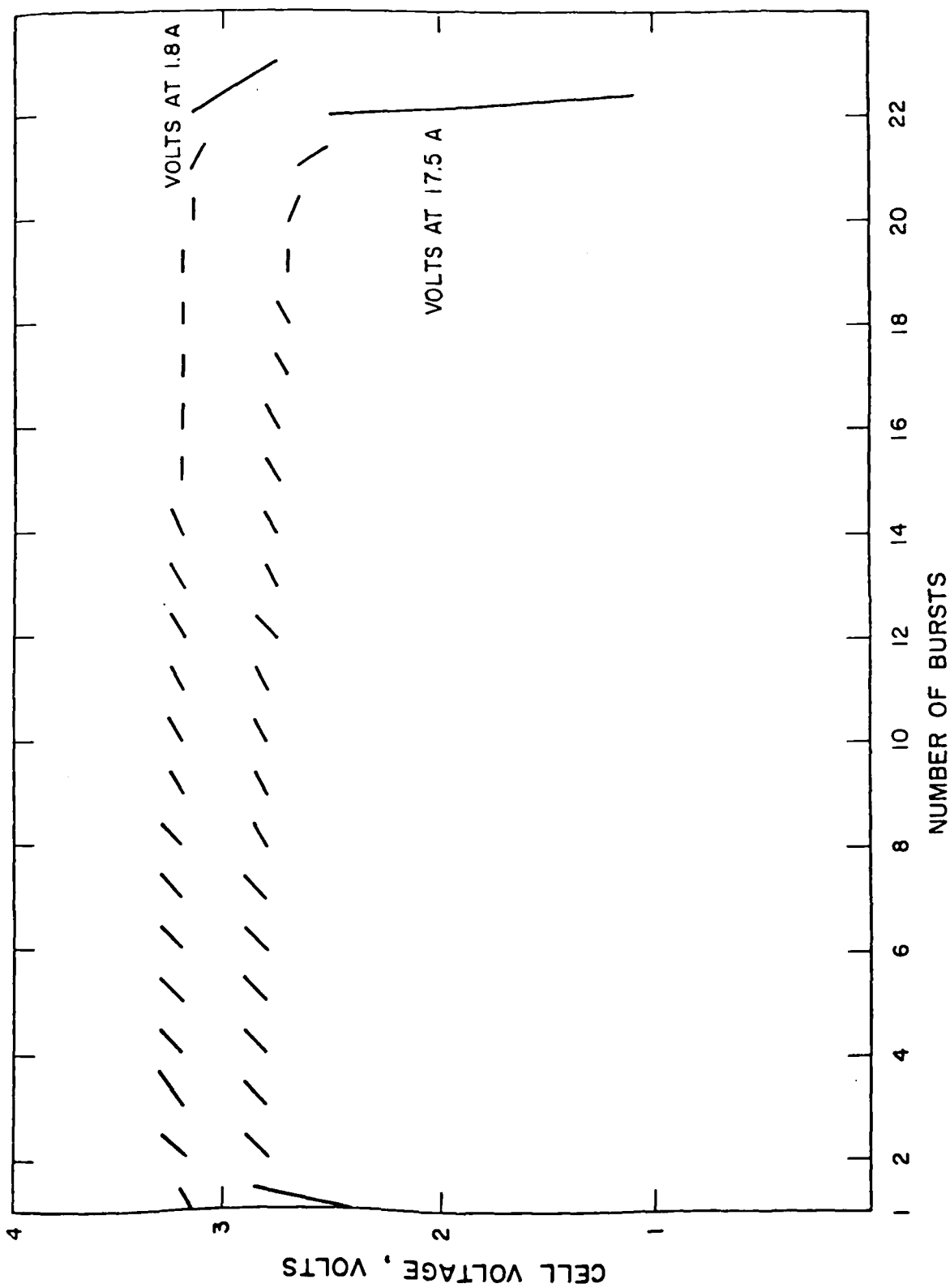


Figure 21. Nonuniform aging two cells with initial voltage 1, level 2 on GIMP test using the old duty cycle.

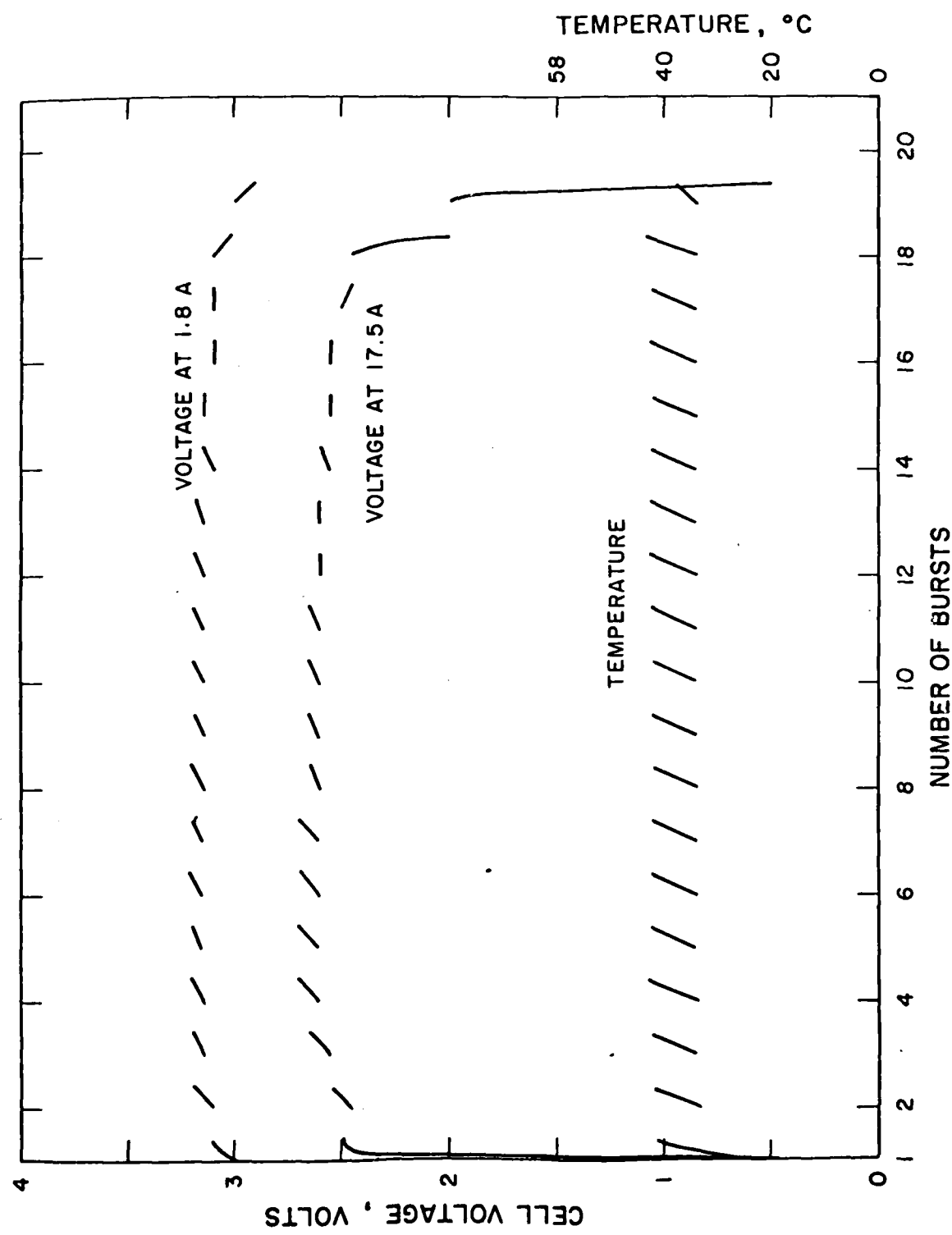


Figure 35. Performance of two D cells with cathode additive 1, level B on GLLD test using the old duty cycle.

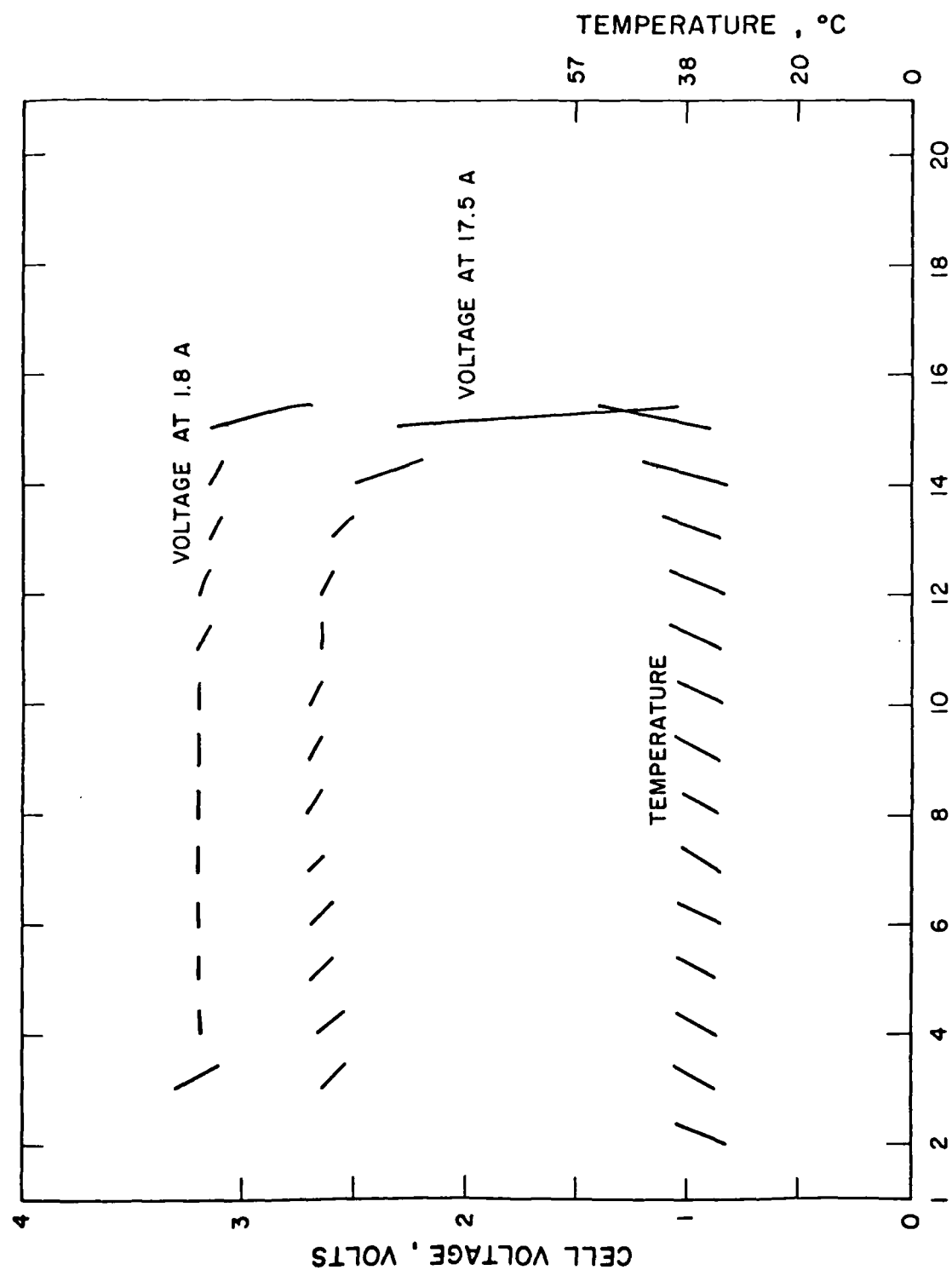


Figure 26. Performance of two D cells with cathode additive 1, level B on GLLD test

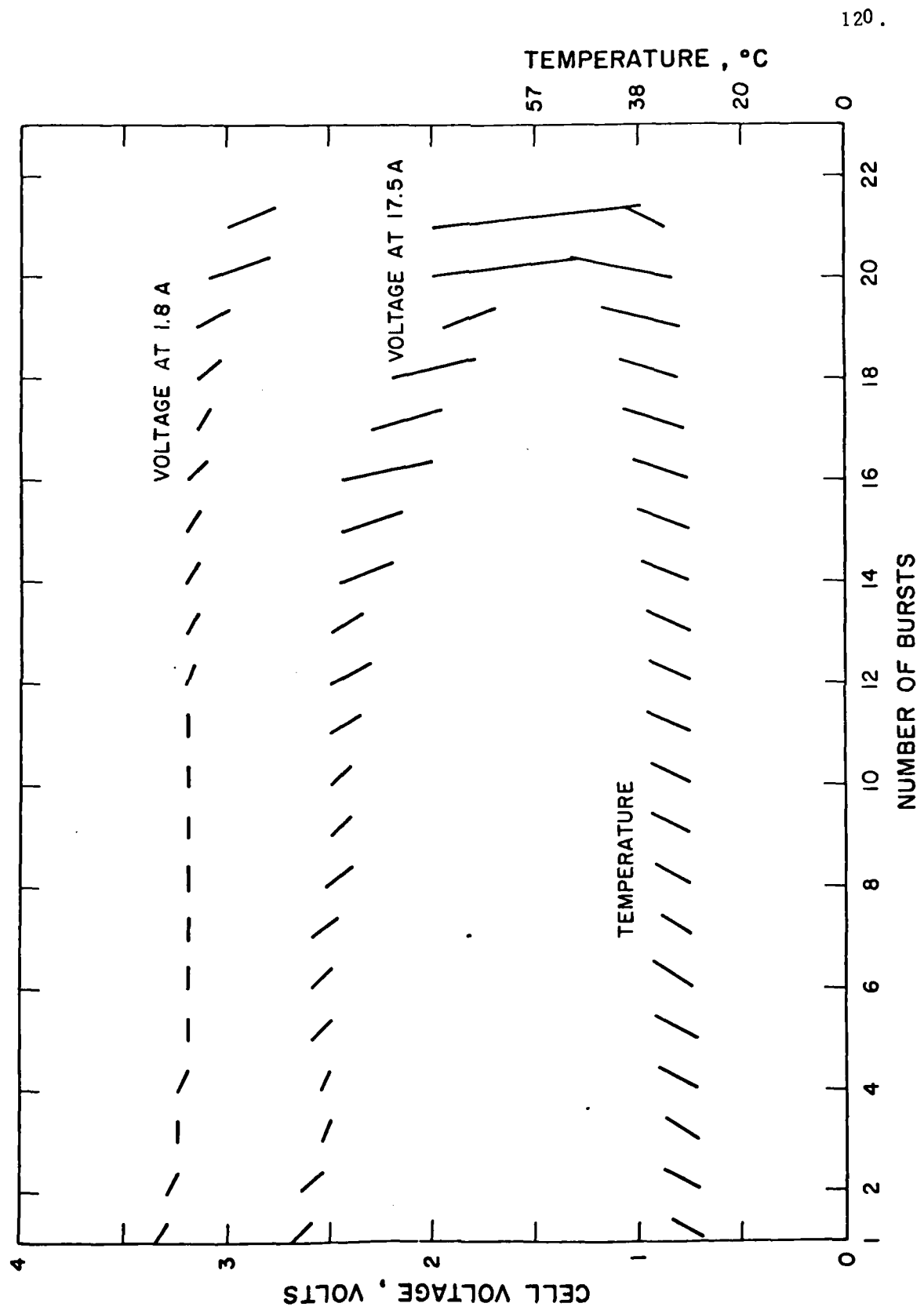


Figure 27. Performance of two D cells with cathode additive 2 at level A the old GLLD load.

121.

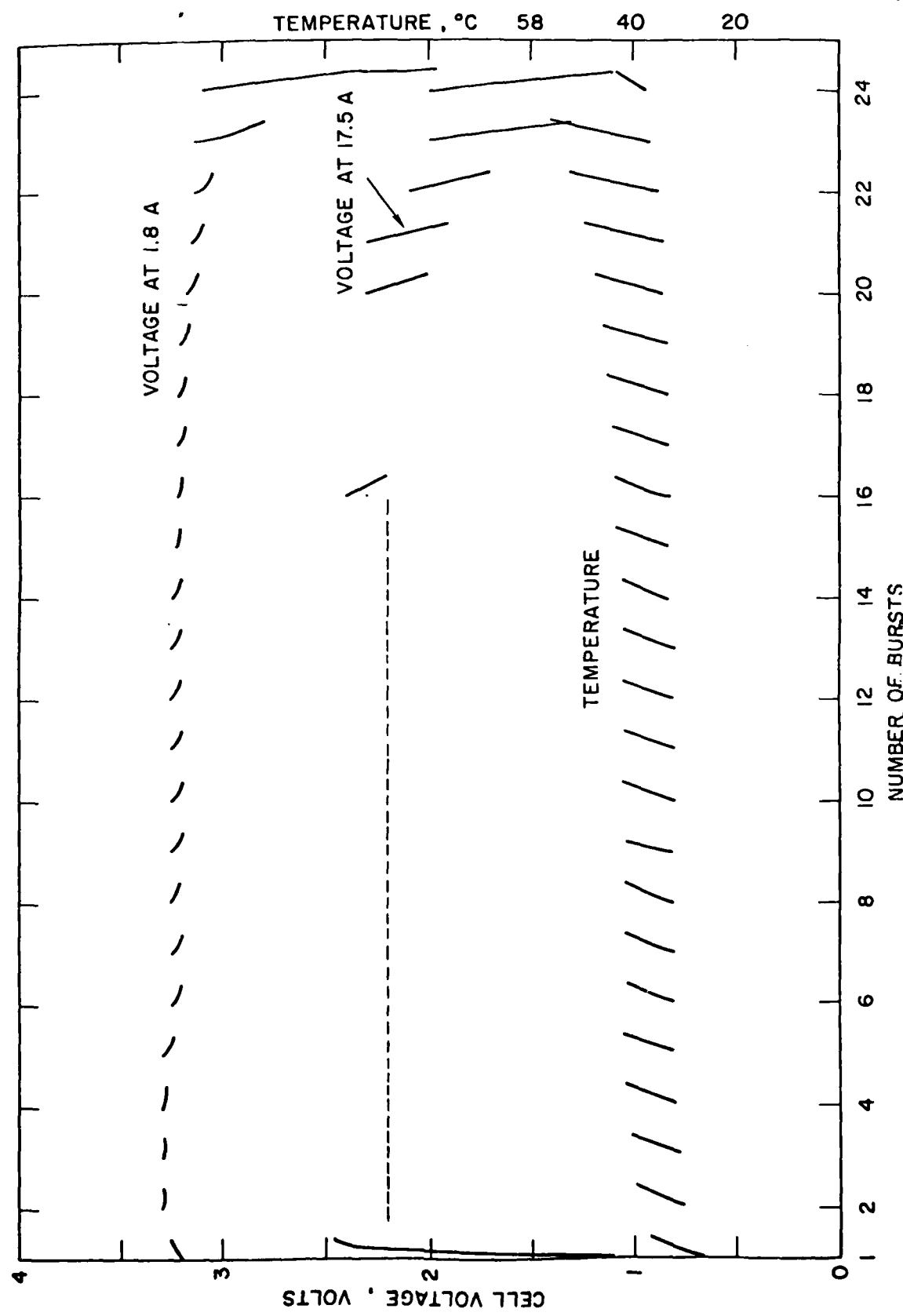


Figure 8. Performance of two D cells with cathode additive 2, level A on old GILD load.

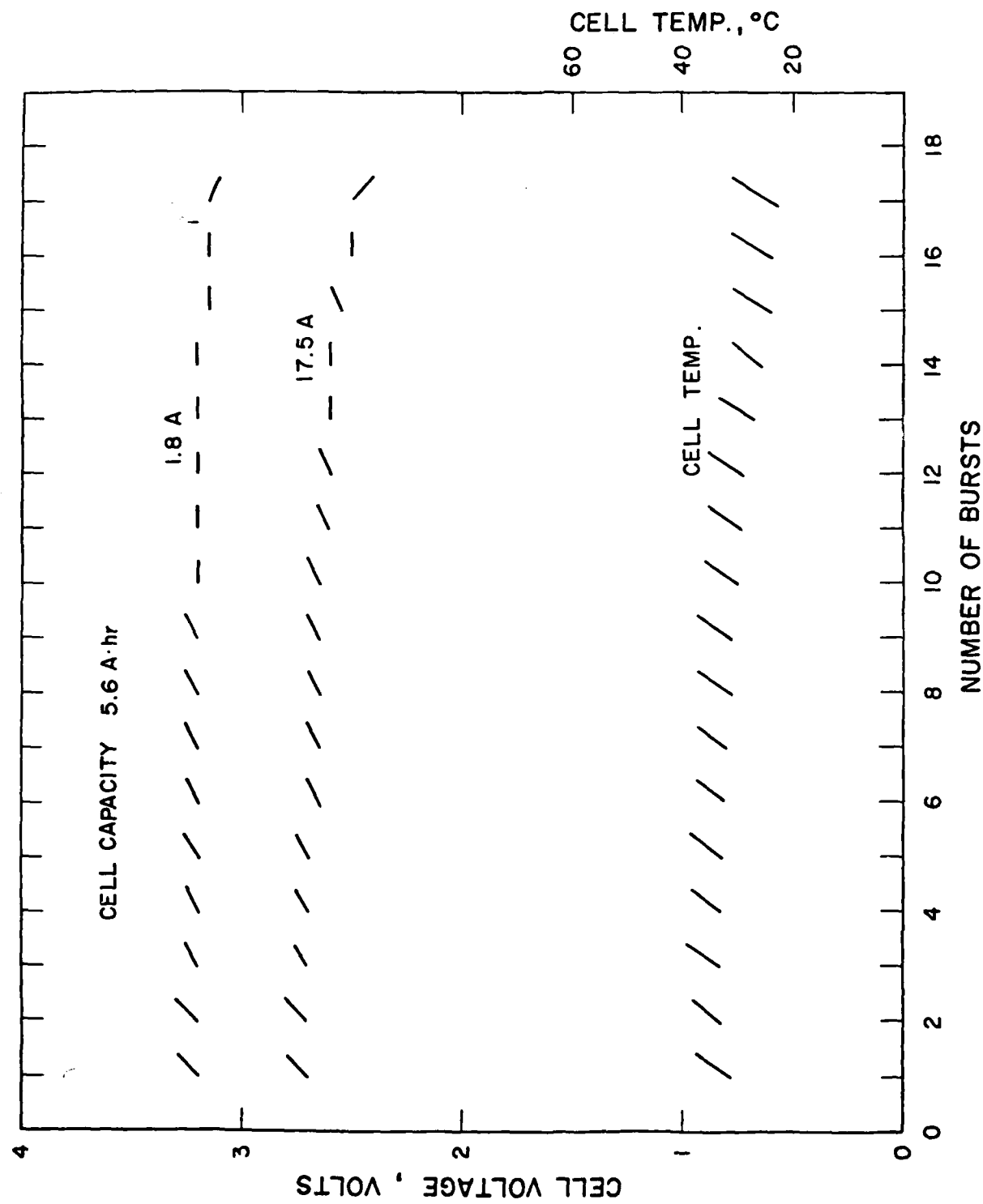


Figure 39. Performance of the two D cells with cathode additive 2, level B on old GLLD load.

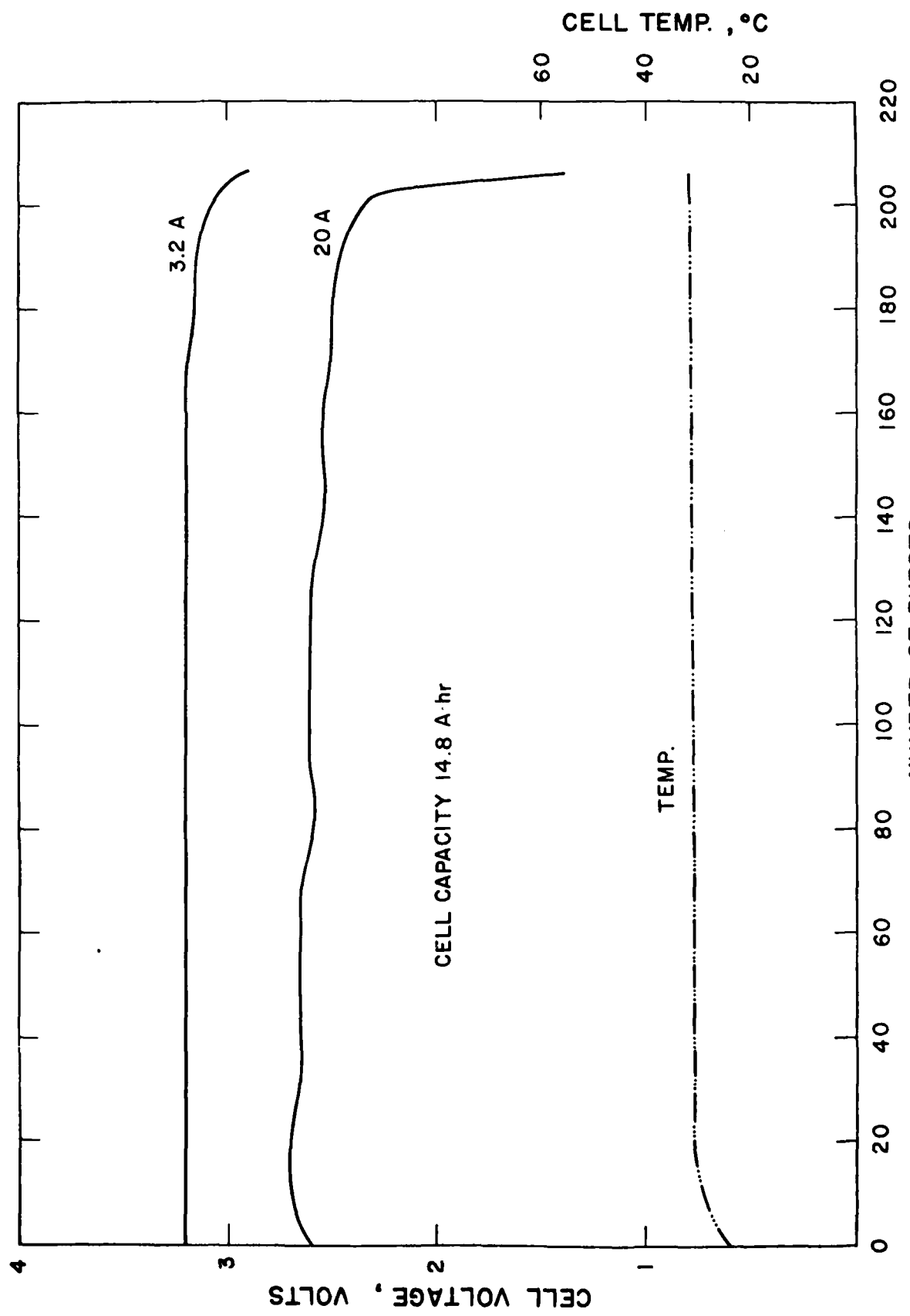


Figure 40. Performance of two D cells with cathode additive 'C' at level C on the new GUD load.

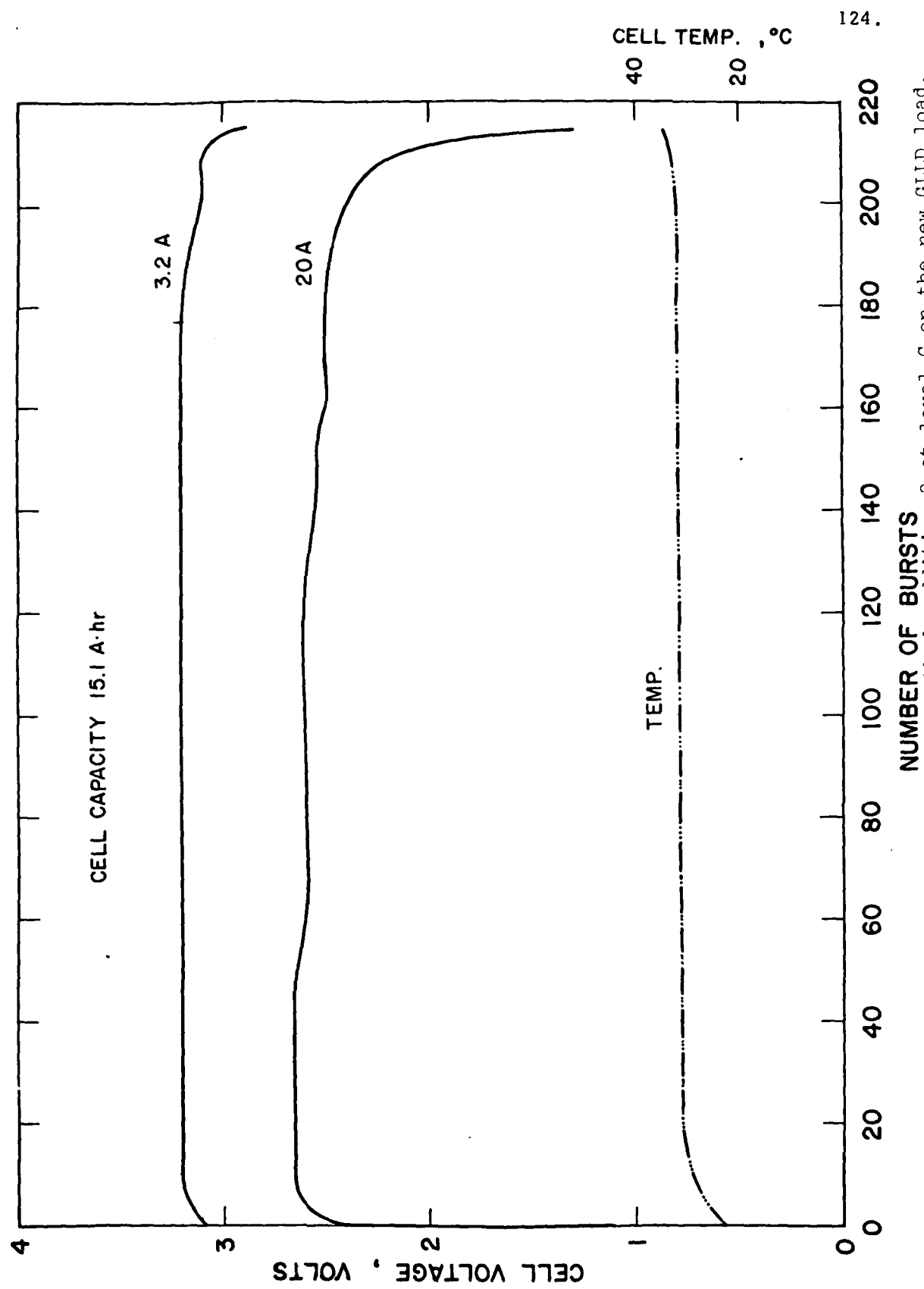


Figure 41. Performance of two D cells with cathode additive 2 at level C on the new GLLD load.

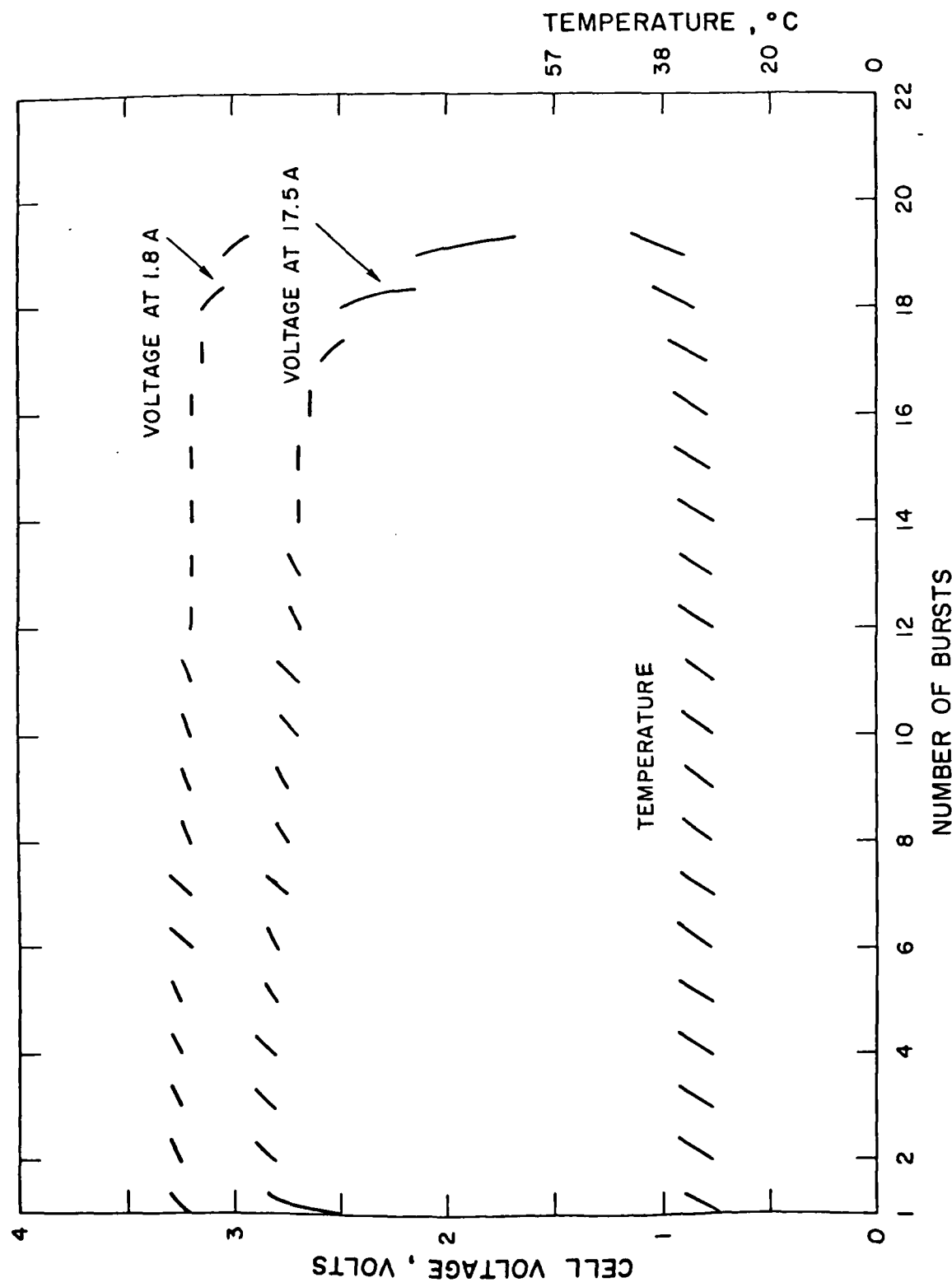


Figure 125. Performance of two D cells with cathode additive 3 on the old G.I.D. load.

126.

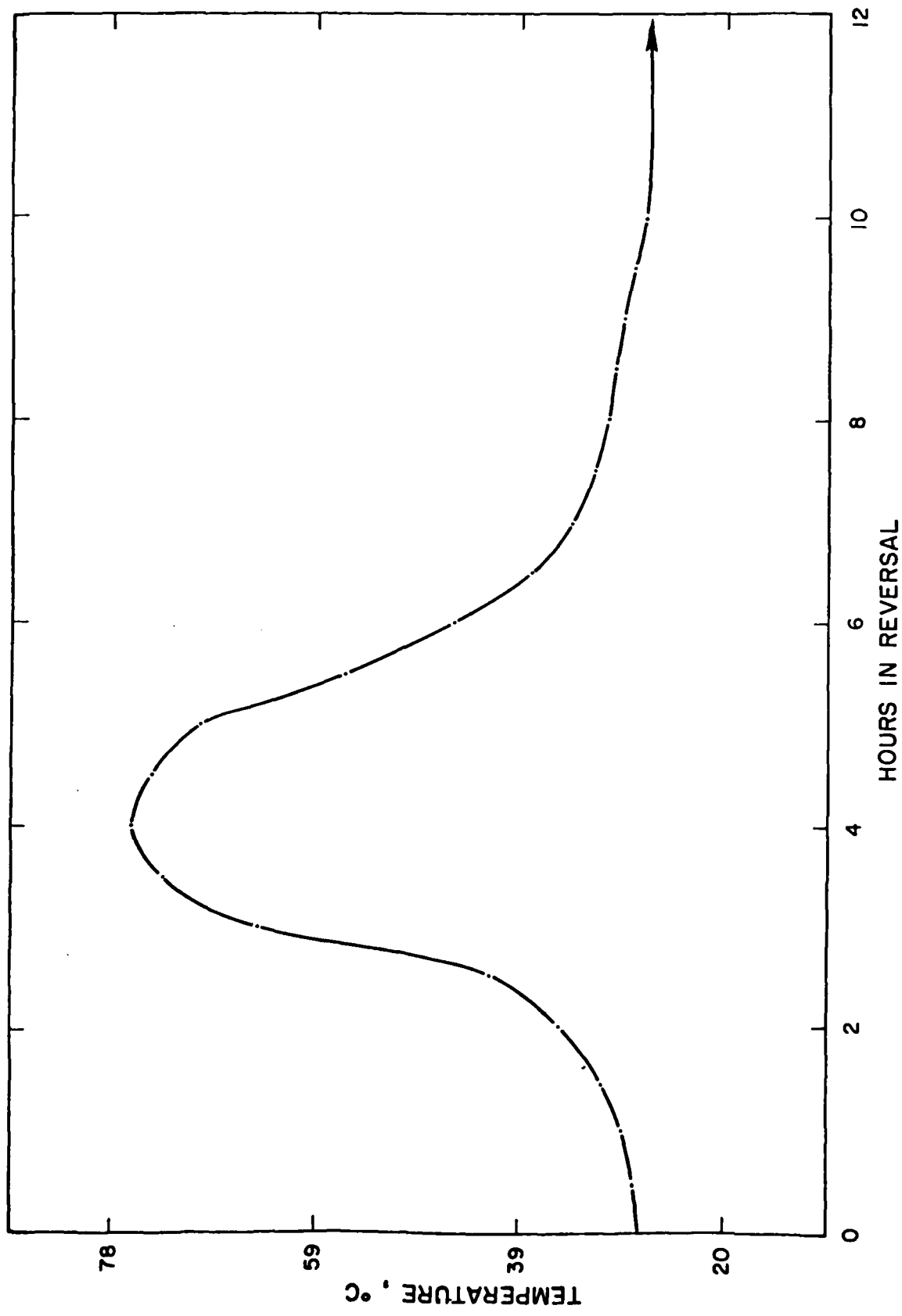


Figure 43. Cell wall temperature of 2 D cells with cathode additive 3 during reversal at 2A

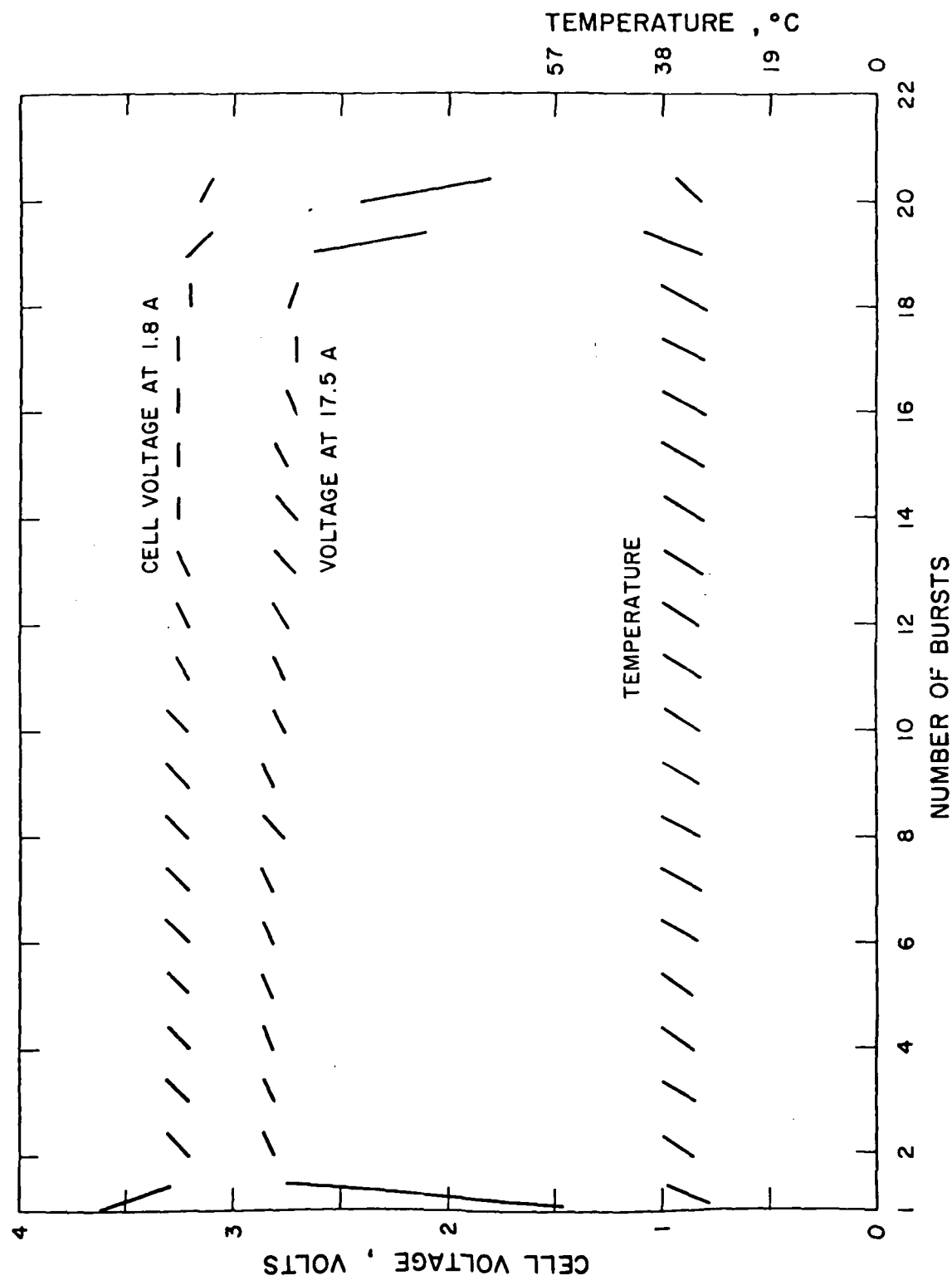


Figure 4b. Performance of two D cells with cathode additive 3 on the old GILD load.

128.

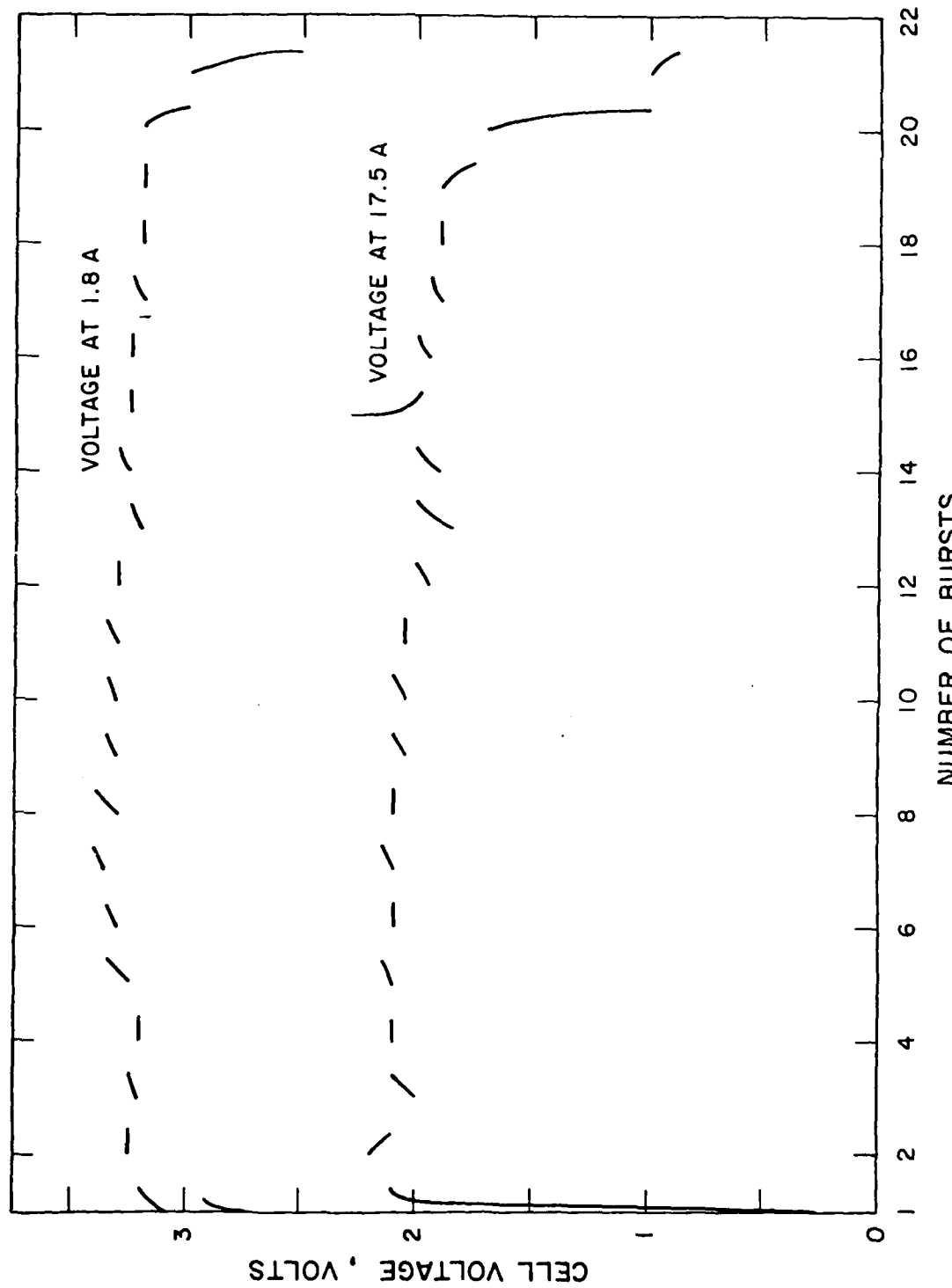
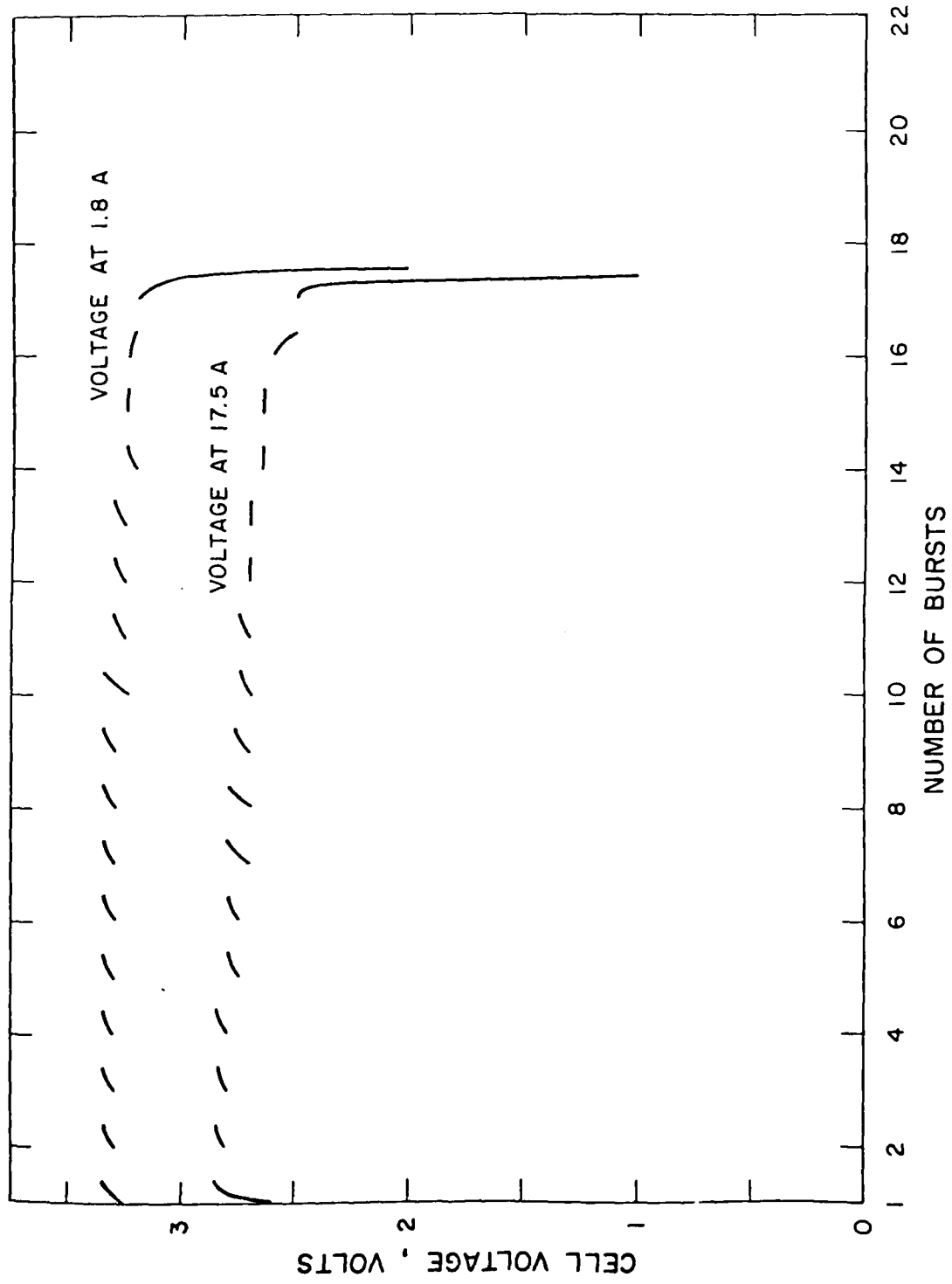


Figure 1.5. Performance of two D cells with cathode additive 4 on the old GLID test



Picture 4f. Performance of two D cells with cathode additive 5 on the old GULP test.

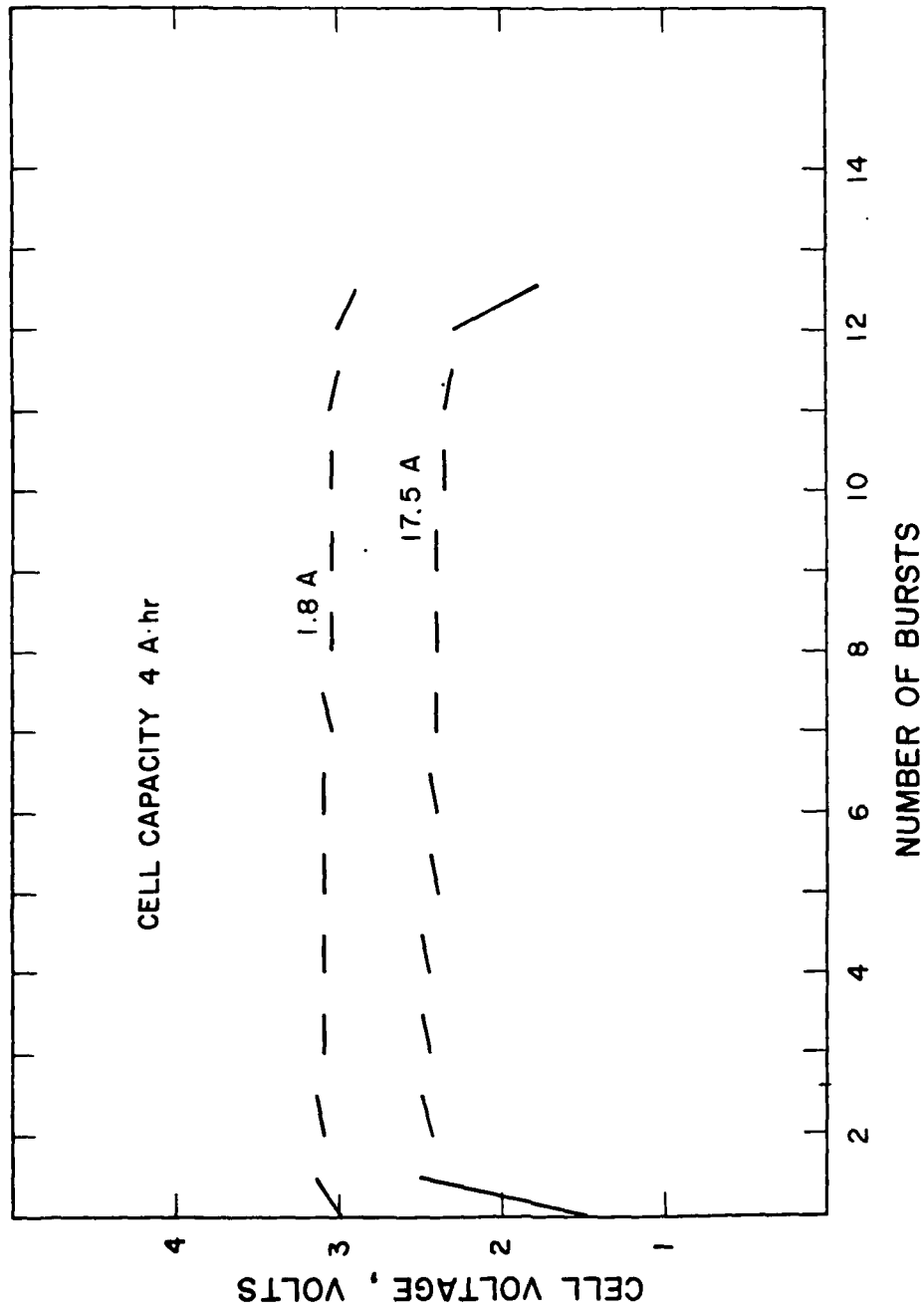


Figure 47. Performance of two D cells with 1.4 M LiAlCl<sub>4</sub> + SOCl<sub>2</sub> electrolyte on the old GLLD duty cycle.

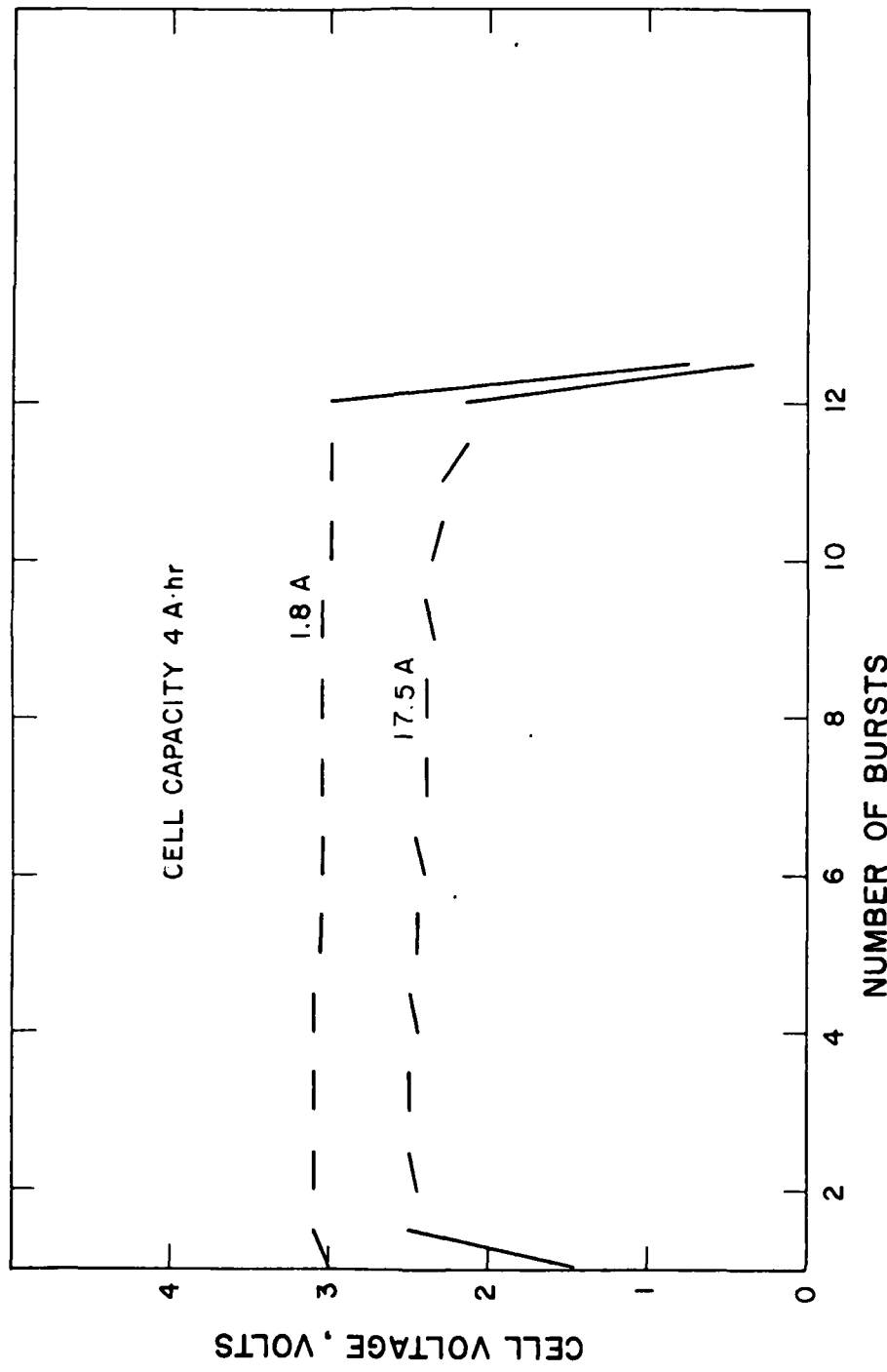


Figure 4. Performance of two cells with 1.0M LiAlCl<sub>4</sub> SOCl<sub>2</sub> electrolyte on the old GILD duty cycle.

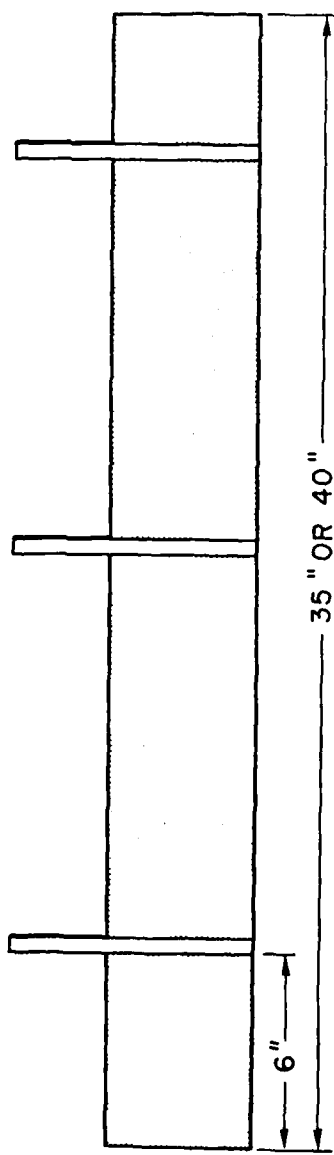


Figure 49. Current collector configuration of long cathodes in n cells.  
(design #10)

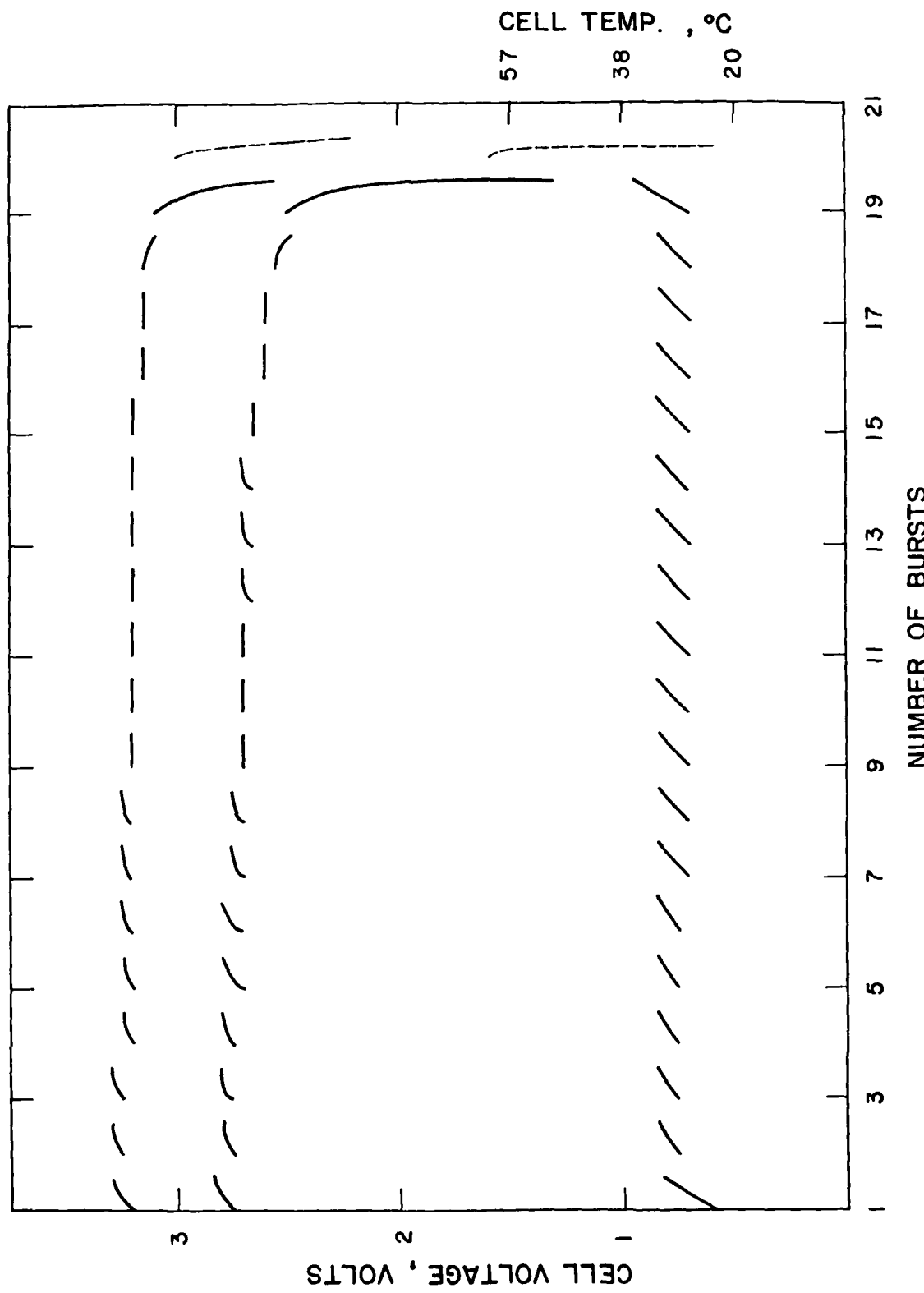


Figure 50. Performance of two D cells with 25% pretreated cathodes on the old GND duty cycle.

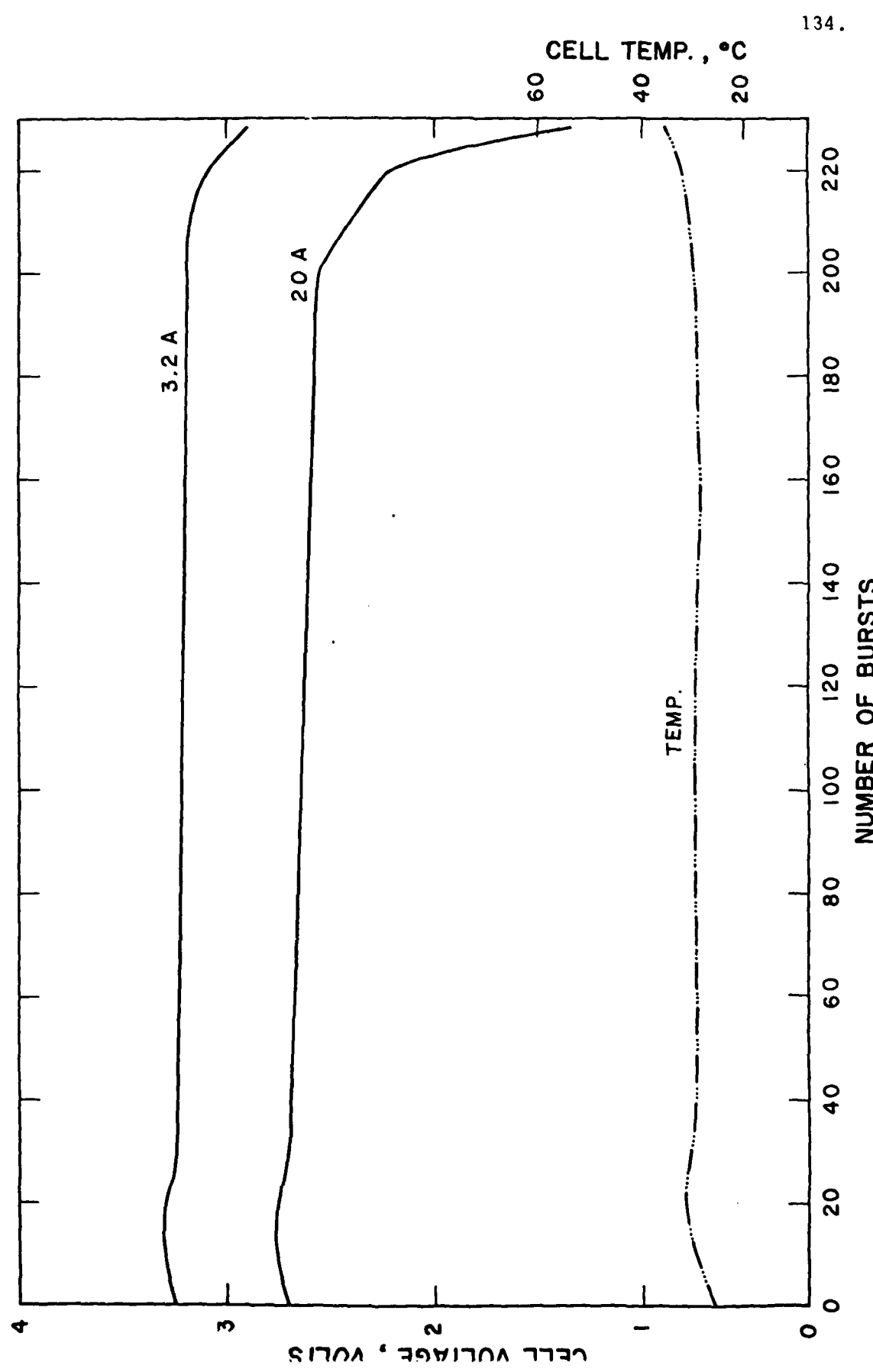


Figure 51. Performance of 2 D cells with 35" cathode on the new GLLD duty cycle.

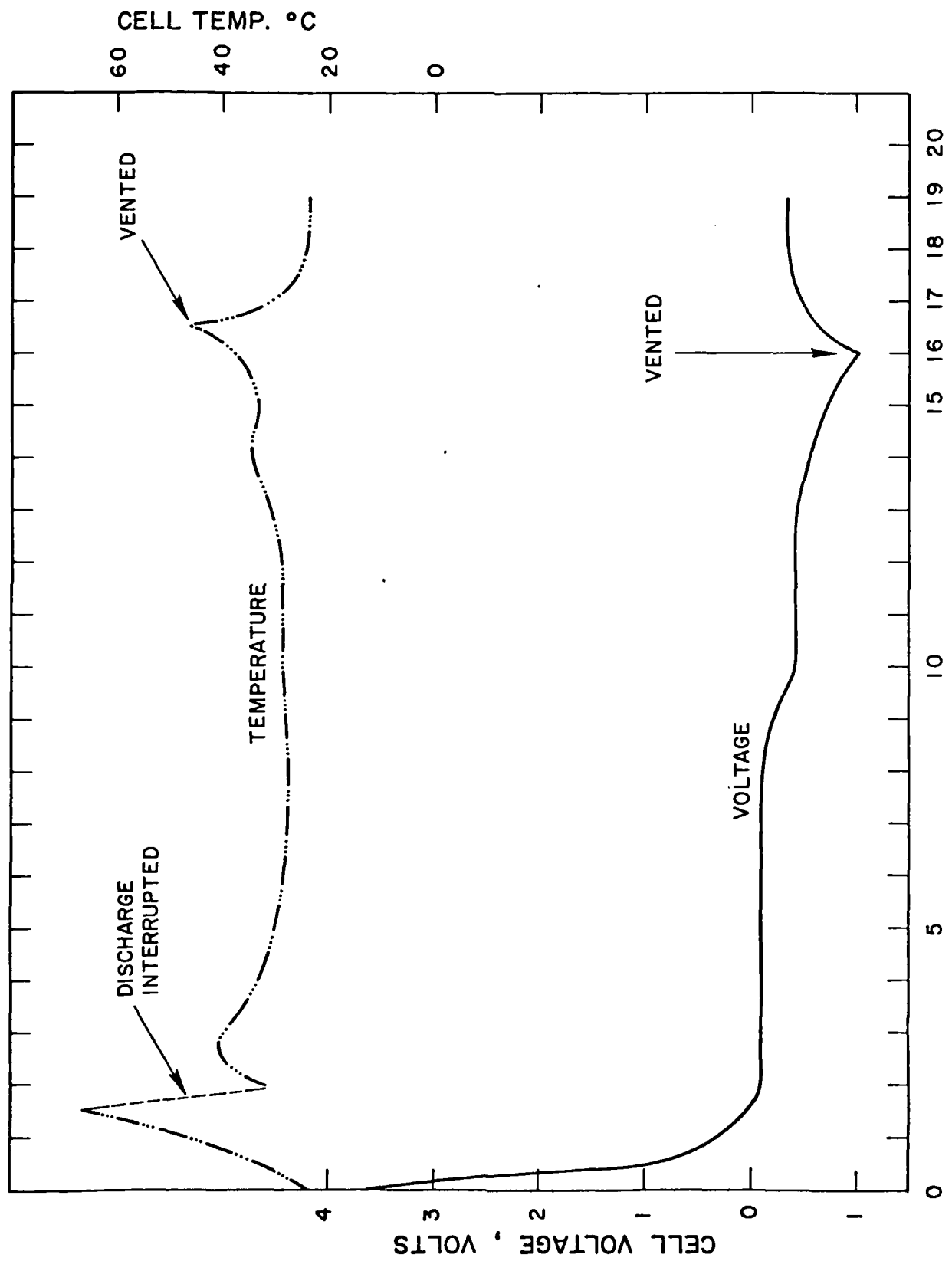


Figure 52. Li/SOCl<sub>2</sub> D cell with 35" pretreated cathode driven into voltage reversal at 2A.

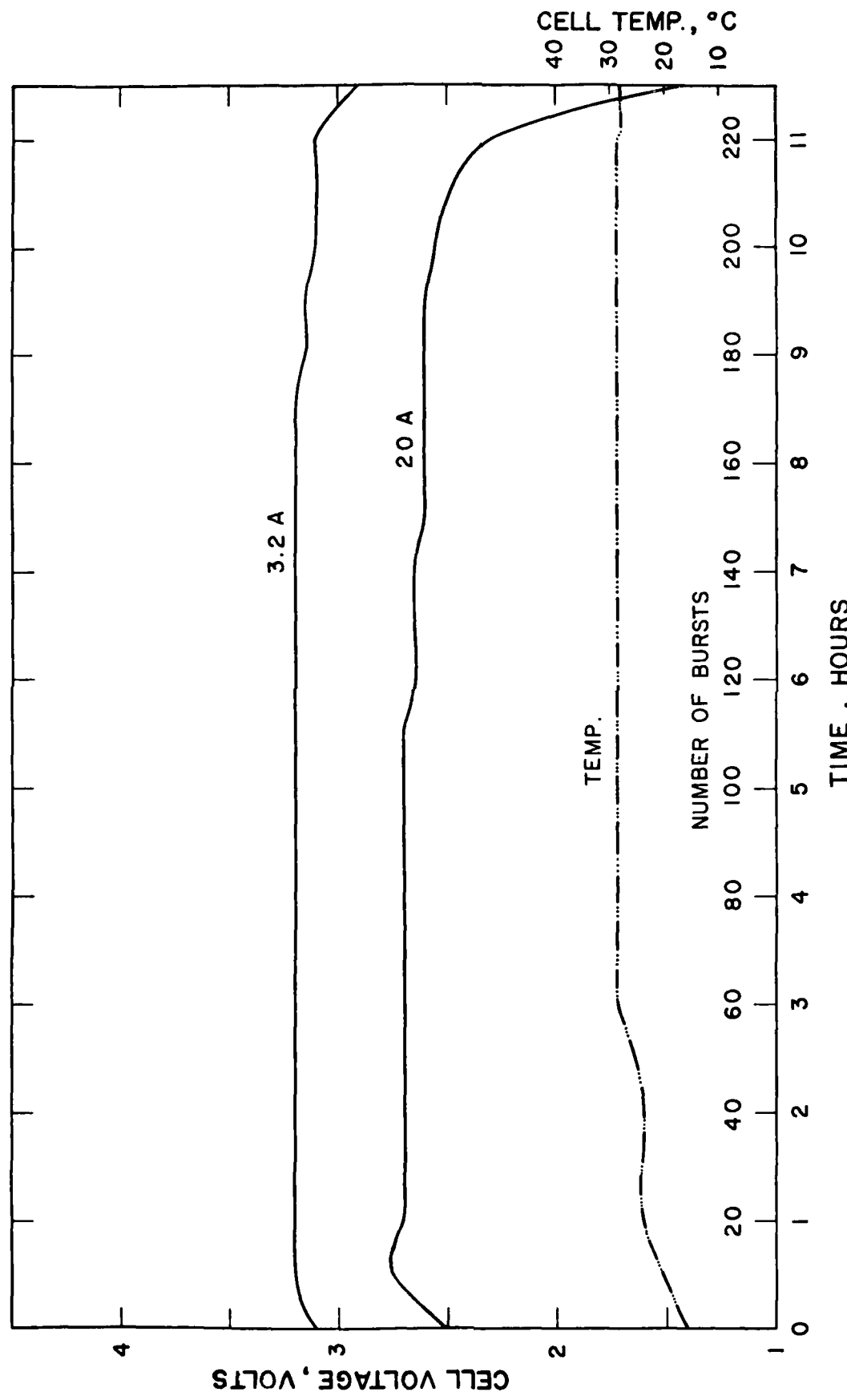


Figure 53. Performance of 2 D cells with 35 inch cathode on the new GLLD duty cycle.

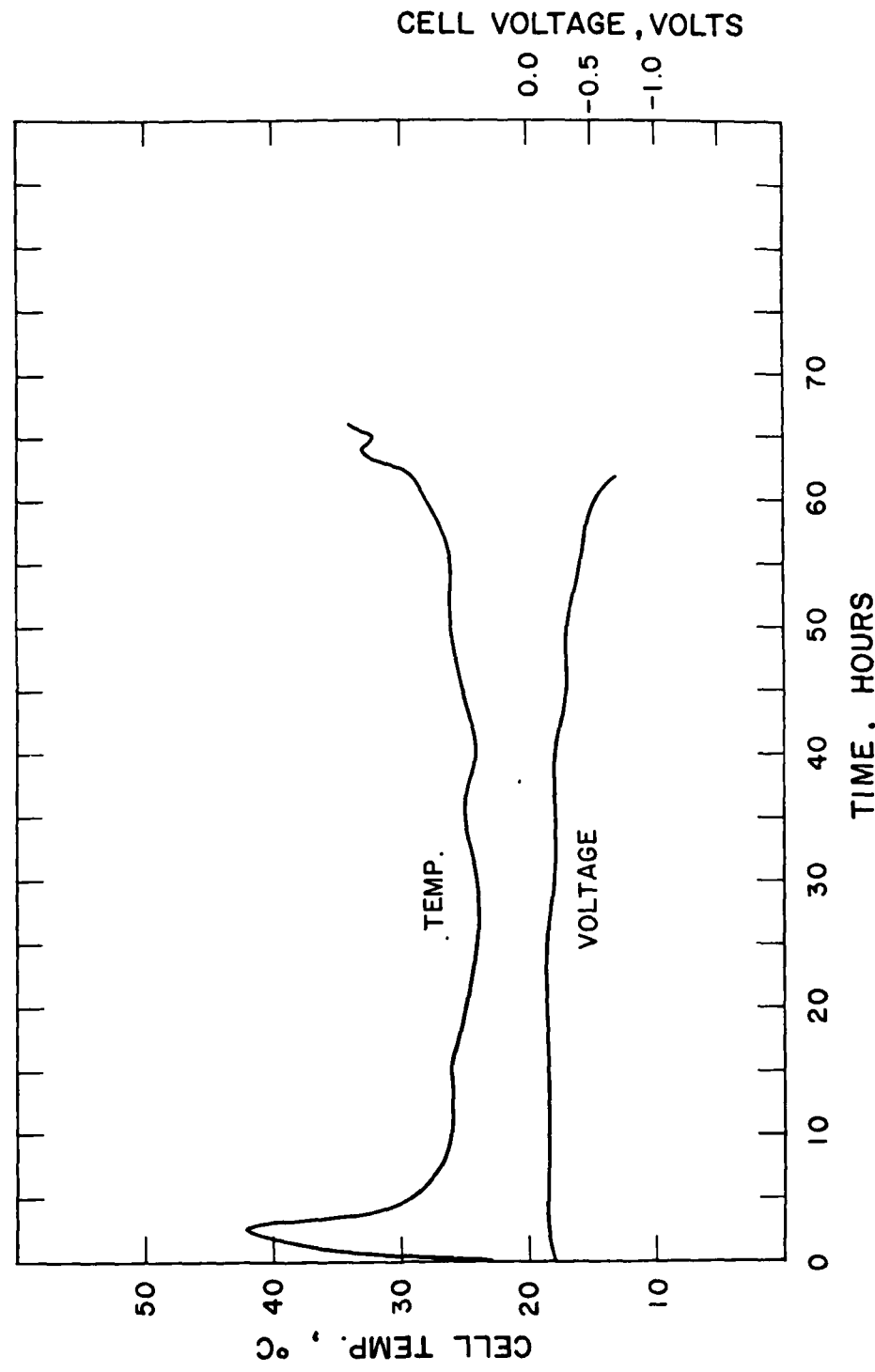


Figure 54. Voltage reversal behavior of the cell pair shown in Figure 53.

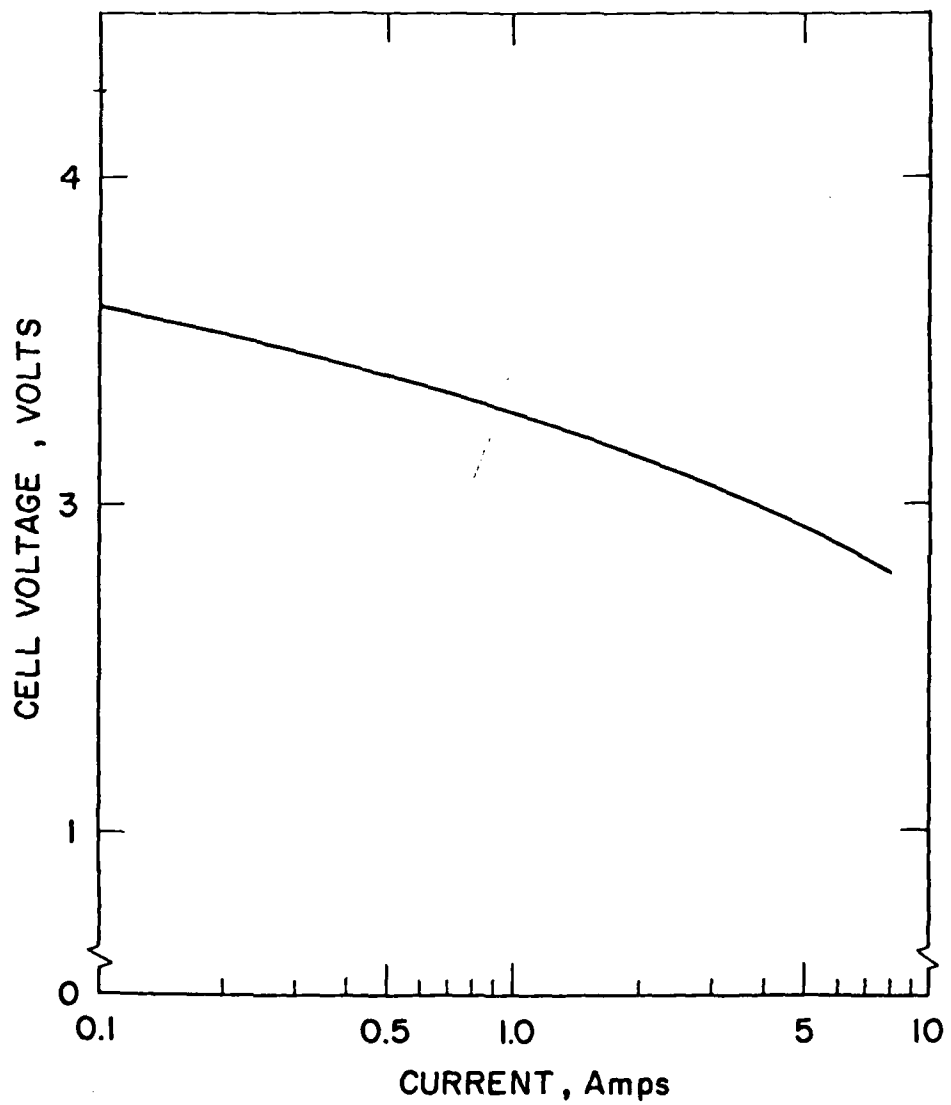


Figure 54a. Polarization curve of a D Cell with 35" long pretreated cathode.

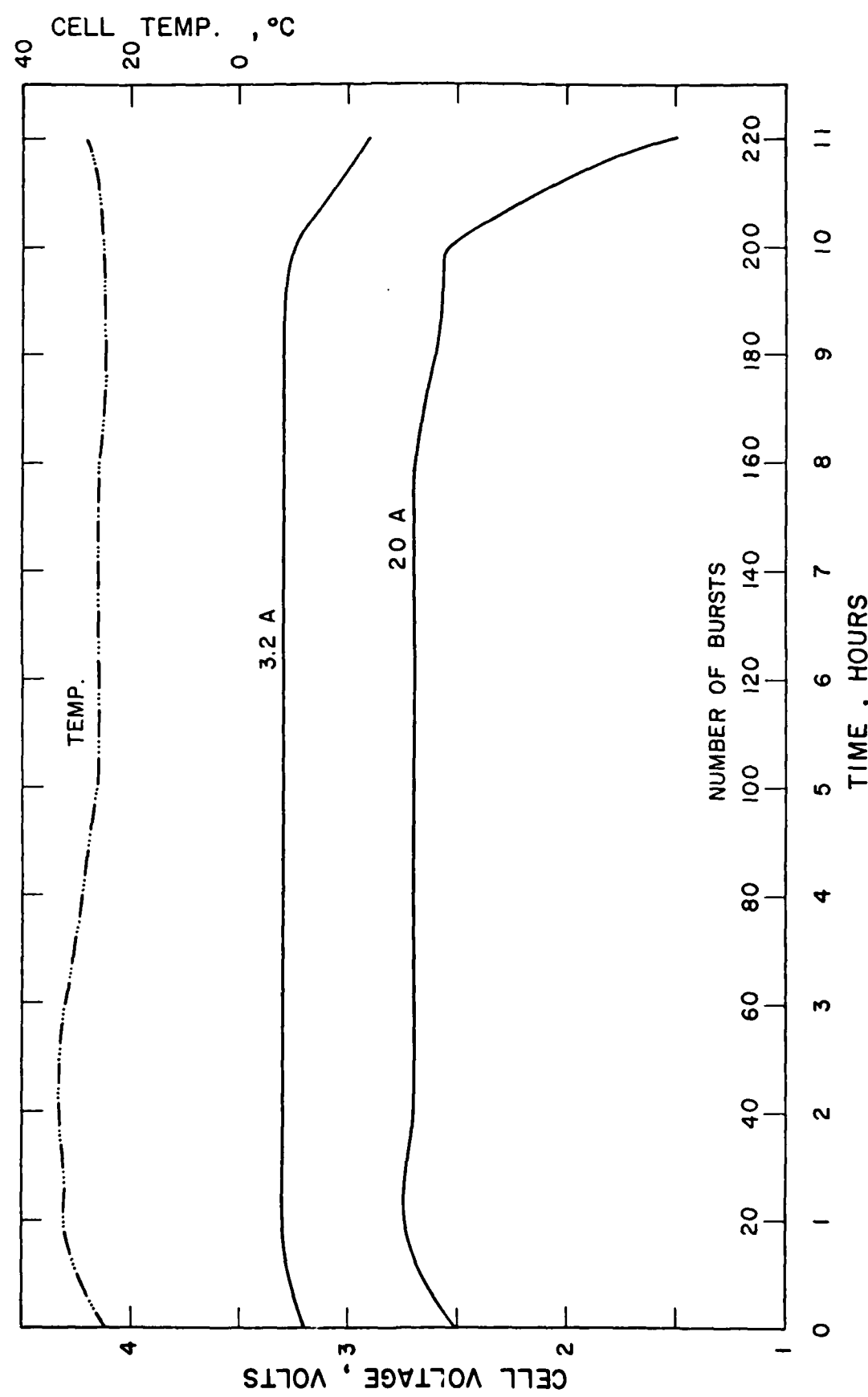


Figure 55. Performance of two D cells with "no" pretreated cathodes on the new GLLN load.

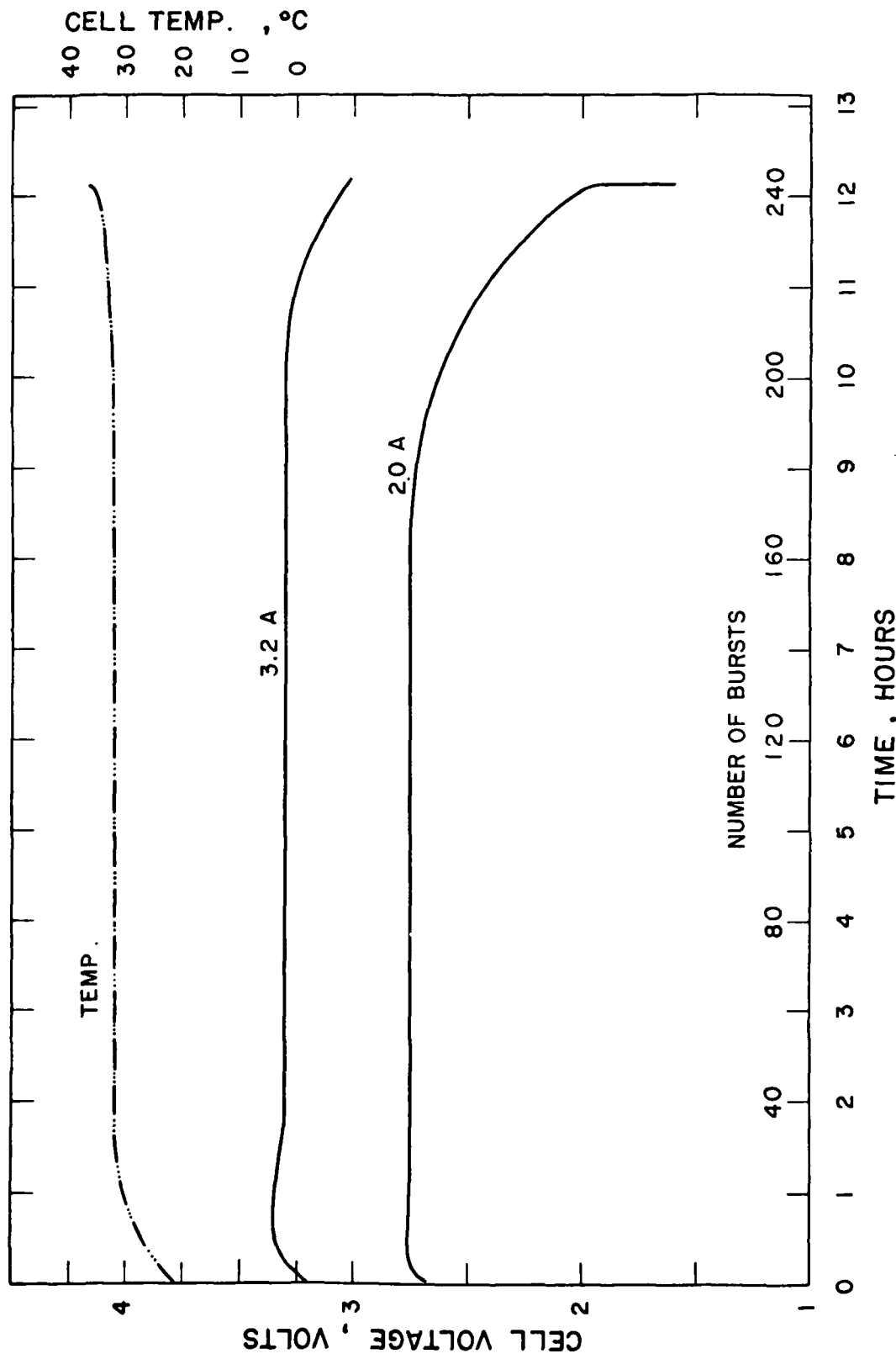


Figure 56. Performance of two D cells with 40" pre-treated cathodes on the new GILD load

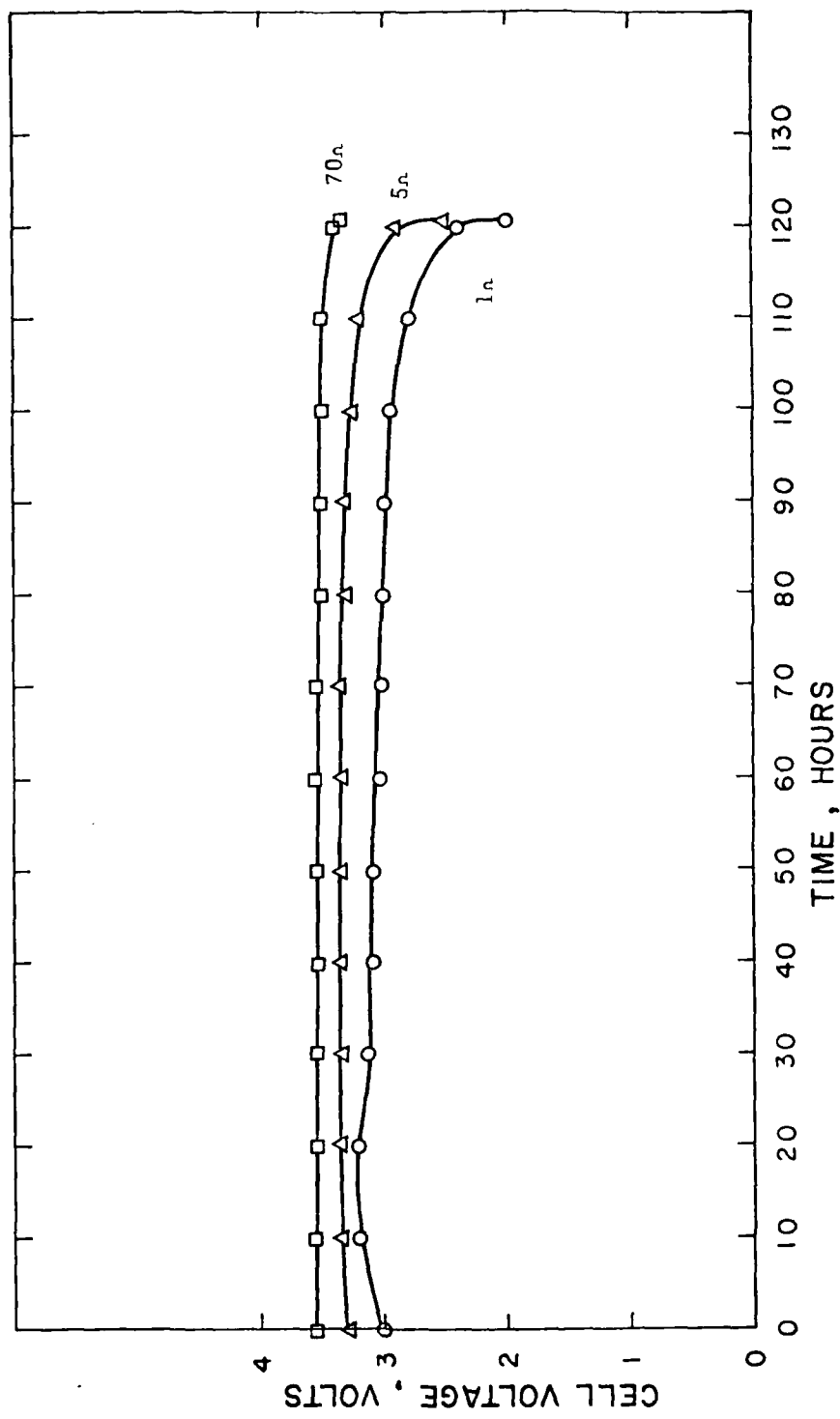


Figure 57. Performance of a D cell with 28 inch cathode on the BA5590 test.

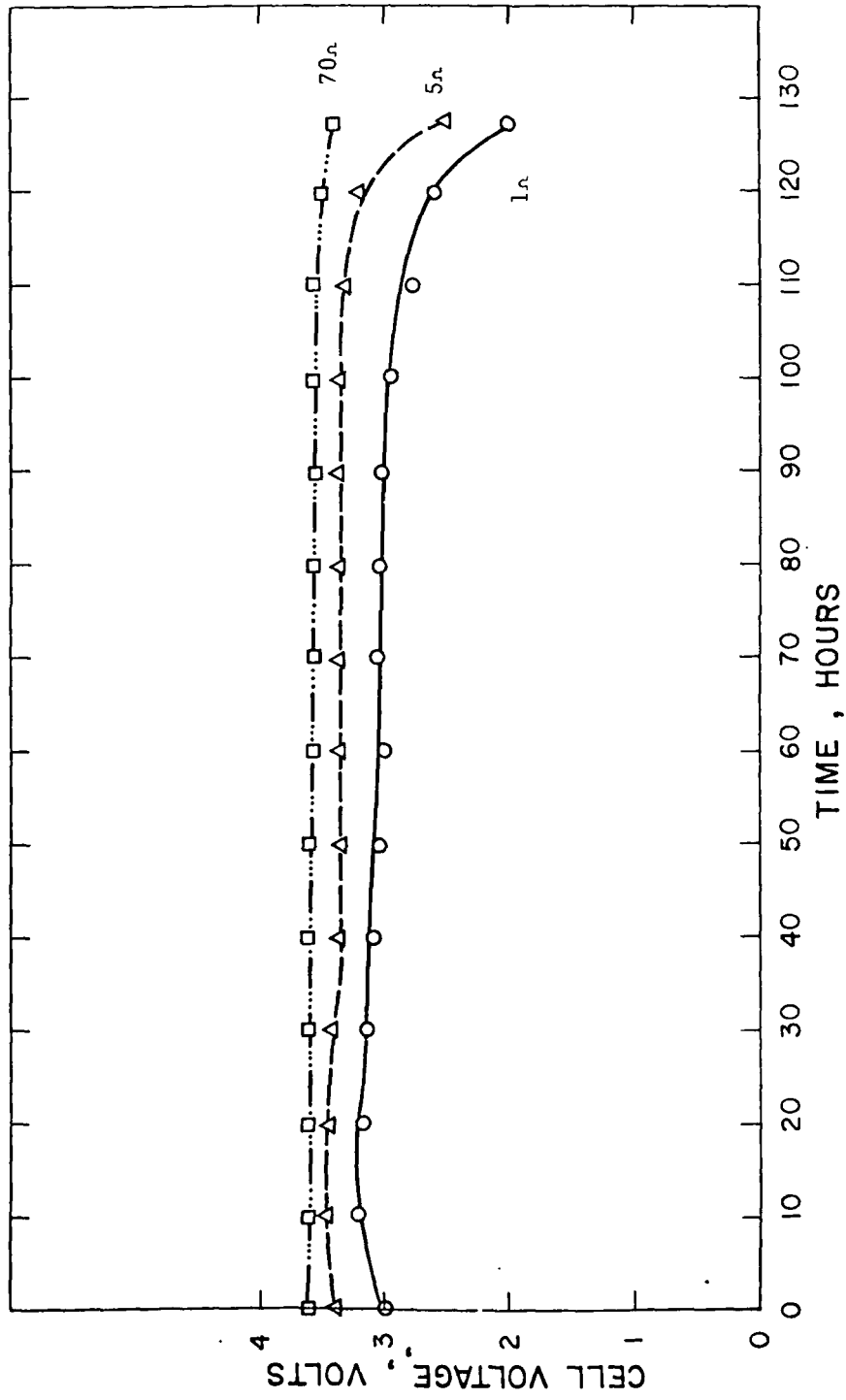


Figure 59. Performance of a D cell with 28 inch cathode on the BA5590 test.

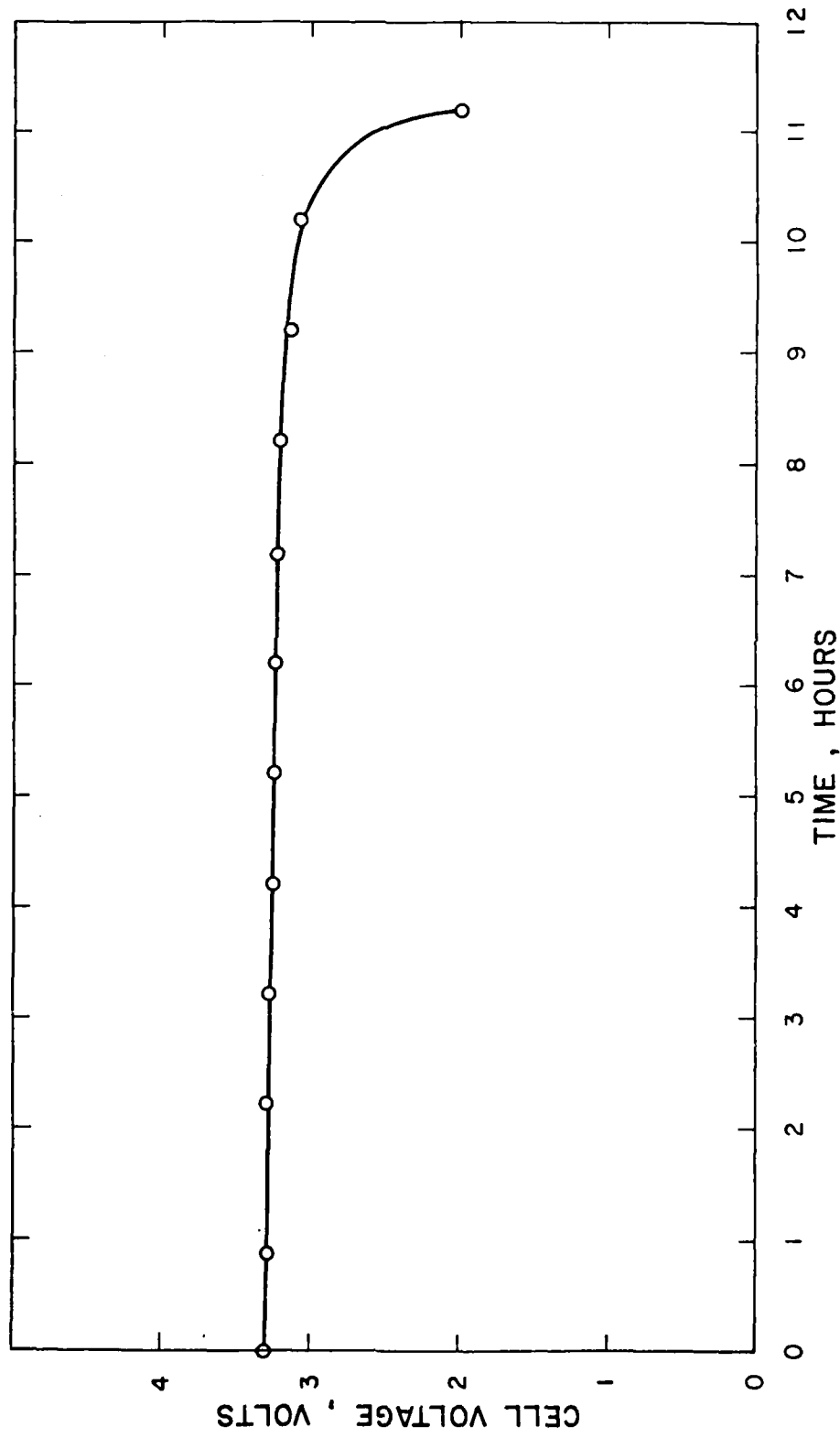


Figure 59. Discharge of a D cell with 28 inch cathode at 1 amp at 25°C.

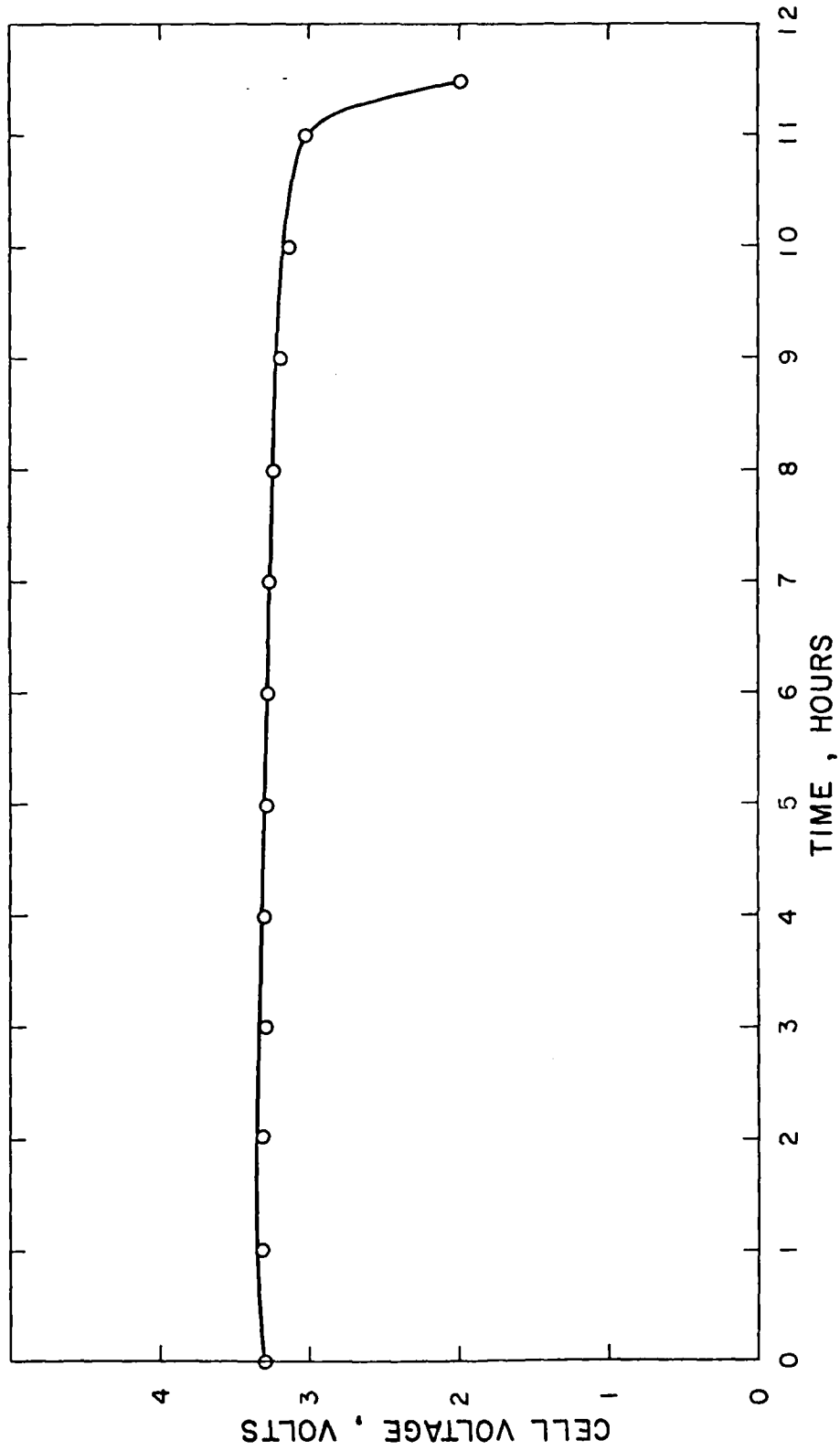


Figure 60. Performance of a D cell with 28 Inch cathode on 1 amp discharge at 25°C.

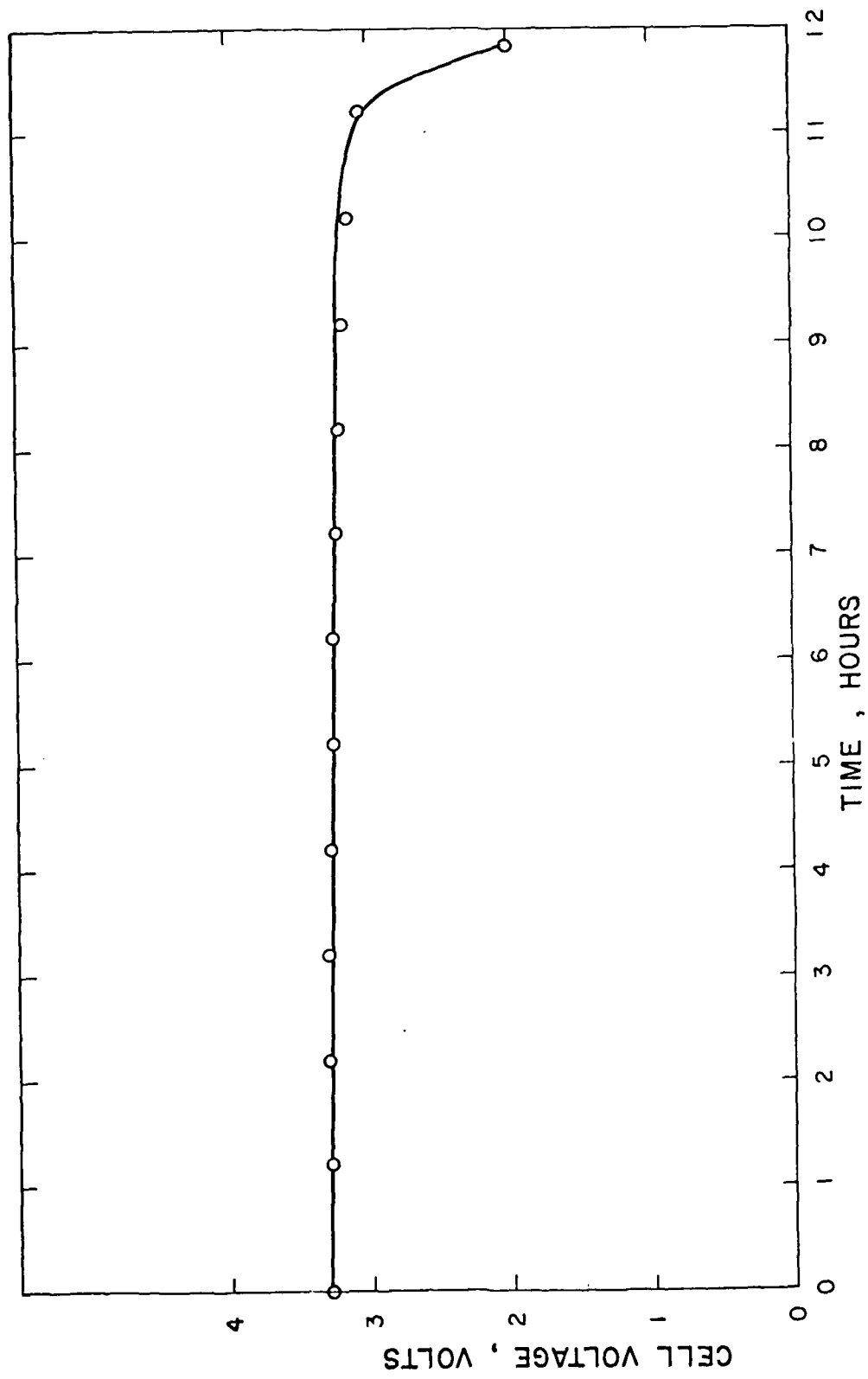


Figure 61. Performance of a D cell with 20 inch cathode at 1 A discharge.

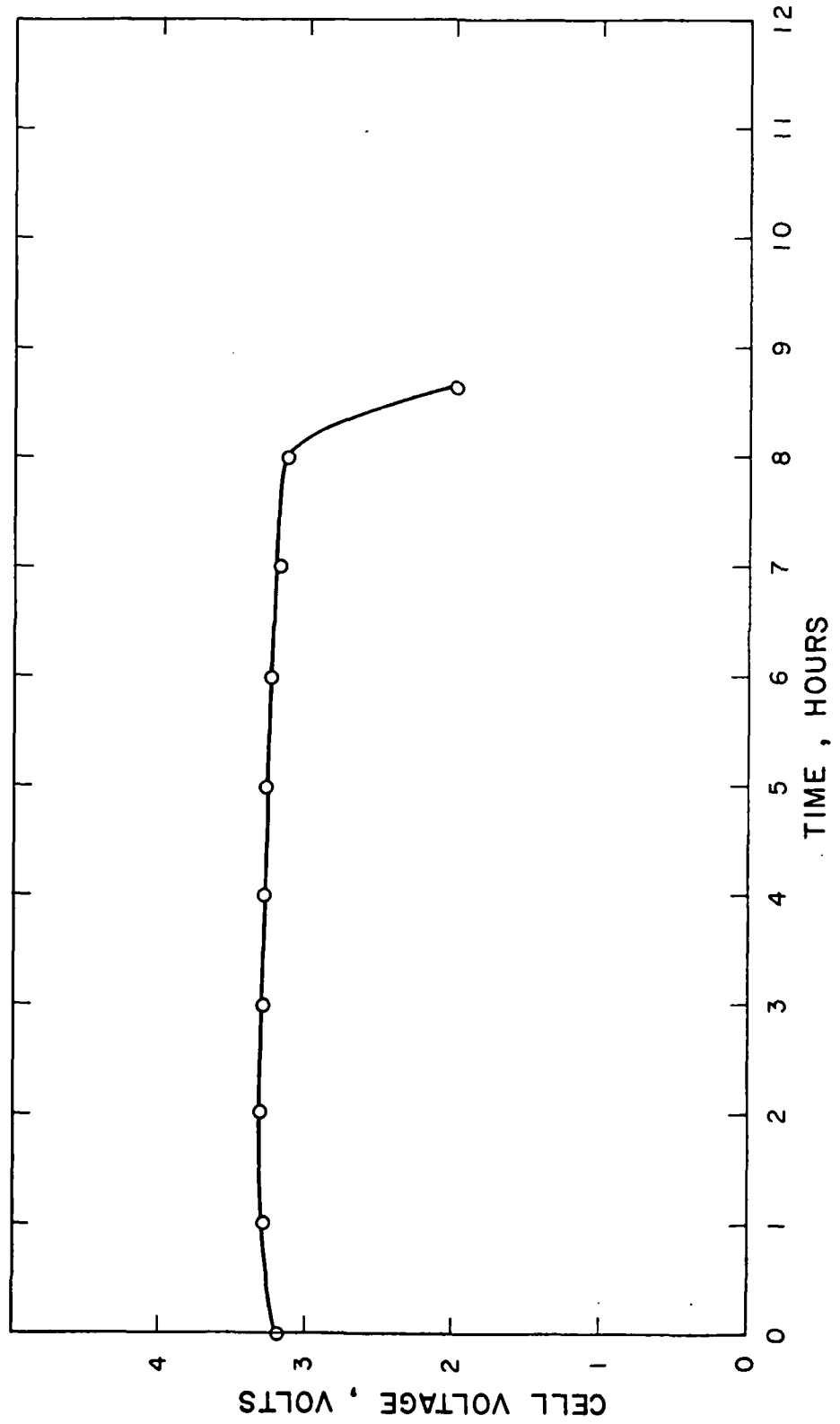


Figure 62. Performance of a D cell with 20 inch pretreated cathode on 1 amp discharge.

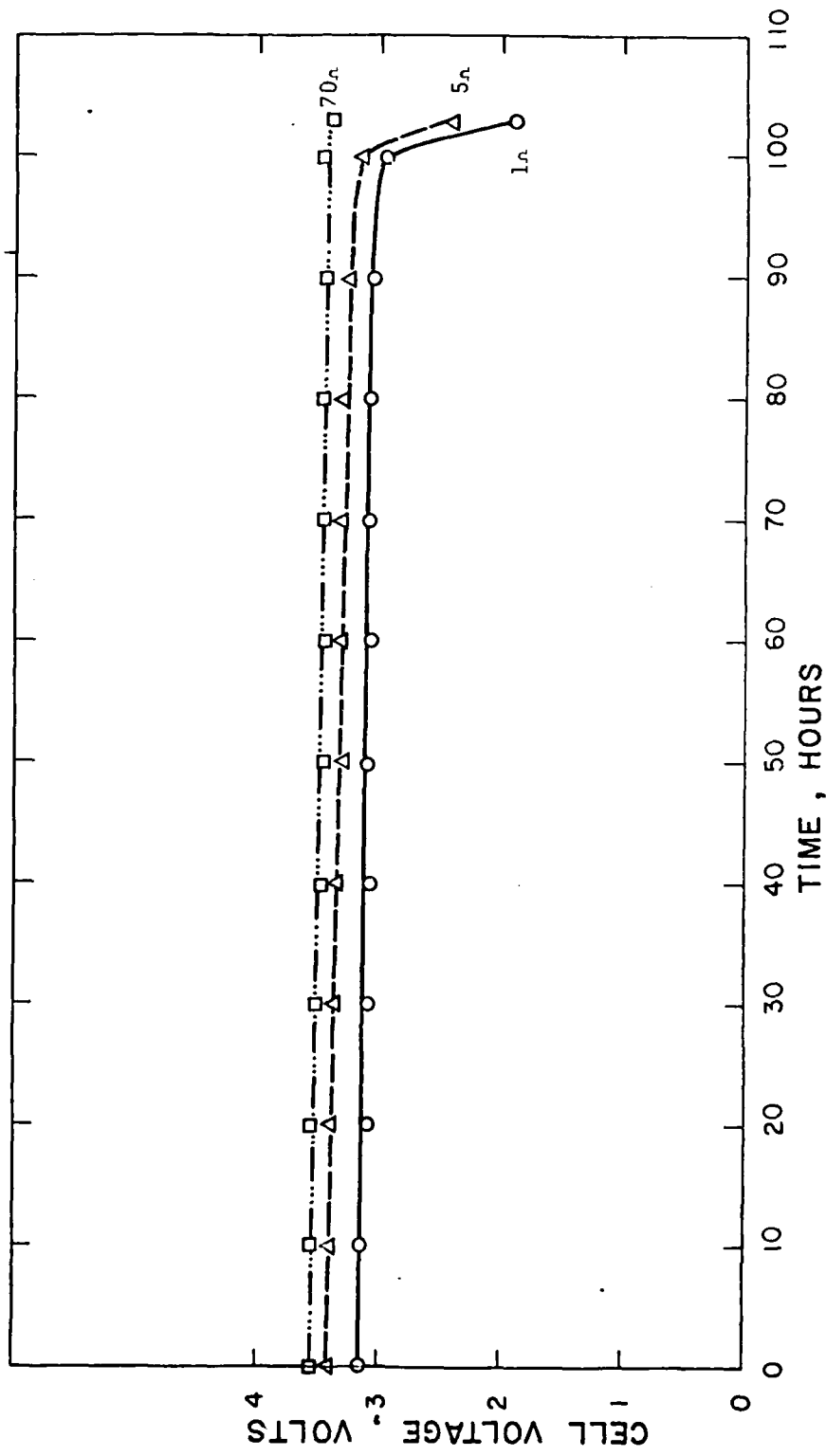


FIGURE 63. Performance of D cell with 26 inch cathode on BAS590 test.

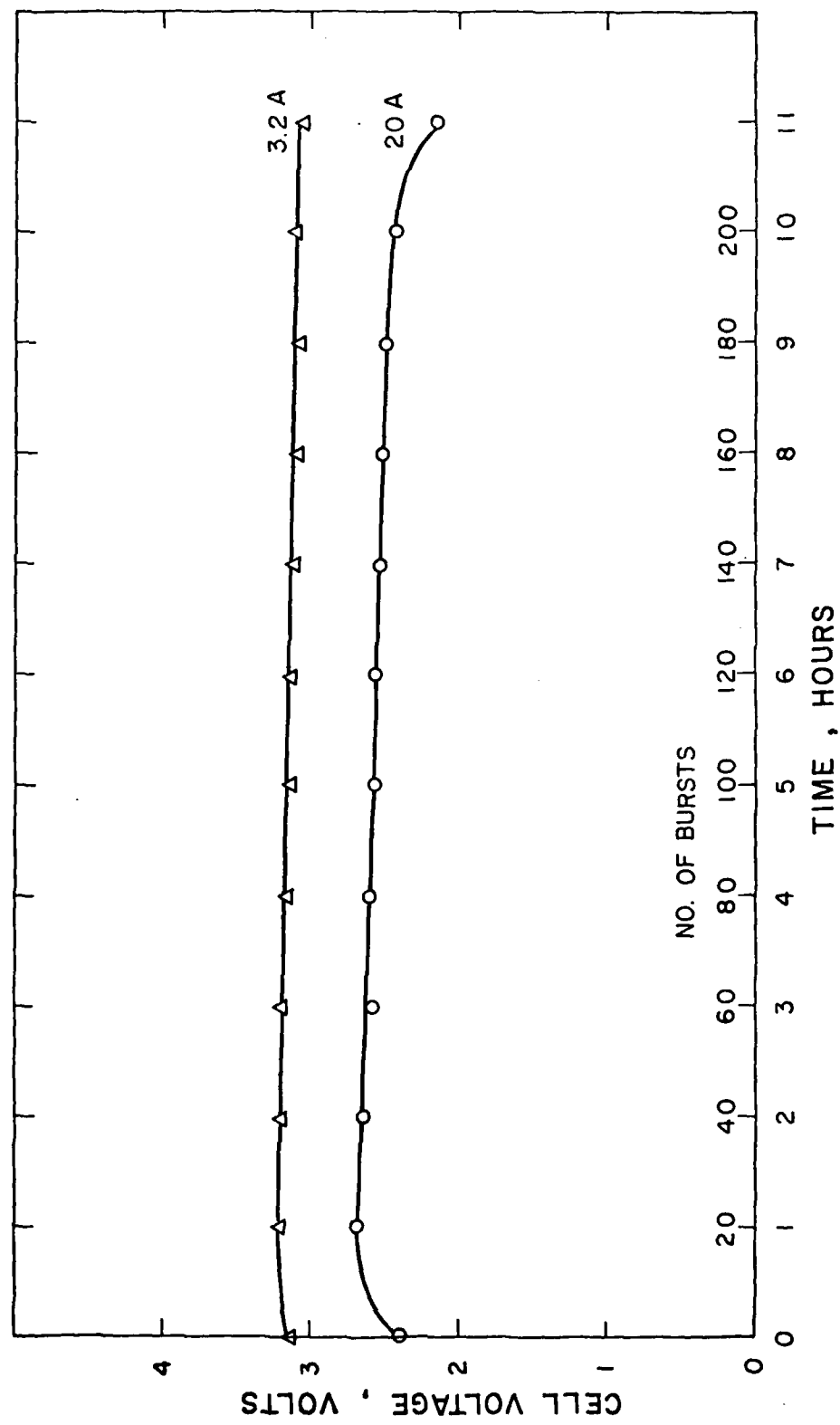


Figure 64. Performance of a pair of D cells with 26 inch cathodes on the new GLLD test.

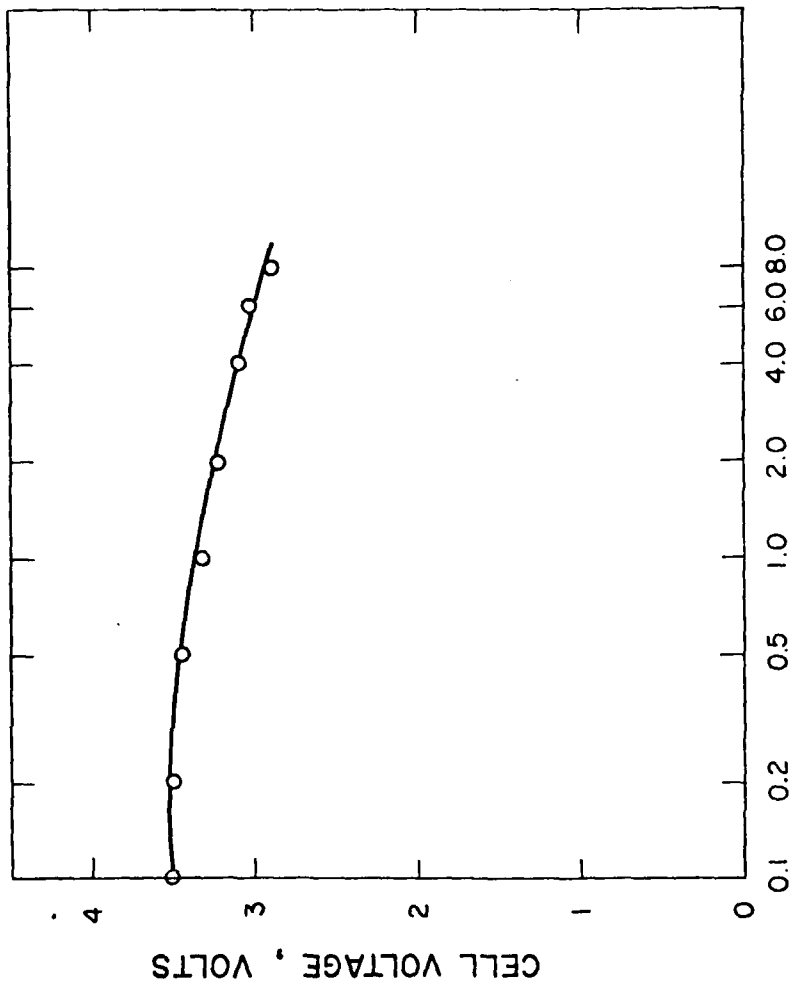


Figure 65. Polarization of an optimized battery, rate D cell at 25°C

150.

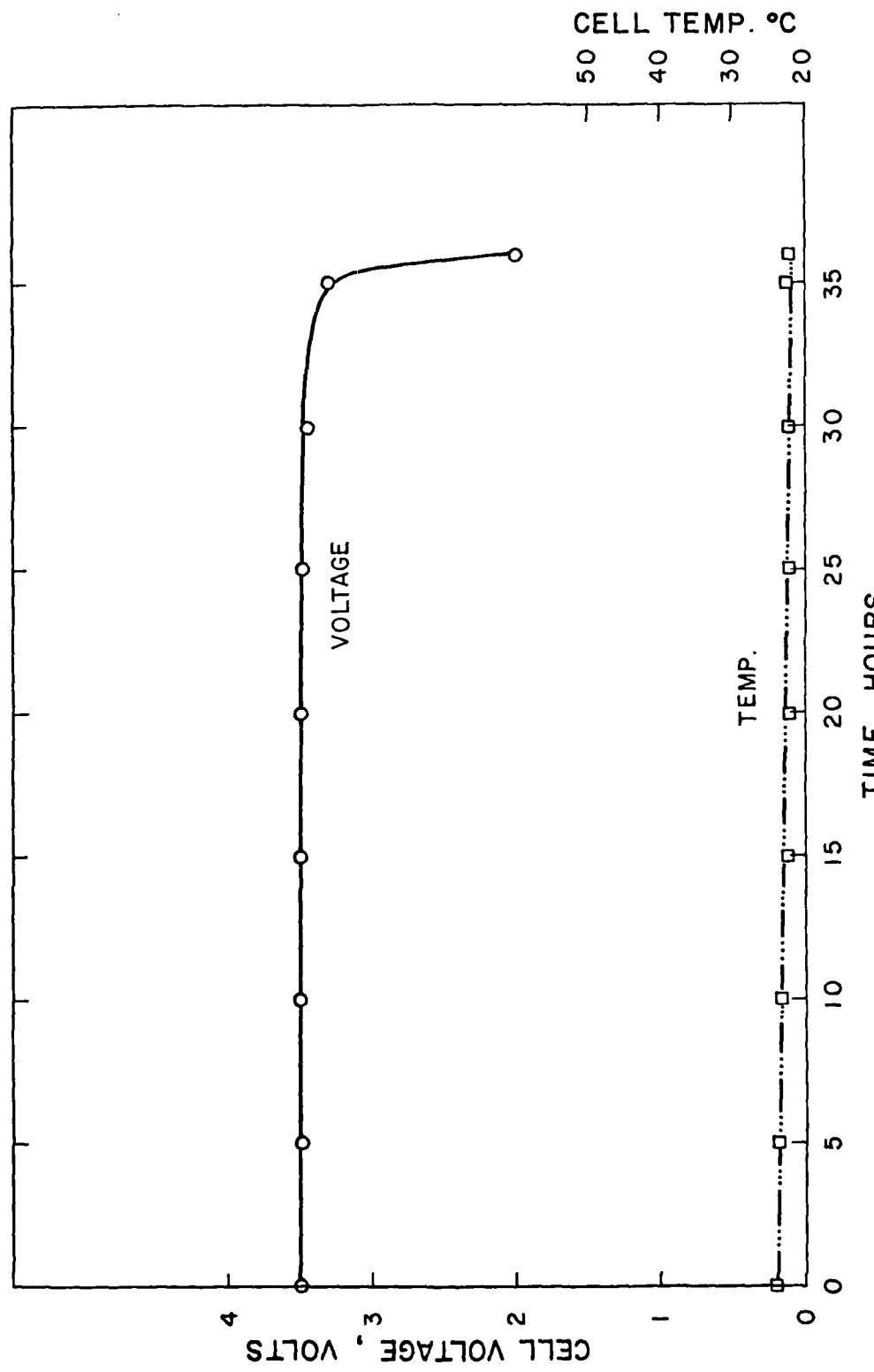


Figure 66. Performance of an optimized high rate D cell on constant current discharge at 0.3A.

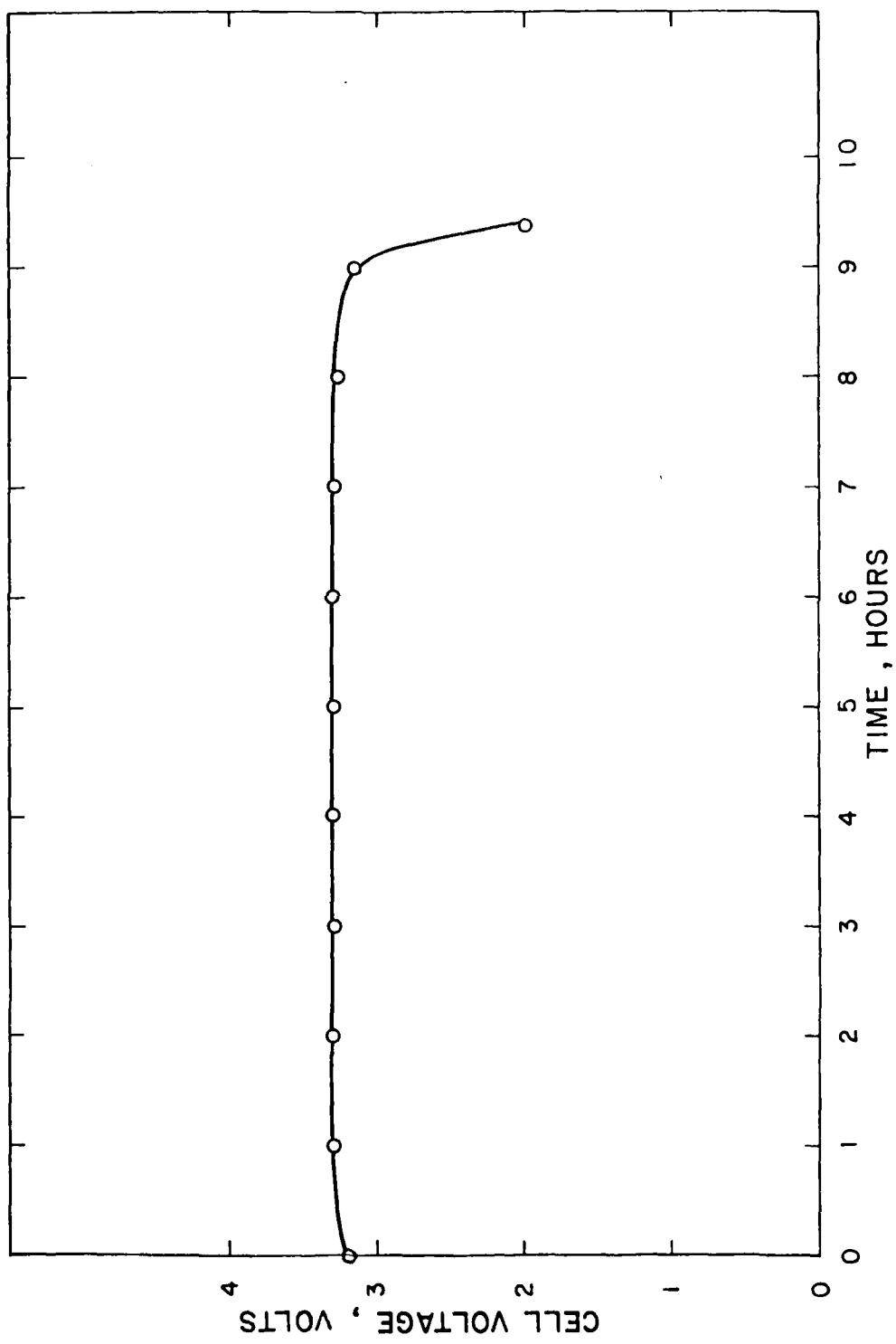


Figure 6.7. Performance of an optimized high rate D cell on discharge at 1A.

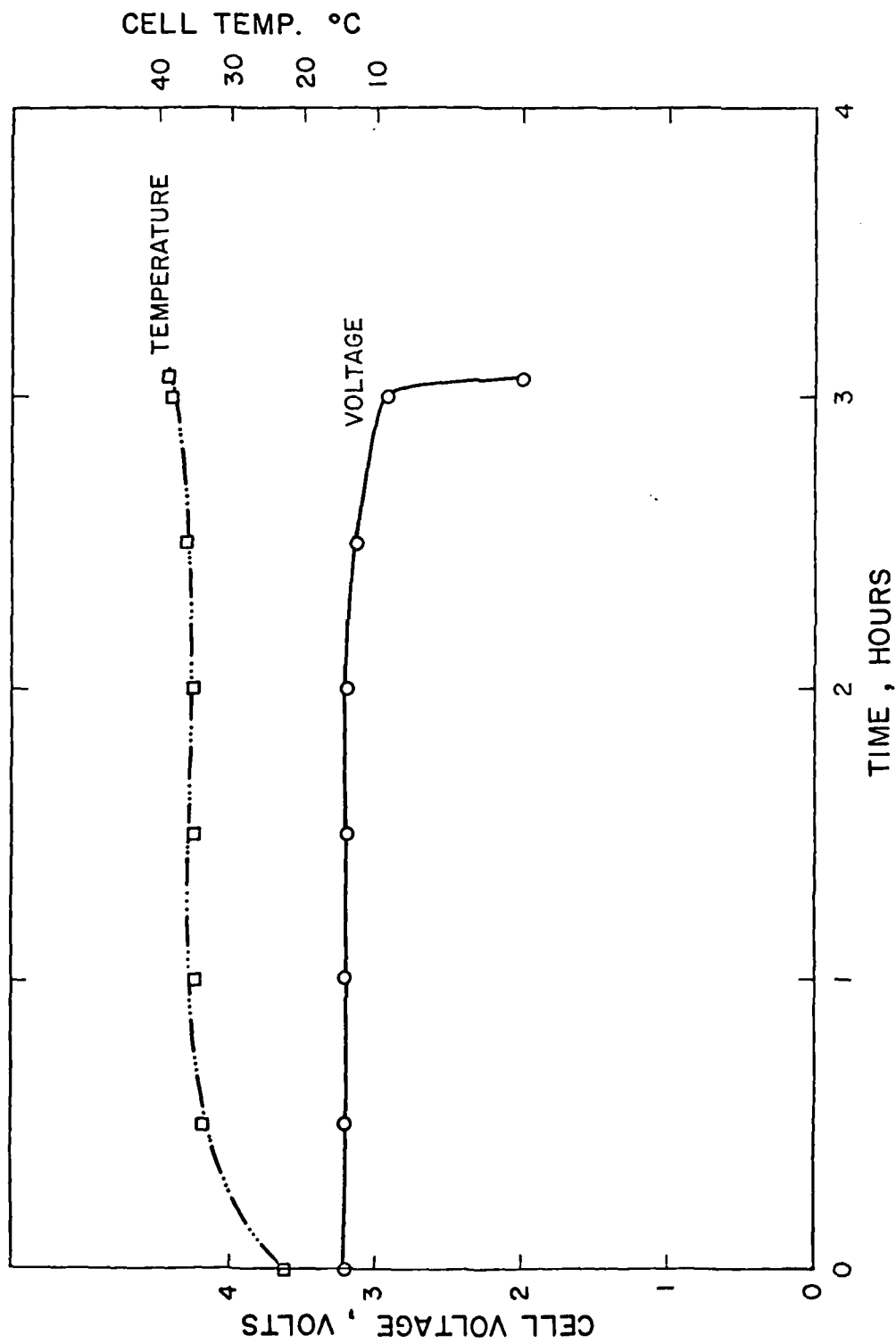


Figure 68. Performance of an optimized high rate D cell on discharge at 3.0A.

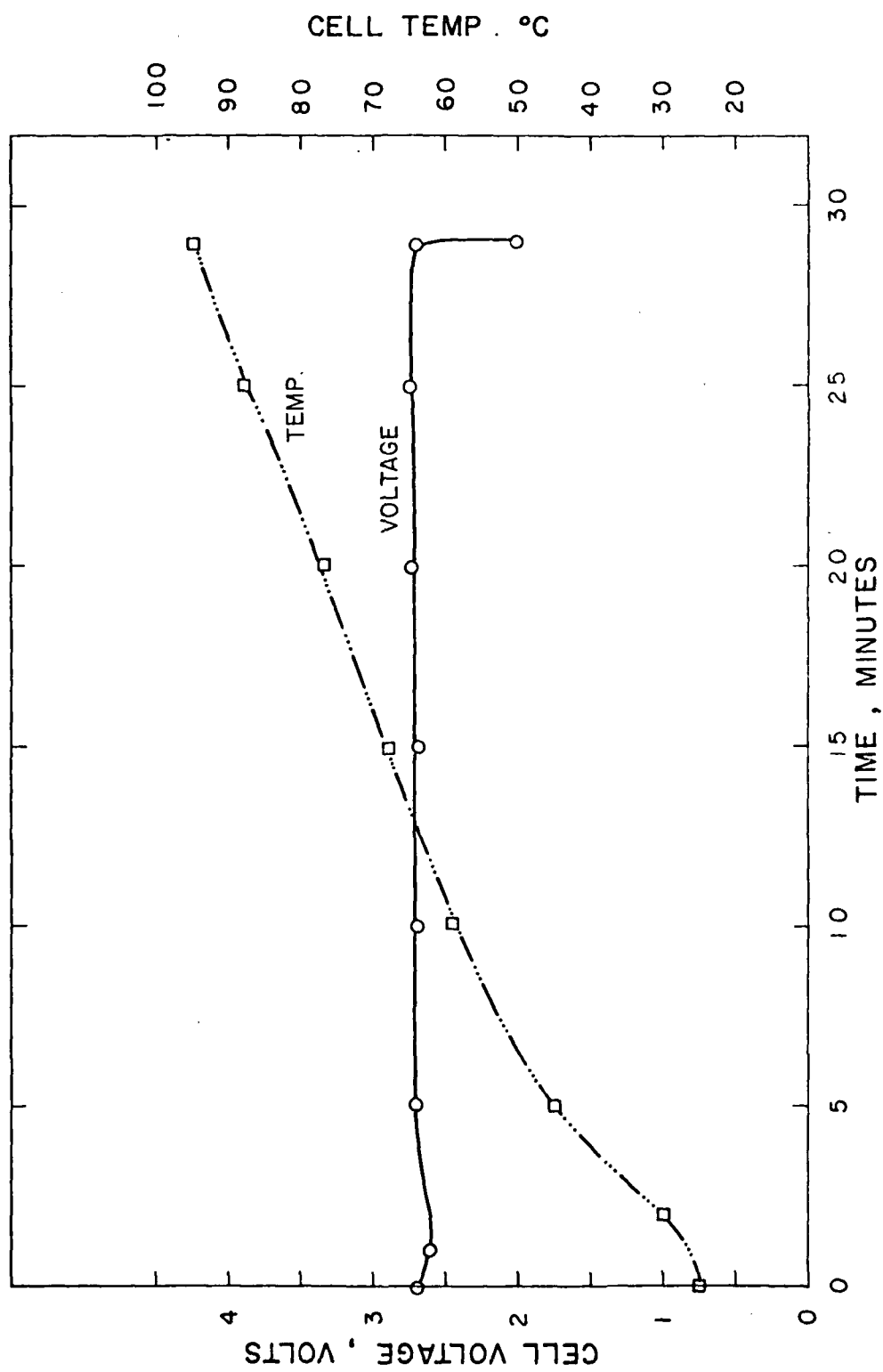


Figure 69. Plot of cell voltage and temperature for an optimized D cell on discharge at 10A.

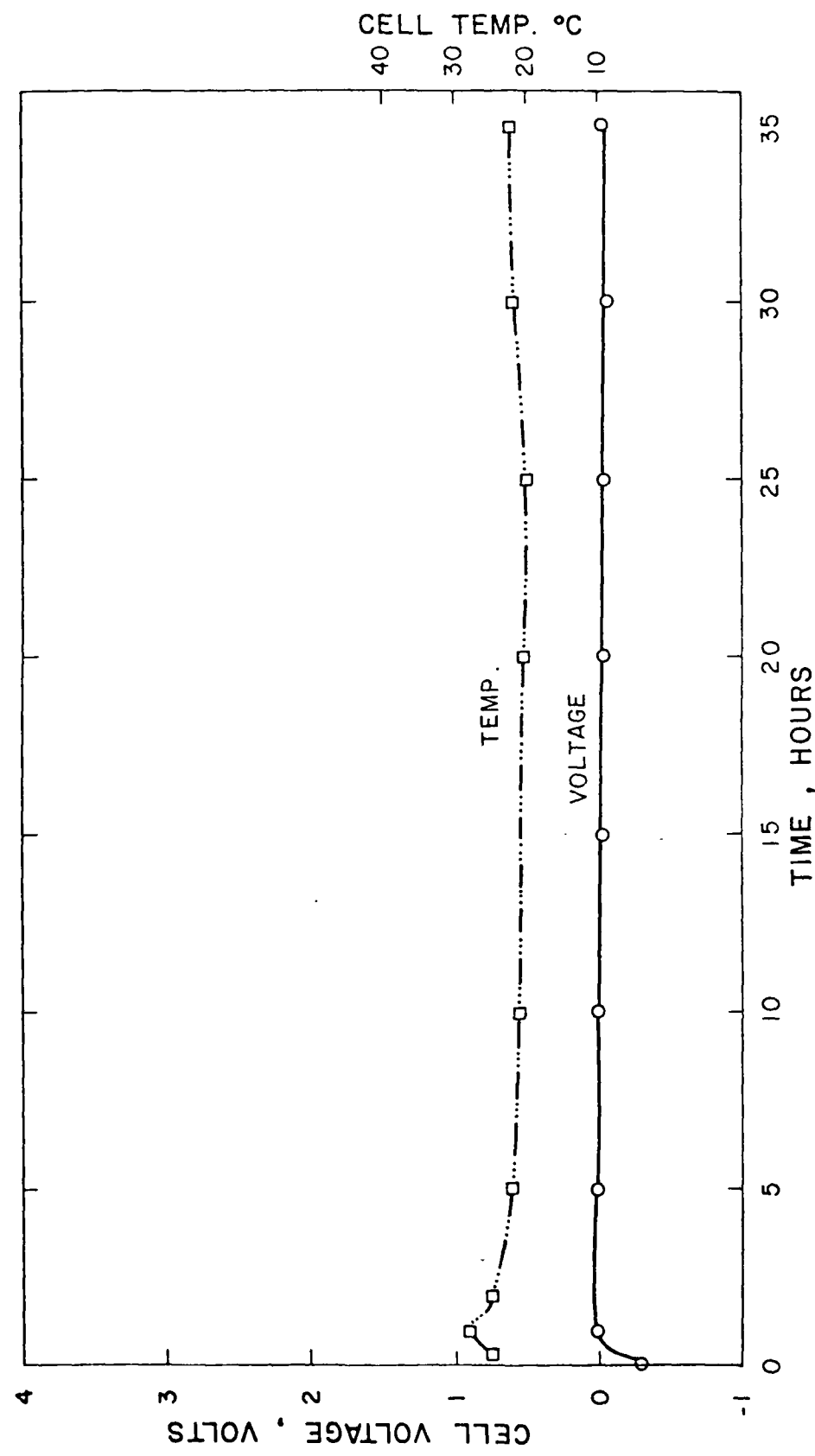


Figure 70. Plot of cell temperature and voltage for an optimized D cell in normal operation,  
at 25°C.

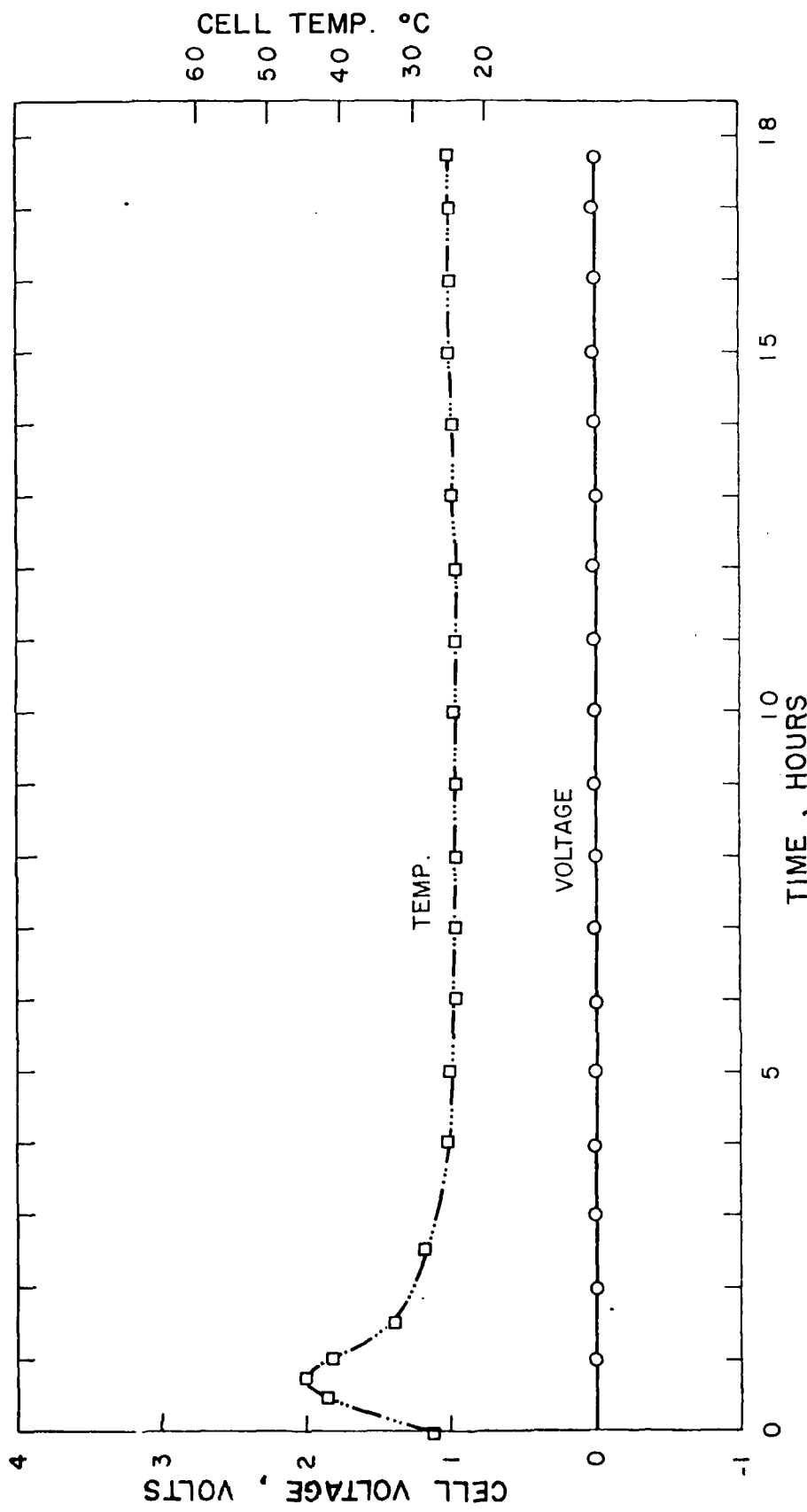


Figure 71. Temperature and voltage for an optimized D cell with cathode additive C in reversal at 1A.

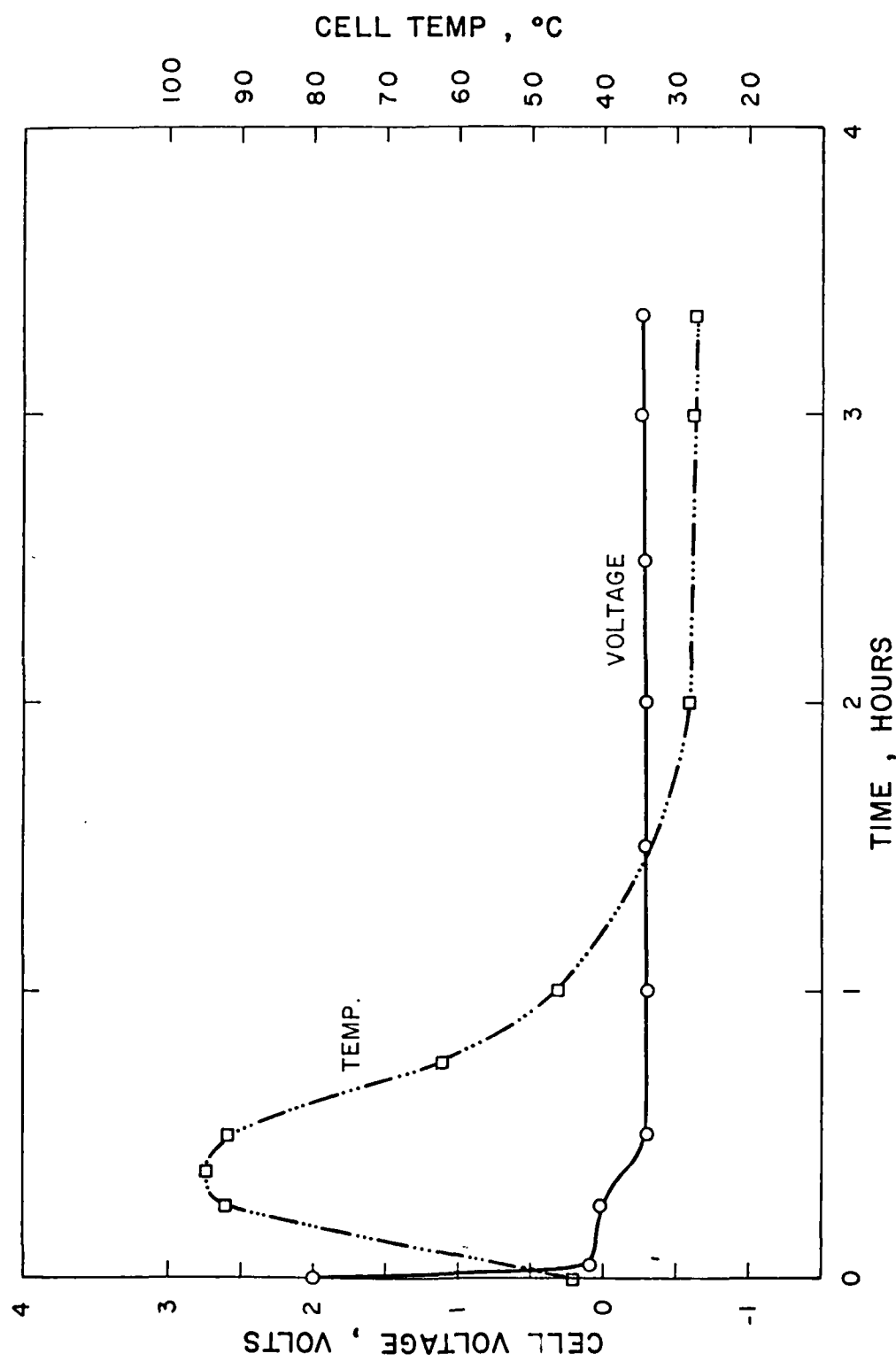


Figure 72. Cell temperature and voltage for an optimized D cell driven into reversal at 3A.

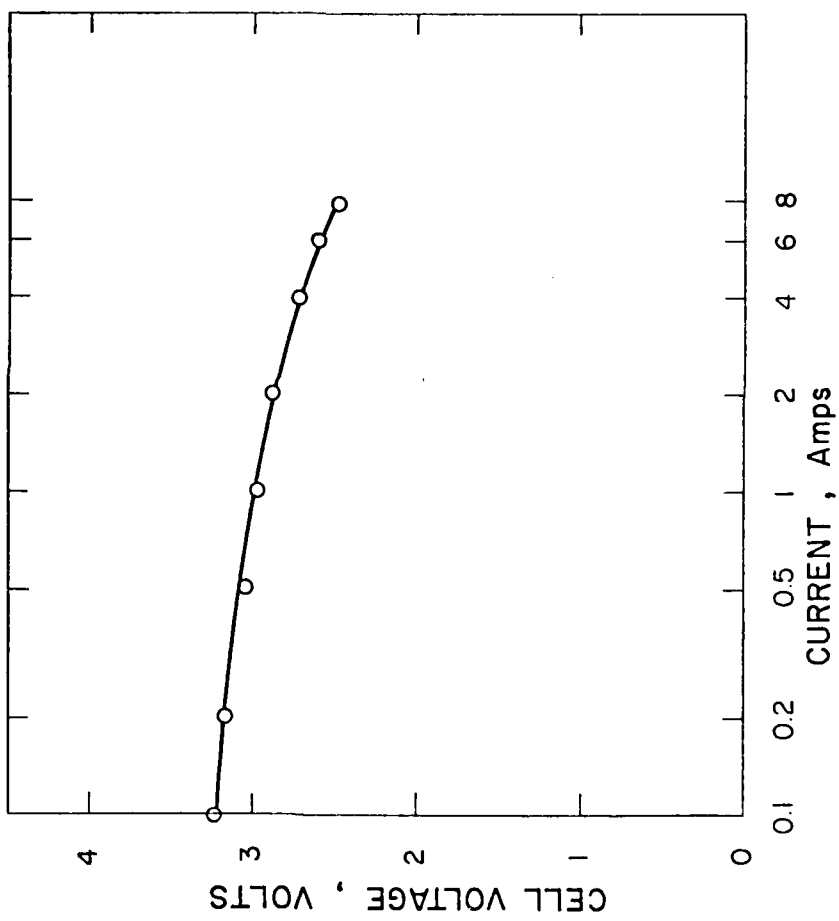


FIGURE 72. Polarization of an optimized D cell at -30°C.

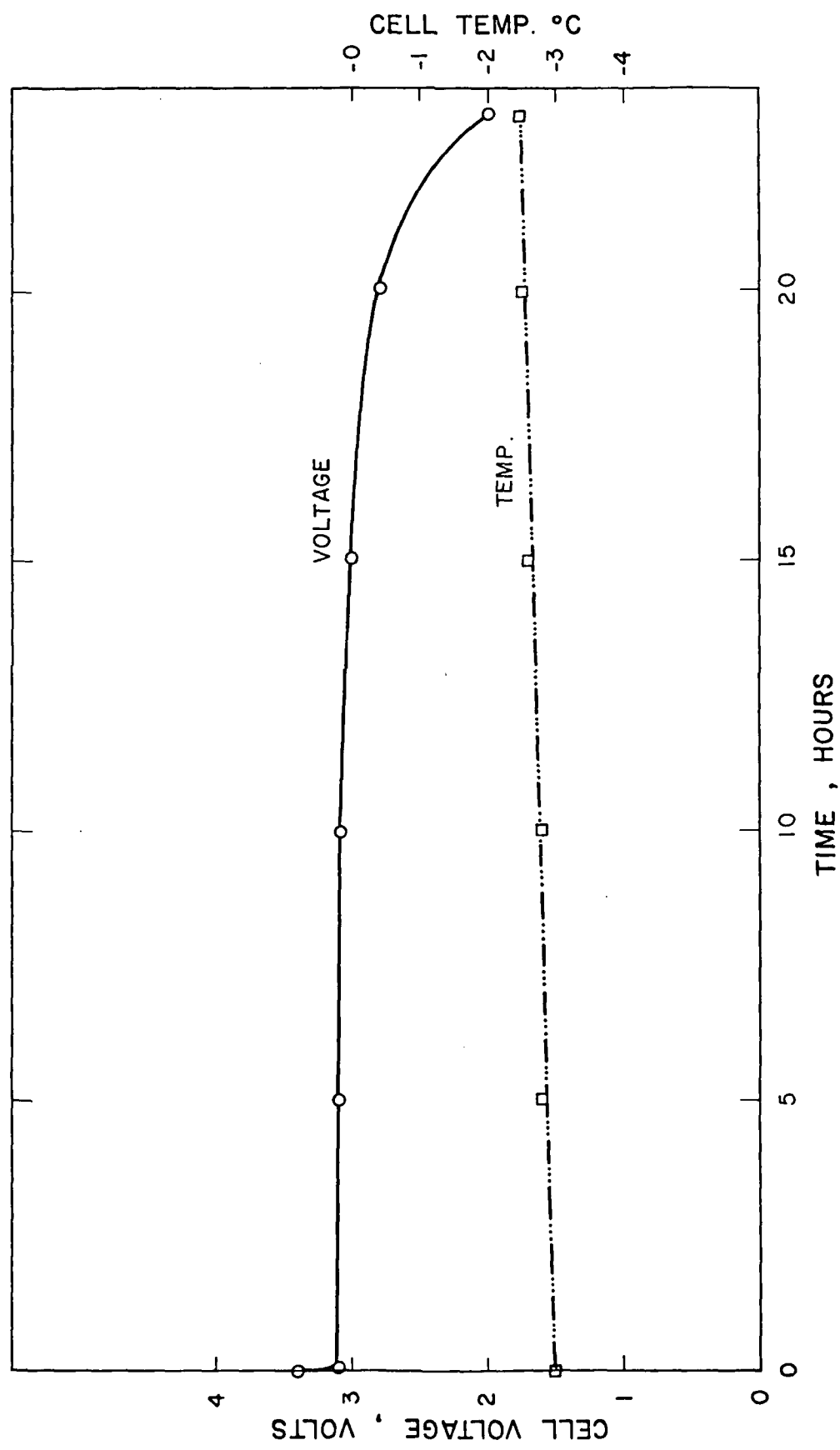


Figure 74. Discharge of an optimized D cell on 0.3A load at -30°C

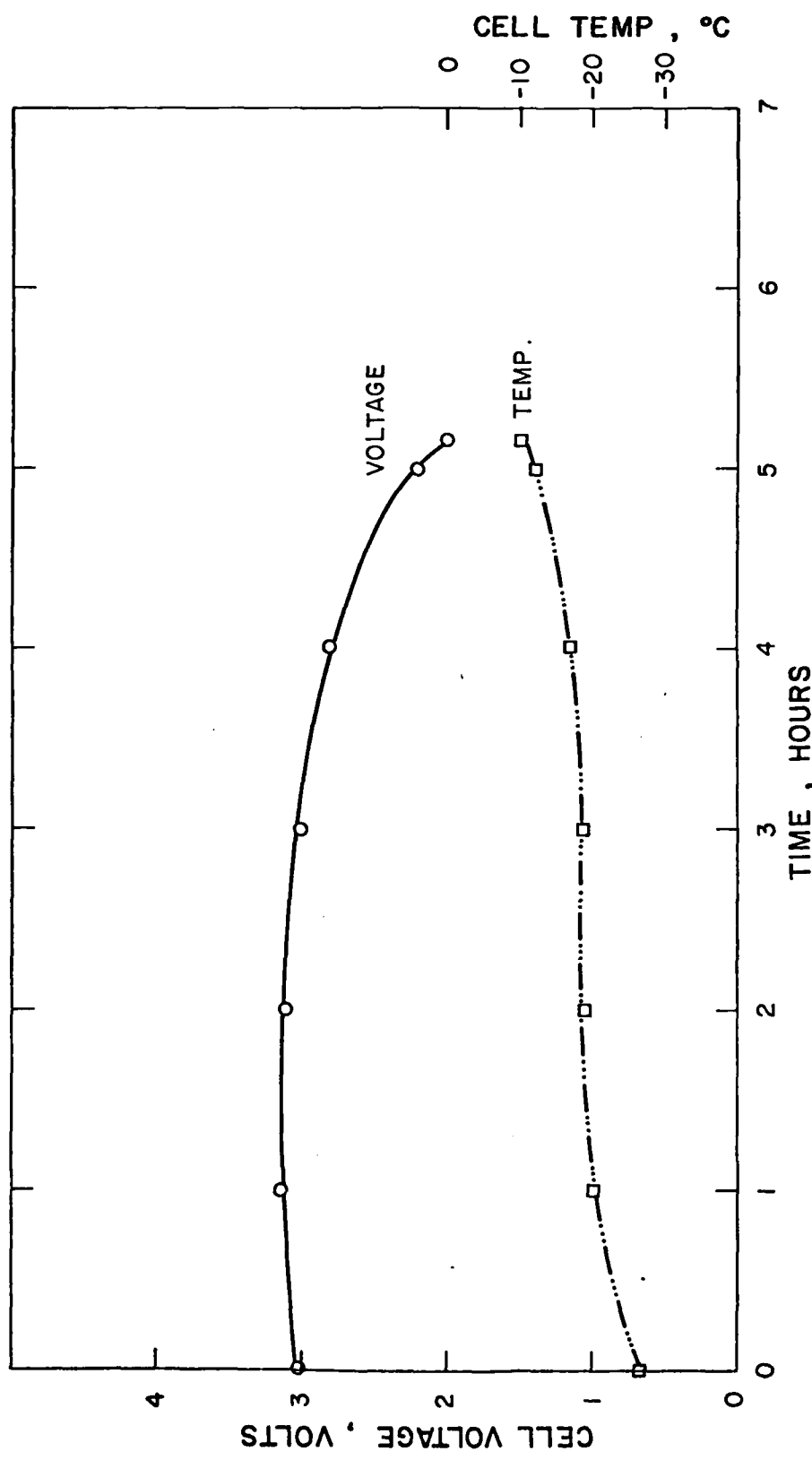


Figure 75. Discharge of an optimized D cell with cathode additive 2 at 1A at -30°C.

160.

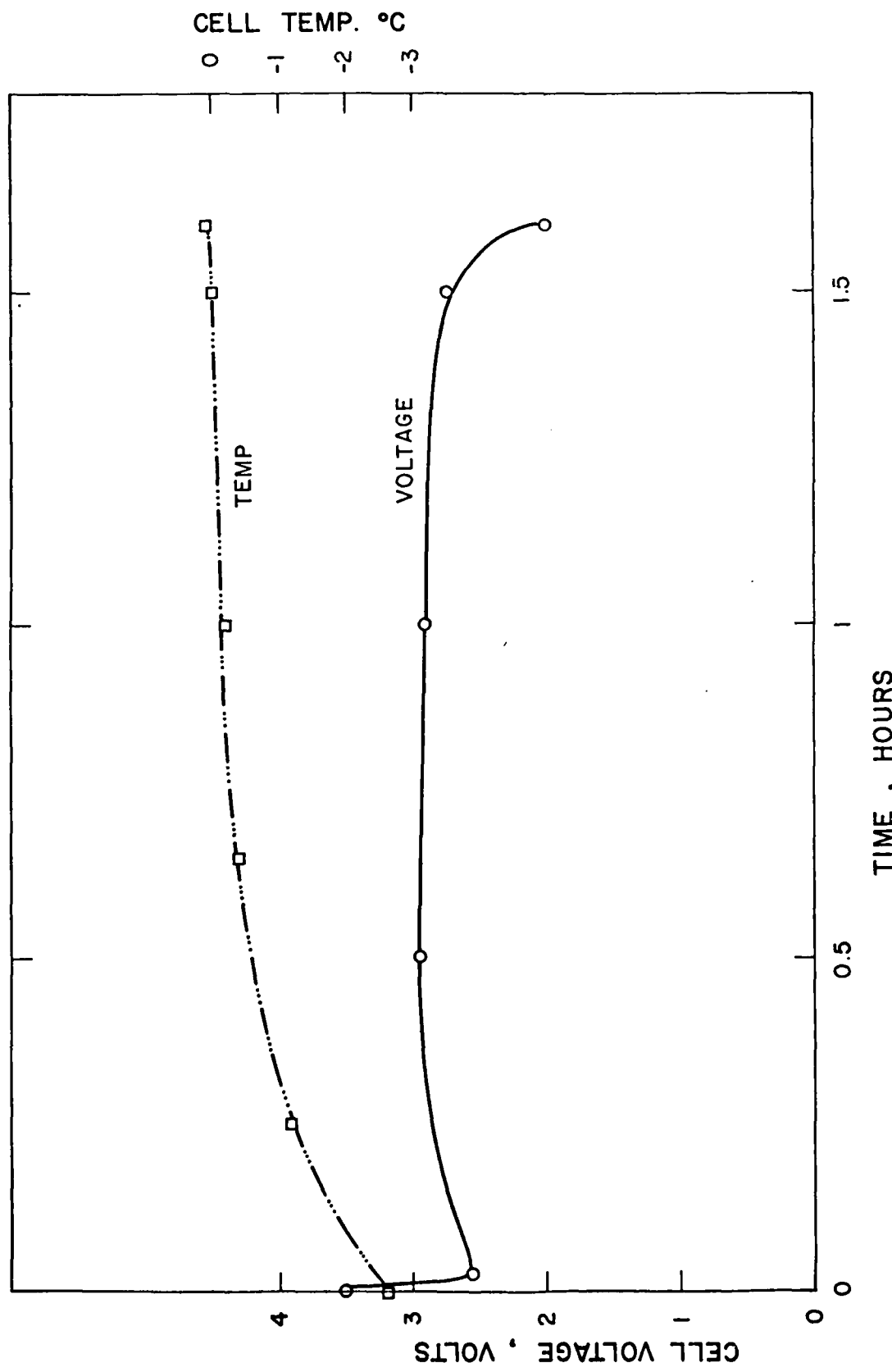


Figure 76. Discharge of an optimized D cell on 3 A load at -30°C.

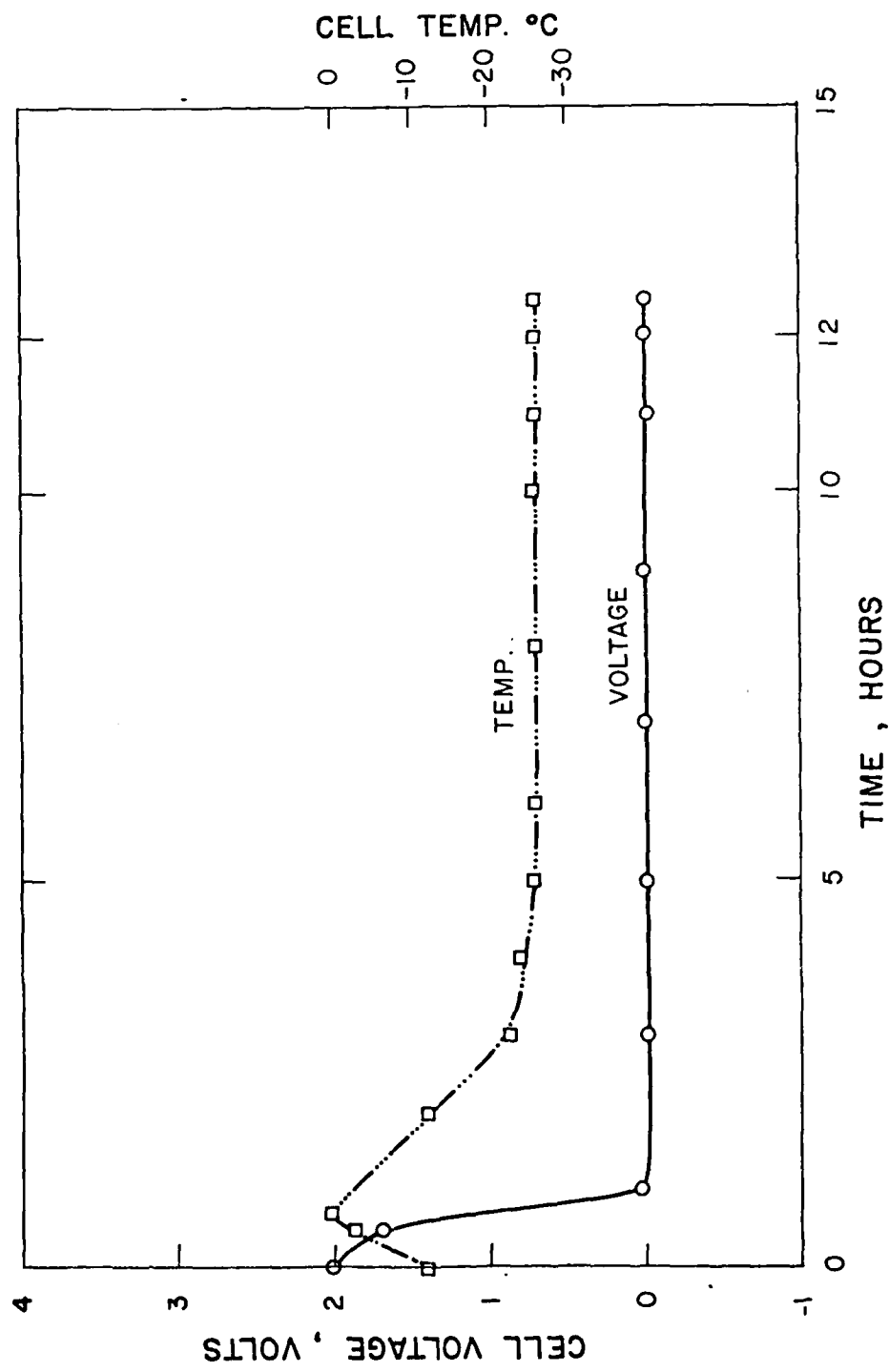


Figure 77. Cell temperature and voltage for an optimized D cell with cathode additive 2 in reversal at 1 A at  $-30^{\circ}\text{C}$ .

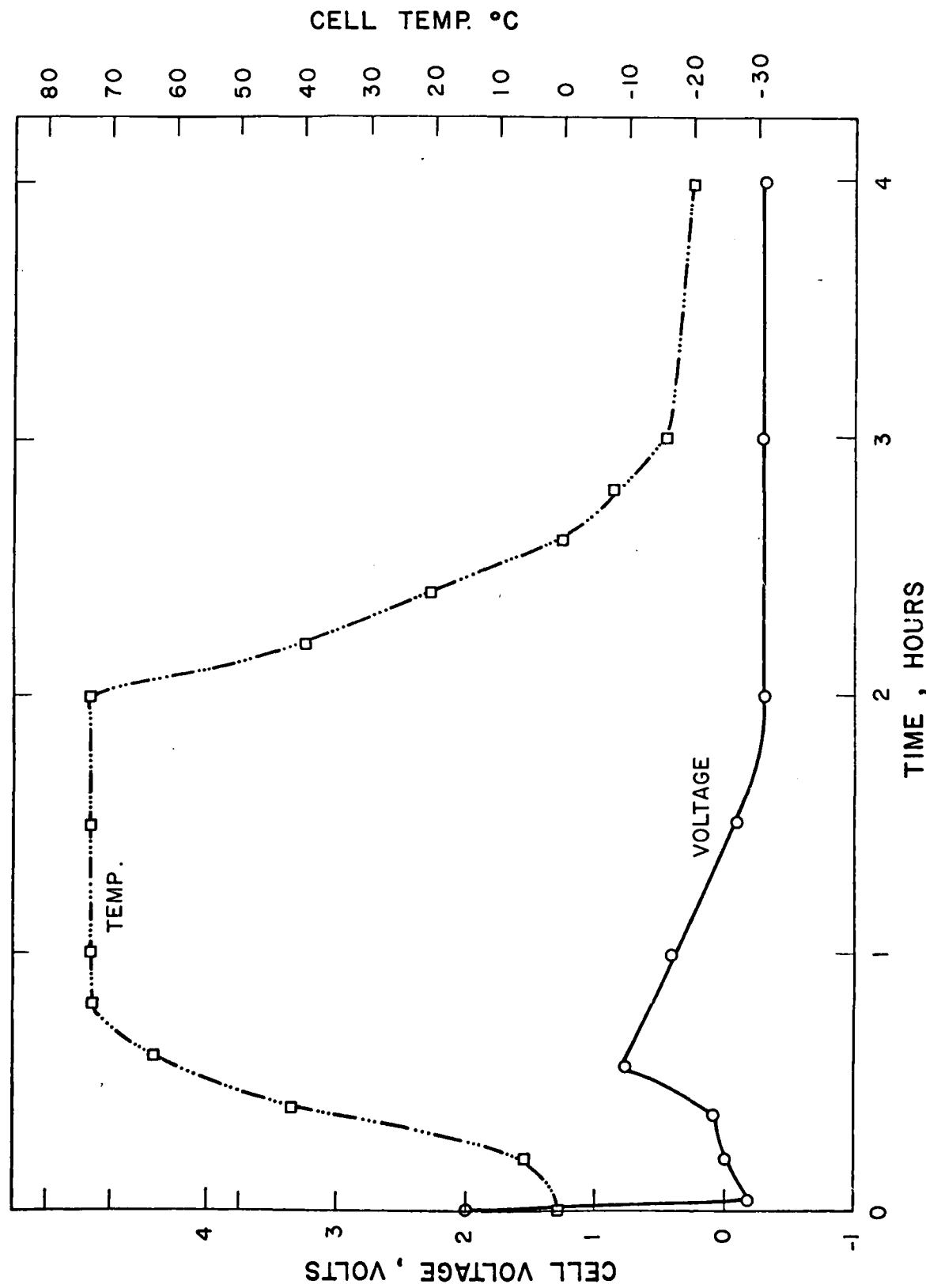


Figure 78. Cell temperature and voltage for an optimized D cell driven into reversal at 3A and -30°C.

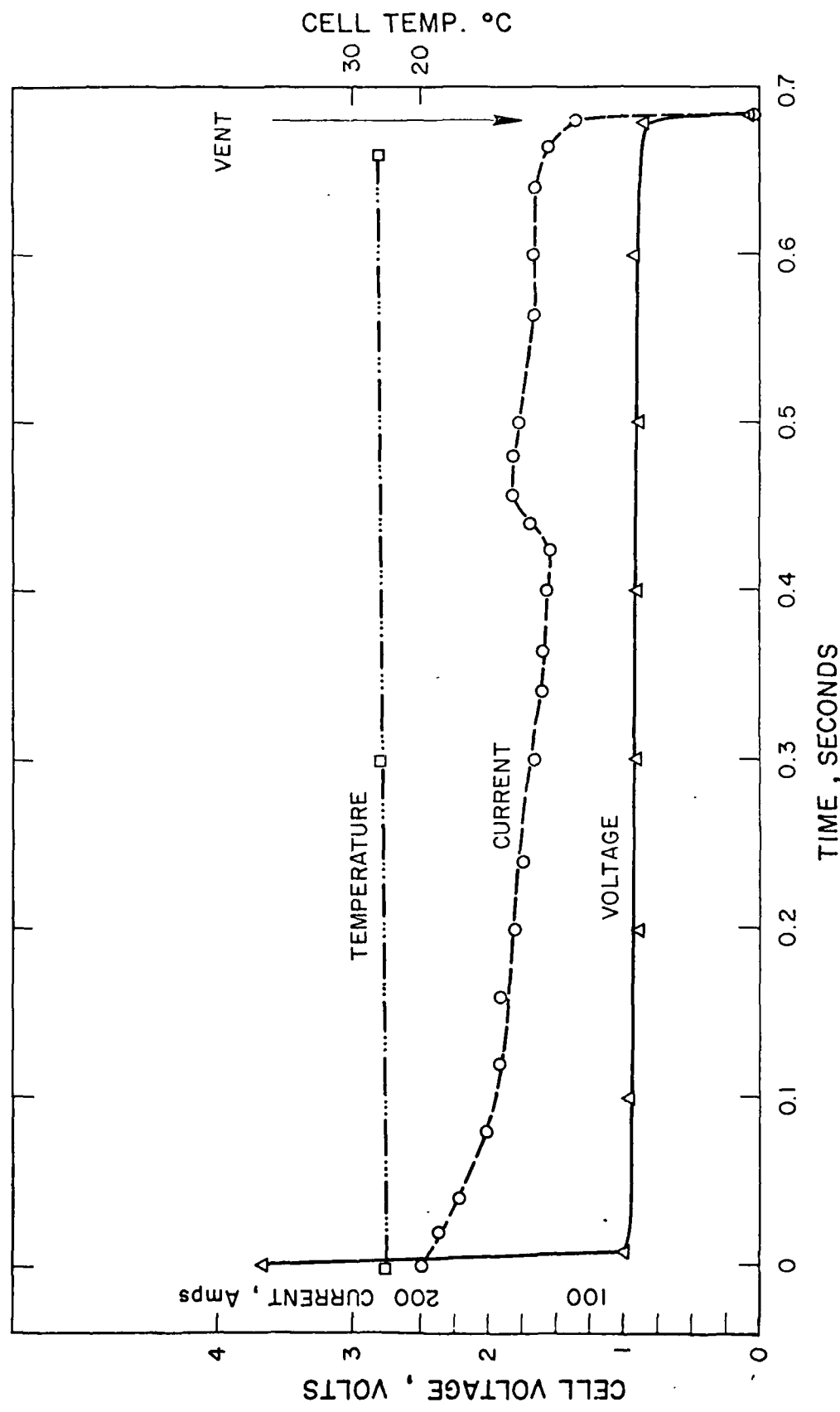


Figure 79. Short circuit current of an optimized high rate D cell.

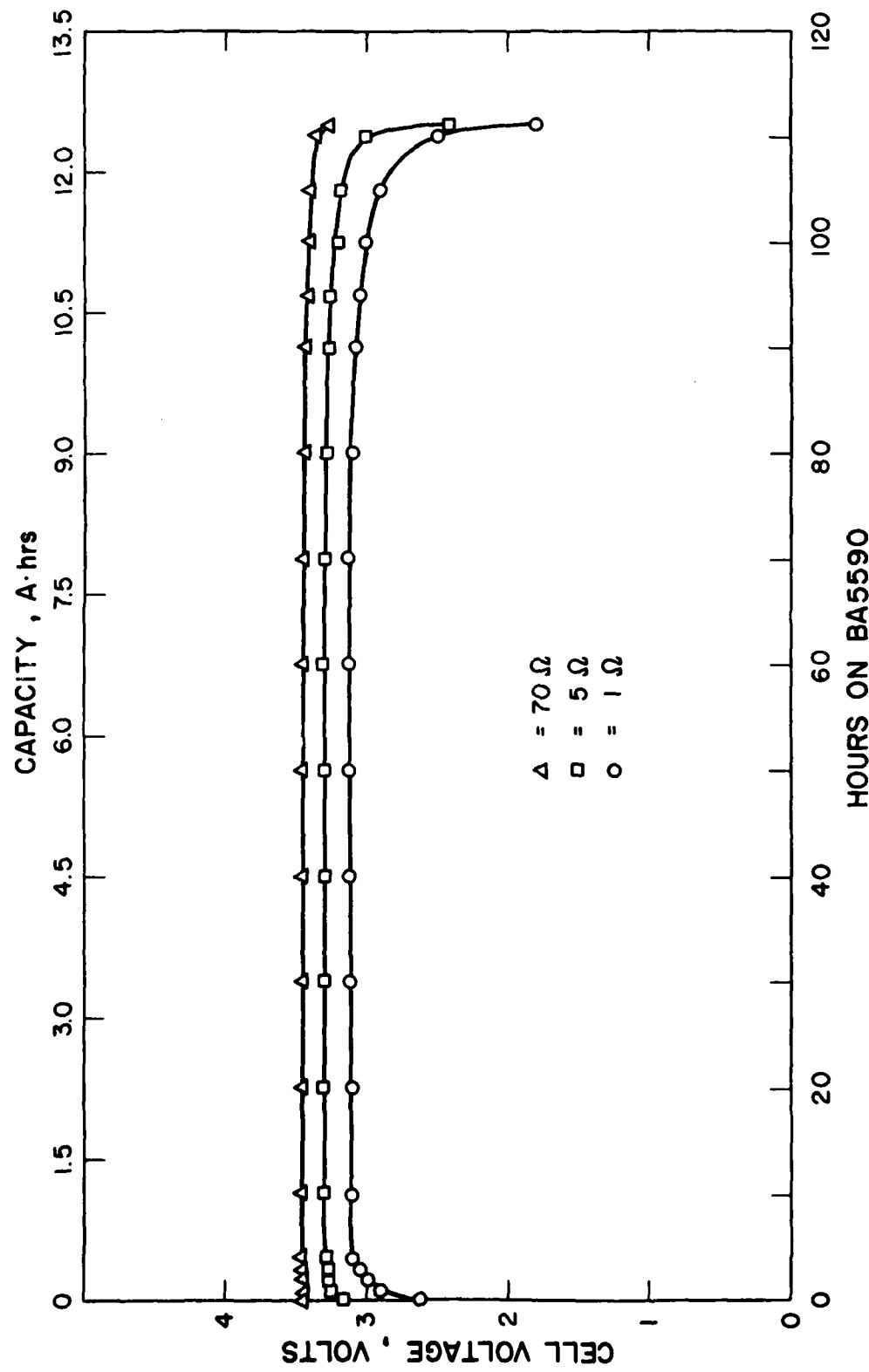


Figure 80. Performance of a high rate D cell on the BA5590 test after two weeks at 72°C.

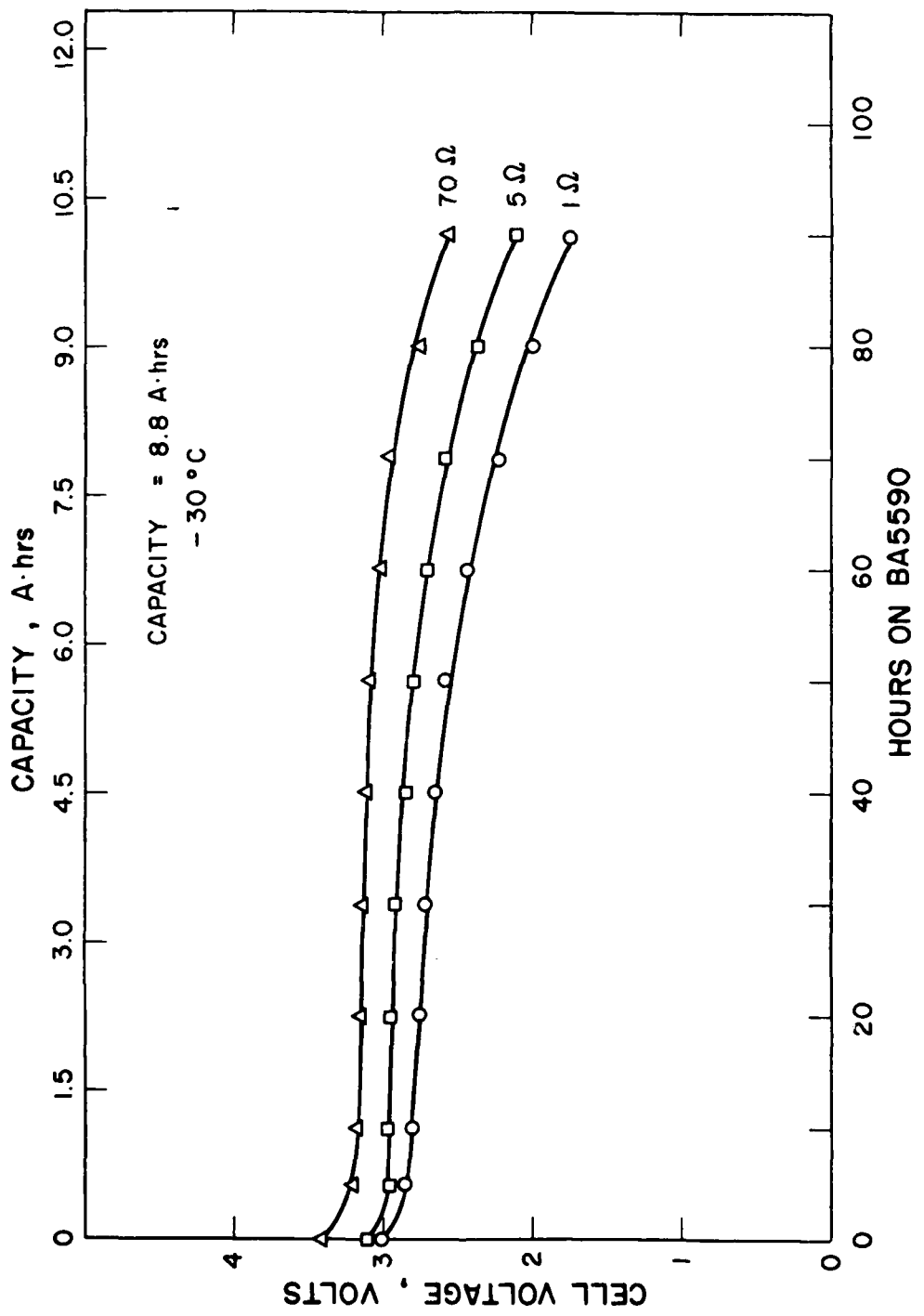


Figure 81. Performance of a D cell at  $-30^{\circ}\text{C}$  on the BA5590 test after two weeks storage at  $72^{\circ}\text{C}$ .

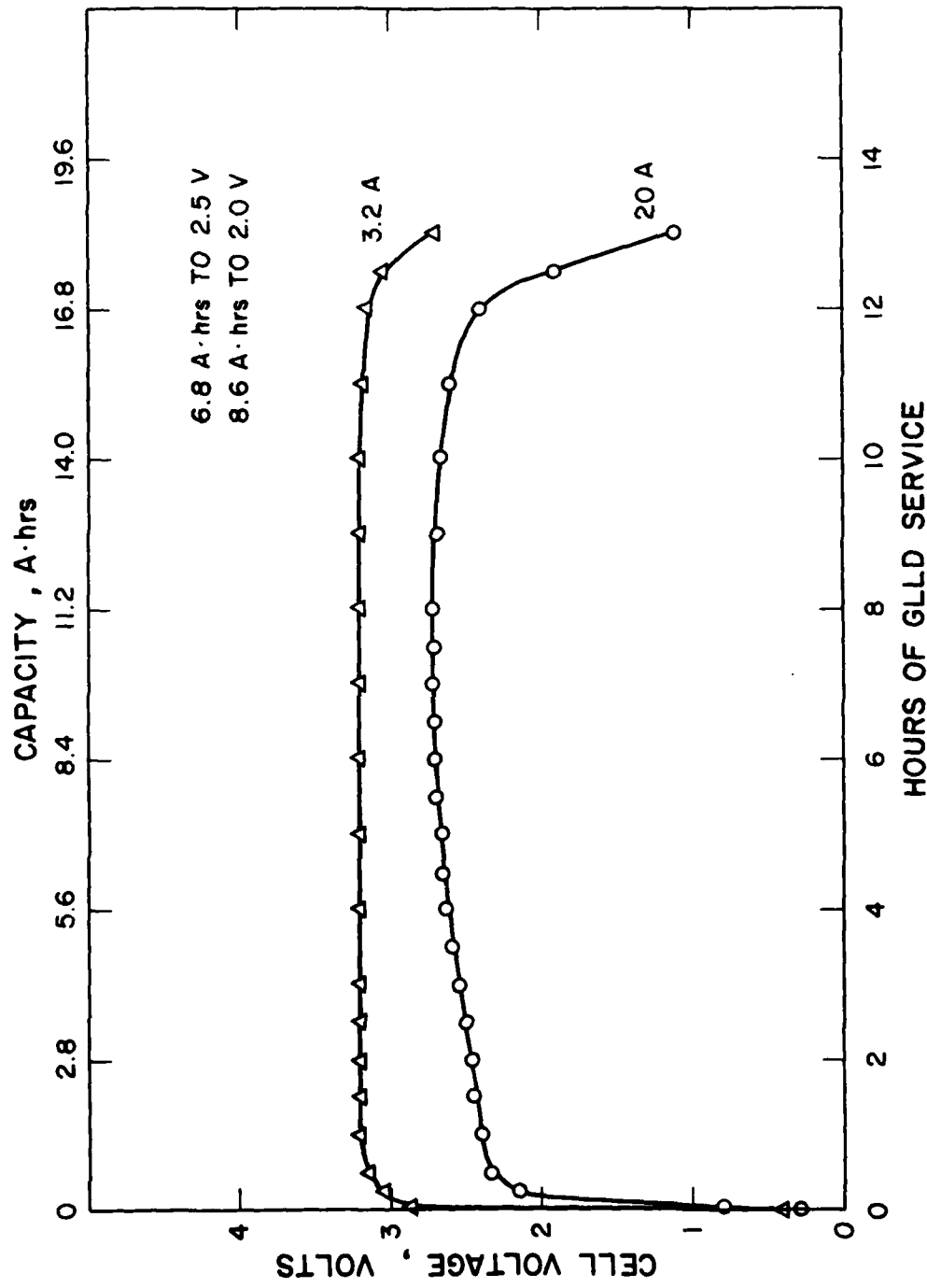


Figure 82. Performance of a pair of D cells on the GLLD test after two weeks storage at 72°C.

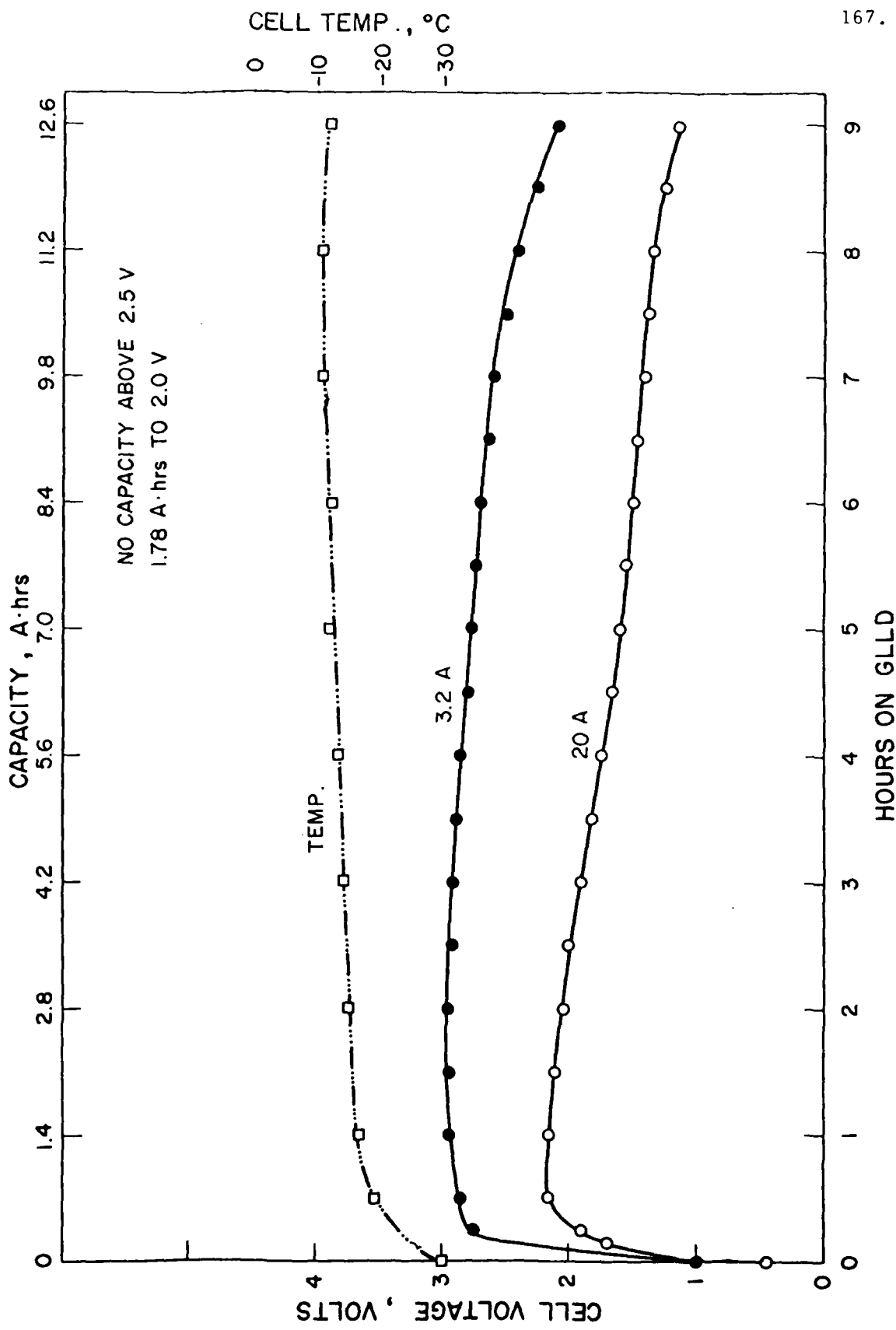


Figure 83. Performance of a pair of D cells on the GLLD test at -30°C after two weeks of storage at 72°C

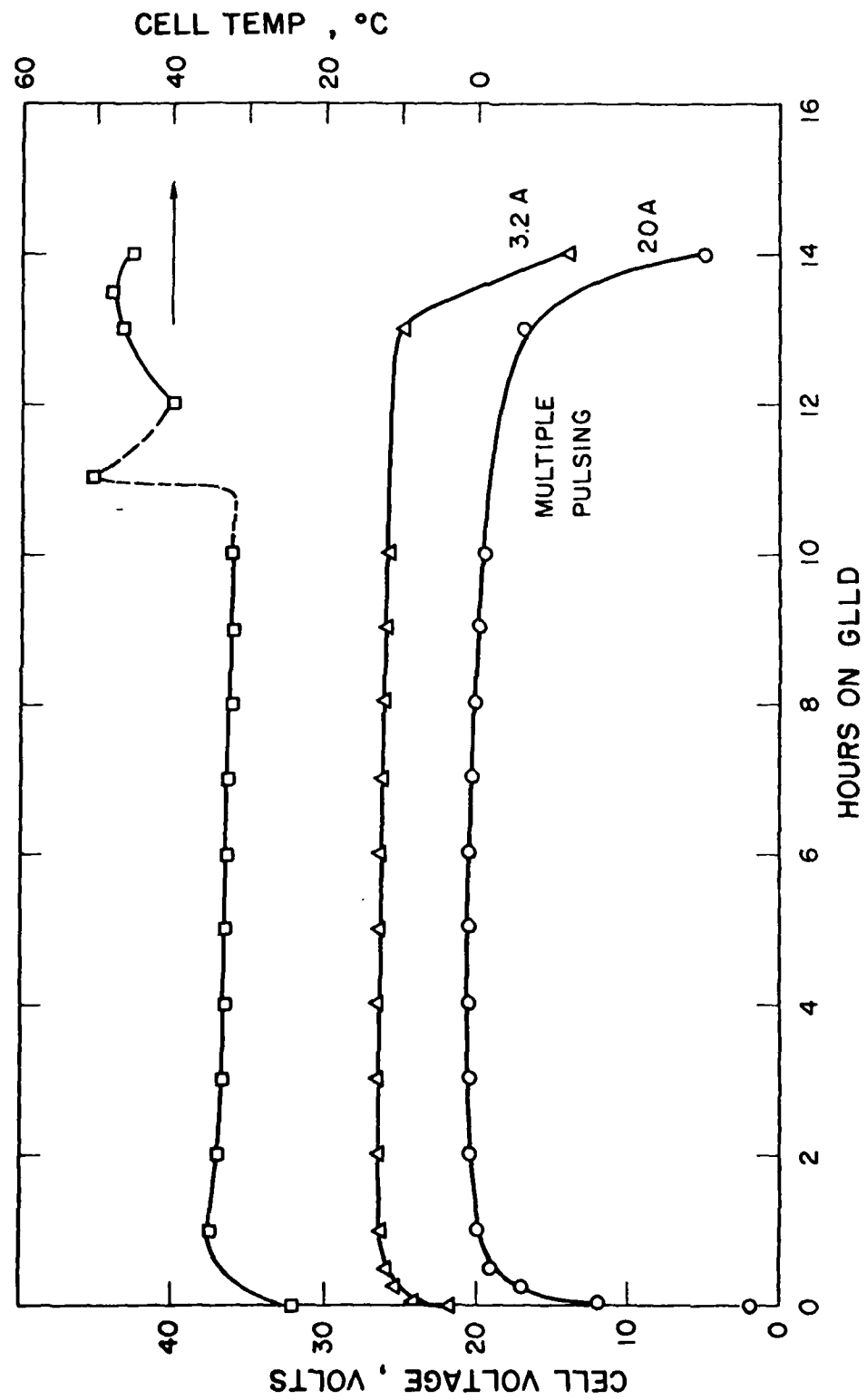


Figure 83a. Performance of a 16 cell GLLD battery on the new GLLD load at 25°C after six months on storage.

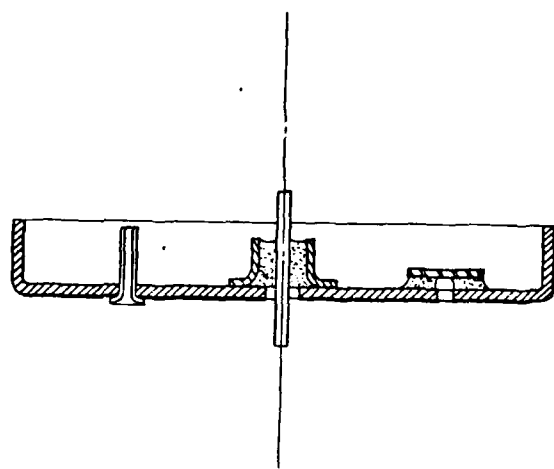


Figure 84. Schematic drawing of the completed 1.8 inch diameter cell top with fill port, vent and G/M feedthrough.

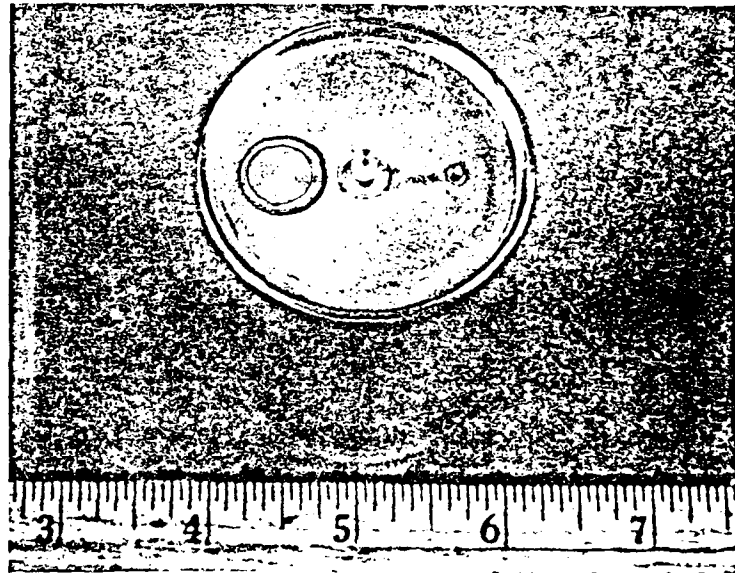


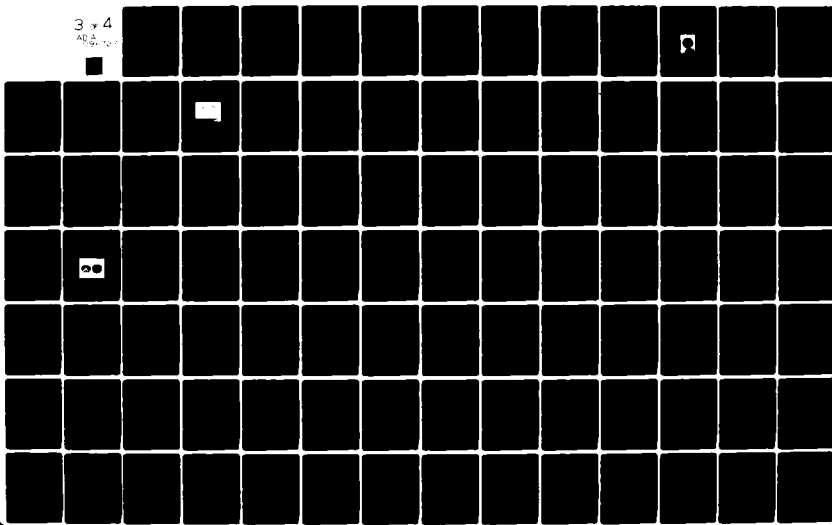
Figure 85. Photograph of the finished 1.8 inch.diameter cylindrical cell.

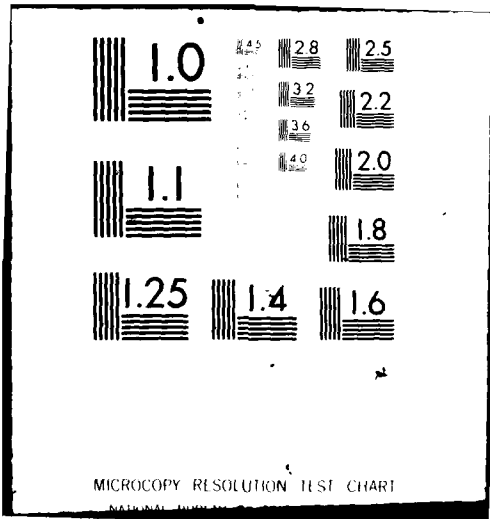
AD-A098 727 DURACELL INTERNATIONAL INC BURLINGTON MA LAB FOR PHYS--ETC F/G 10/3  
LITHIUM-THIONYL CHLORIDE BATTERY, (U)  
APR 81 D WONG, W BOWDEN, N HAMILTON

DAA807-78-C-0563  
DELET-TR-78-0563-F NL

UNCLASSIFIED

3 x 4  
AB<sup>2</sup>...  
AB<sup>2</sup>...  
AB<sup>2</sup>...





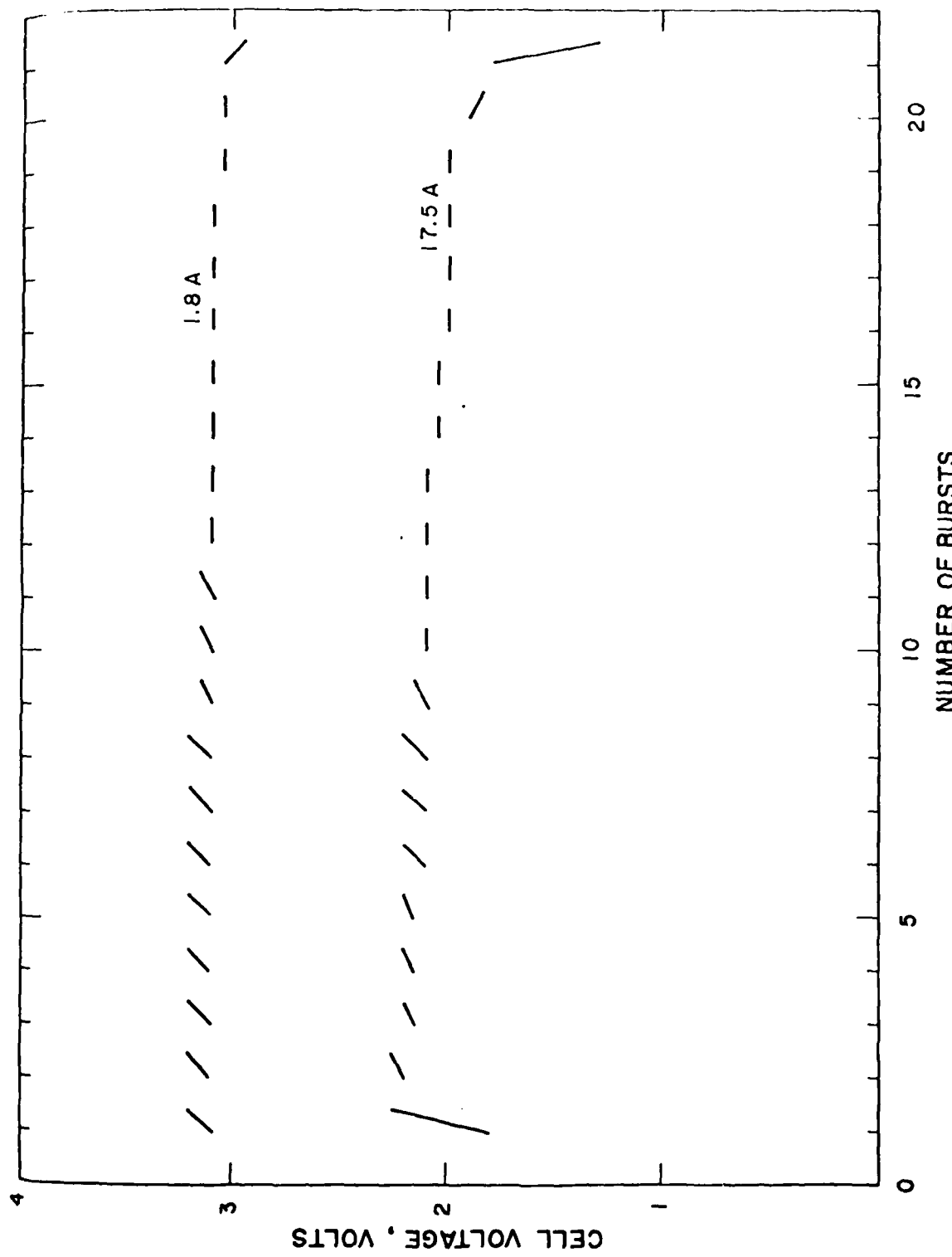


Figure 86. Performance of a 1.8 inch diameter cylindrical cell on the old GLID test cycle.

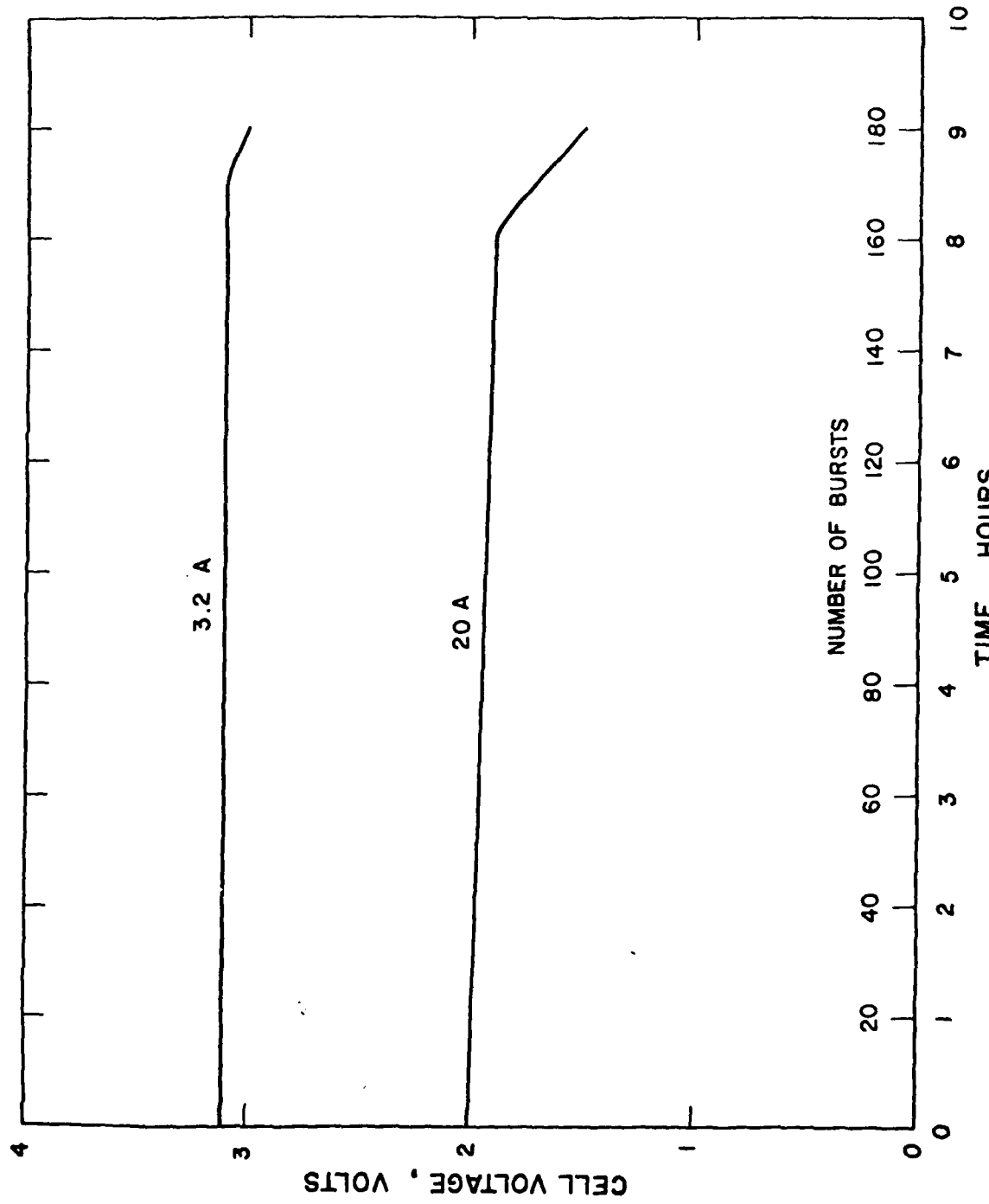


Figure 87. Performance of a 1.8 inch diameter cylindrical cell on the new GLLD test cycle.

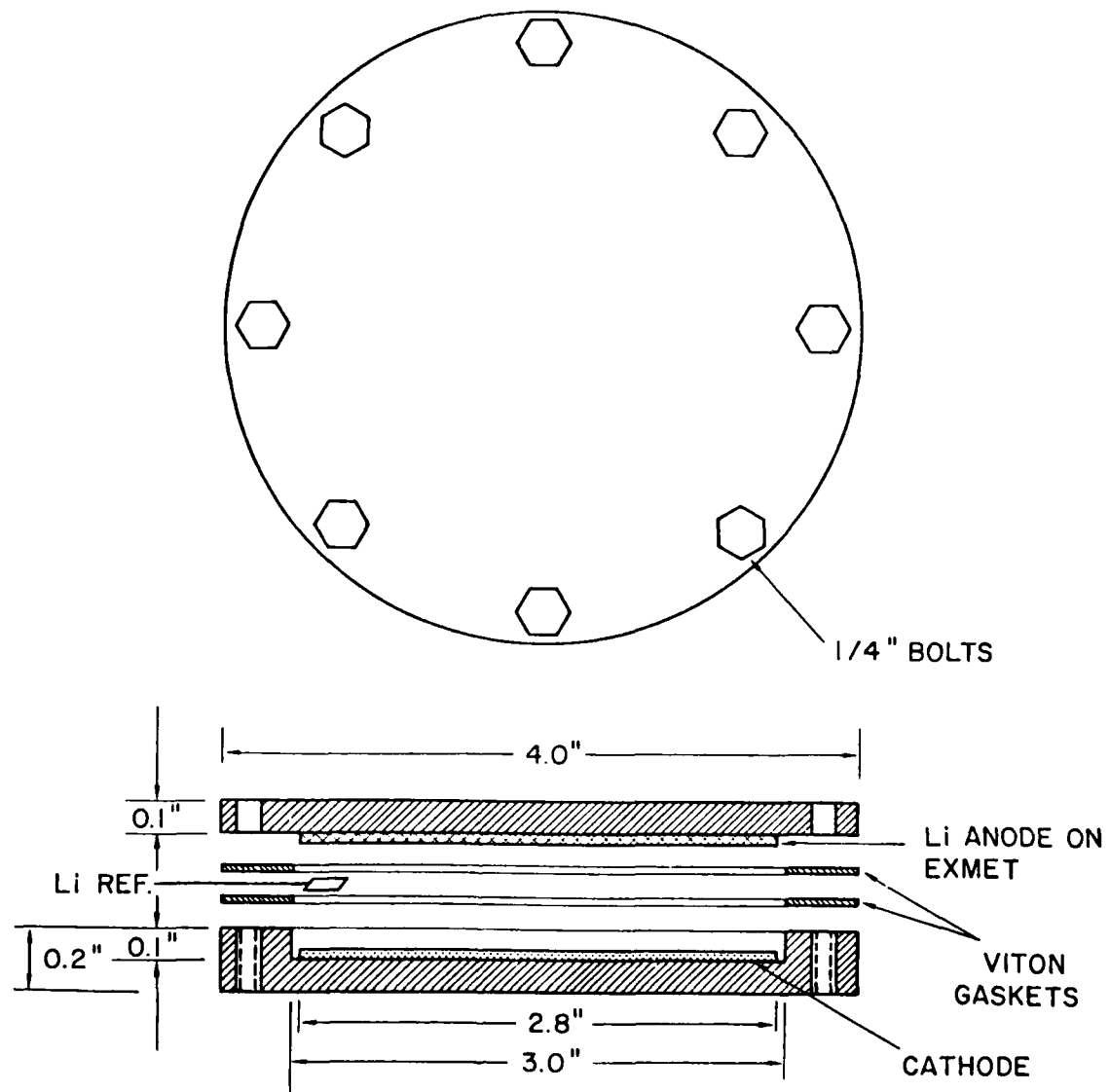


Figure 88. Schematic view of the experimental demountable flat cylindrical cell.

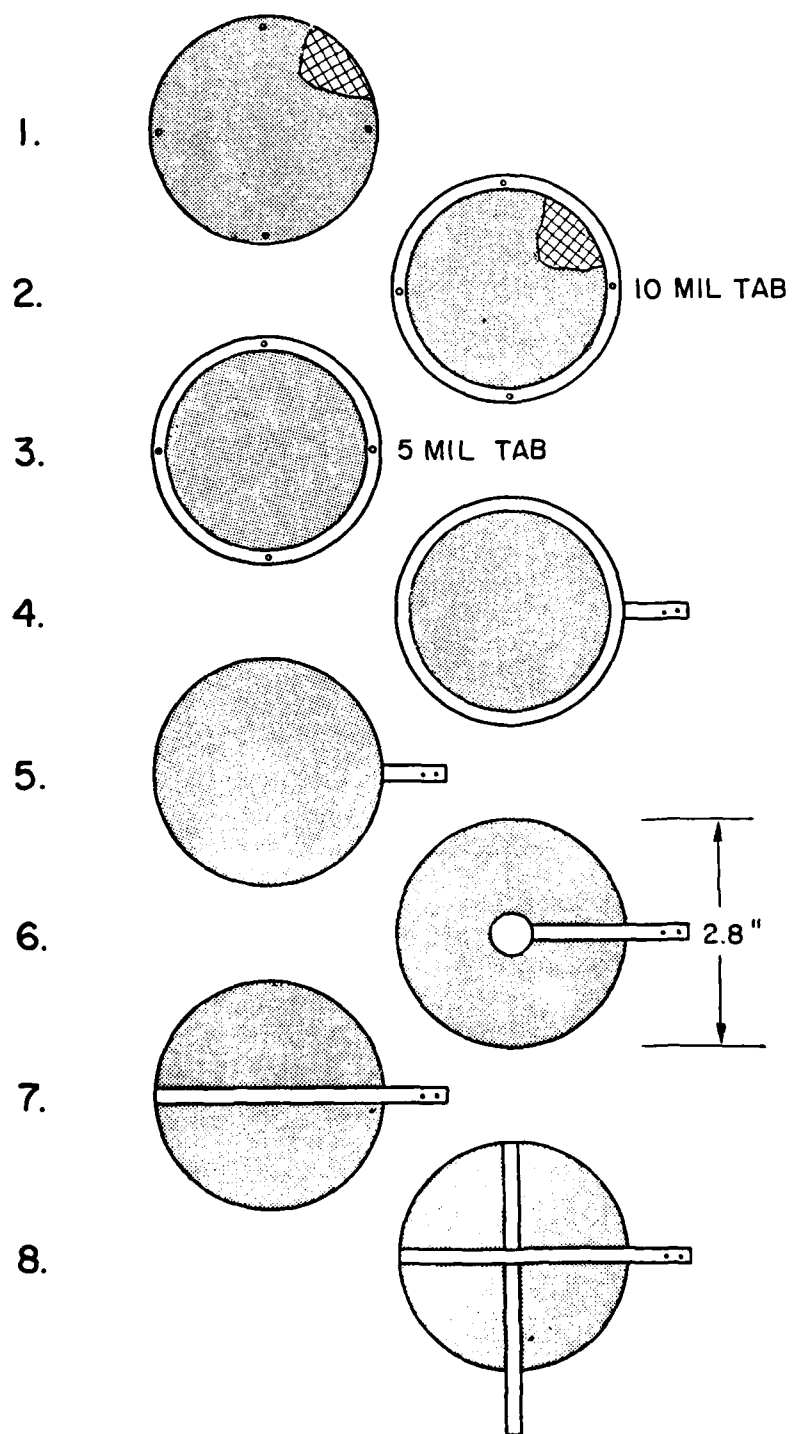


Figure 89. Current collector designs for the 2.8 inch diameter disc cathodes.

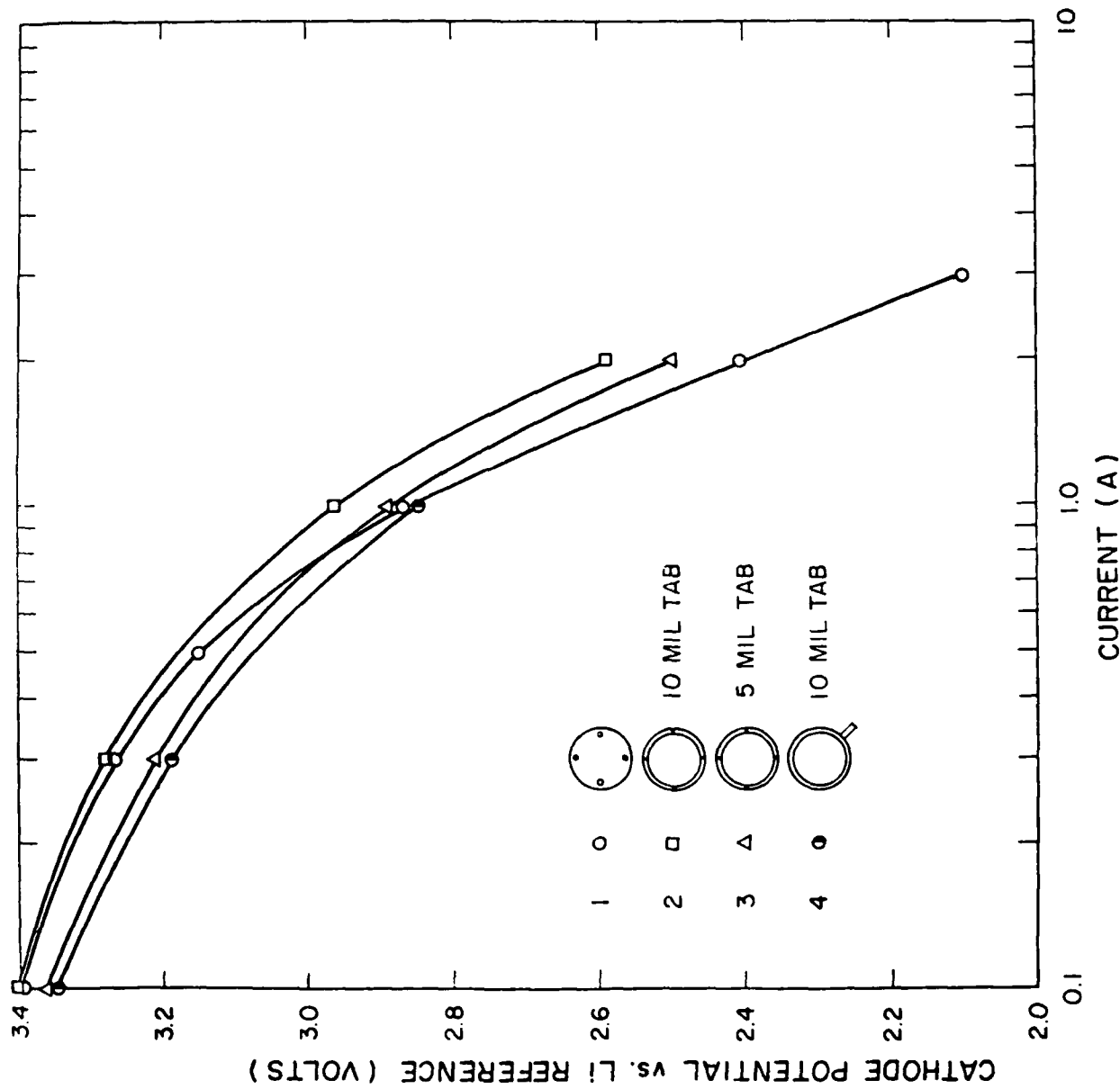


Figure 90. Polarization characteristics of disc shaped cathodes with various current collector designs.

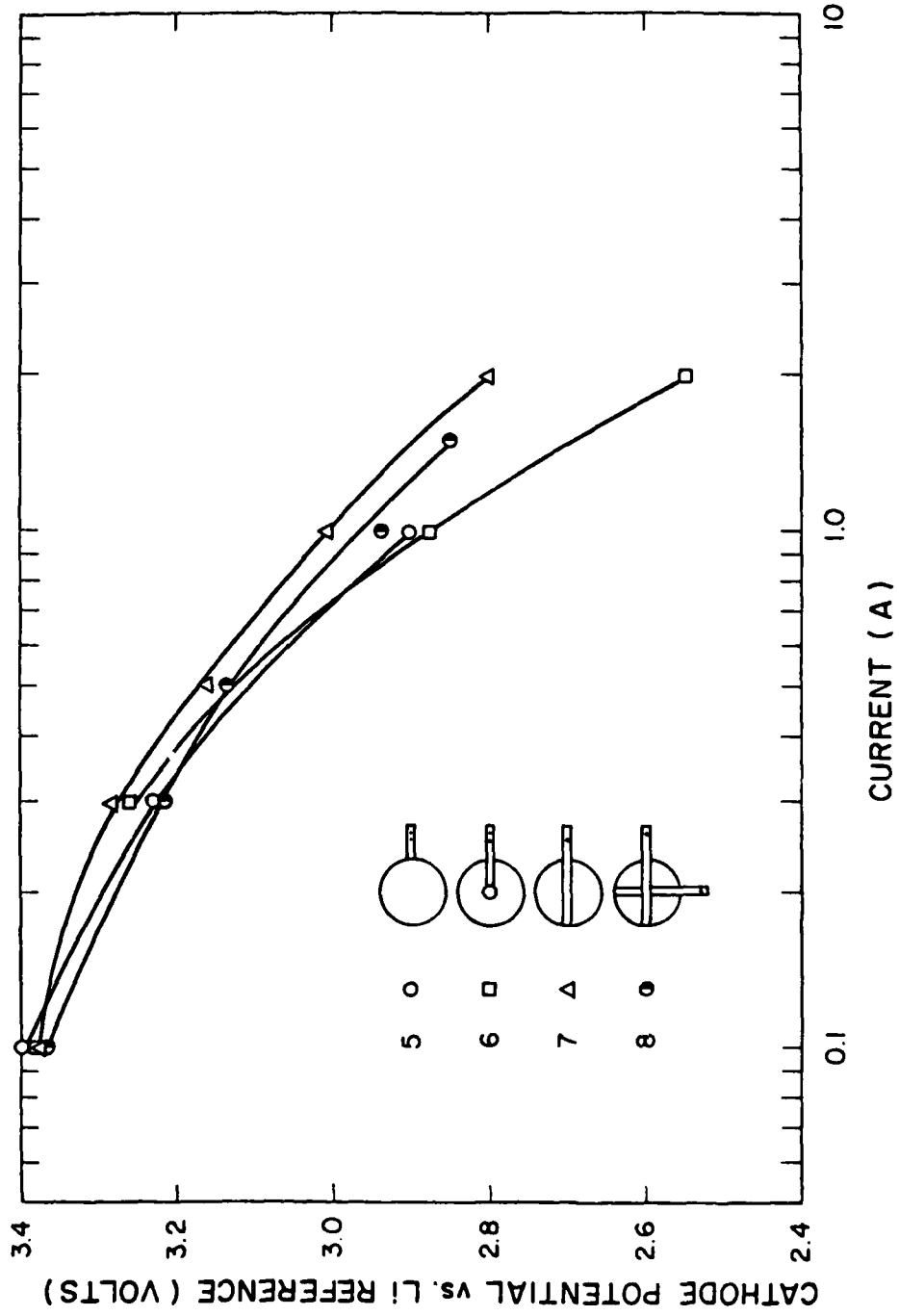


Figure 91. Polarization characteristics of disc shaped cathodes with various current collector designs.

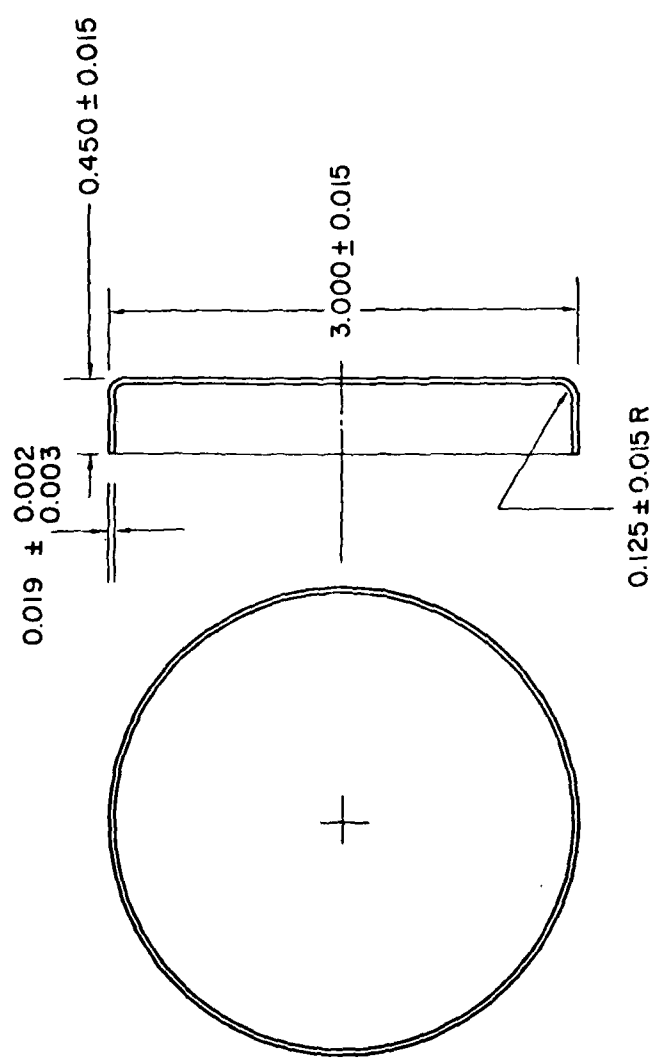
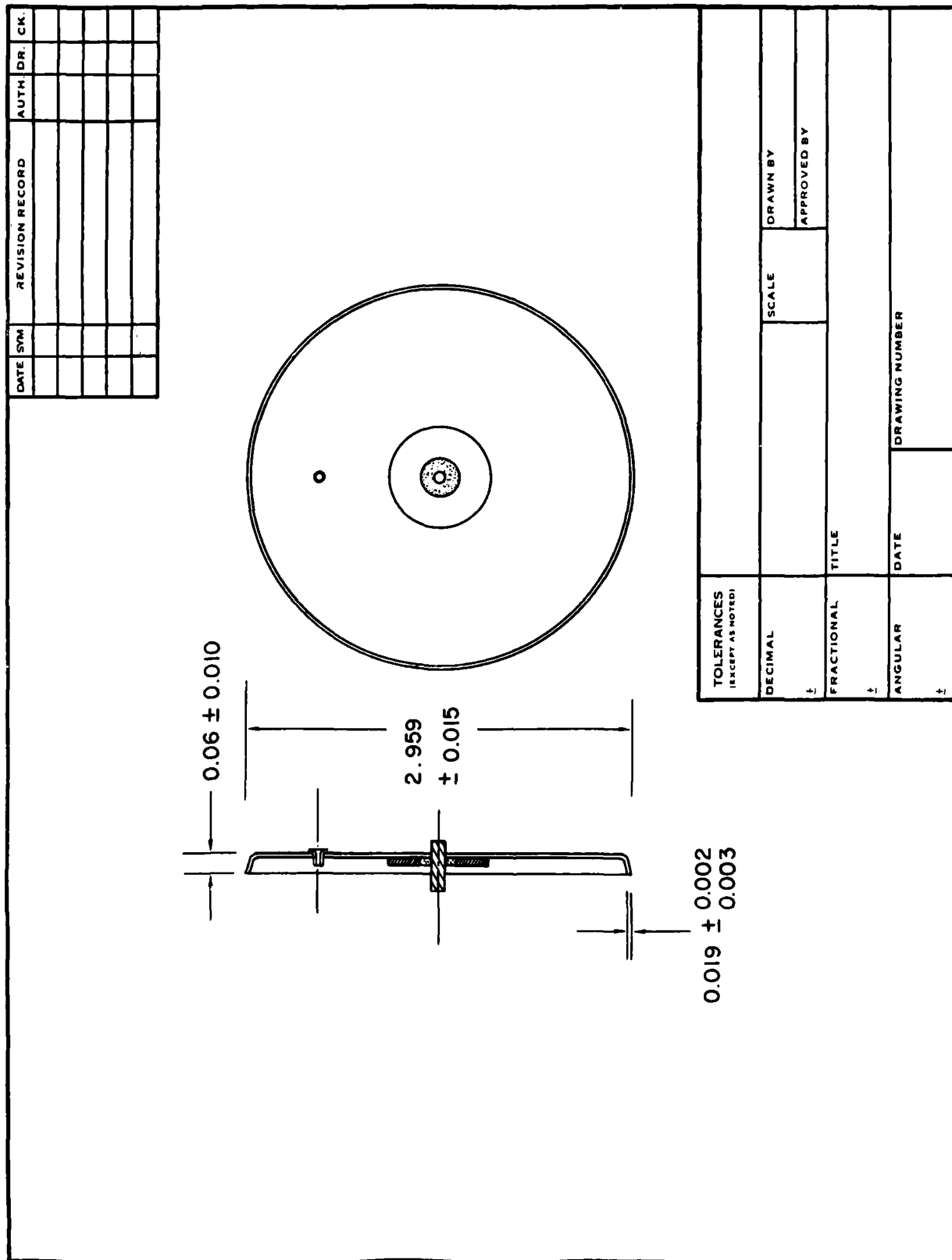
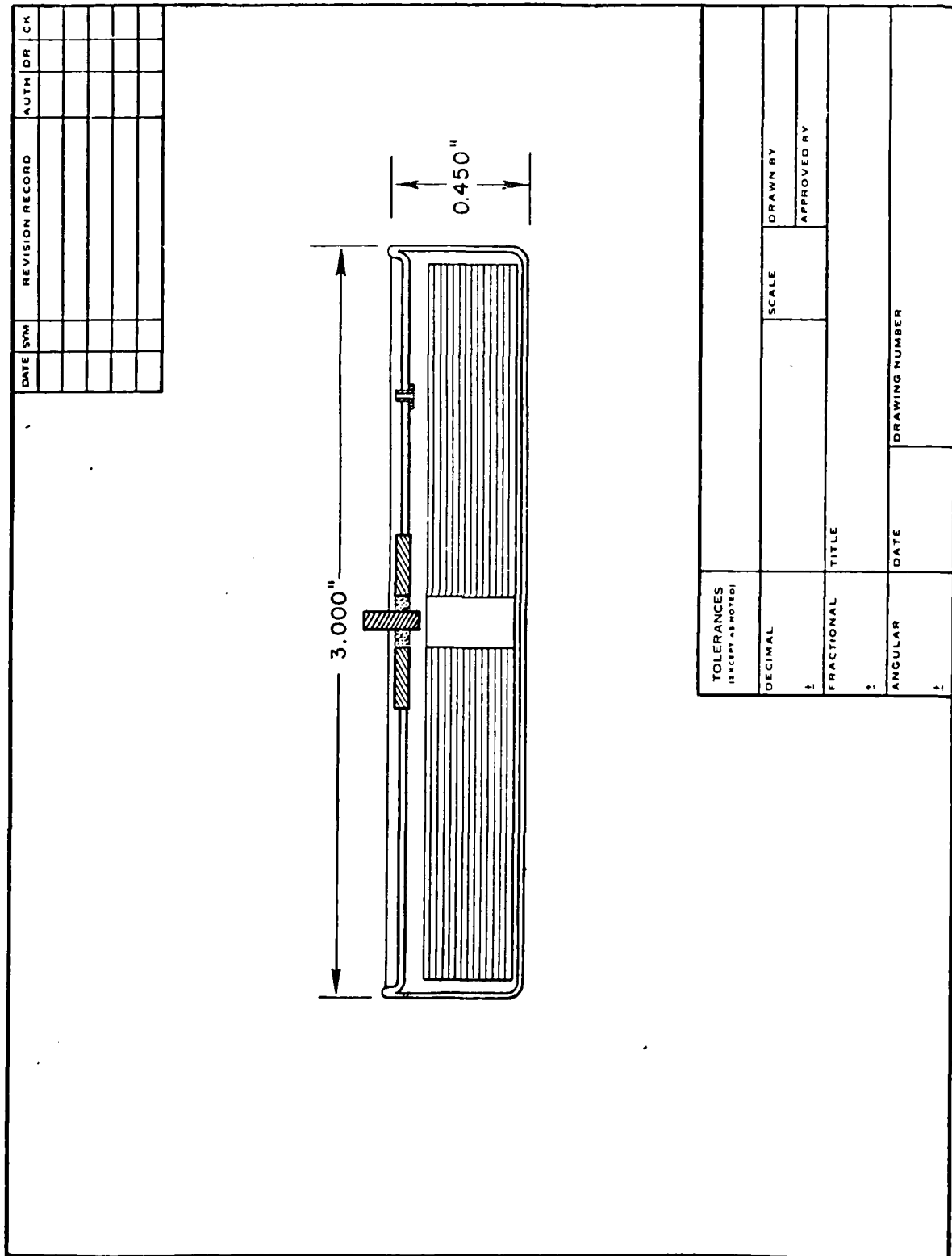


Figure 92. Flat cylindrical cell container.



K+E ALBANESE © 105465  
ENGINEERS' STANDARD FORM  
MADE IN U.S.A.  
Figure 93. Flat cylindrical cell top with G/M seal and the  
electrolyte fill port.



**K-E** STANDARD SECTION  
CROSS-SECTION OF THE HERMETIC FLAT CYLINDRICAL CELL

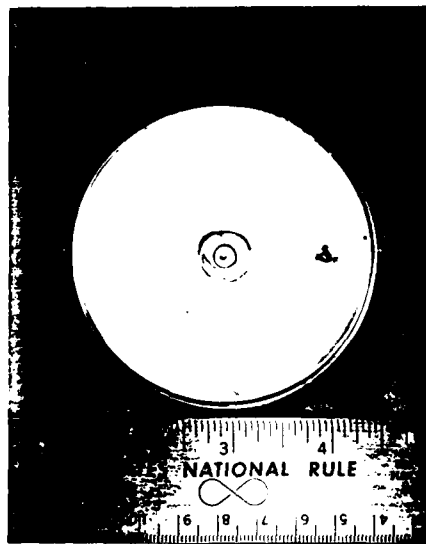


Figure 95. Photograph of a hermetic thin flat cylindrical cell.

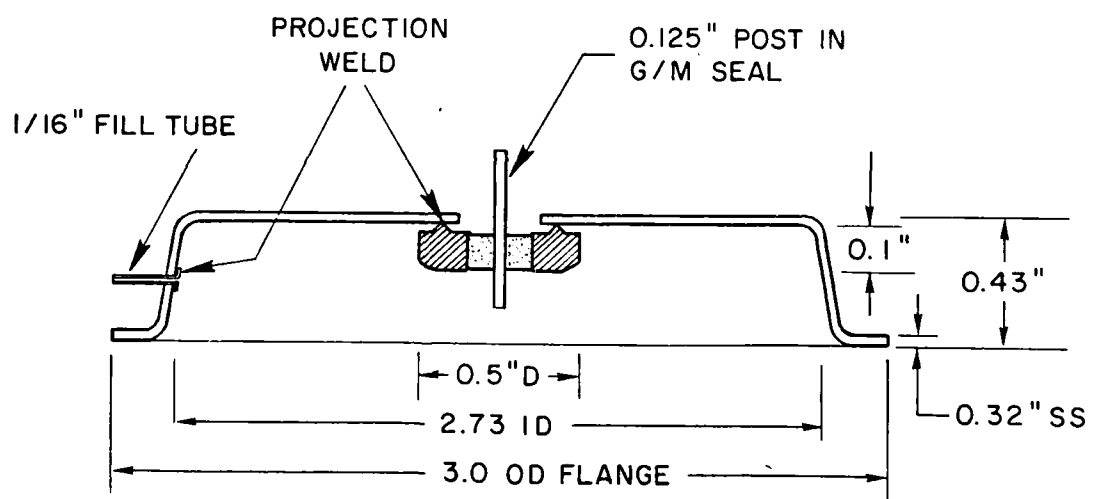


Figure 96. Top of hermetically sealed flat cell with G/M seal and fill tube.

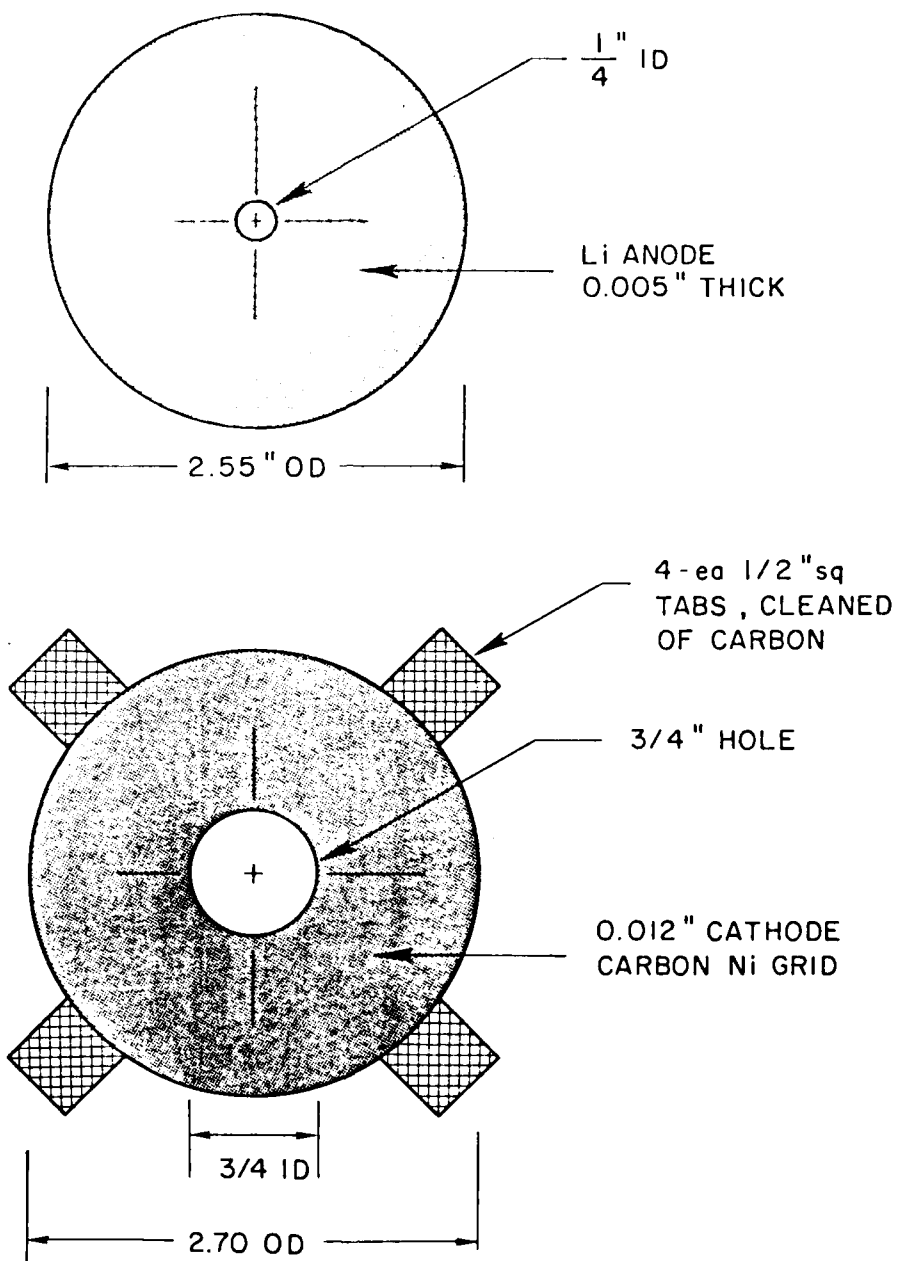


Figure 97. The anode and cathodes for a flat cell.

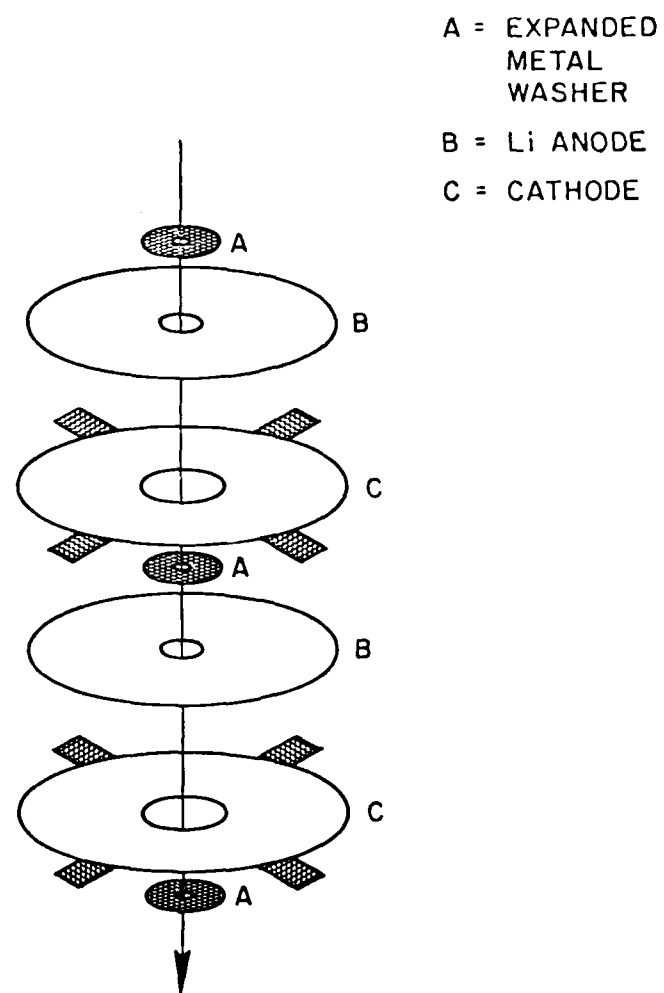


Figure 98. Assembly stacking sequence for the flat cell

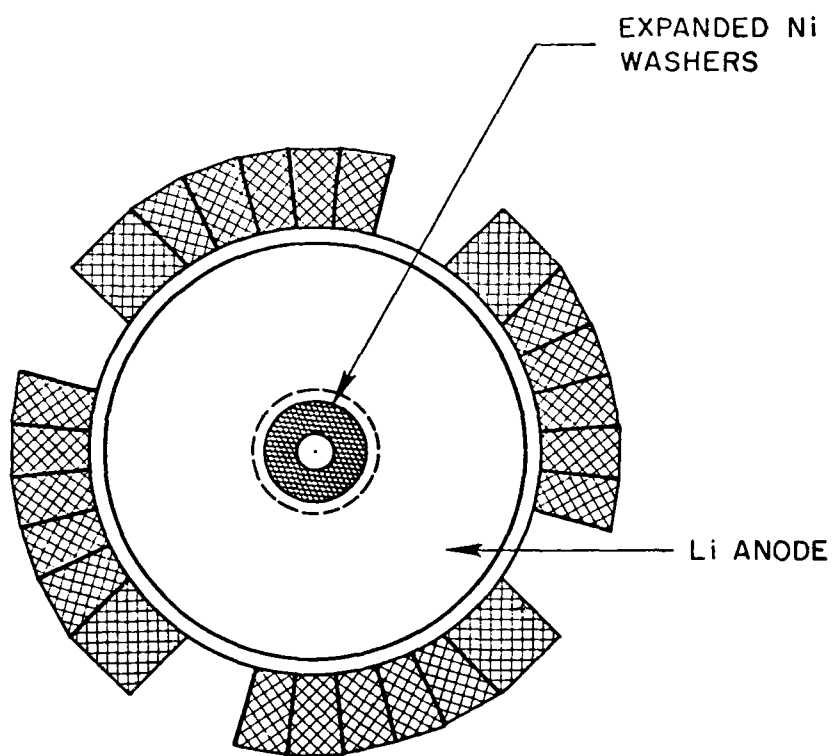


Figure 98a. Top view of an assembled flat cell.

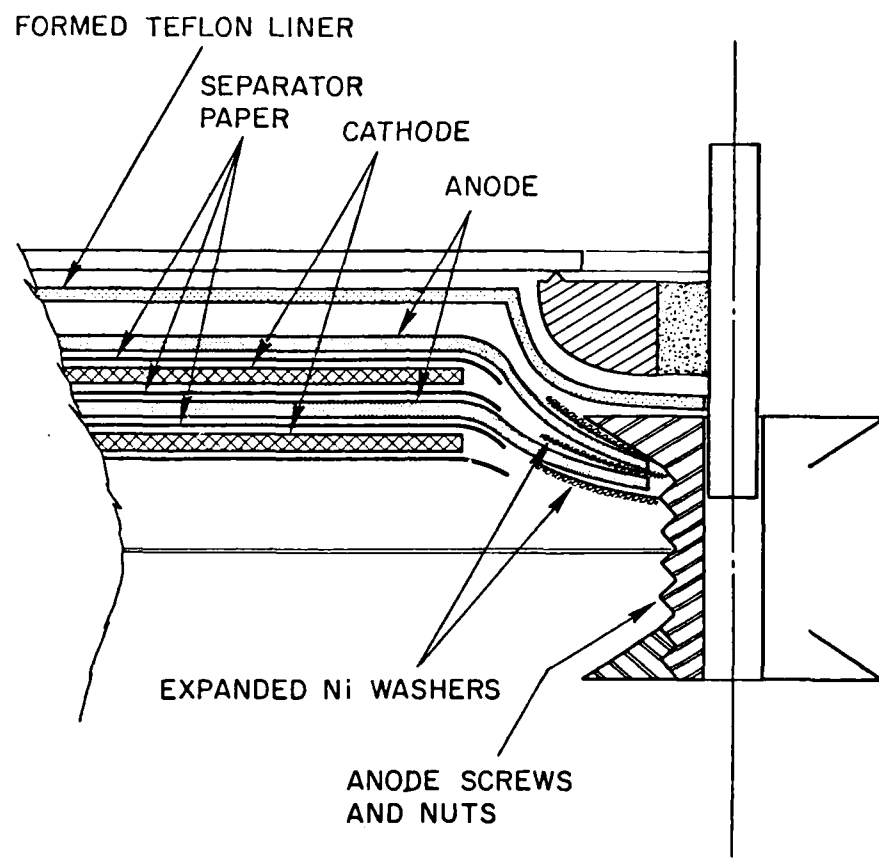


Figure 99. Lithium anode contact detail.

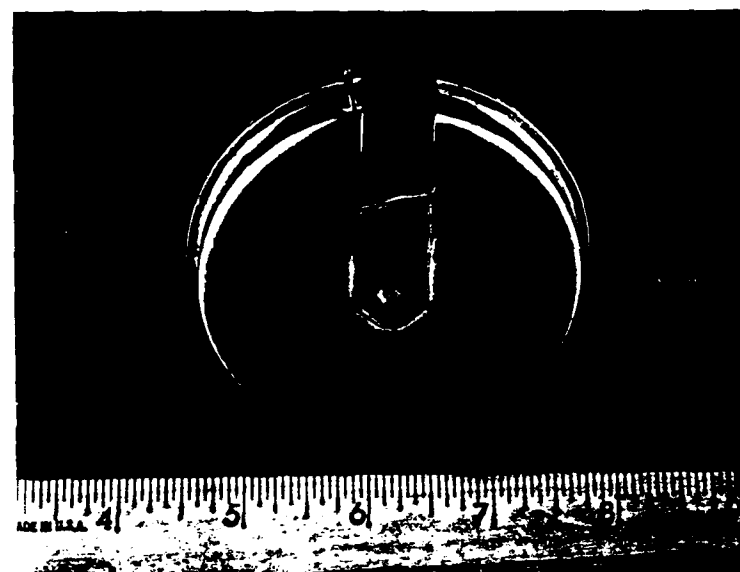


Figure 100. Photograph of finished flat cell.

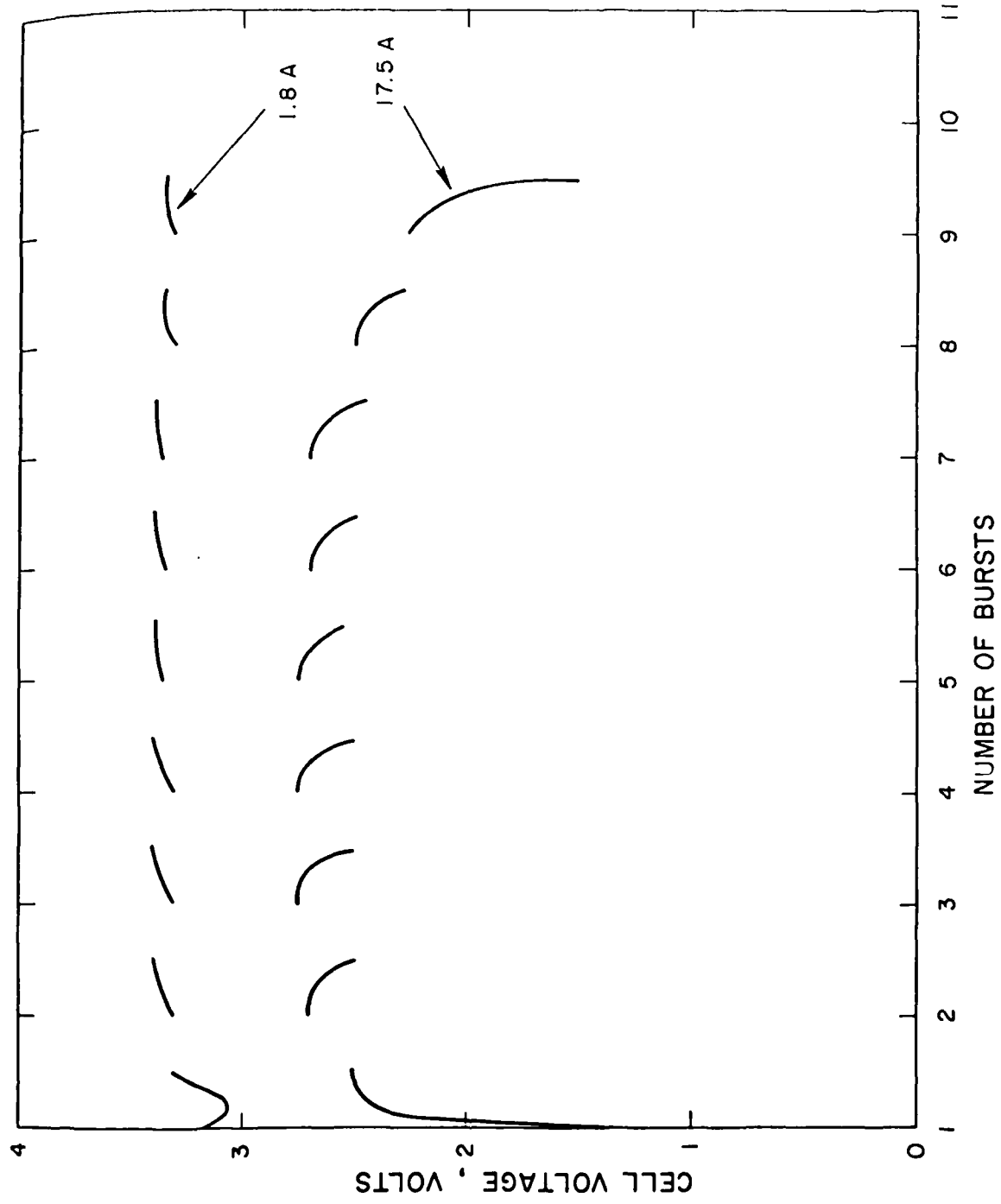


Figure 101. Performance of the thin flat cylindrical cell on the old GLLD test.

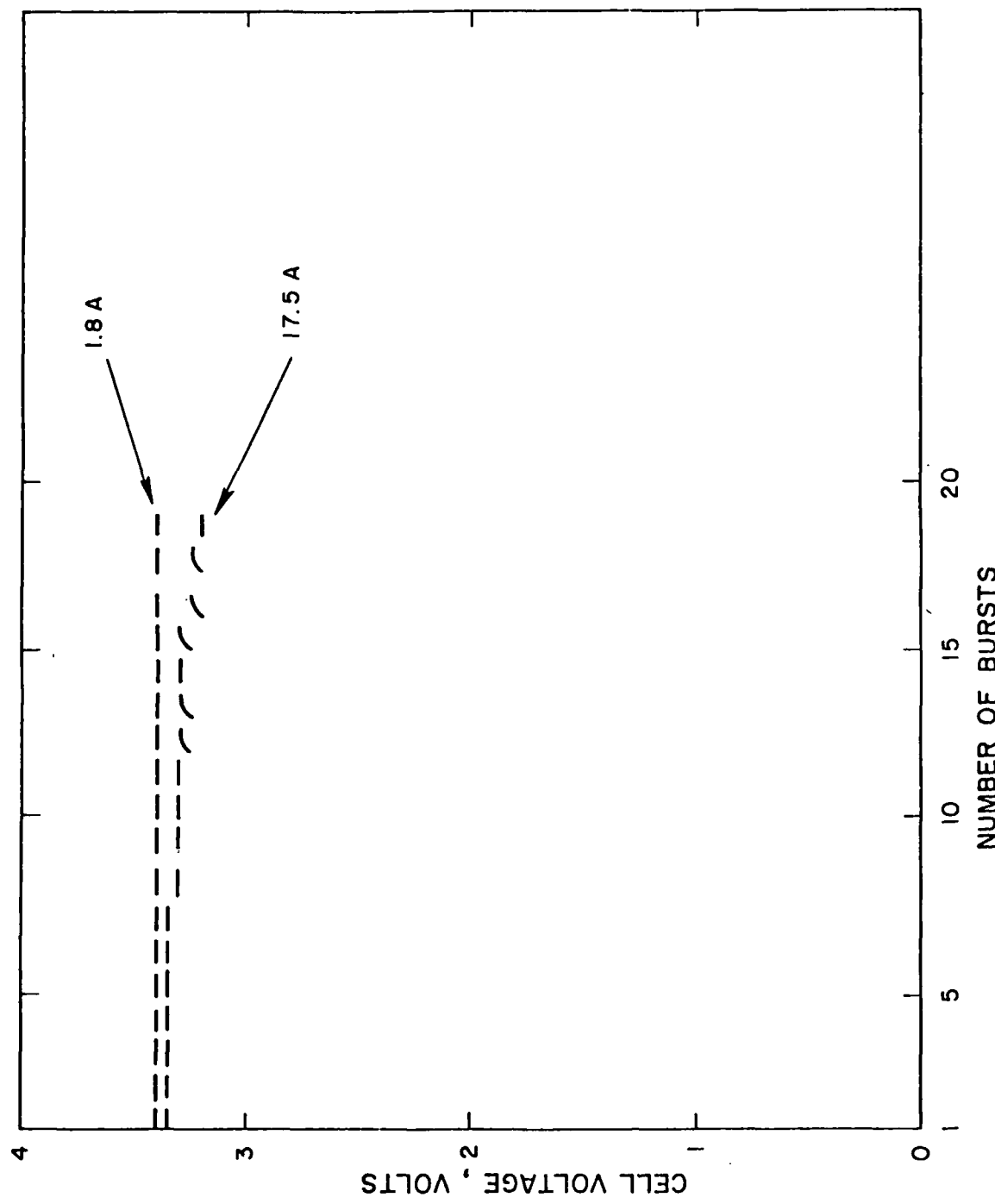


Figure 102. Performance of a thick flat cell with 40 cathodes and 41 anodes on the old GLLD load.

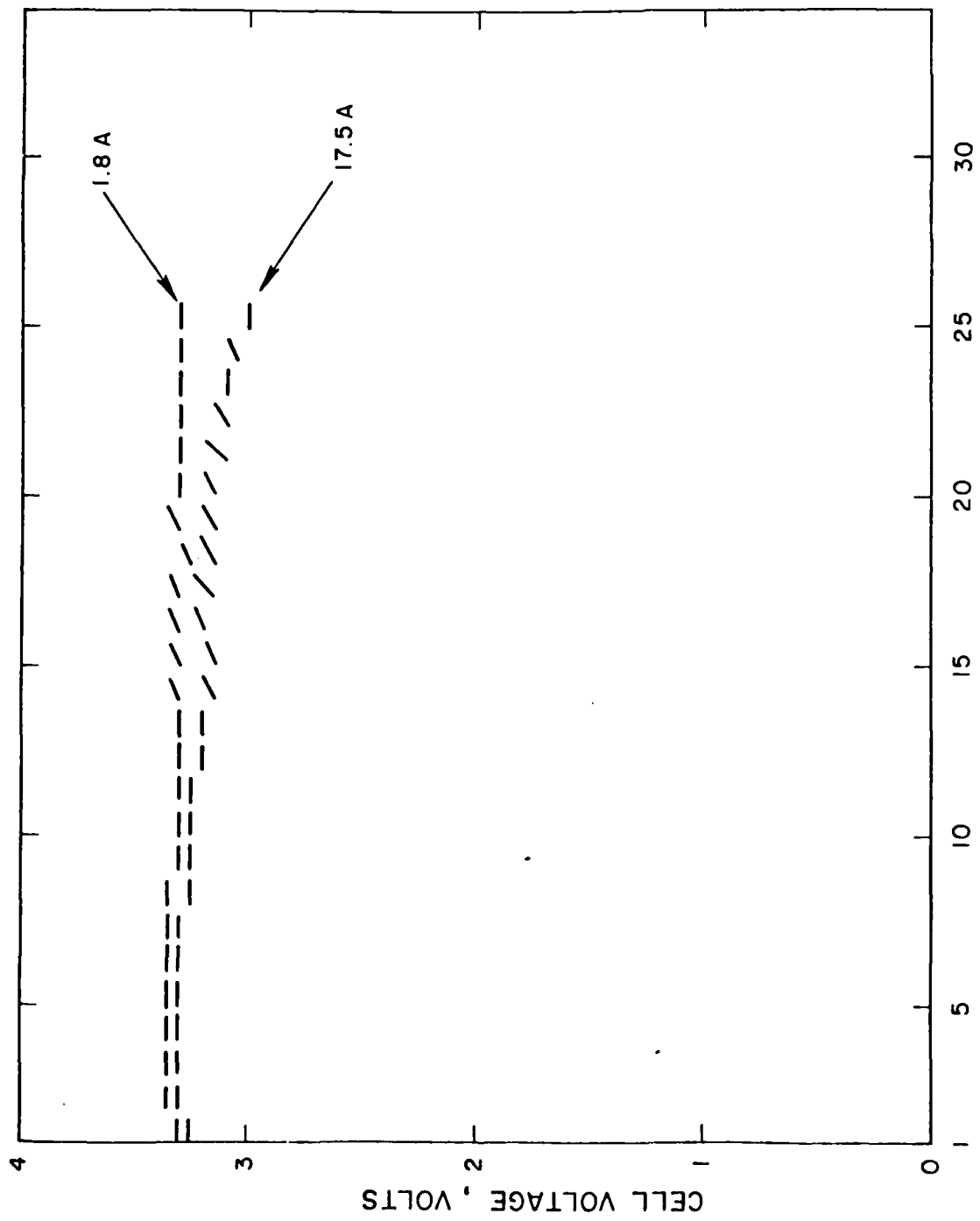


Figure 103. Performance of a thick flat cell with 35 cathodes and 36 anodes on the old GLLD duty cycle.

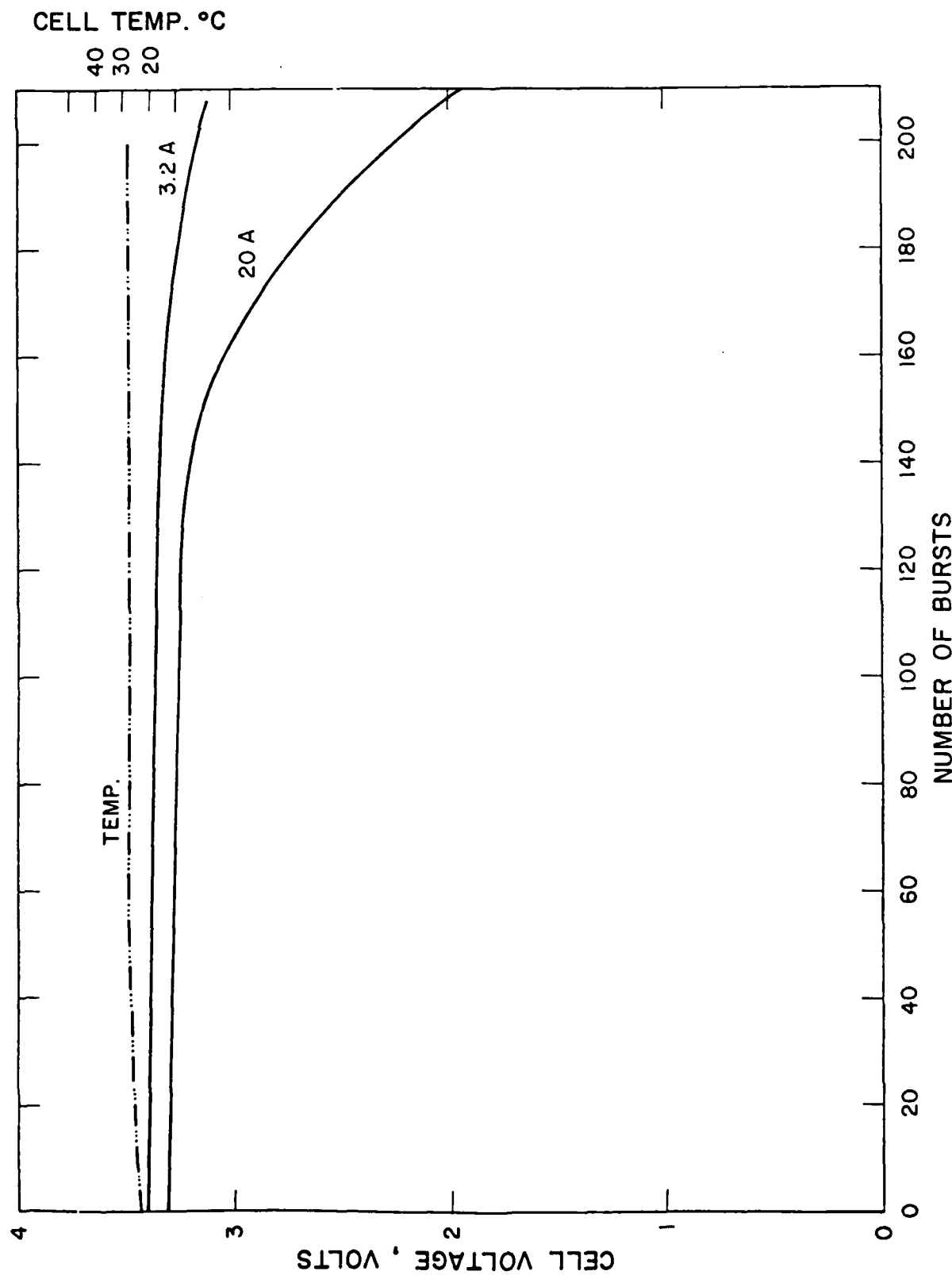


Figure 104. Performance of a flat cell with thick anodes on the new GLLD load.

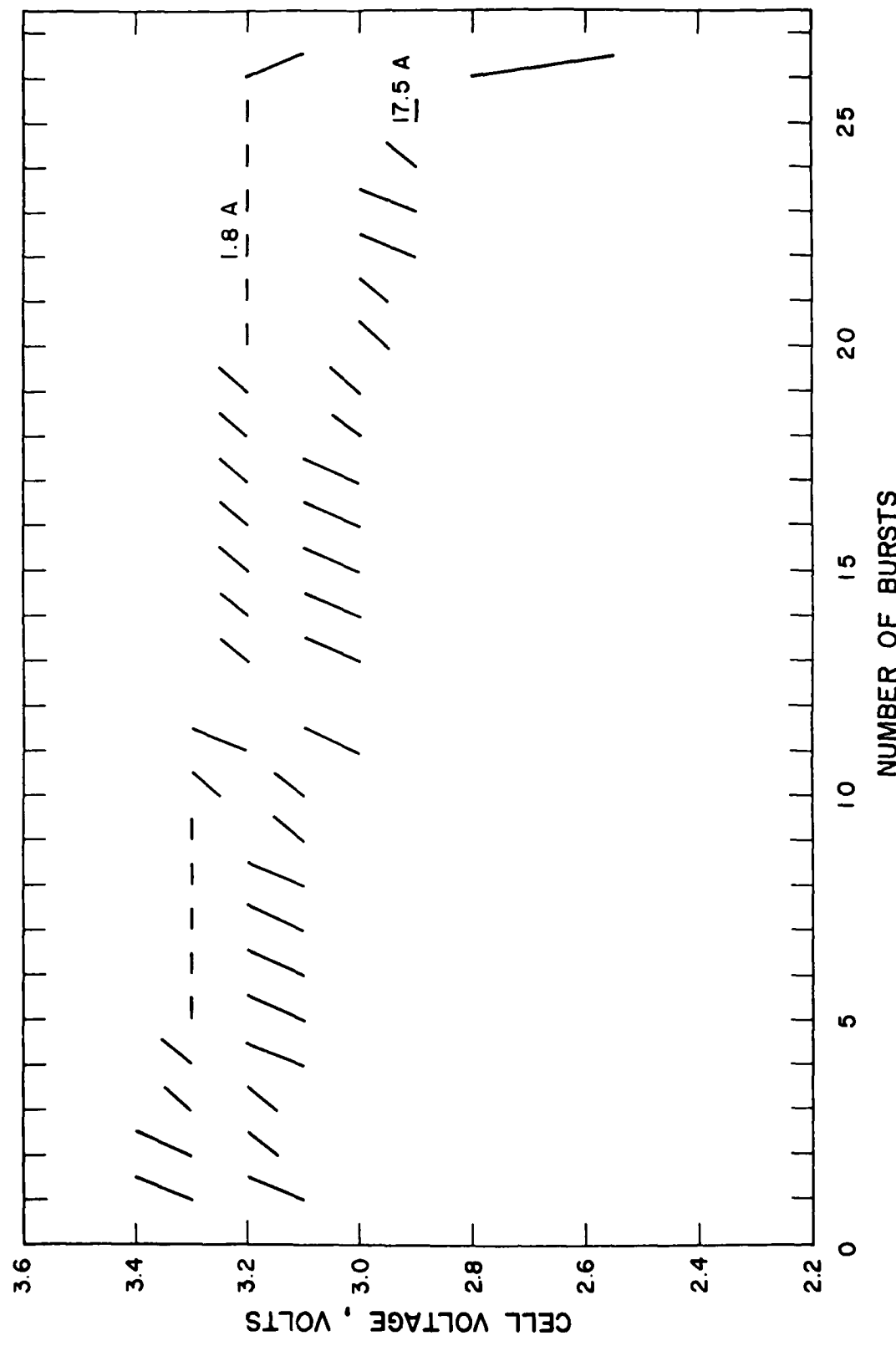


Figure 105. Performance of a flat cell with 32 cathodes on the old GLID test at 25°C.

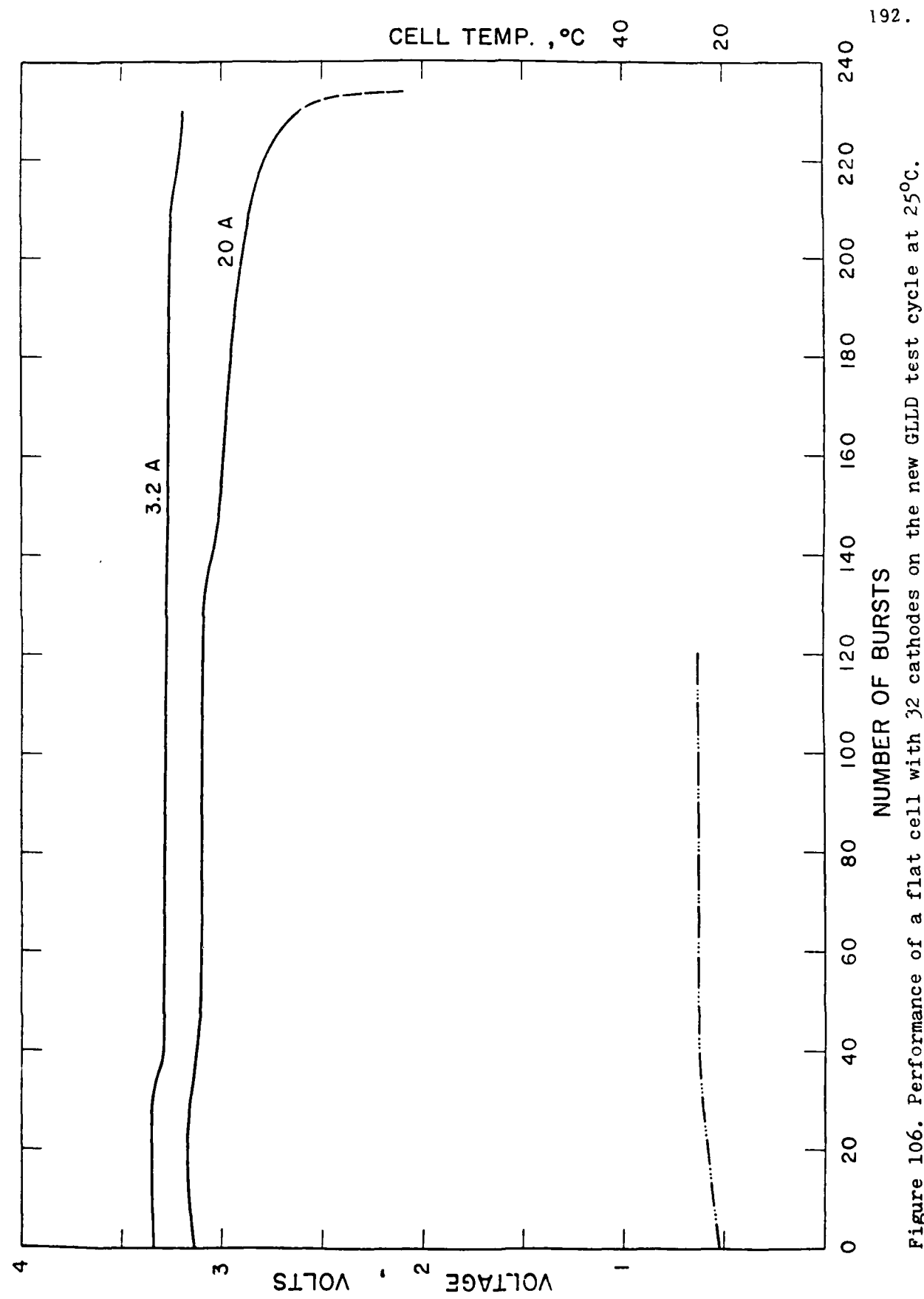


Figure 106. Performance of a flat cell with 32 cathodes on the new GLLD test cycle at 25°C.

193.

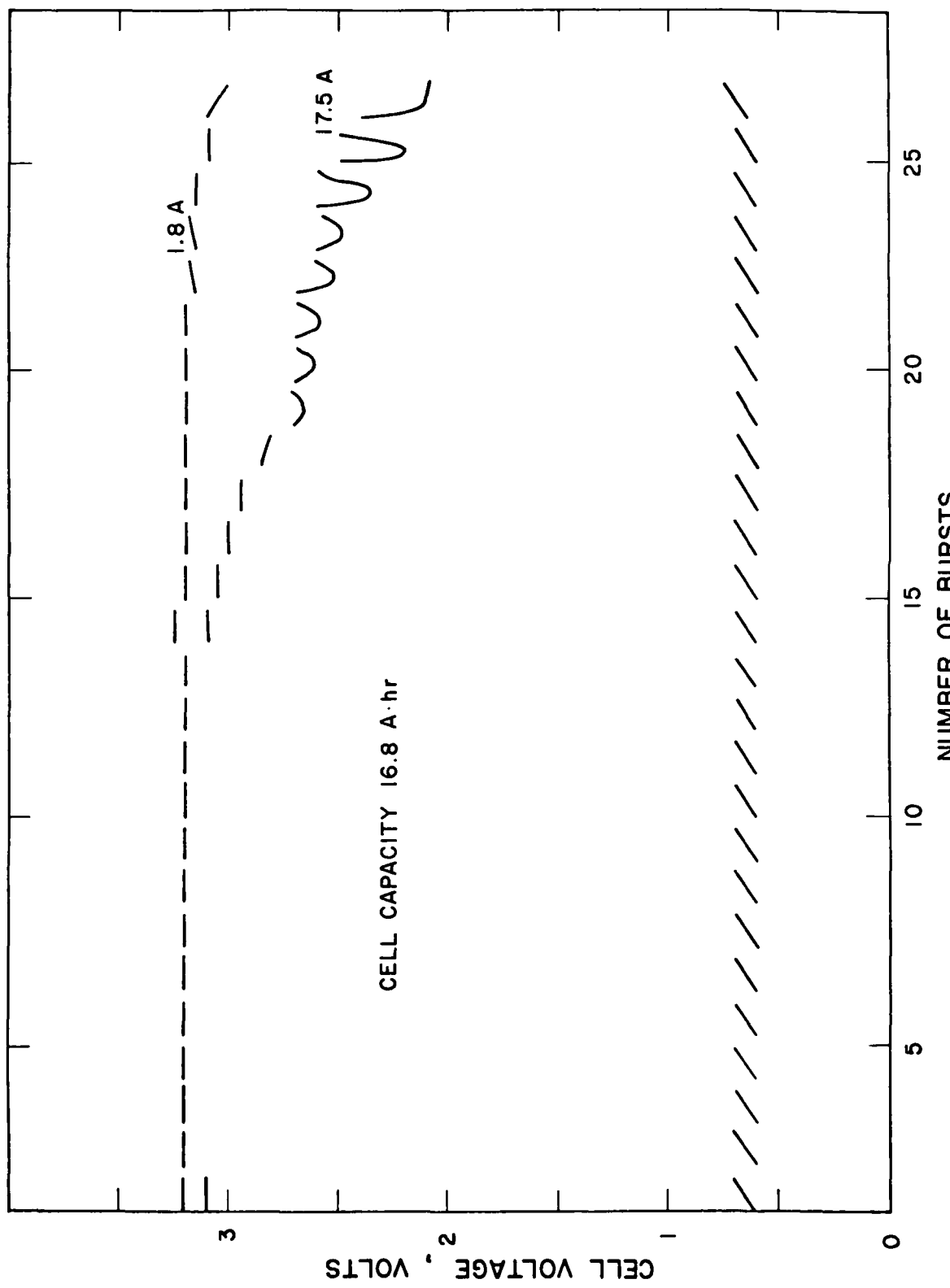
CELL TEMP. °C  
38      19

Figure 107. Performance of a flat cell with 40 cathodes on the old GLLD load at 25°C.

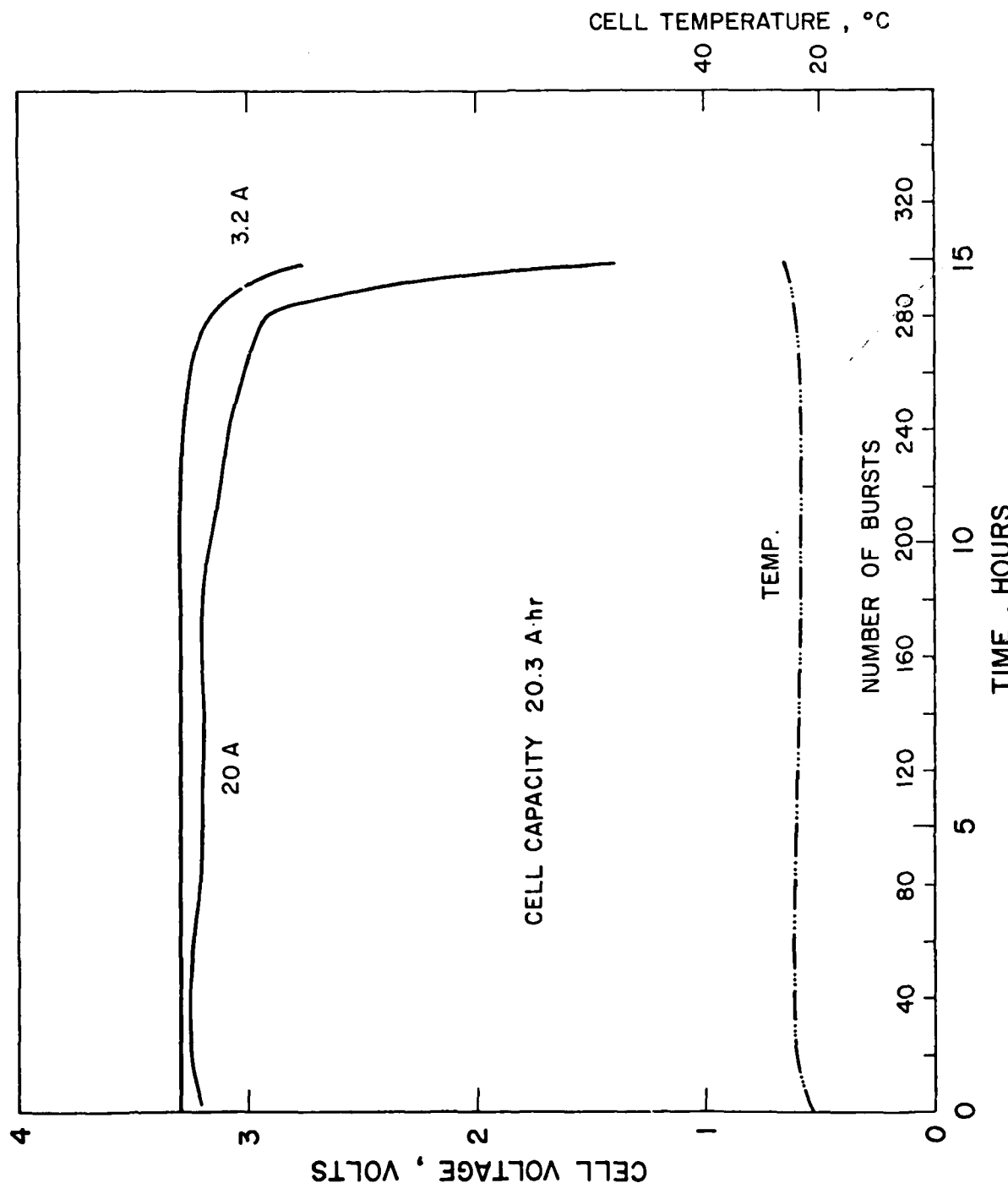


Figure 108. Performance of a flat cell with 36 cathodes on the new GLLD load at 25°C.

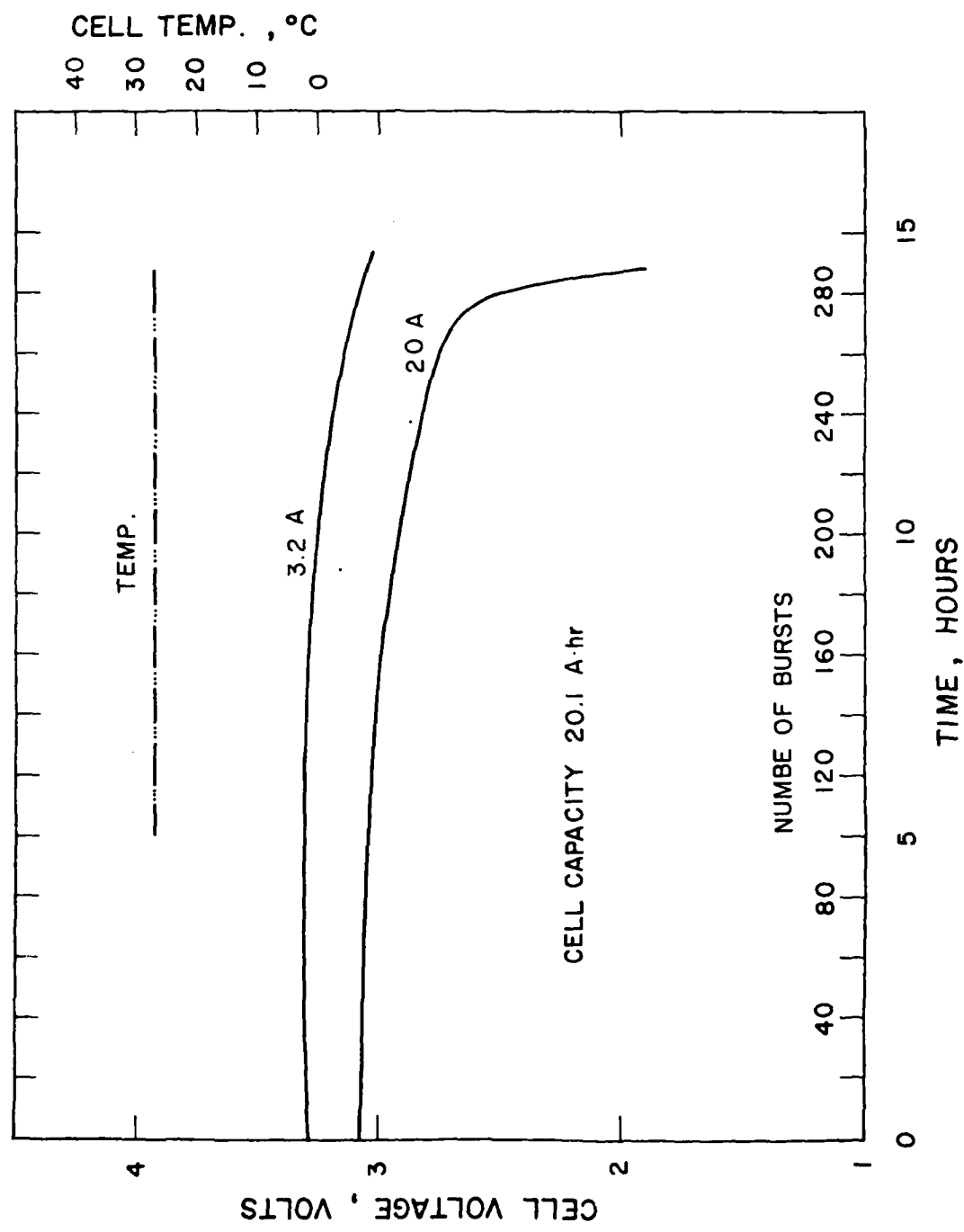


Figure 109. Performance of a flat cell with 36 cathodes on the new GLLD load at 25°C.

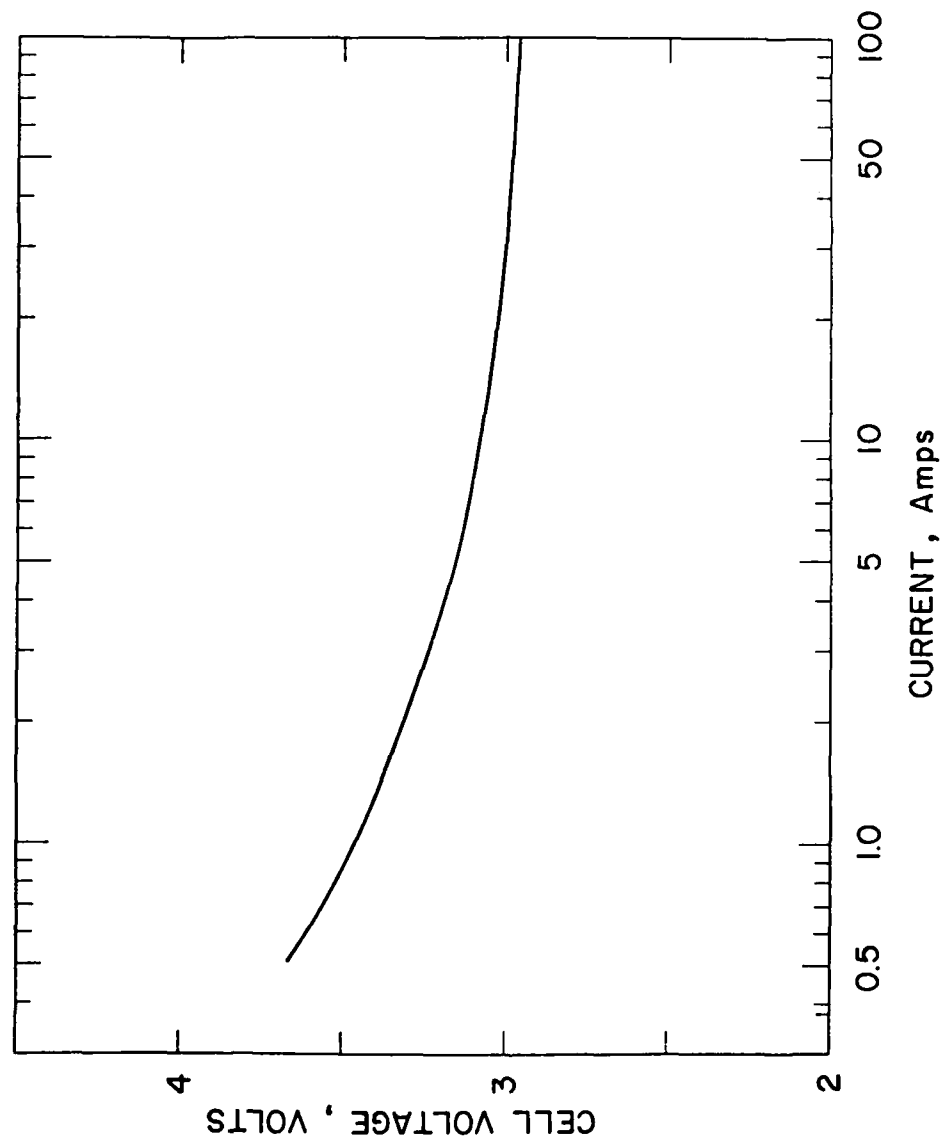


Figure 110. Voltage - current curve of a flat cell with 36 cathodes.

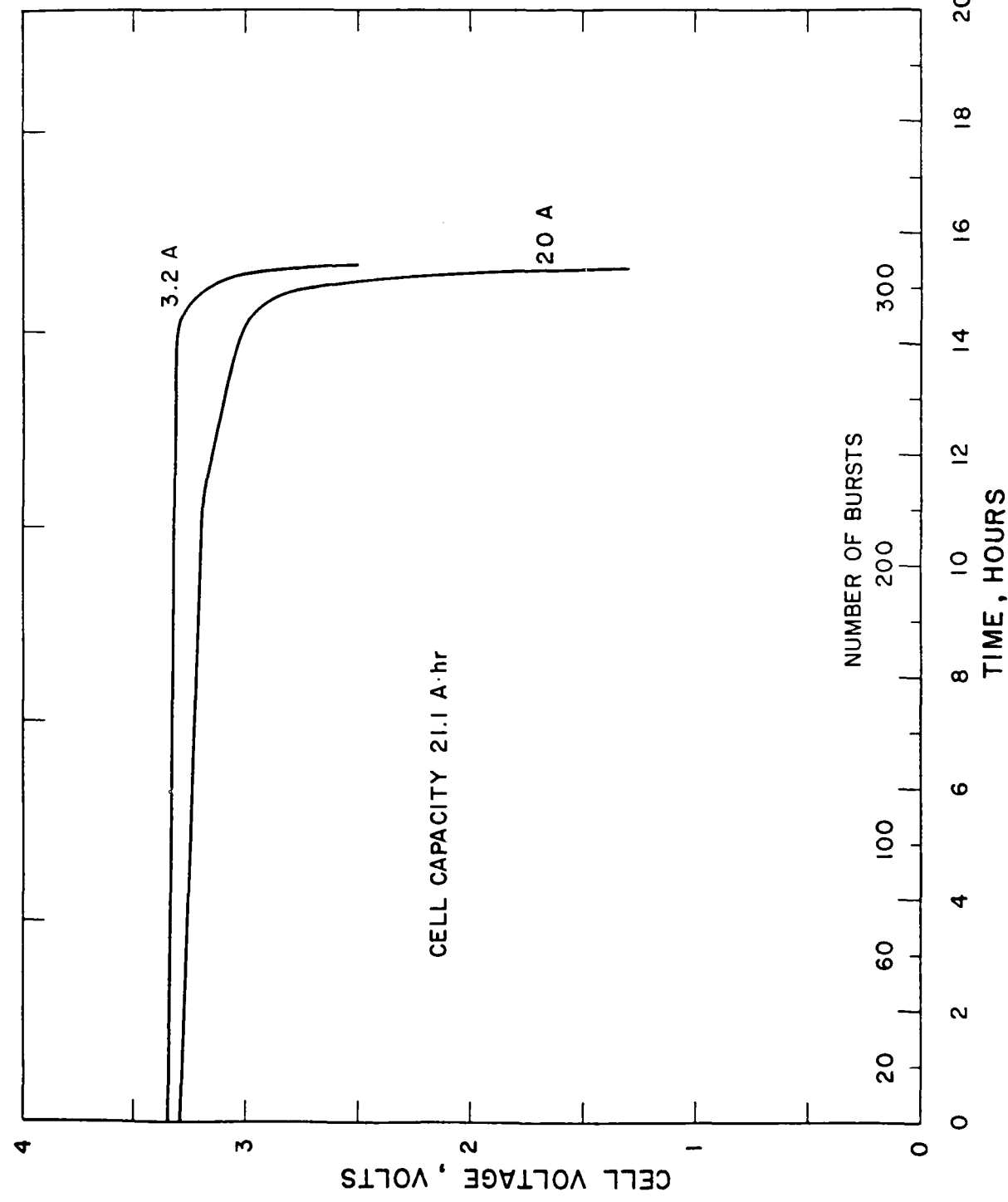


Figure 111. Performance of a flat cell with cathode additive 1 at level A on the new GLLD test.

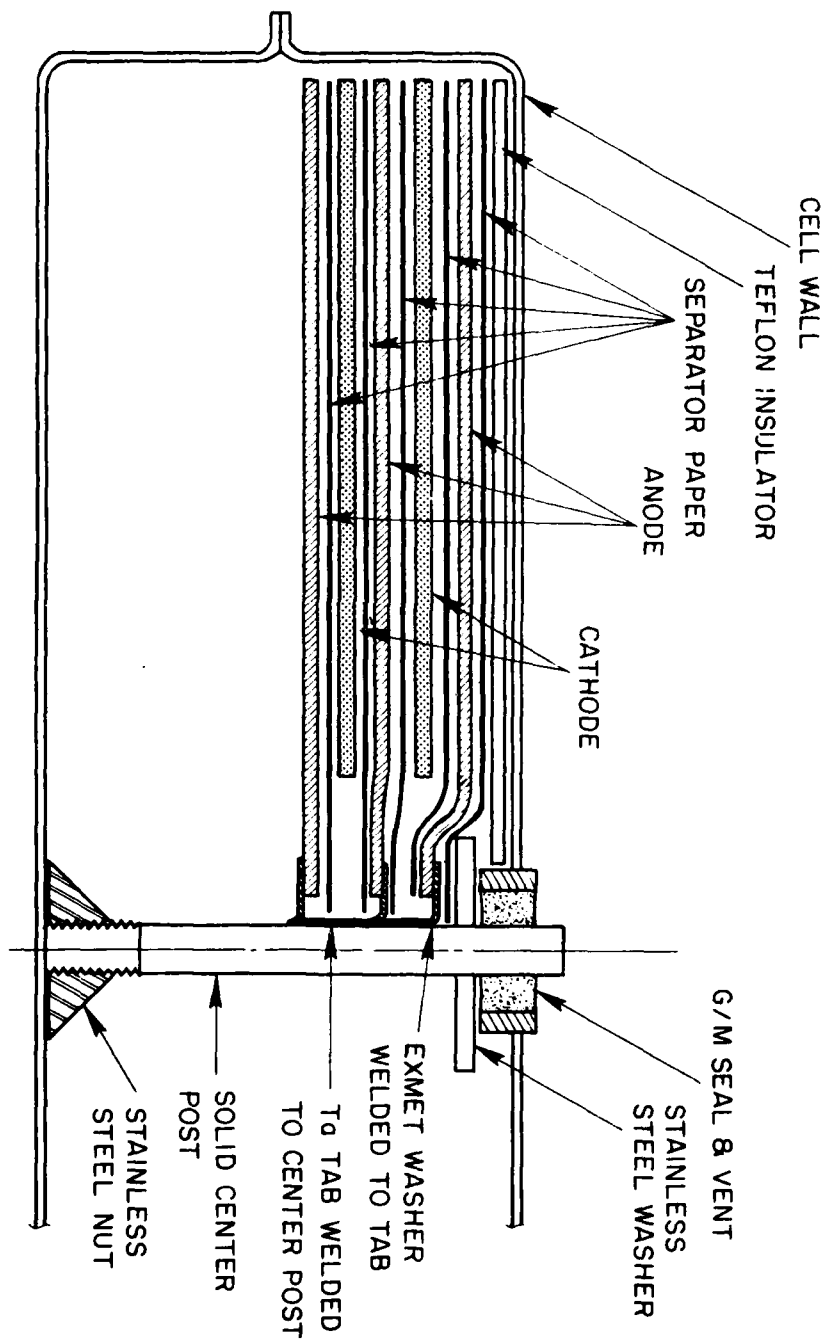


Figure 112. Lithium anode contact detail of finalized version of the flat cell.

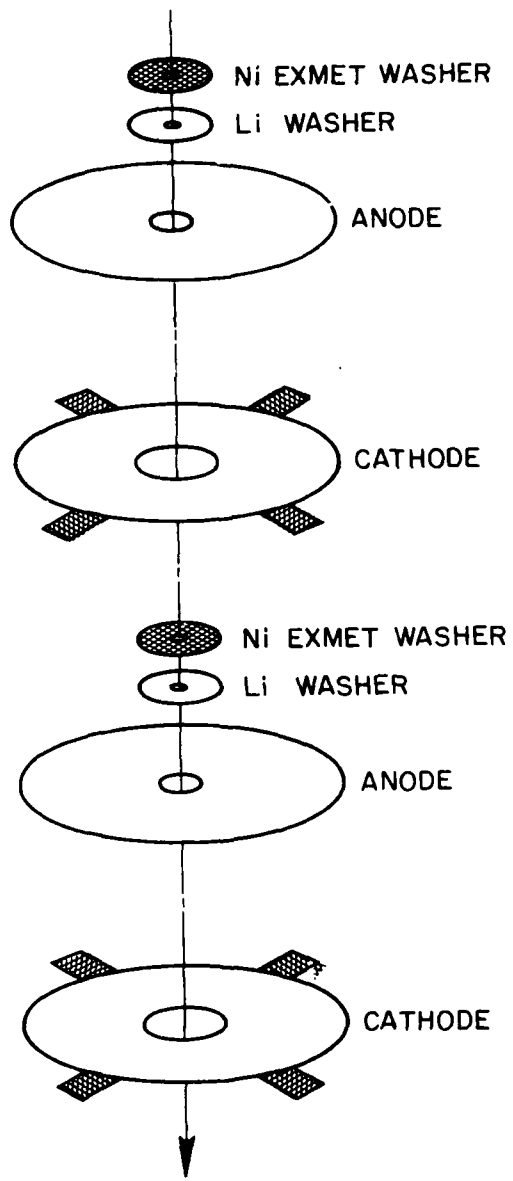


Figure 113. Assembly stacking sequence for the flat cell.

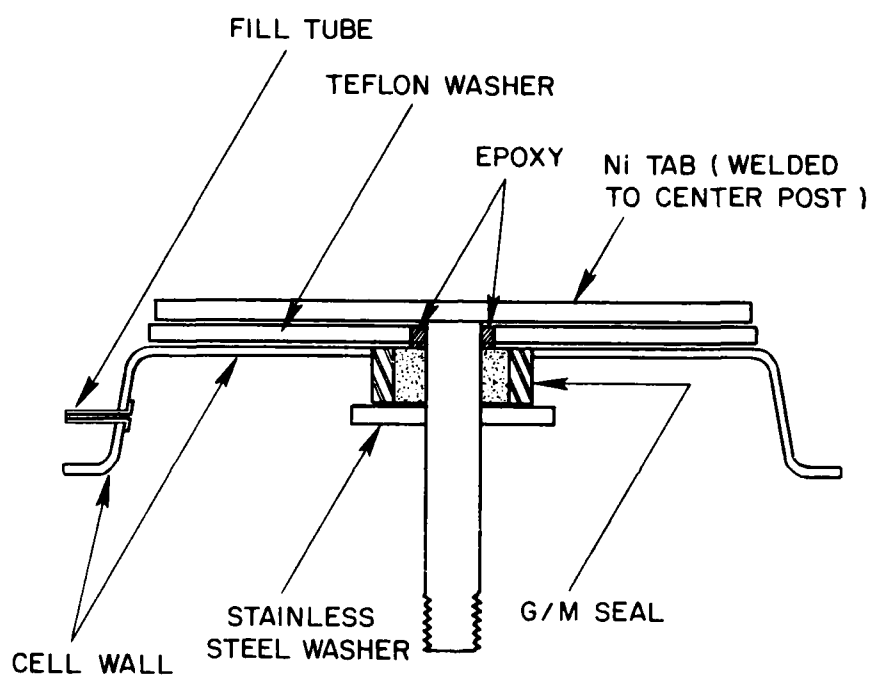


Figure 114. Top of hermetically sealed flat cell showing G/M seal, nickel tab and fill tube.

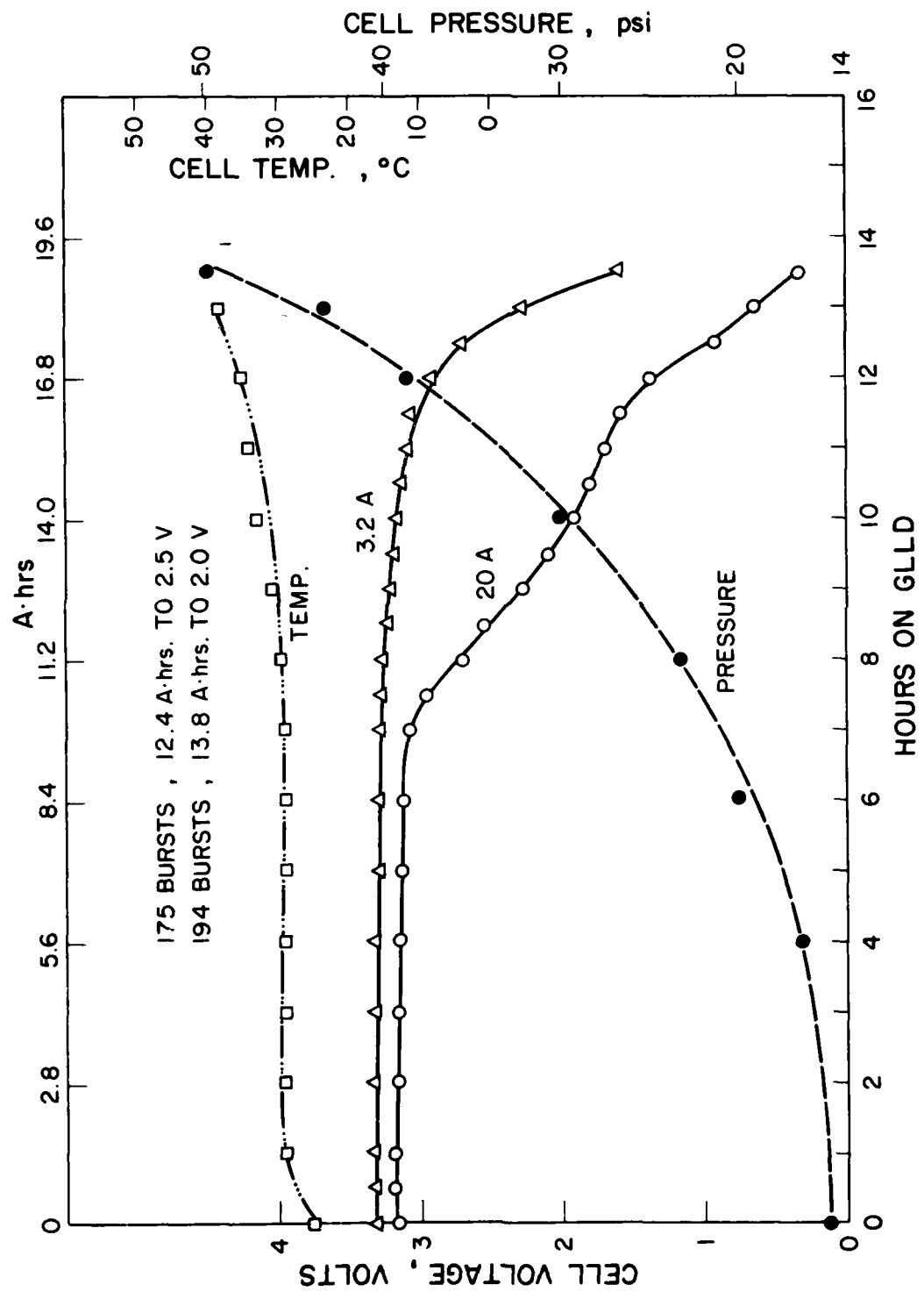


Figure 115. Performance of a fresh flat cell with new electrode design on the GLLD test at room temperature.

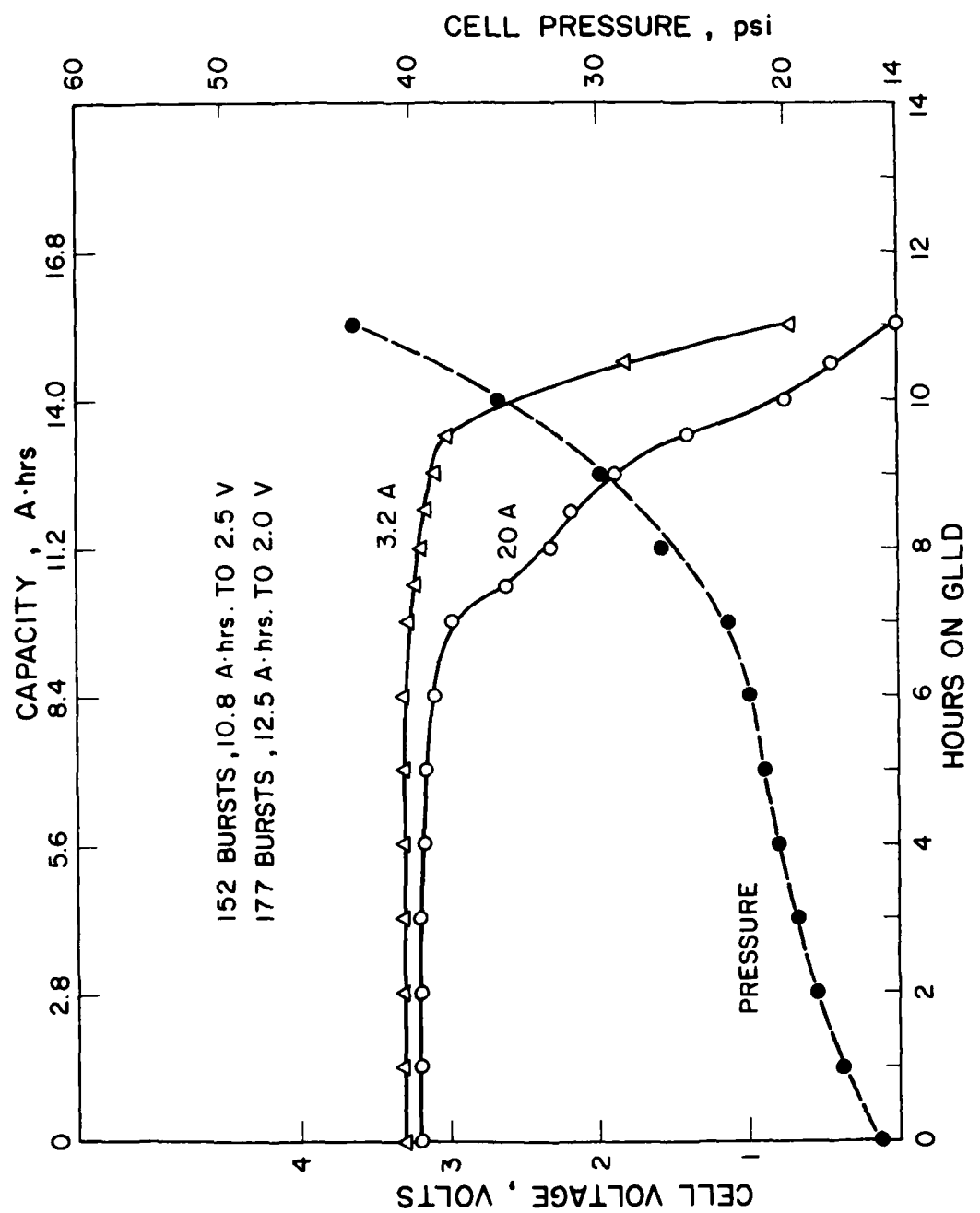


Figure 116. Performance of a fresh flat cell with new electrode design on the new GLLD test at room temperature.

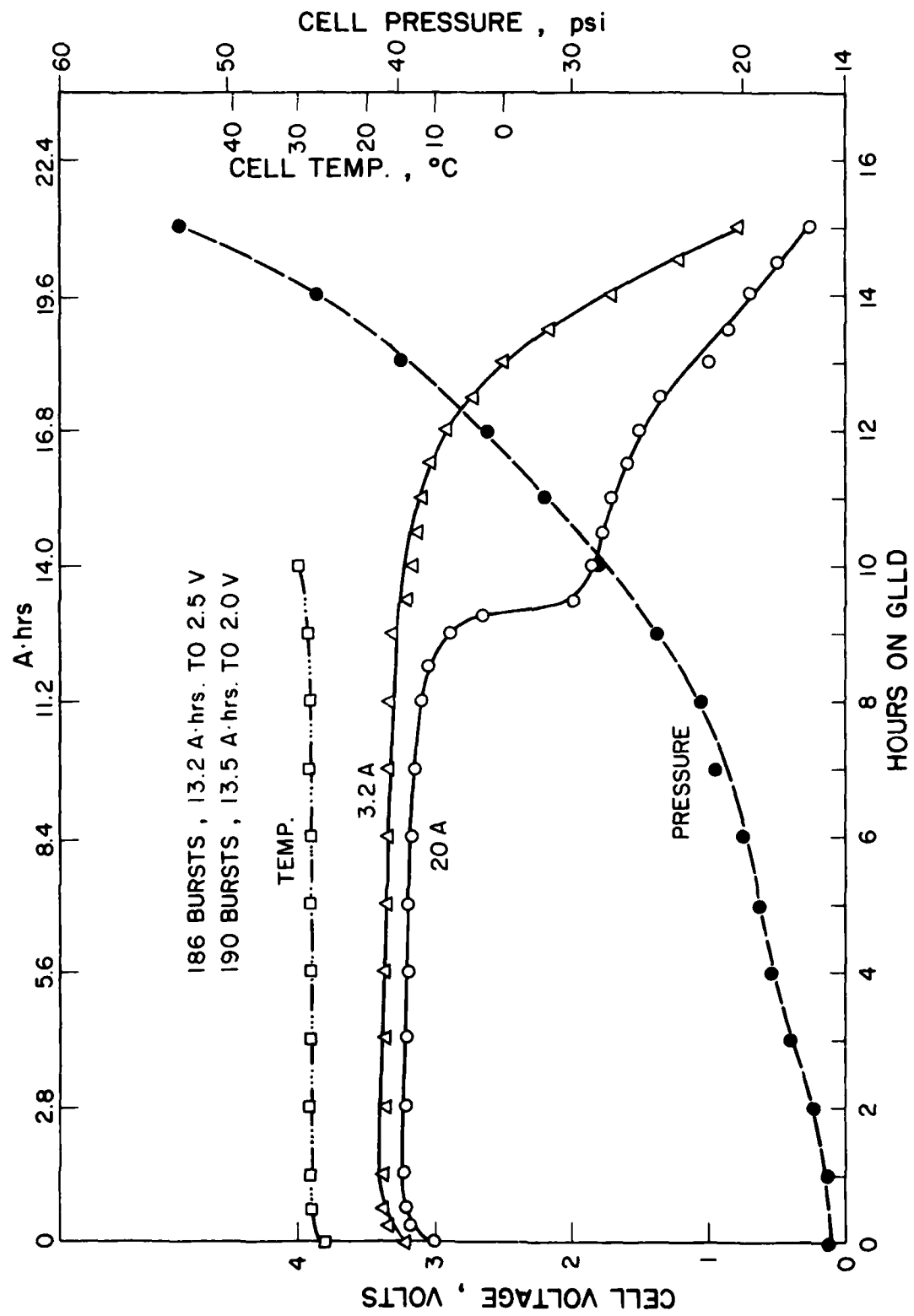


Figure 117. Performance of a fresh flat cell with old electrode design on the new GLLD test at room temperature.

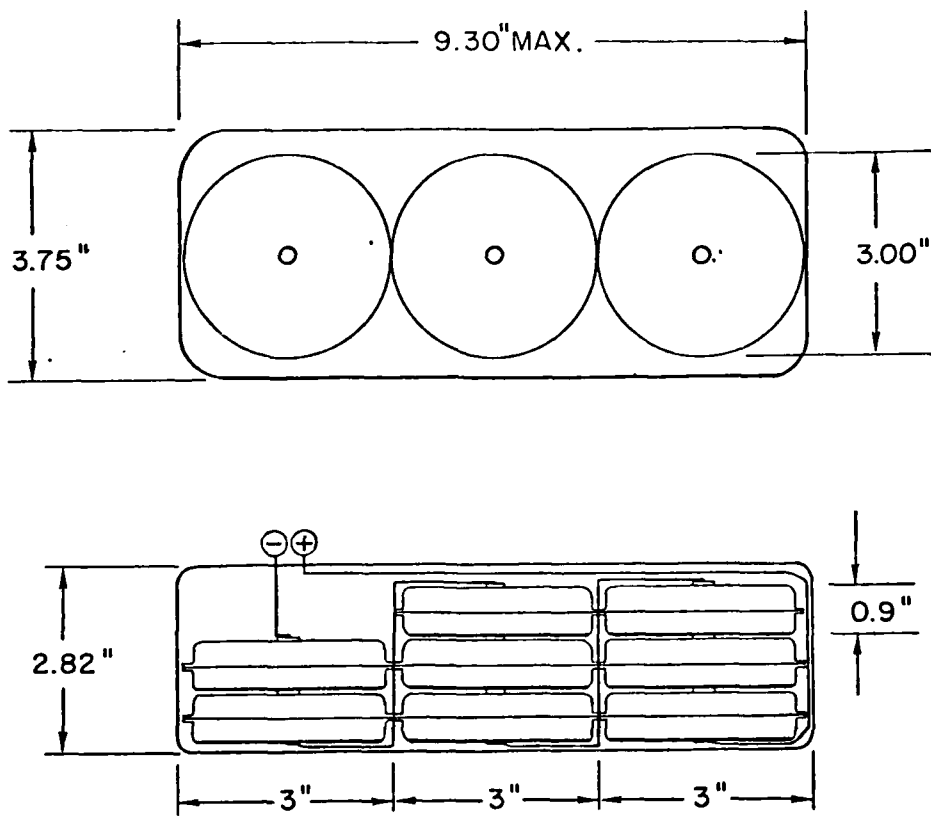


Figure 118. Schematic outline for the GLLD battery using 8 3" O.D.,  
0.90" thick flat cells.

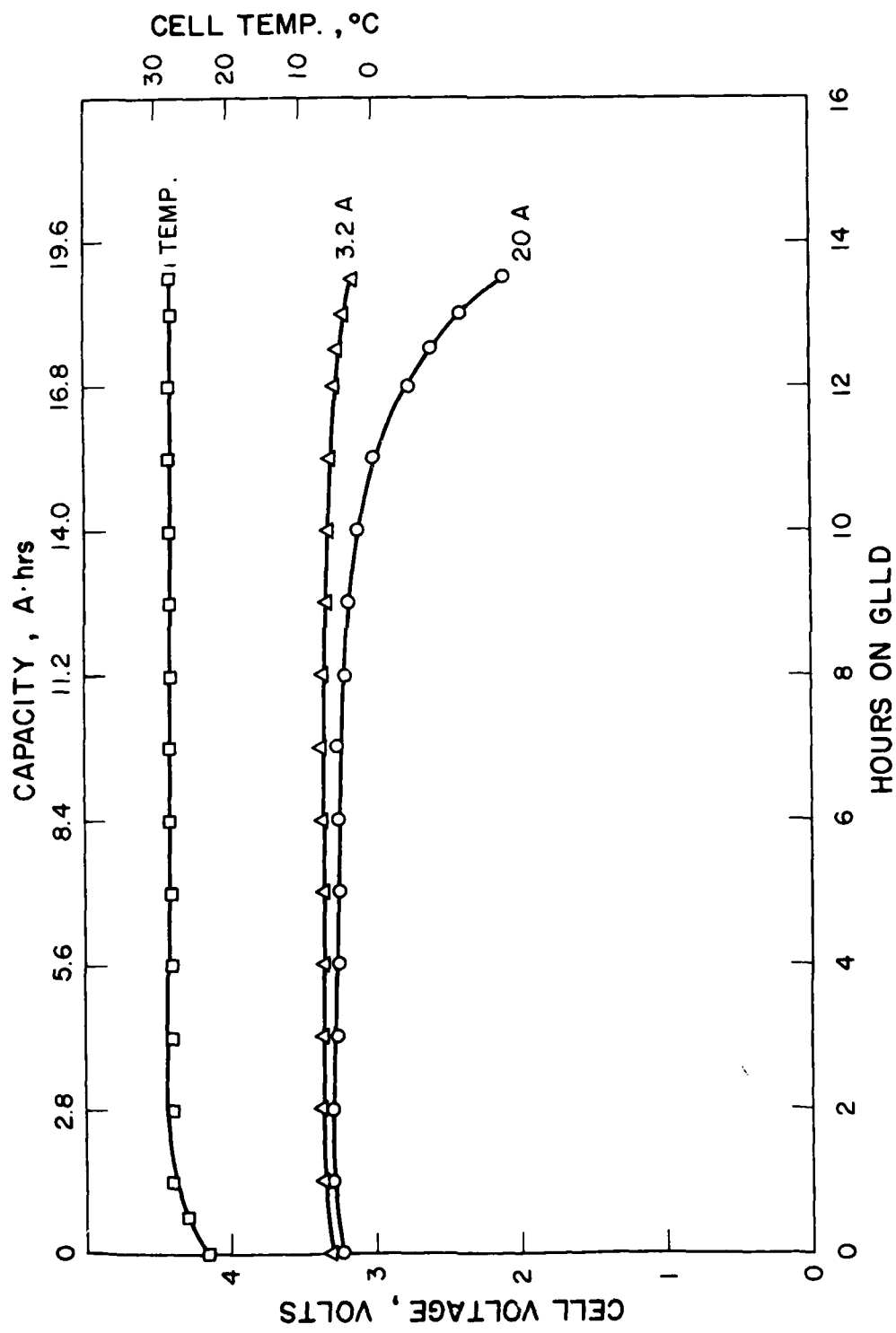


Figure 119. Performance of a fresh flat cell on the new GLLD test at 25°C.

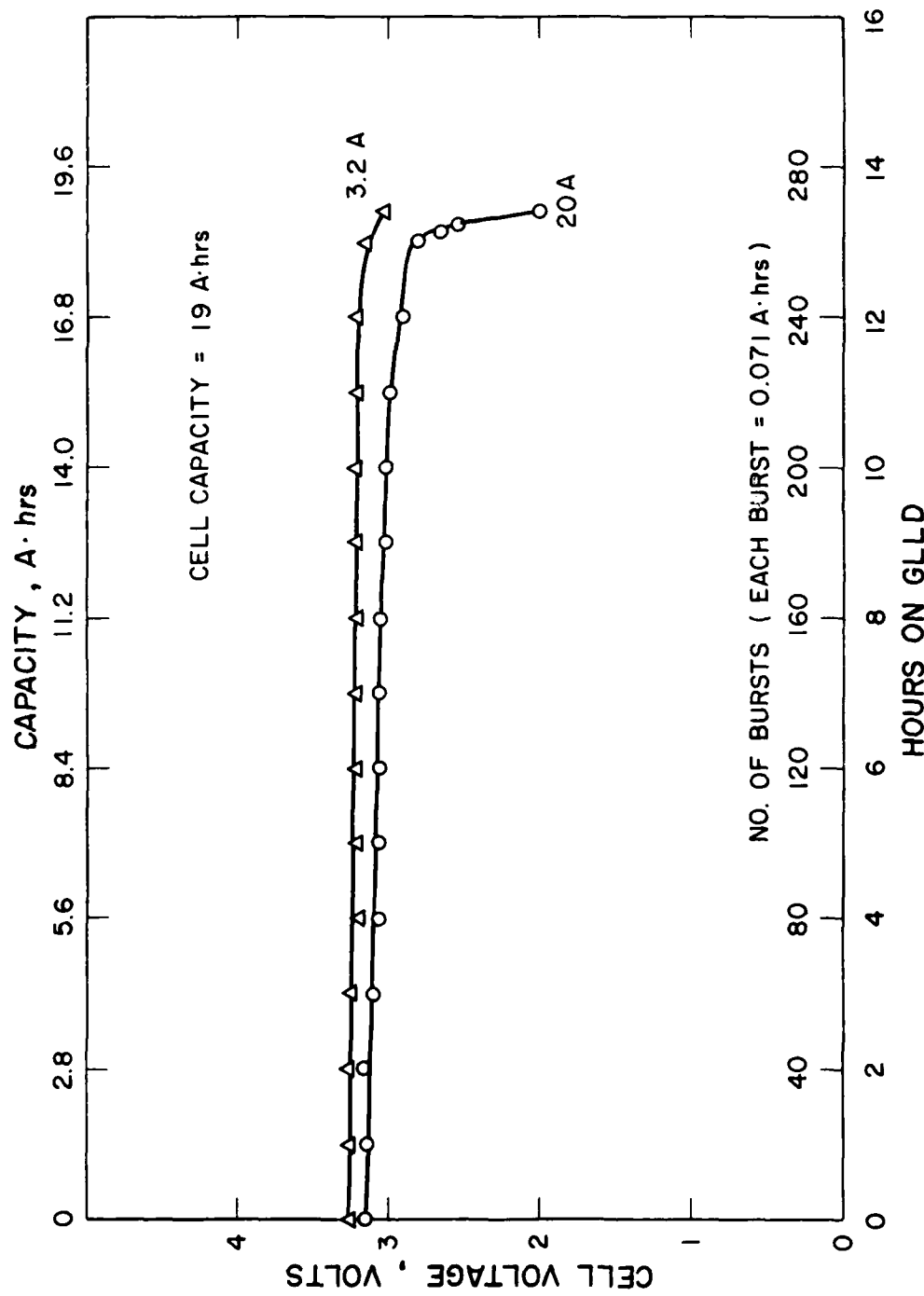
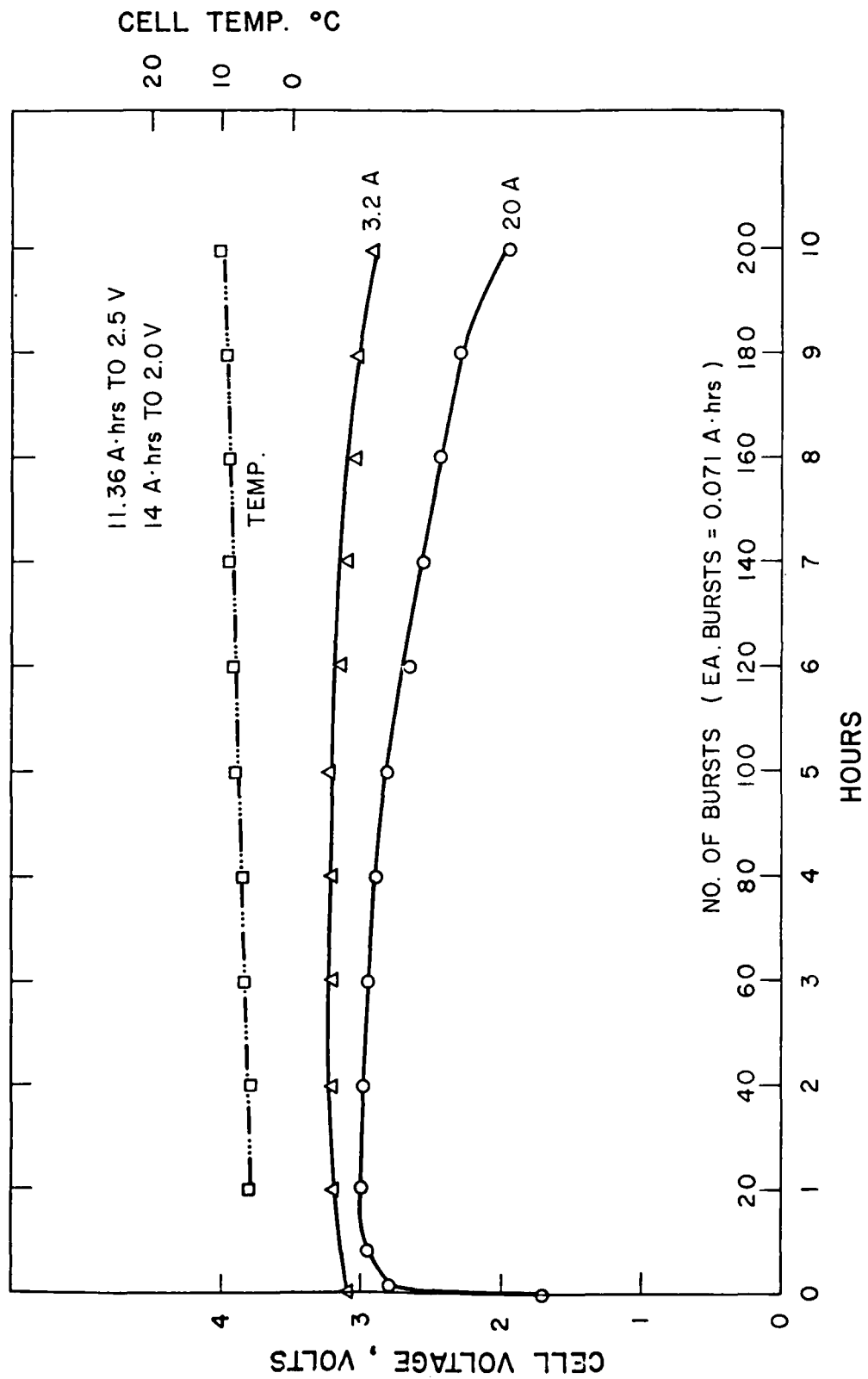


Figure 120. Performance of a fresh flat cell on the new GLLD test at 25°C.



**Figure 121.** Performance of a fresh flat cylindrical cell on the new GLLD test at 0°C.

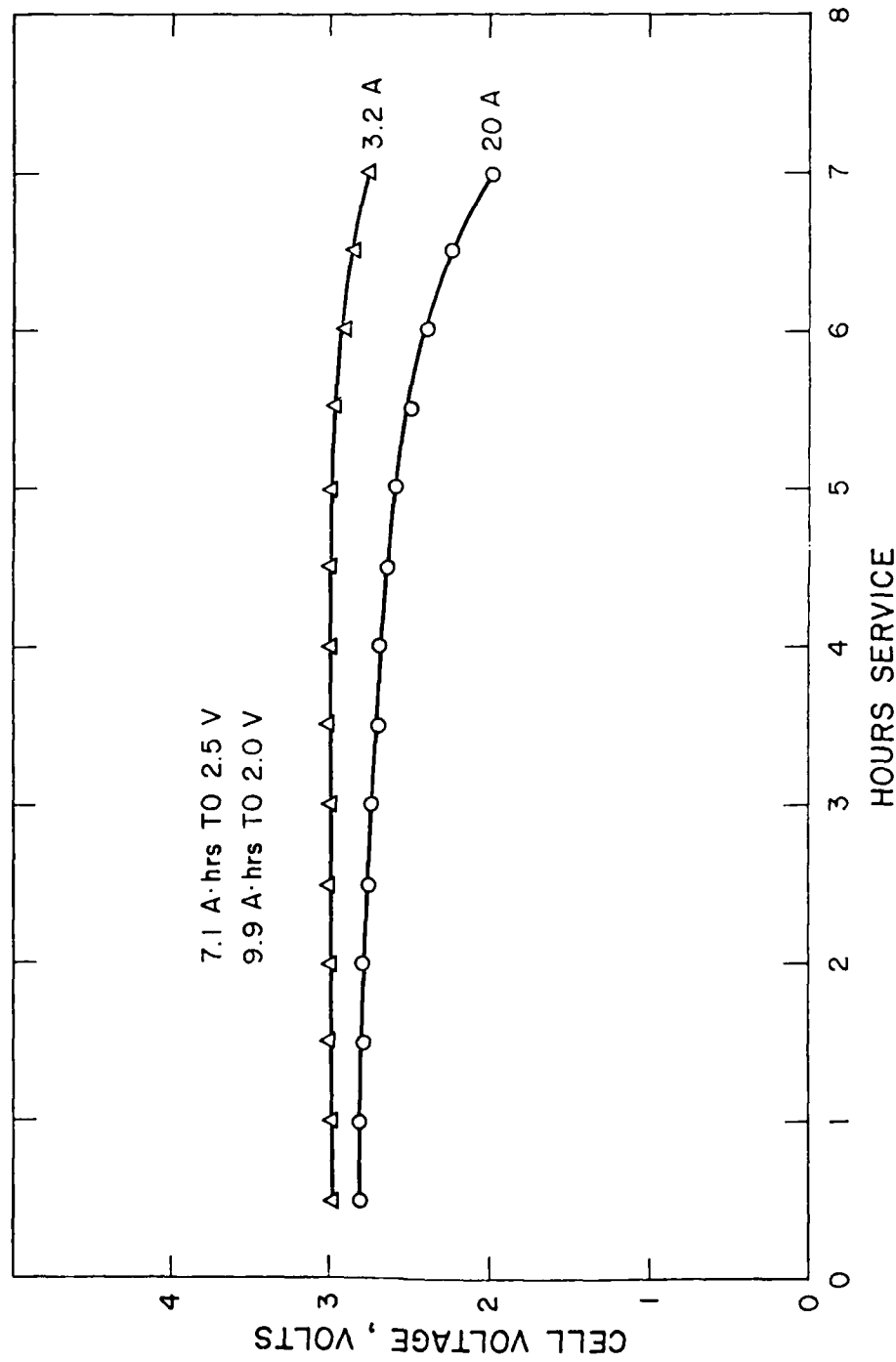


Figure 122. Performance of a fresh flat cell on the new GLID load at -30°C.

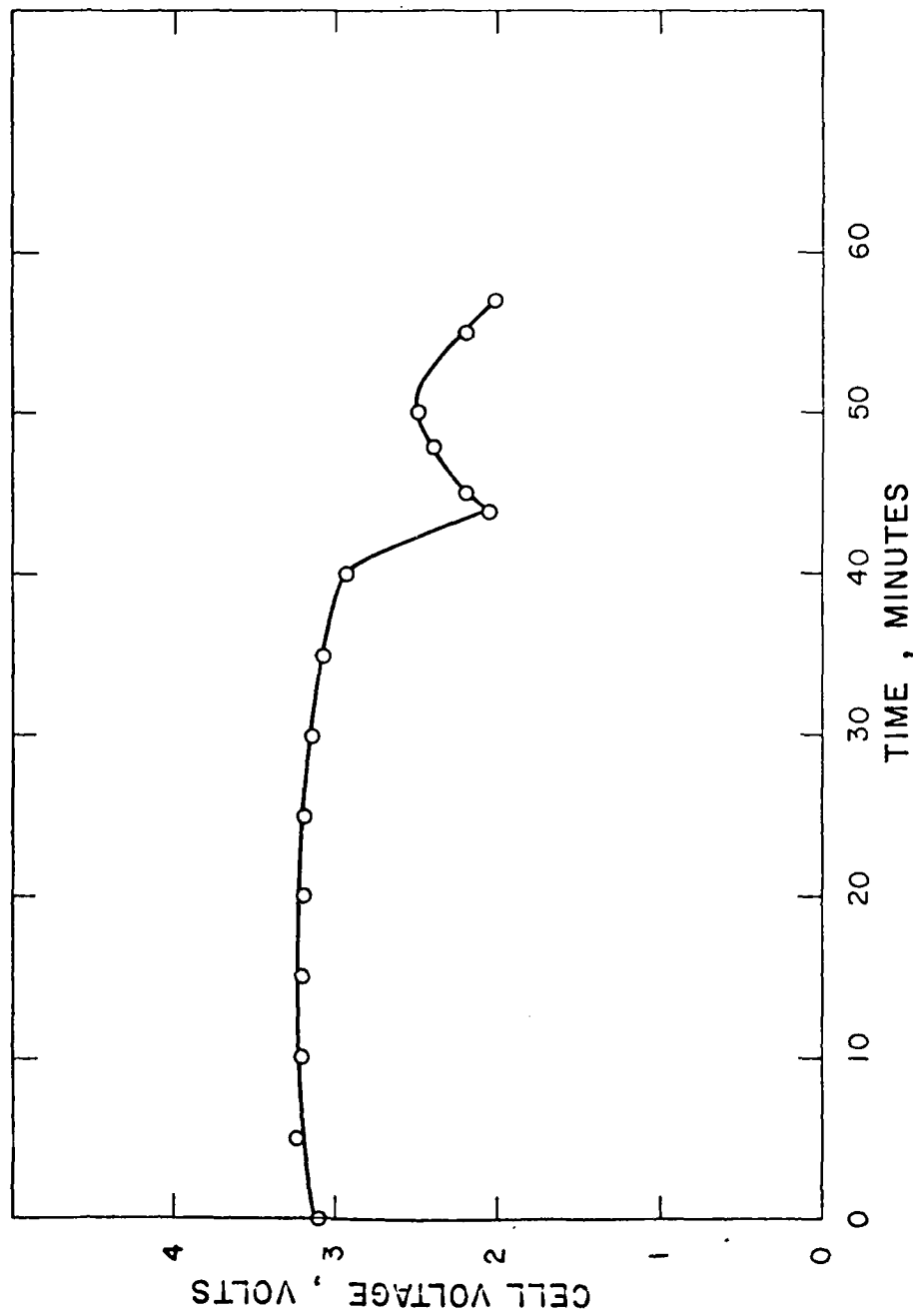


Figure 123. Performance of a fresh flat cell on 20A constant current discharge.

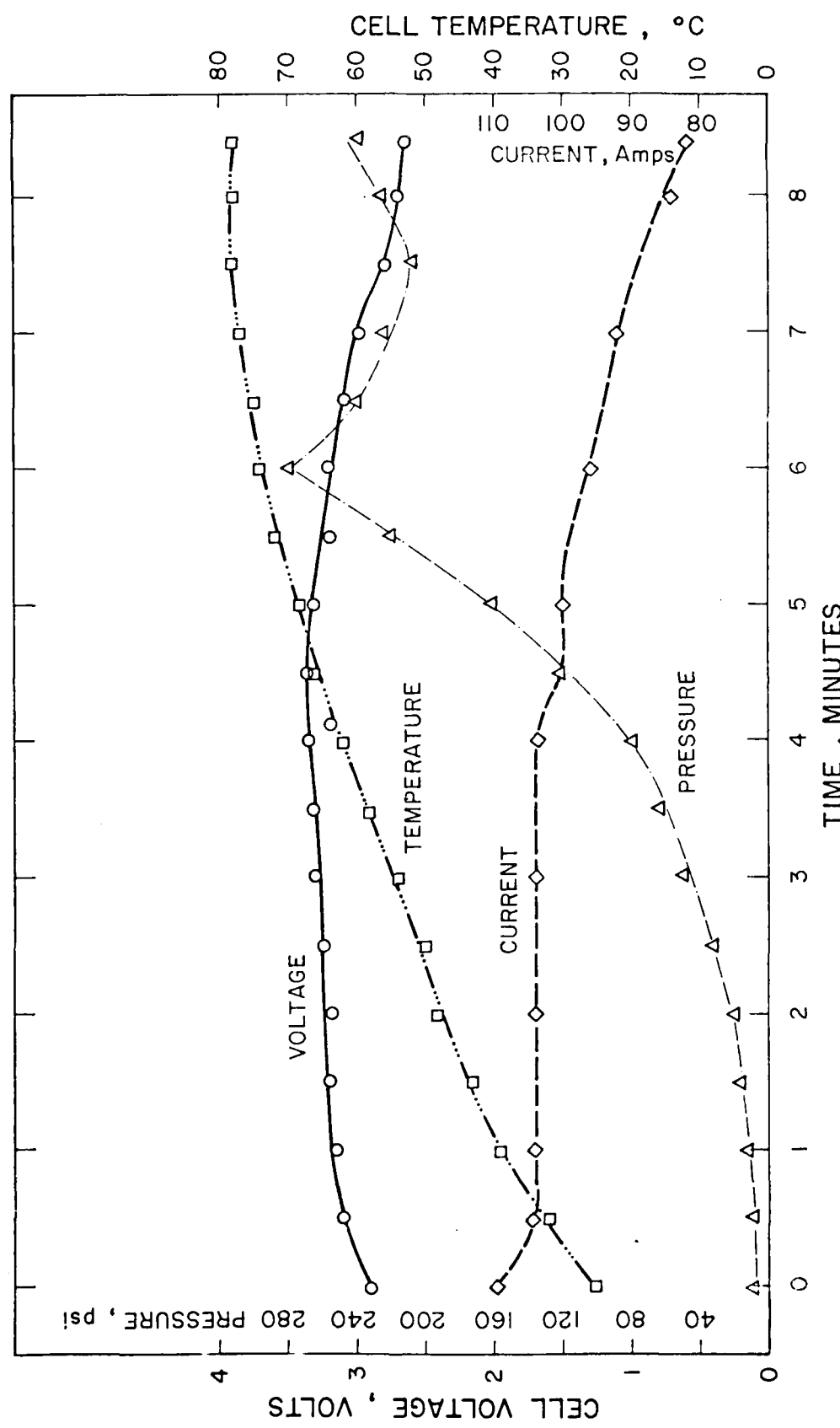


Figure 124. Voltage, temperature and internal pressure profiles of a fresh flat cylindrical cell on 100A at 25°C.

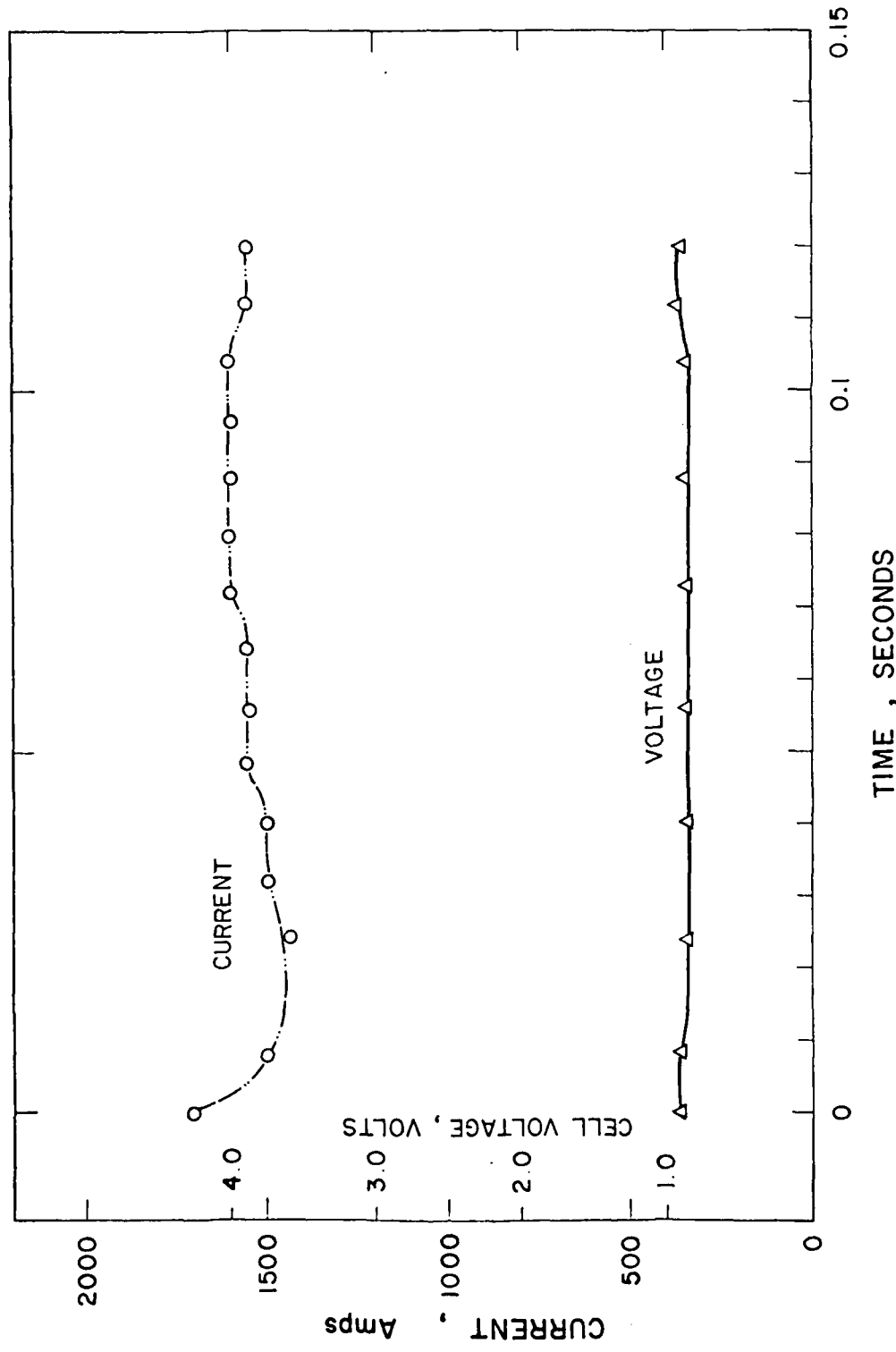


Figure 125. Short circuit performance of a flat cylindrical cell.



Figure 126. Photograph of a fresh and a shorted flat cell.

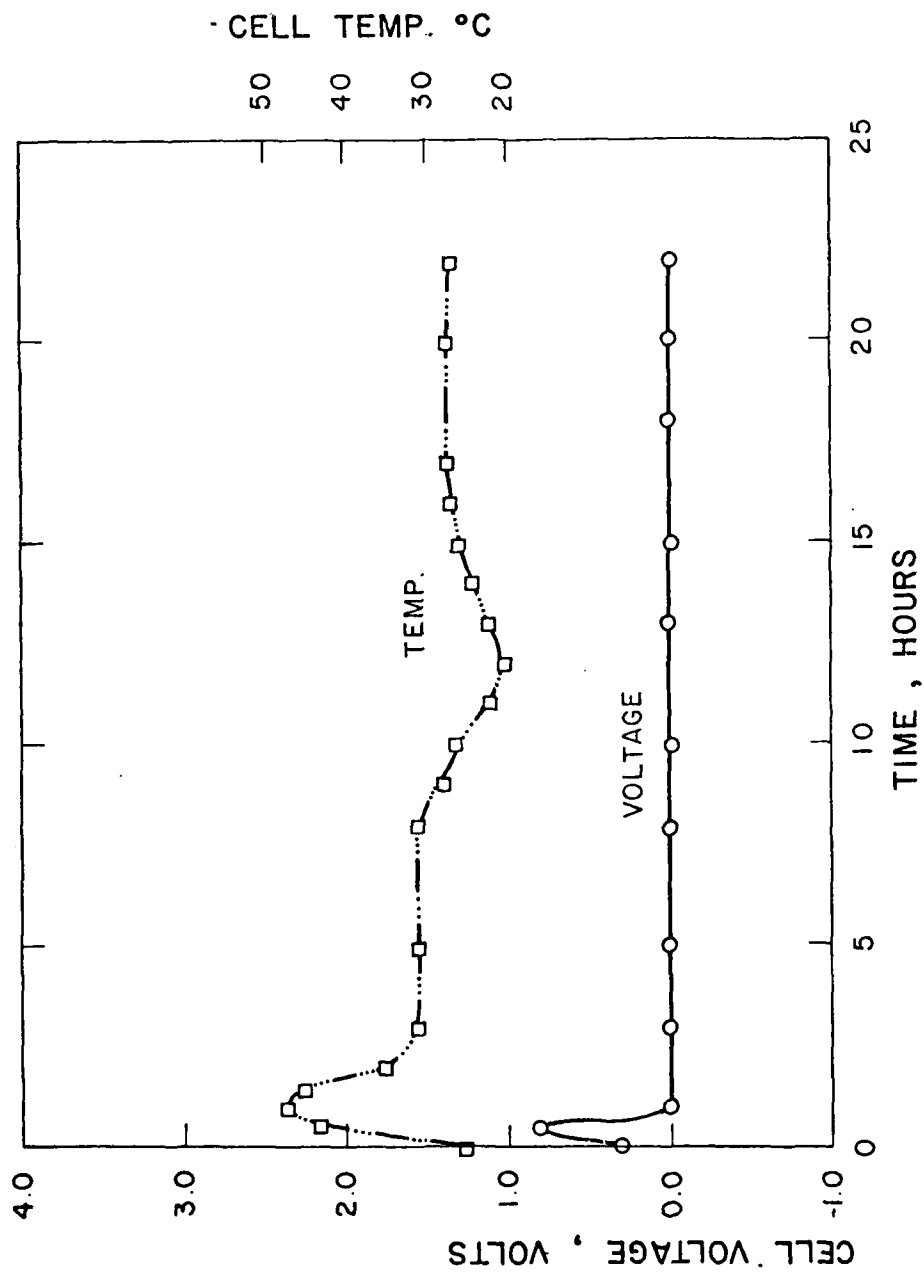


Figure 127. Voltage and temperature profiles of a flat cell on force-discharge at a constant current of 3.0A at 25°C.

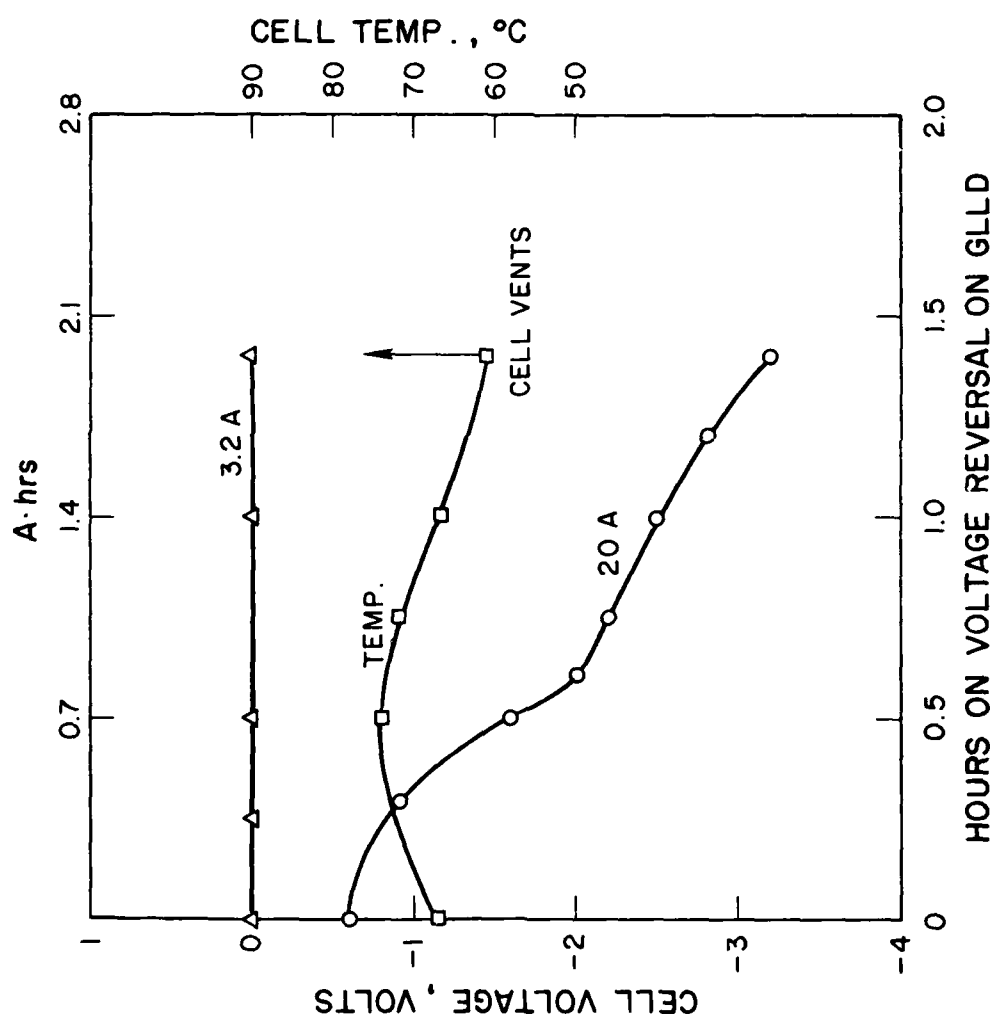


Figure 128. Behavior of a flat cell during voltage reversal on the new GLLD cycle.

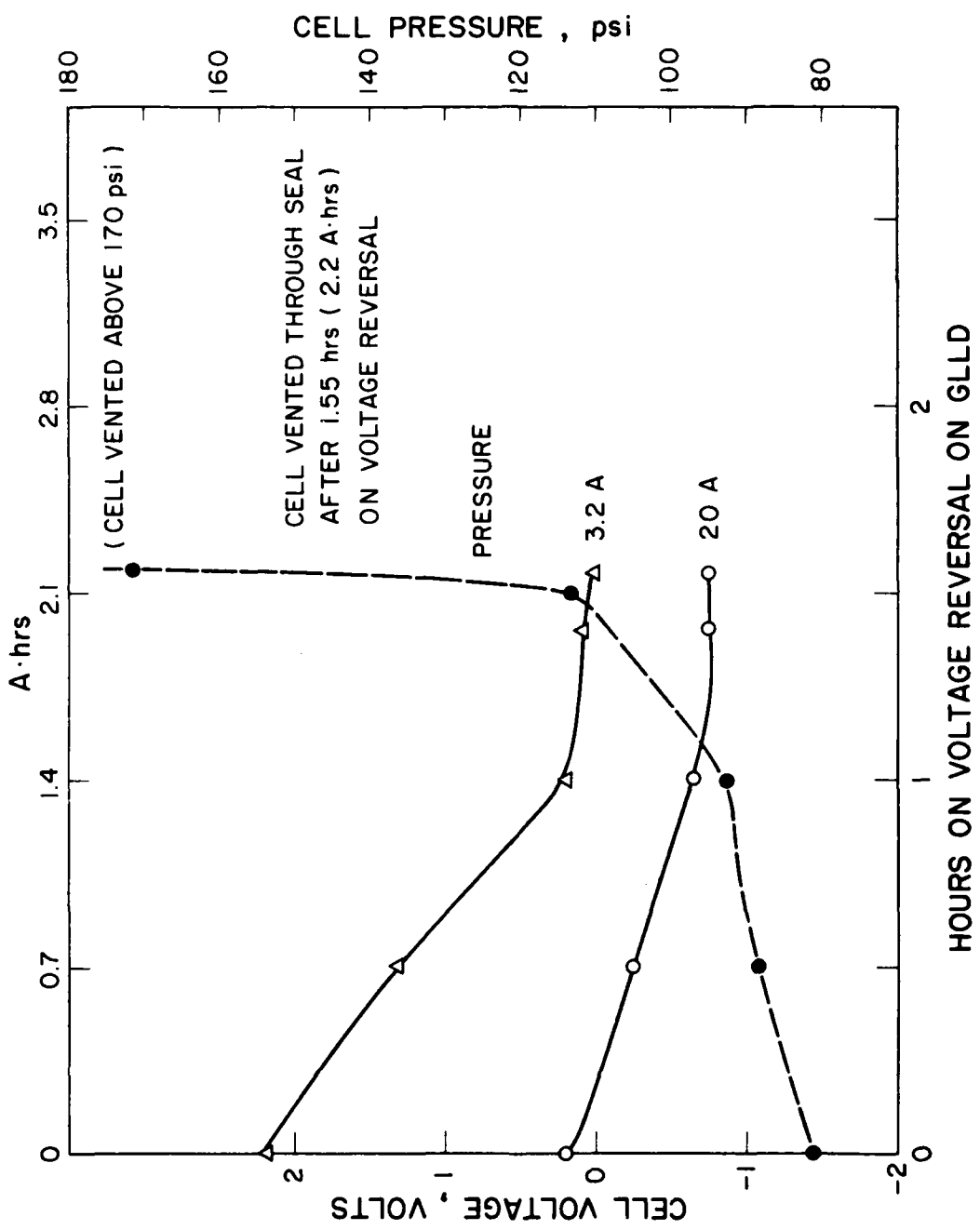


Figure 129. Behavior of a flat cell during voltage reversal at 3.2A and 20A on the new GLLD cycle.

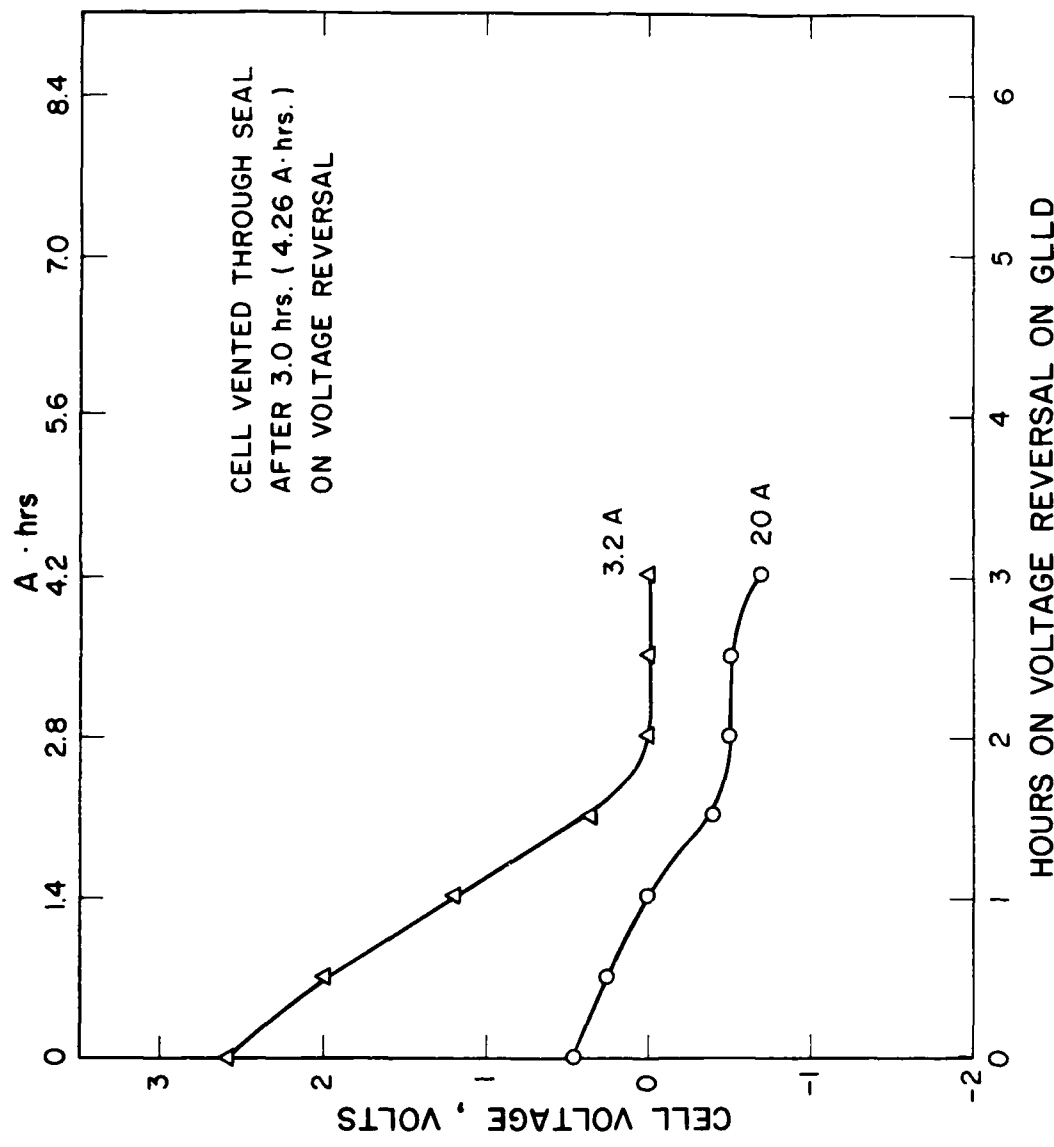


Figure 130. Behavior of a flat cell during voltage reversal at 3.2A and 20A on the new GLLD cycle.

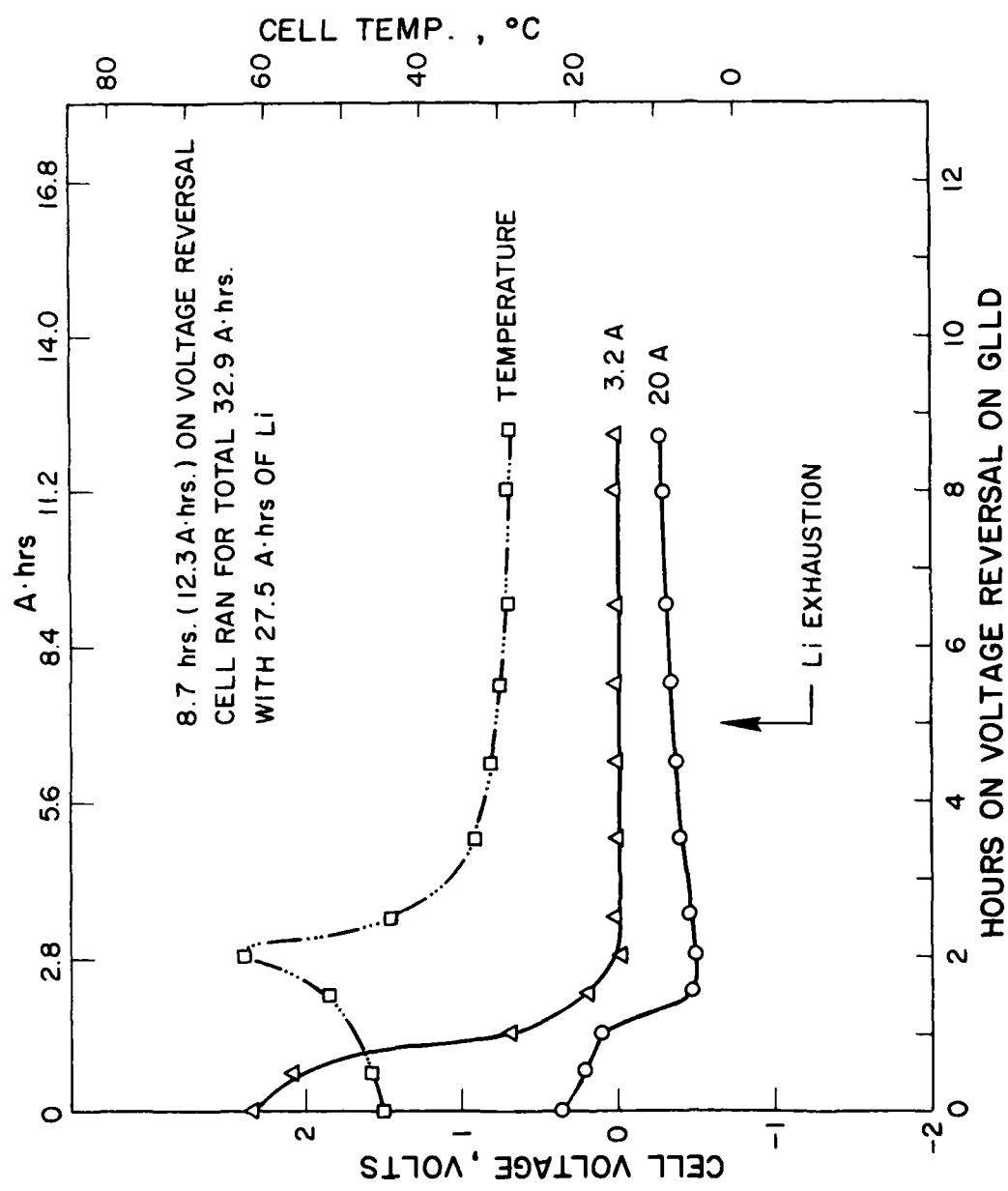
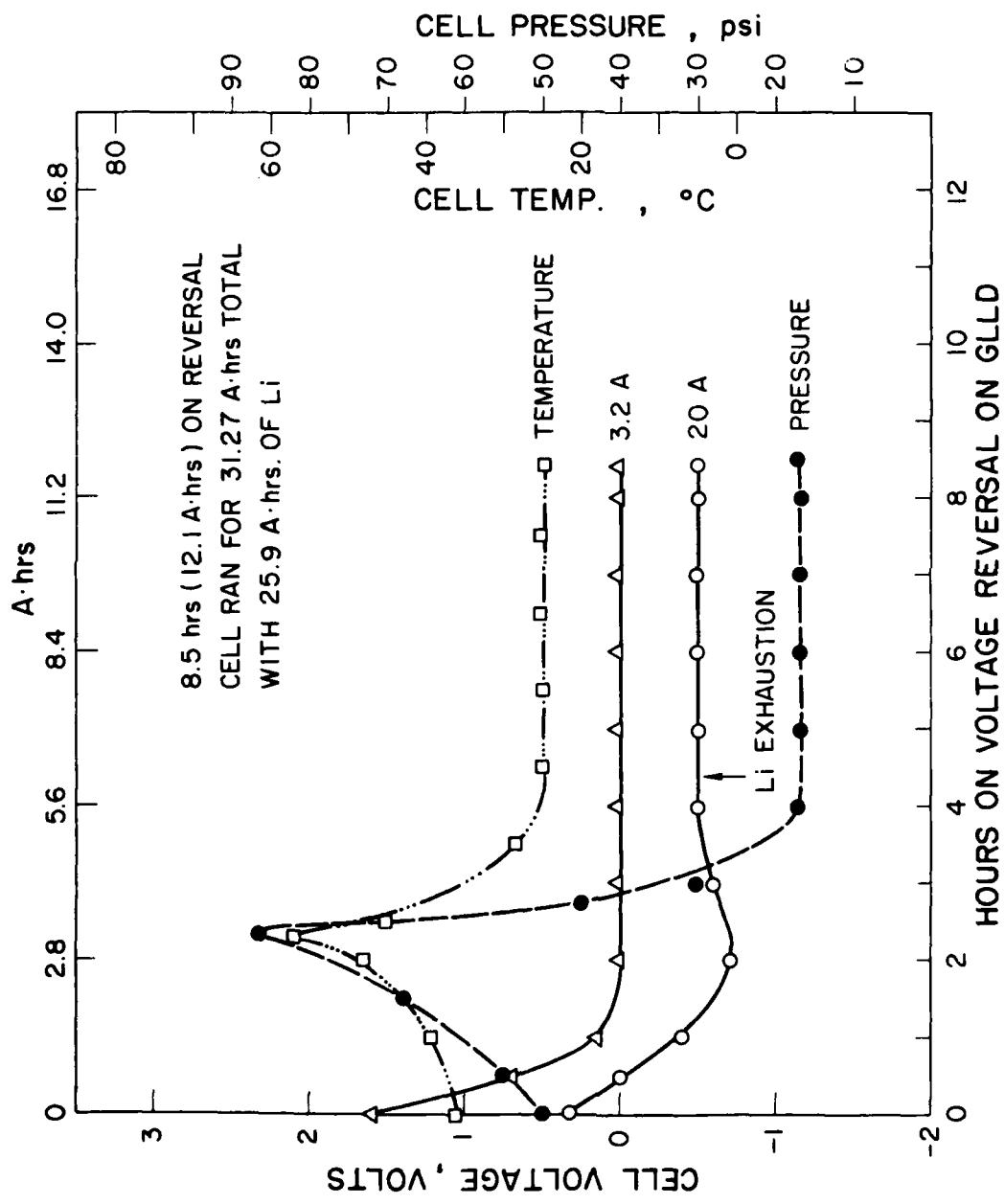


Figure 131. Behavior of a flat cell during voltage reversal on the new GLLD Cycle.



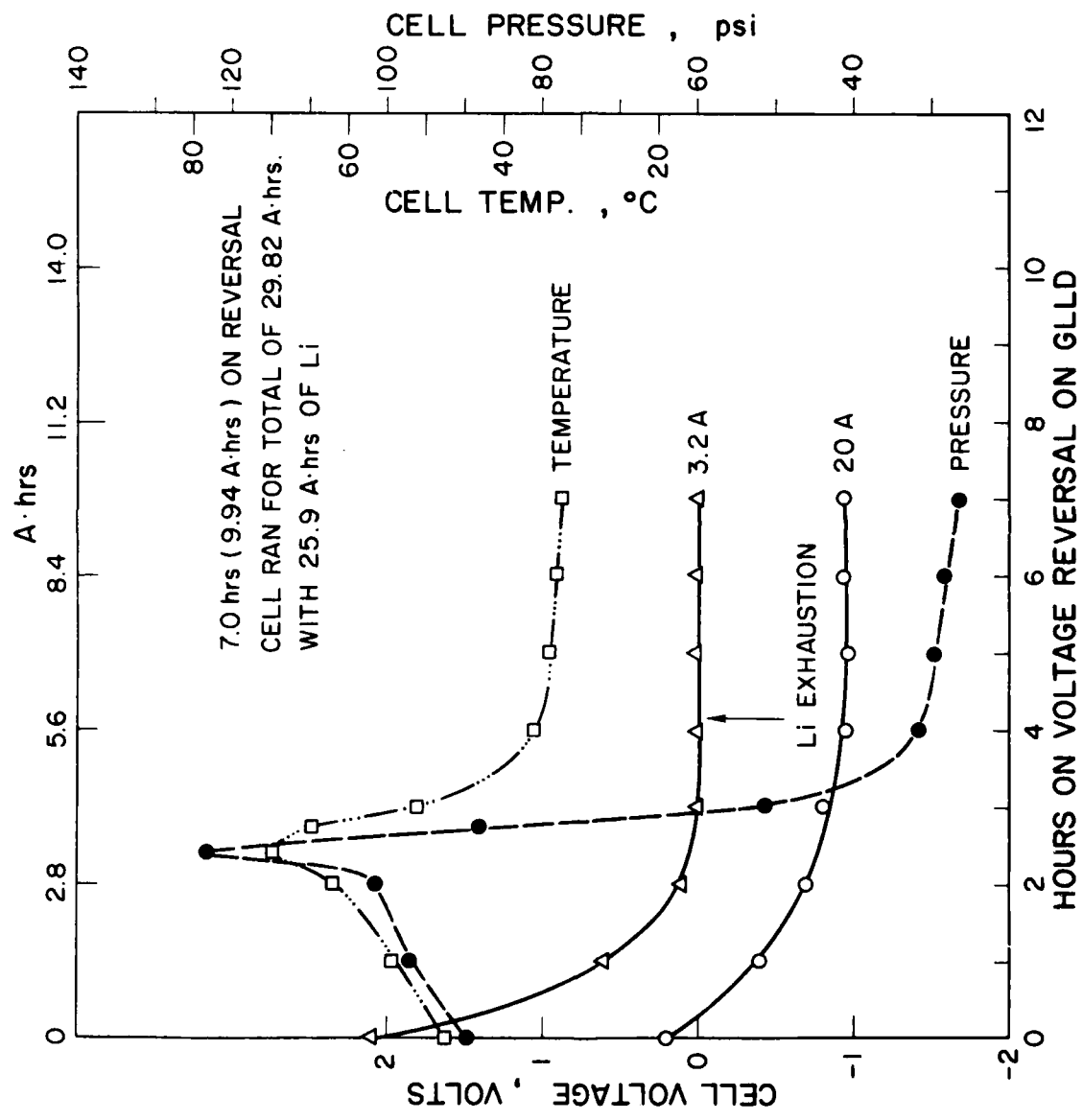


Figure 133. Behavior of a flat cell during voltage reversal on the new GLLD cycle

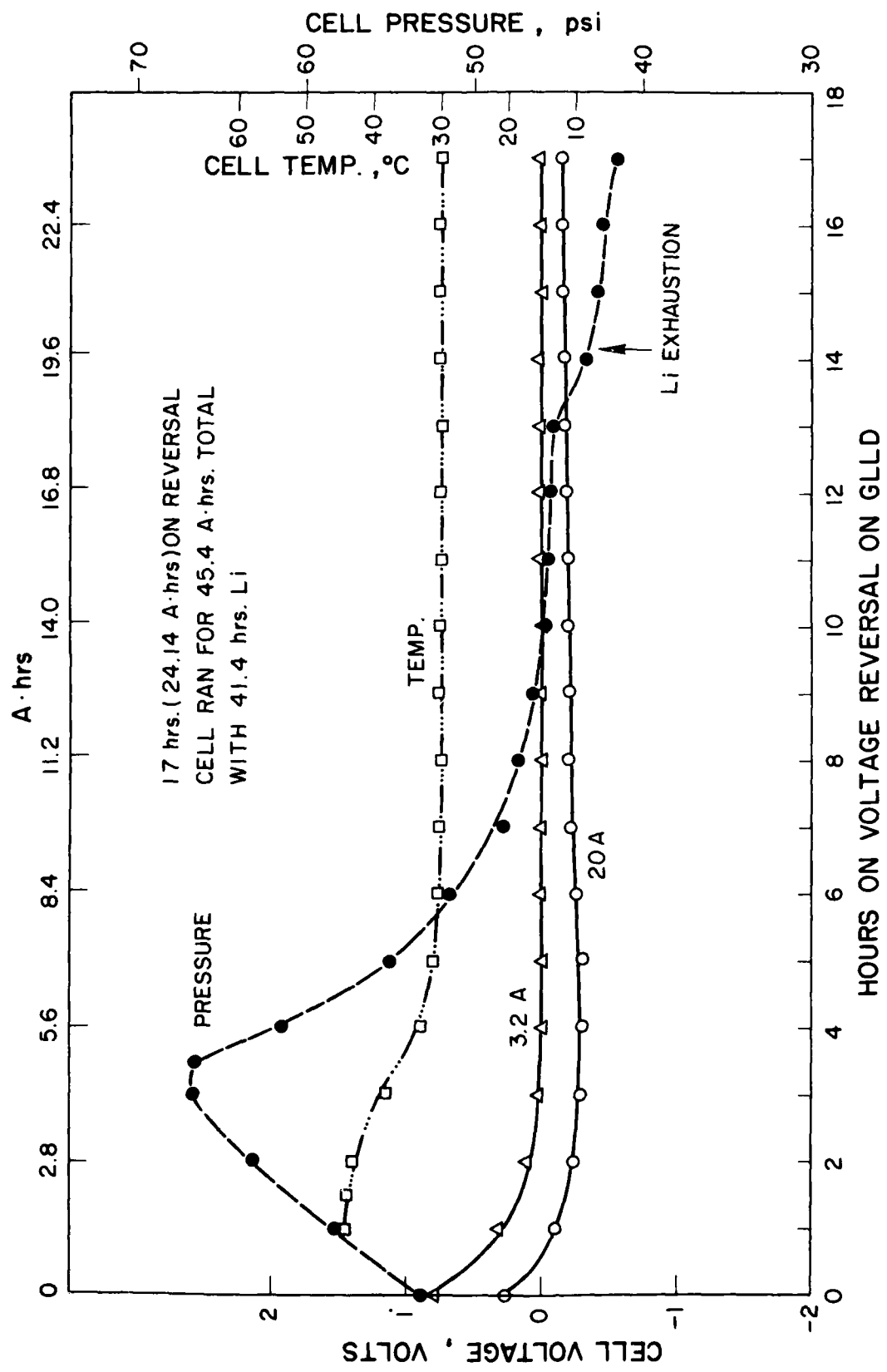


Figure 134. Behavior of a lithium excess flat cell during voltage reversal on the new GLLD load.

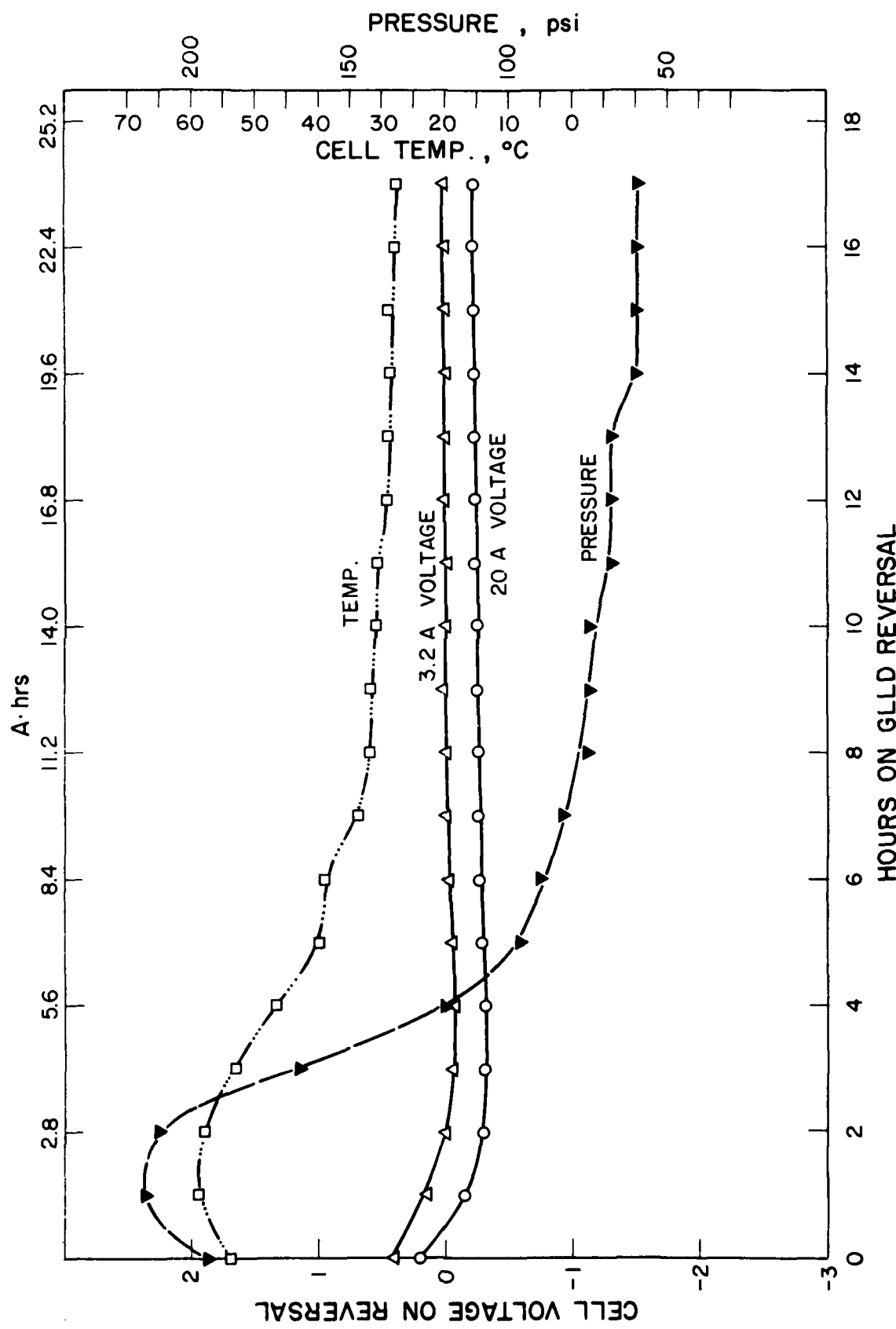


Figure 135. Performance of a lithium excess flat cell during voltage reversal at the new GLLD load.

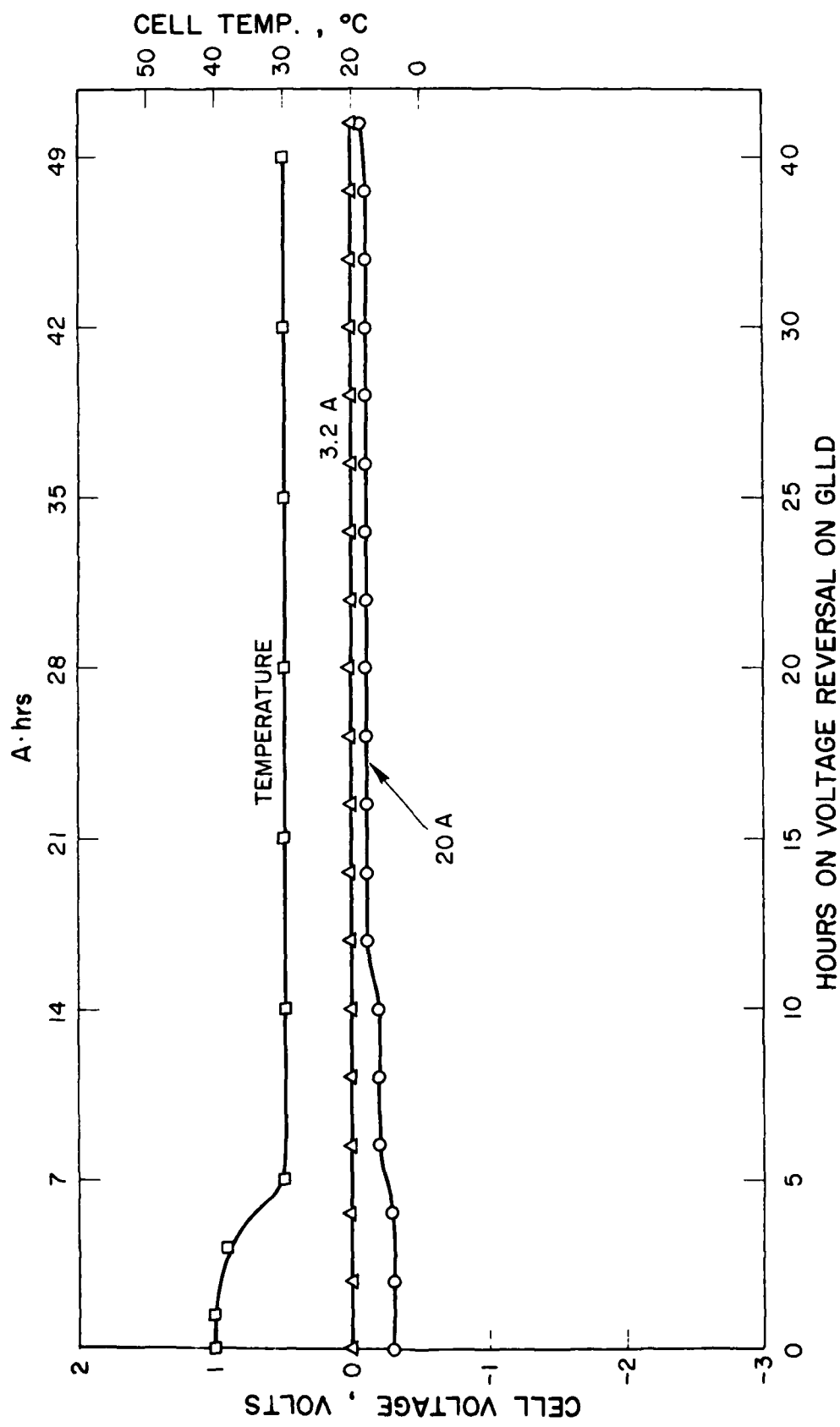


Figure 136. Performance of a lithium excess flat cell during voltage reversal on the new GLLD load.

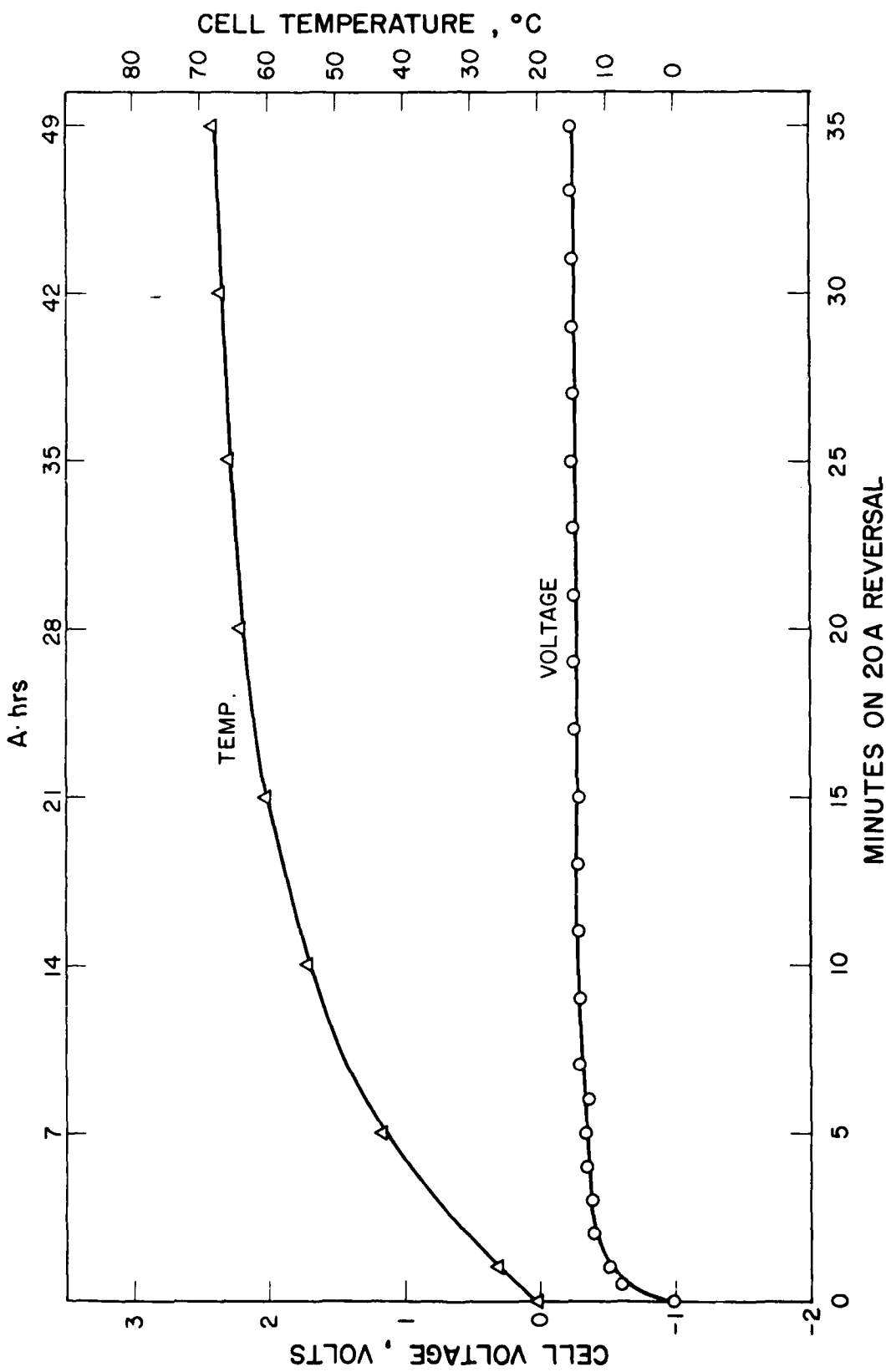


Figure 137. Performance of a lithium excess flat cell on voltage reversal at 20A.

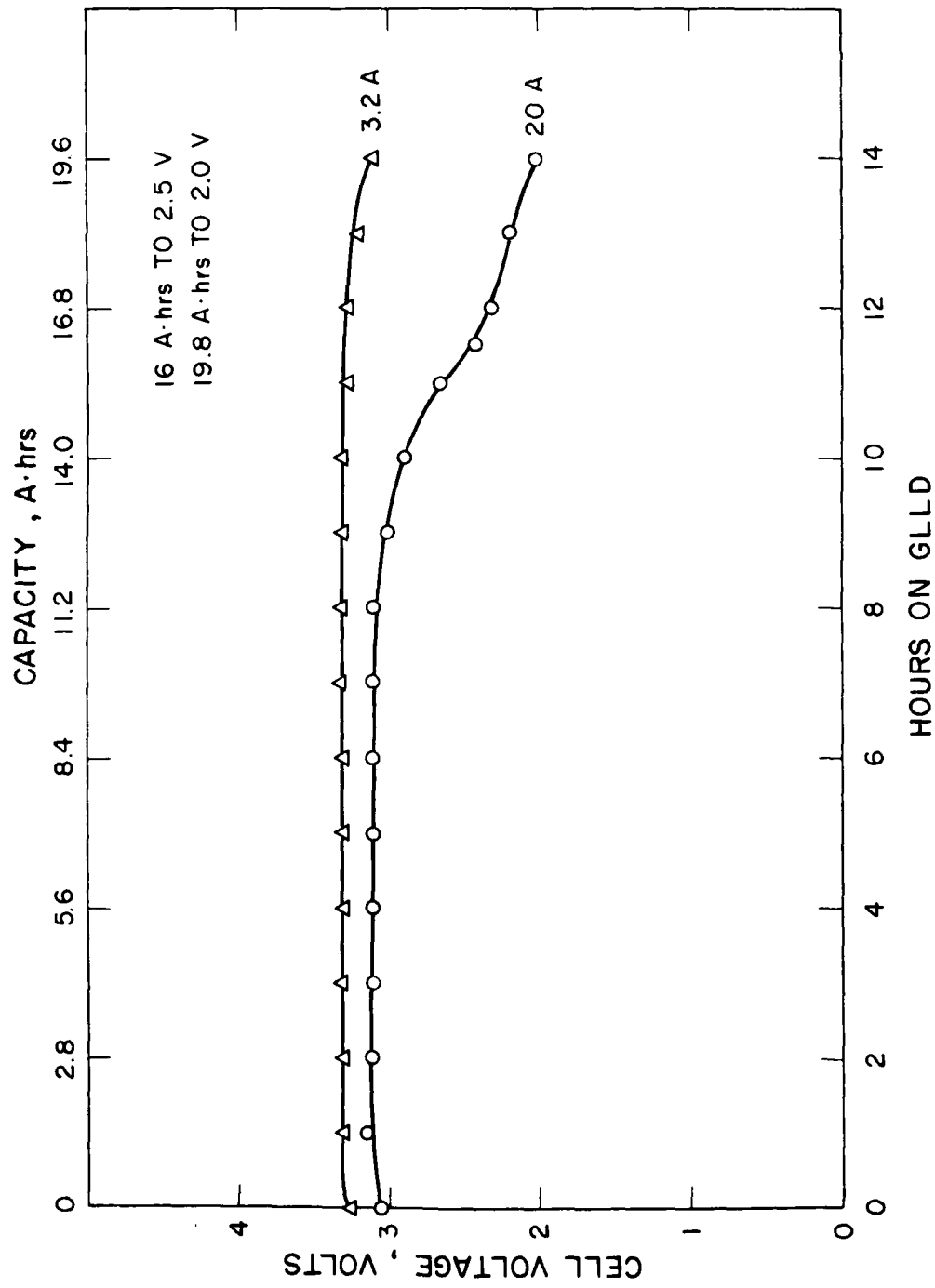


Figure 138. Performance of a flat cell on the new GLLD test at room temperature after three days at room temperature.

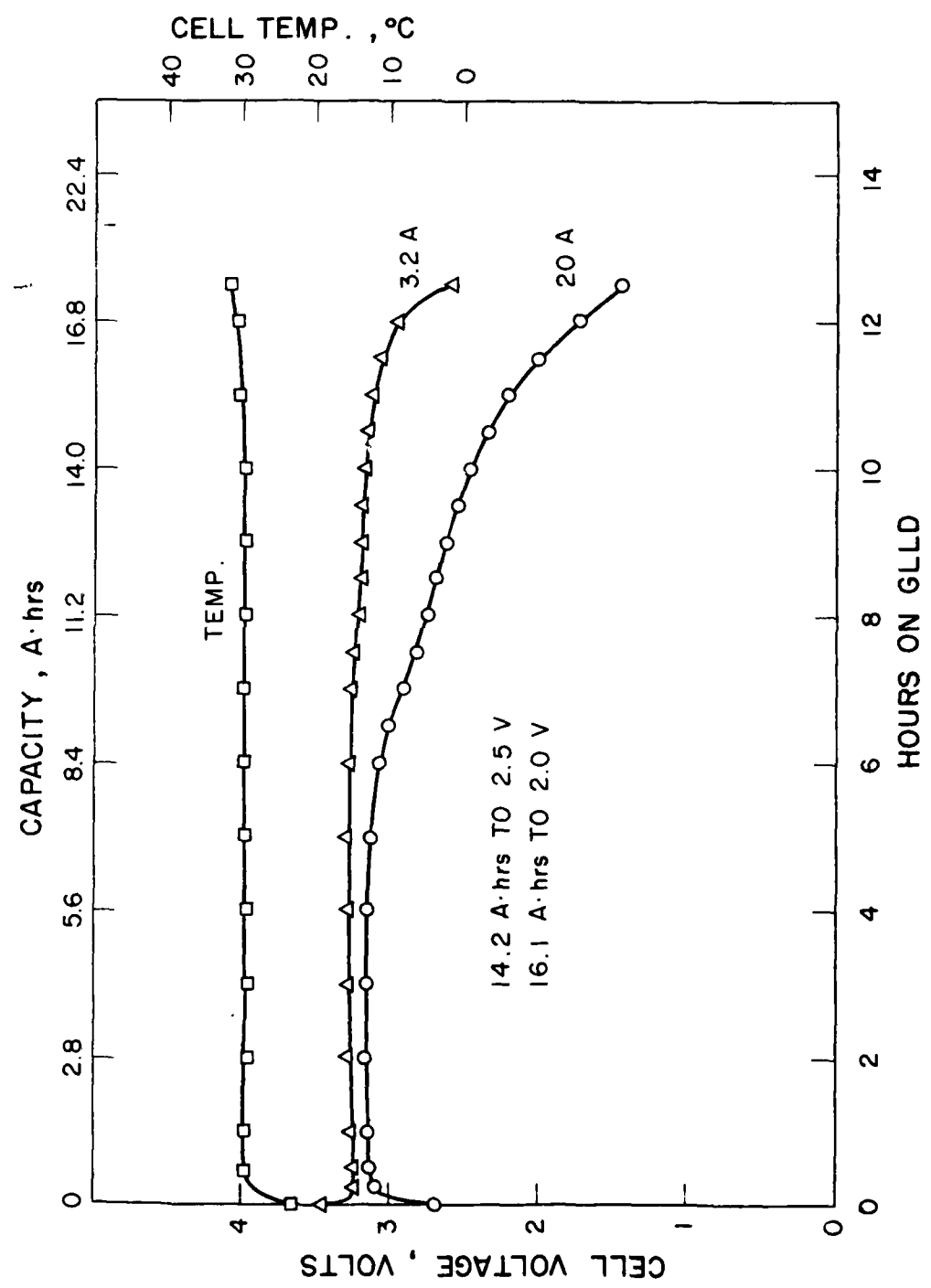


Figure 139. Performance of a flat cell on the new GLLD test at room temperature after one week at room temperature.

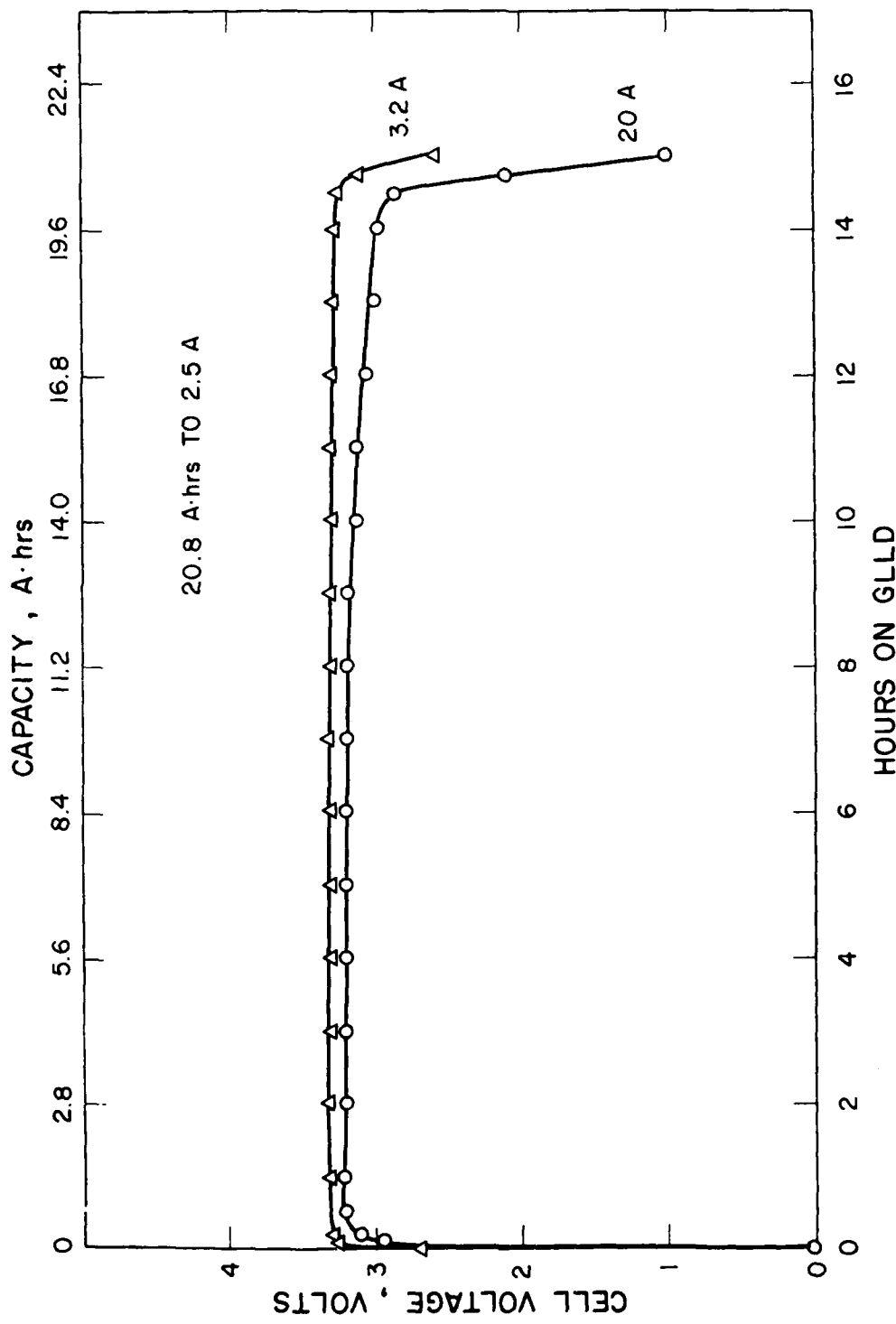


Figure 140. Performance of a flat cell on the new GLLD test at room temperature after one week at room temperature.

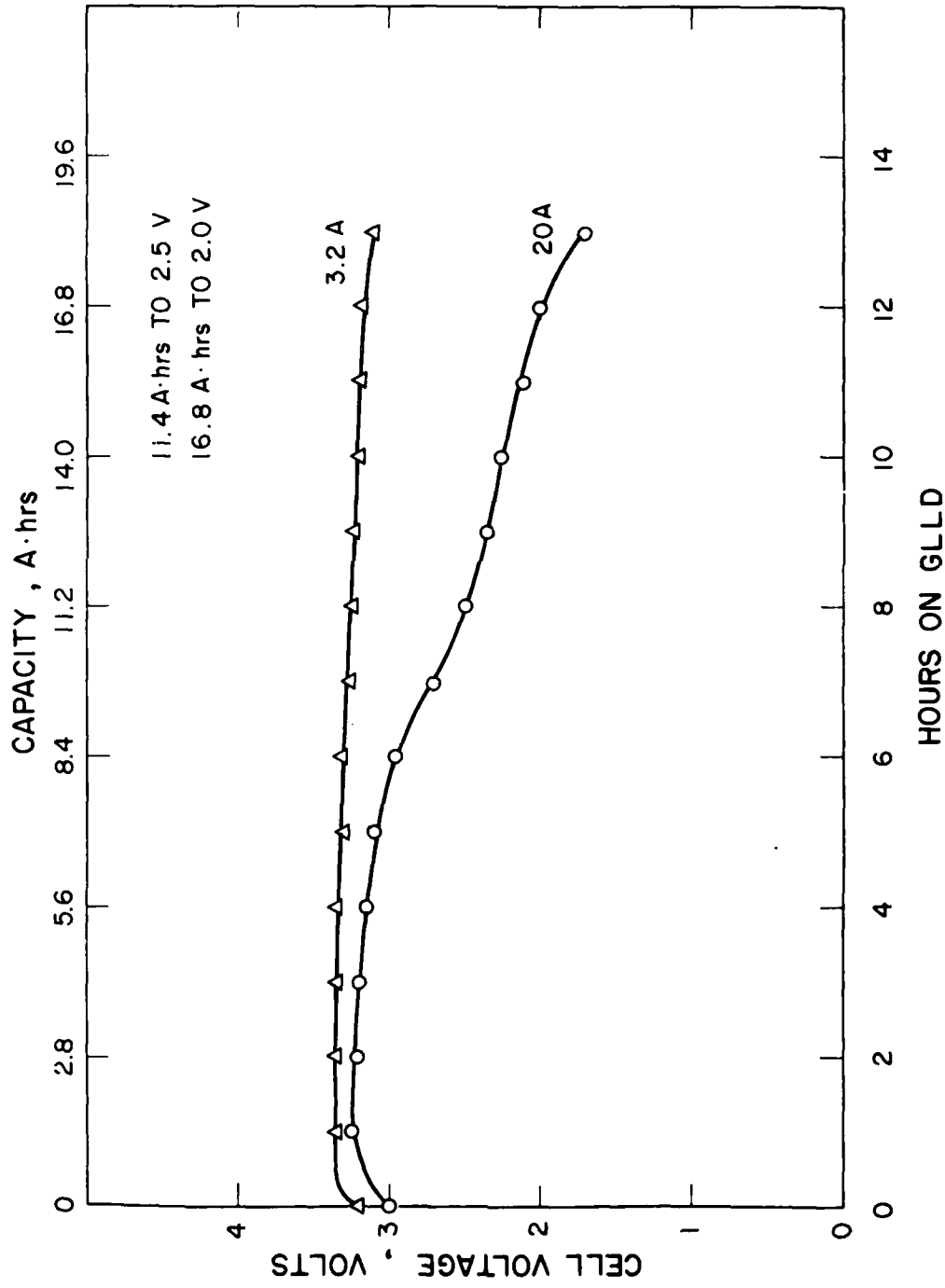


Figure 141. Performance of a flat cell on the GLLD test at room temperature after two weeks at room temperature.

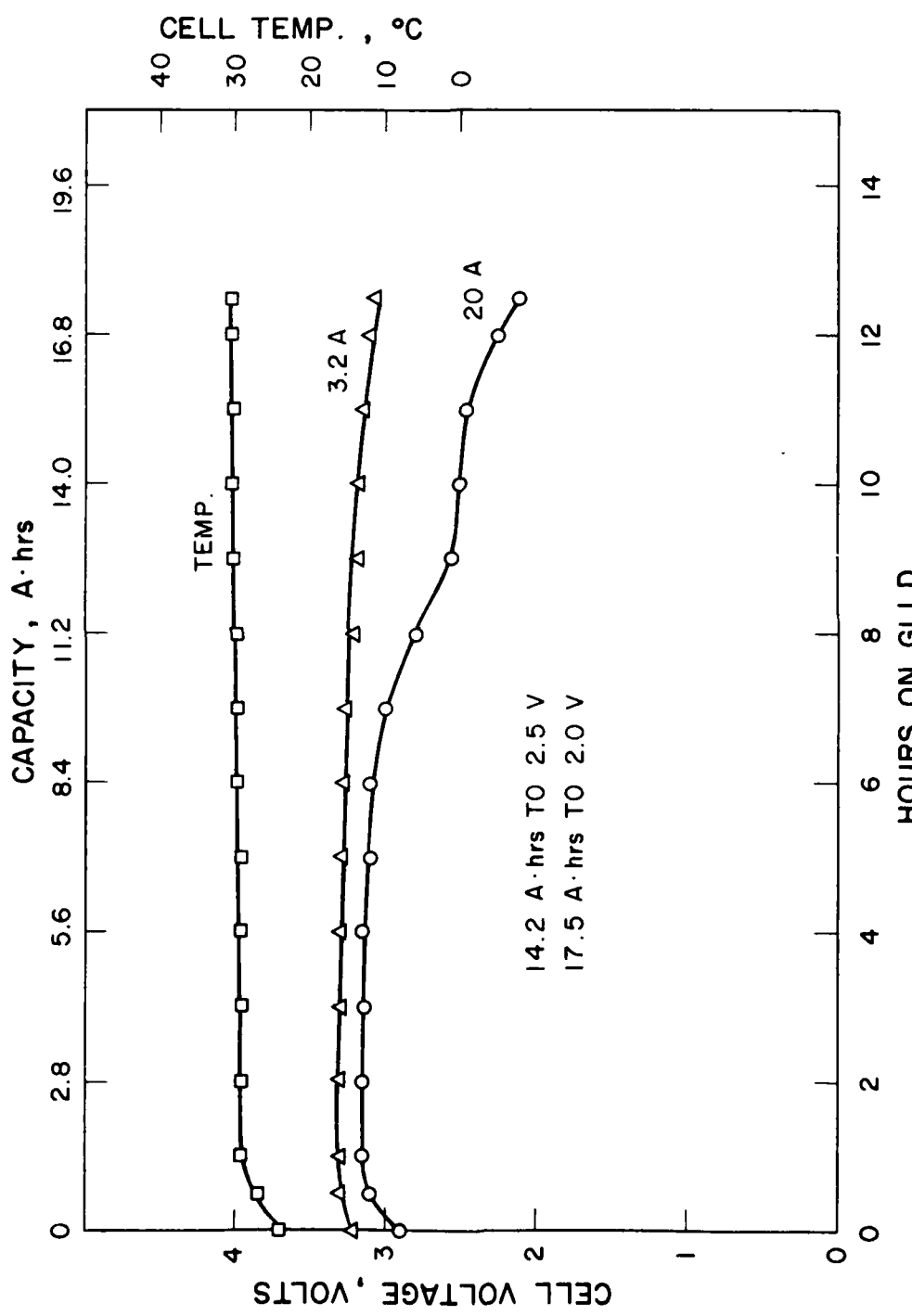


Figure 142. Performance of a flat cell on the GLLD test at room temperature after three weeks at room temperature.

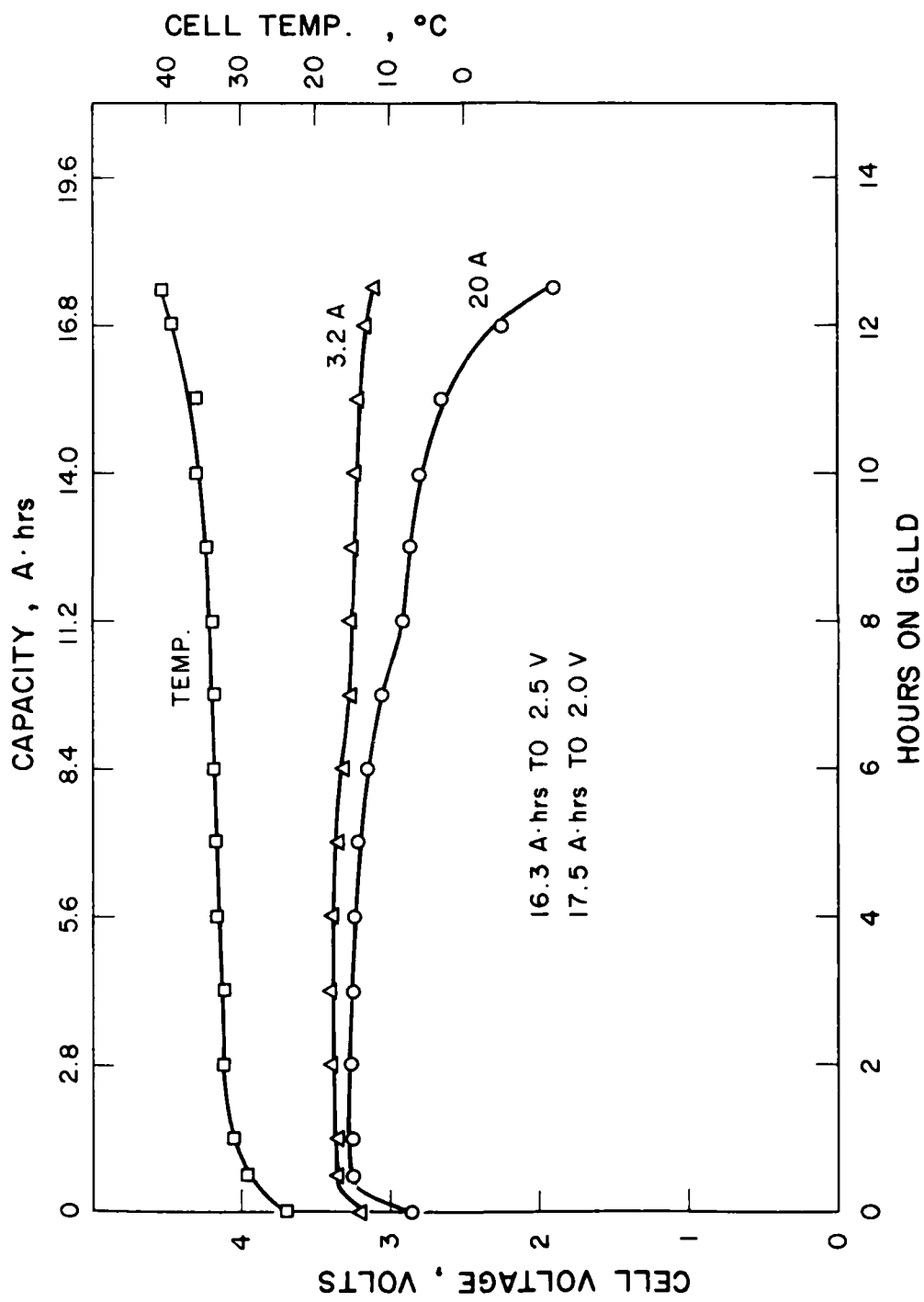


Figure 143. Performance of a flat cell on the GLLD test at room temperature after six weeks at room temperature.

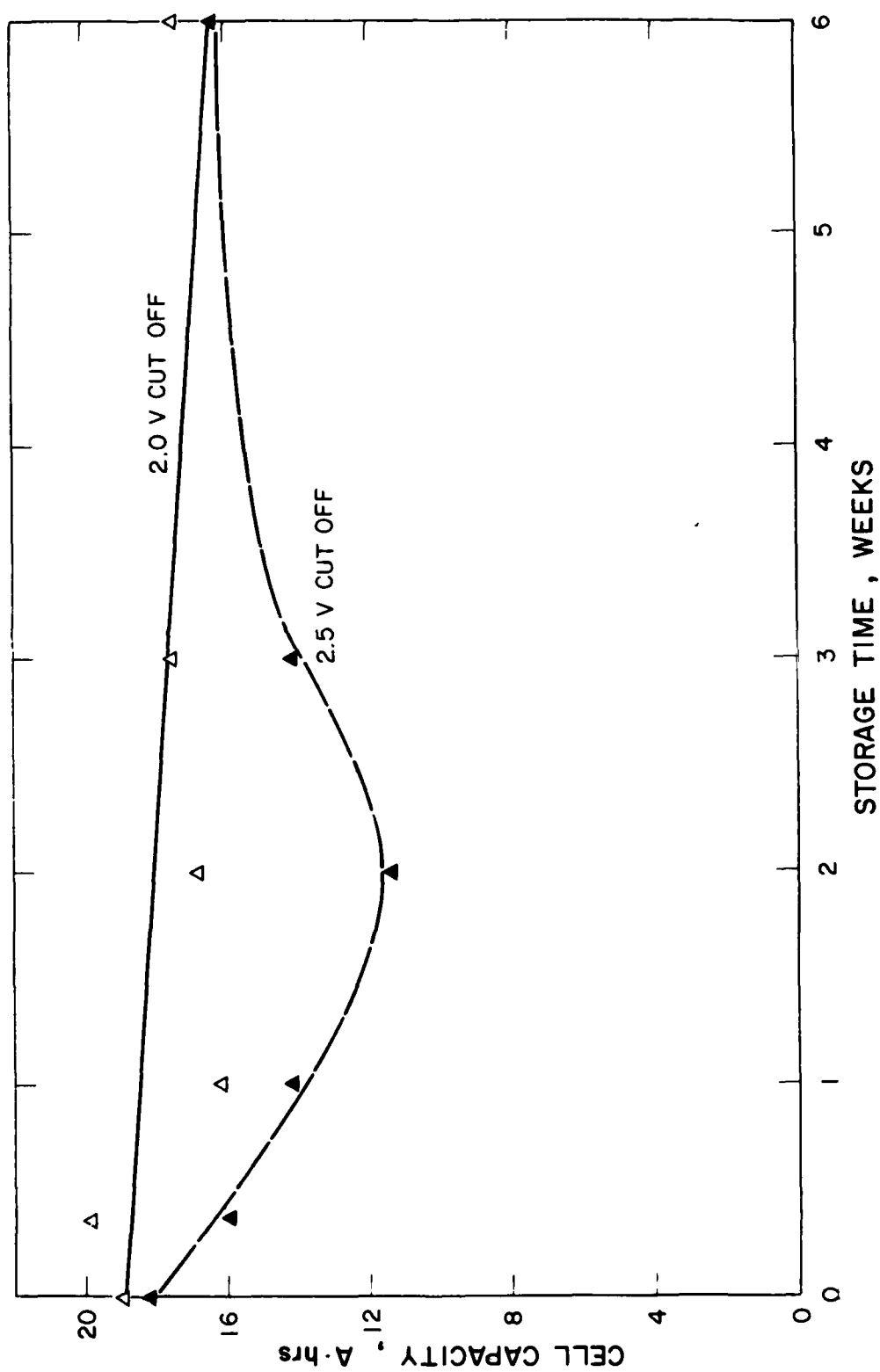


Figure 144. Plot of capacity on GLLD test vs. storage time for flat cylindrical cells.

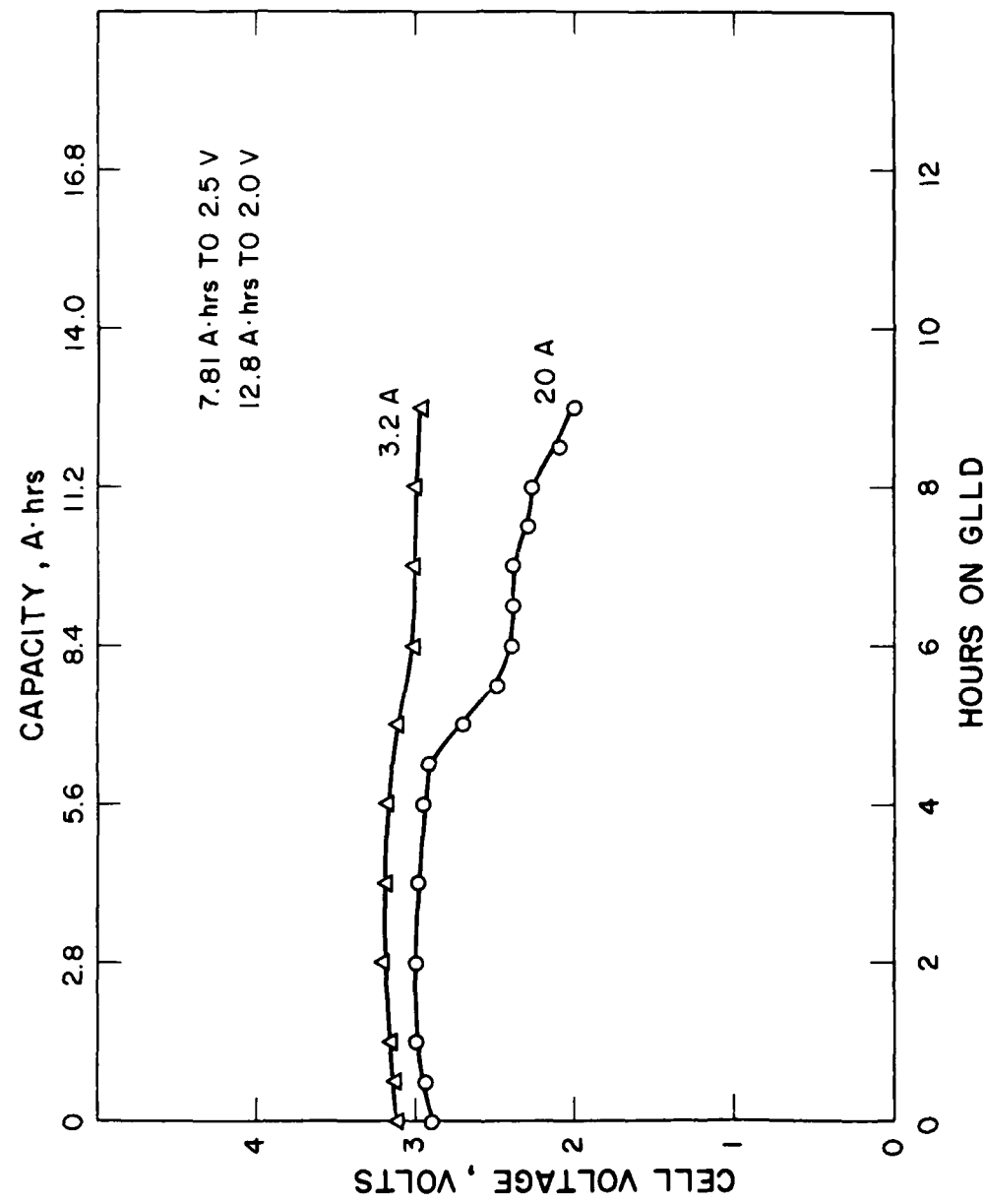


Figure 145. Performance of a flat cell on the new GLLD test at 0°C after three weeks at room temperature.

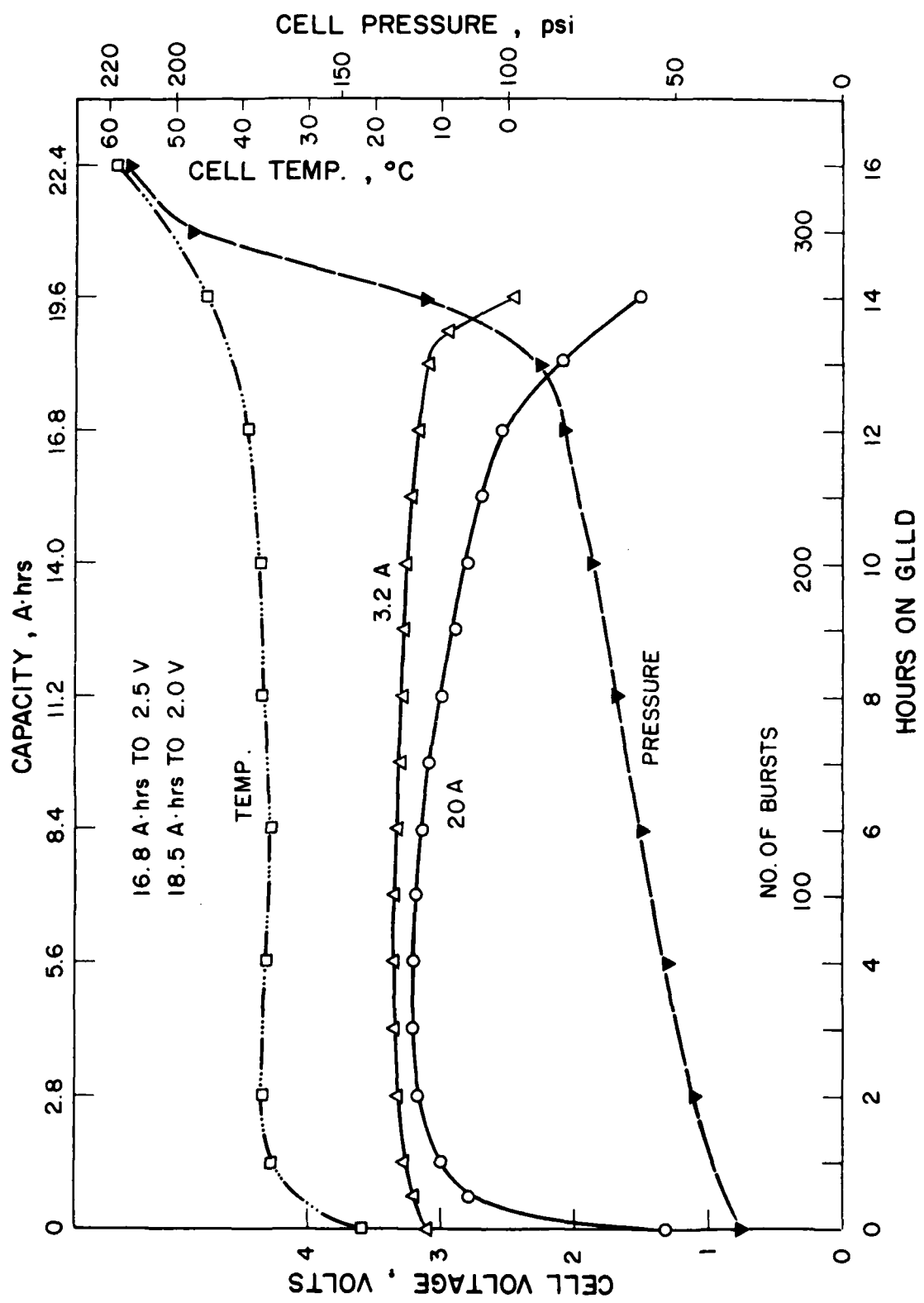


Figure 146. Performance of a flat cell on GLLD test at room temperature after two days at 50°C and two days at 72°C.

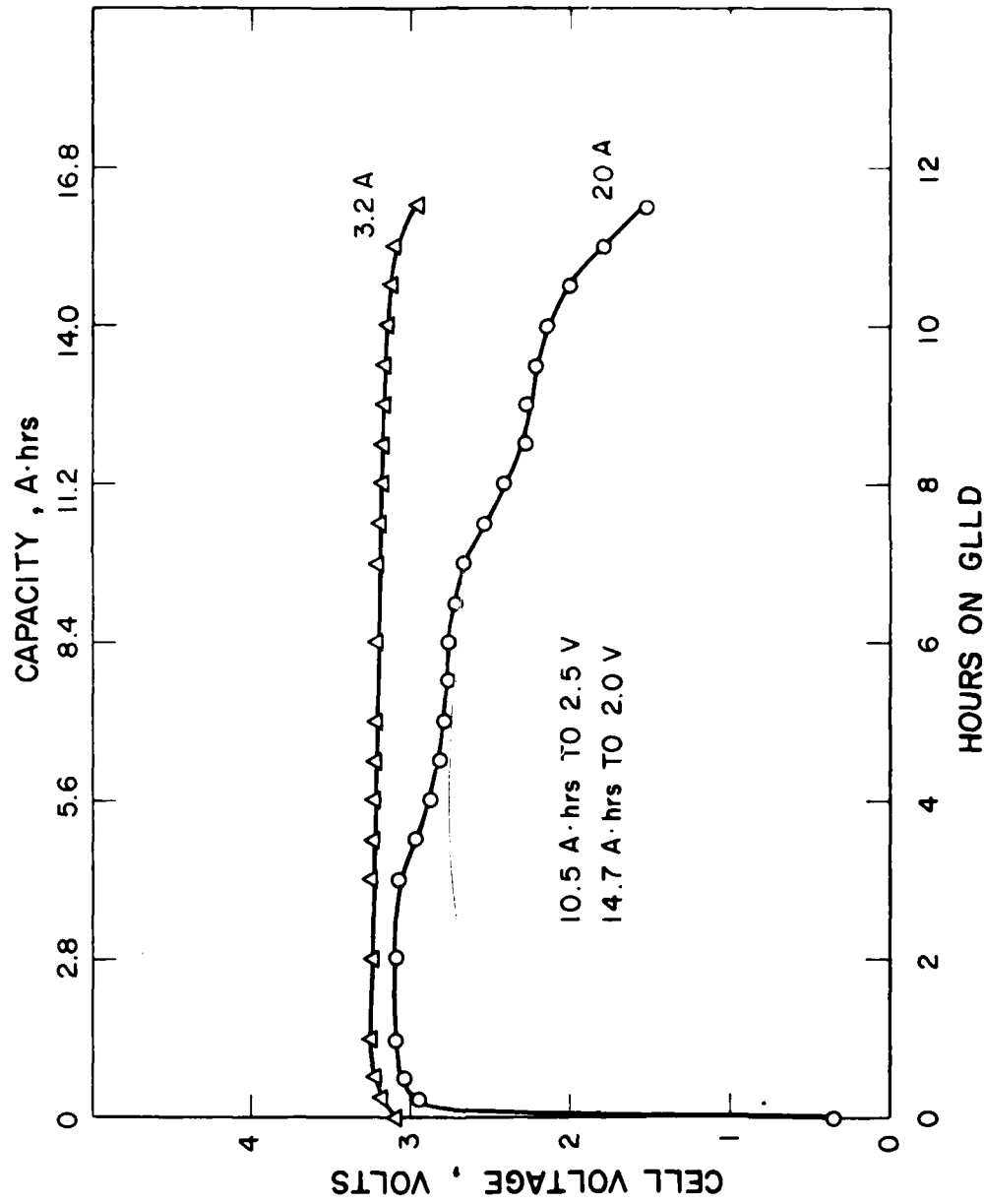


Figure 147. Performance of a flat cell with cathode additive 1 on the new GLLD test at room temperature after 2 days at 72°C and 3-1/2 days at room temperature.

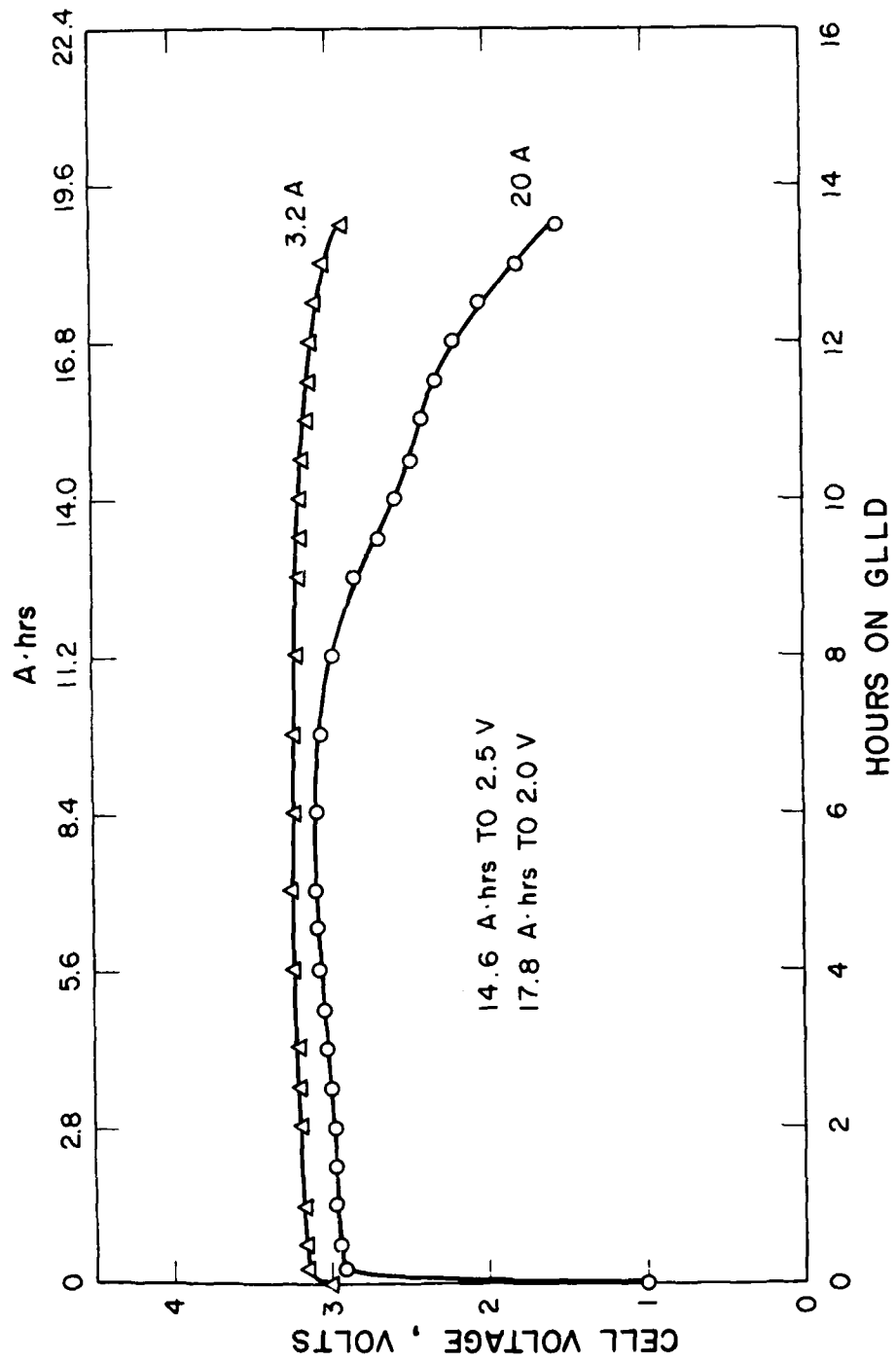


Figure 148. Performance of a cell with vacuum dried cathodes on the new GLLD test at room temperature after 1 day at 72°C and 3-1/2 days at room temperature.

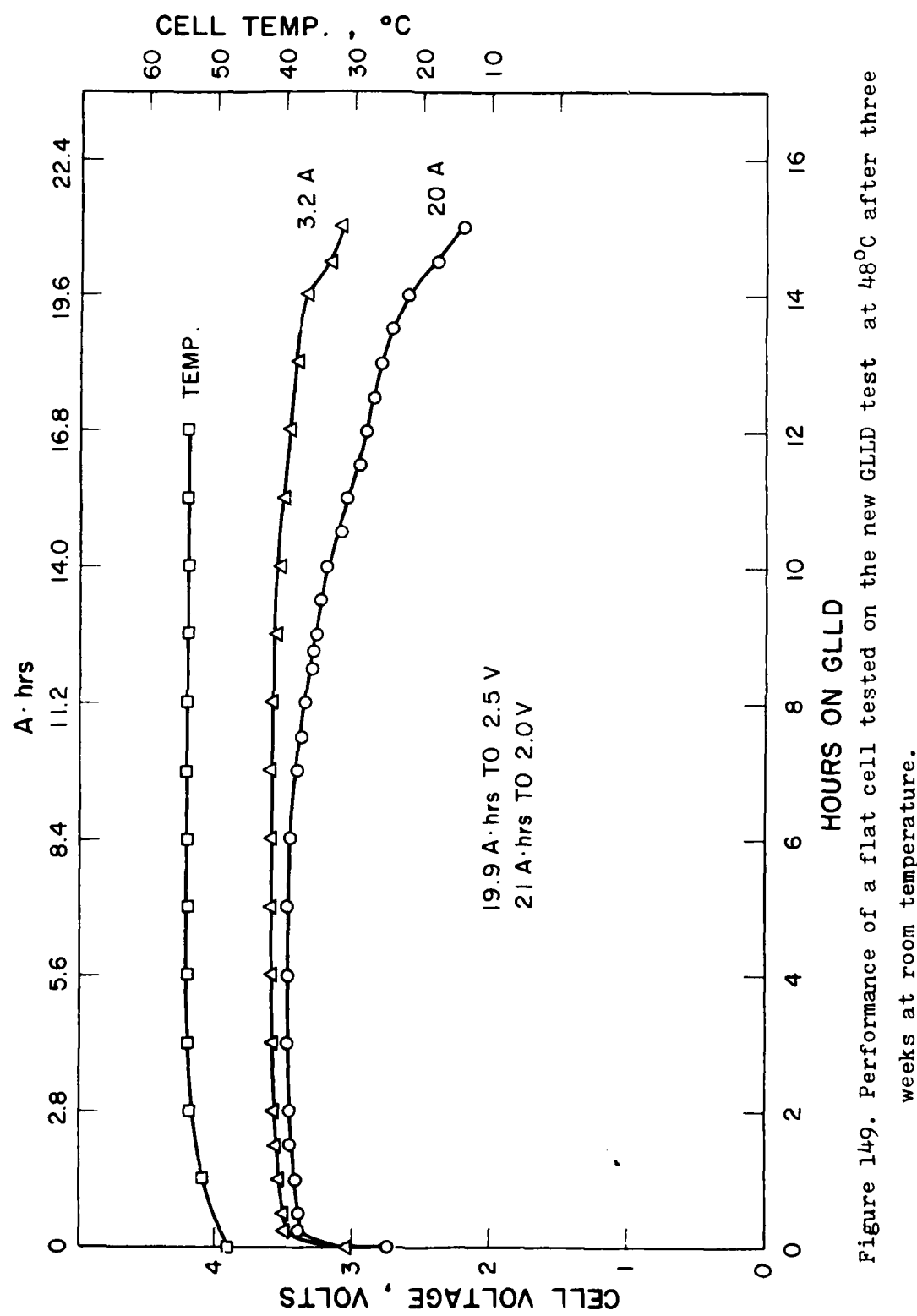


Figure 149. Performance of a flat cell tested on the new GLLD test at 48°C after three weeks at room temperature.

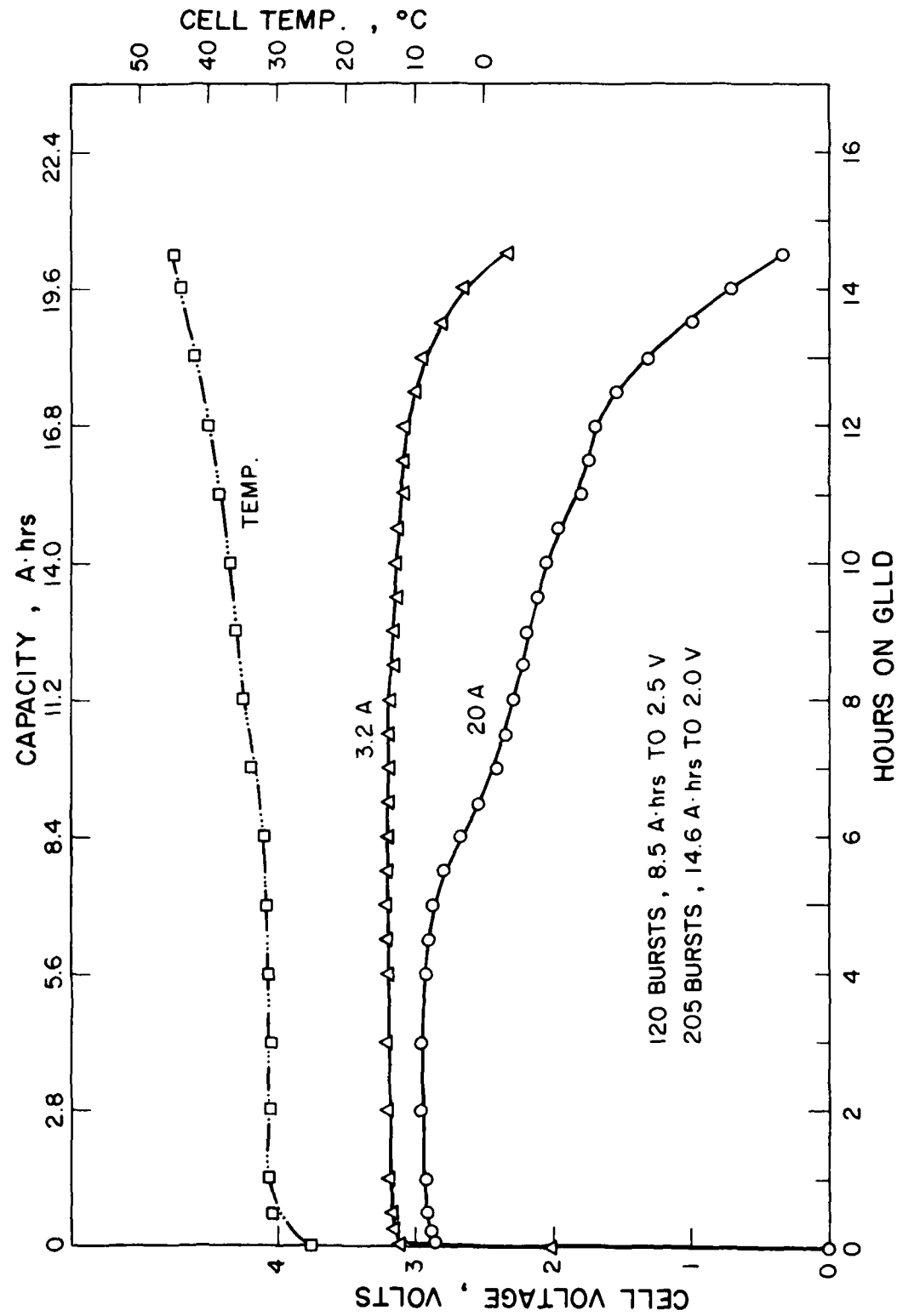


Figure 150. Performance of a flat cell with new design on GLLD test after 2.5 days at 72°C.

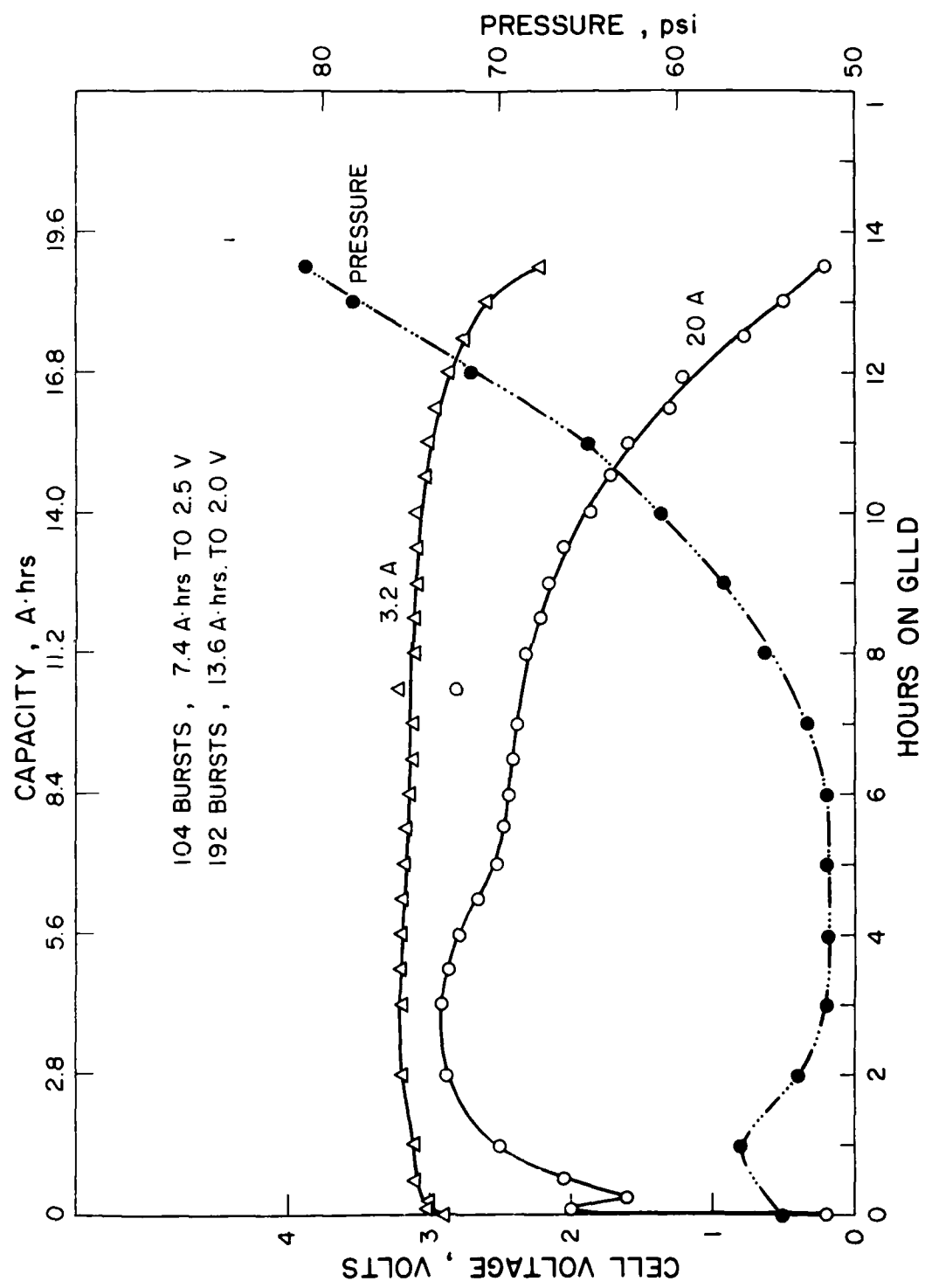


Figure 151. Performance of a flat cell on the new GLLD test at room temperature after 5 days at 72°C.

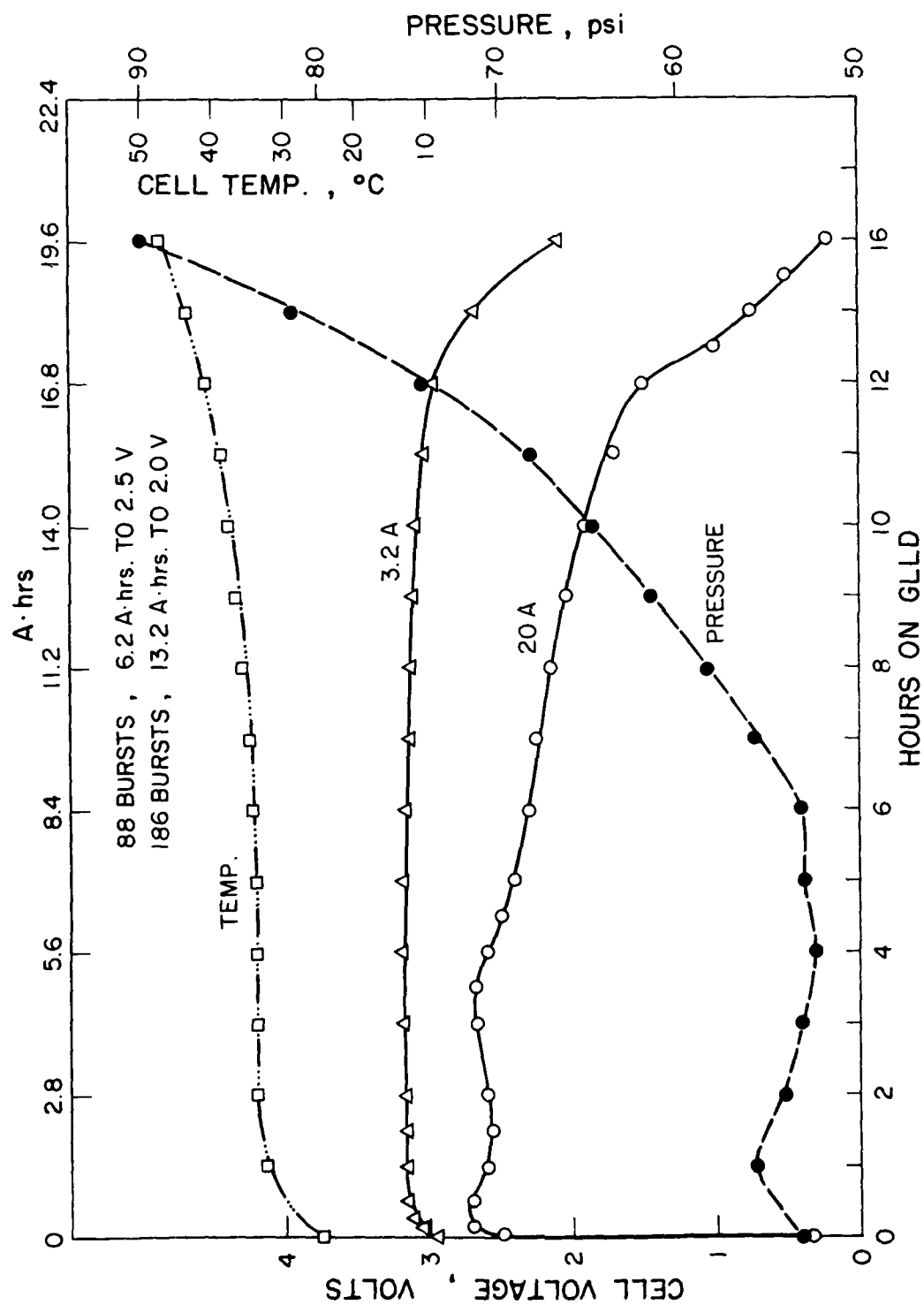


Figure 152. Performance of a flat cell on the new GLLD test at room temperature after 5 days at 72°C.

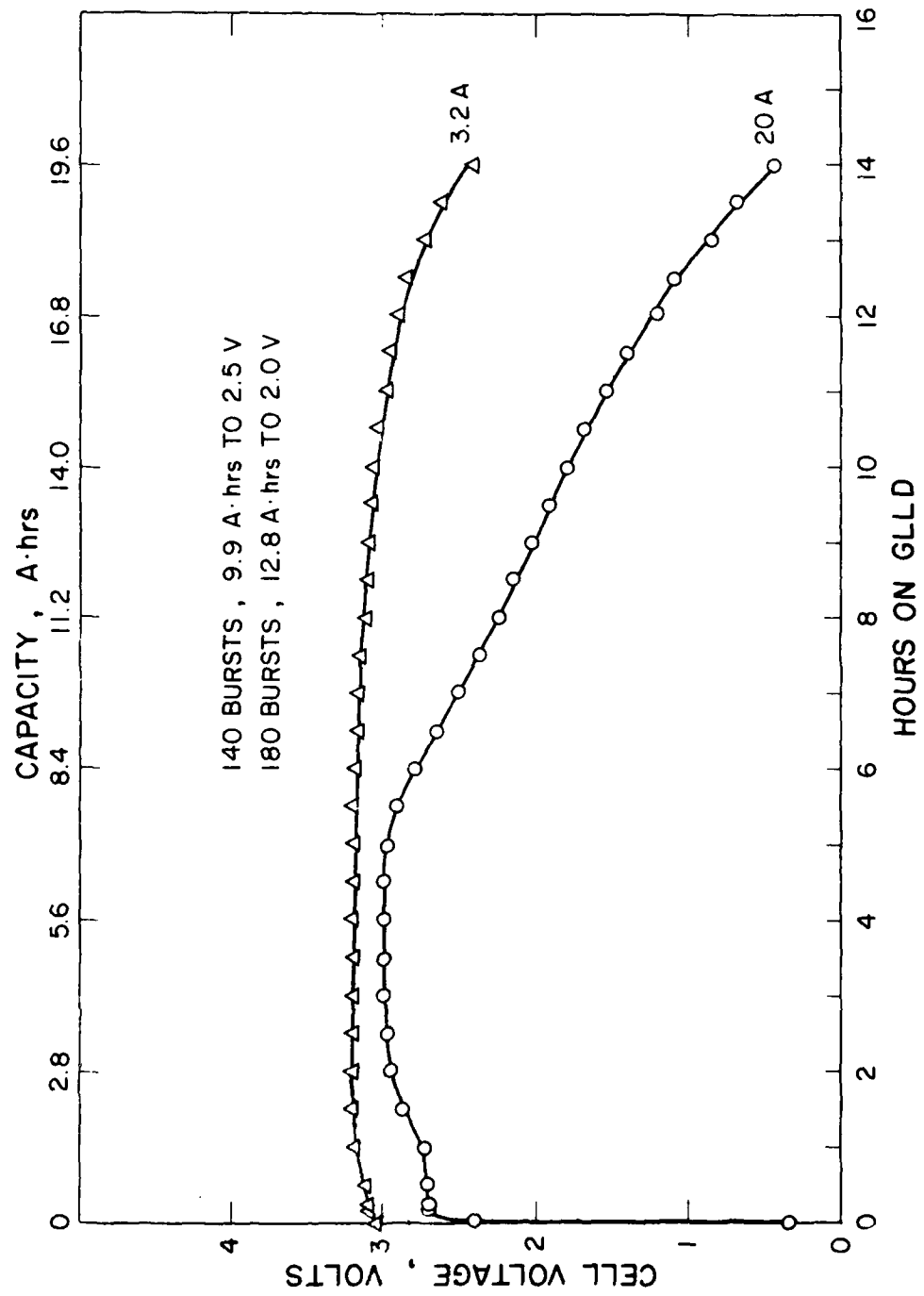


Figure 153. Performance of a flat cell on the new GLLD test at room temperature after 5 days at 72°C.

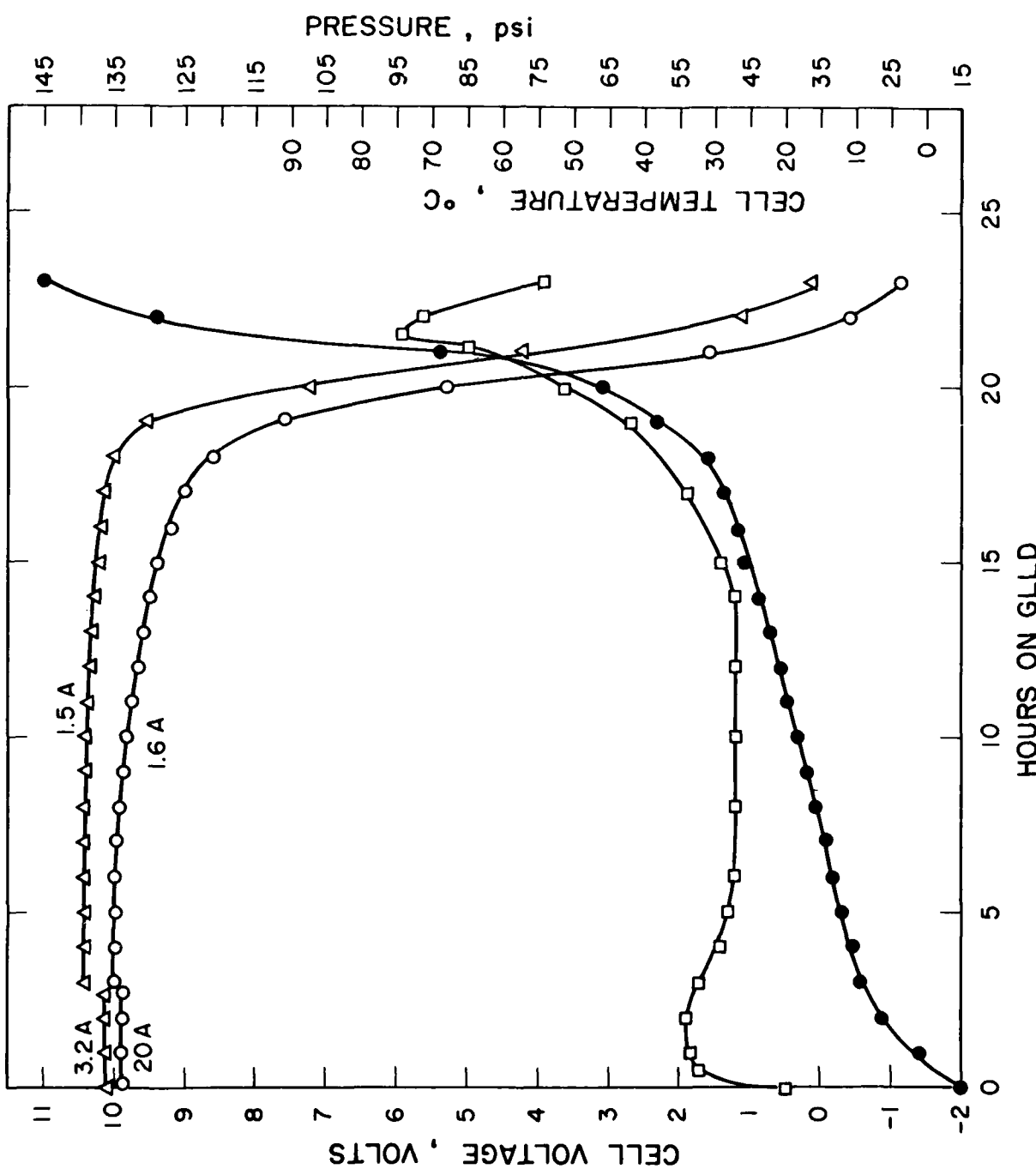


Figure 154. Performance of a three cell stack on the new GLLD cycle at 25°C.

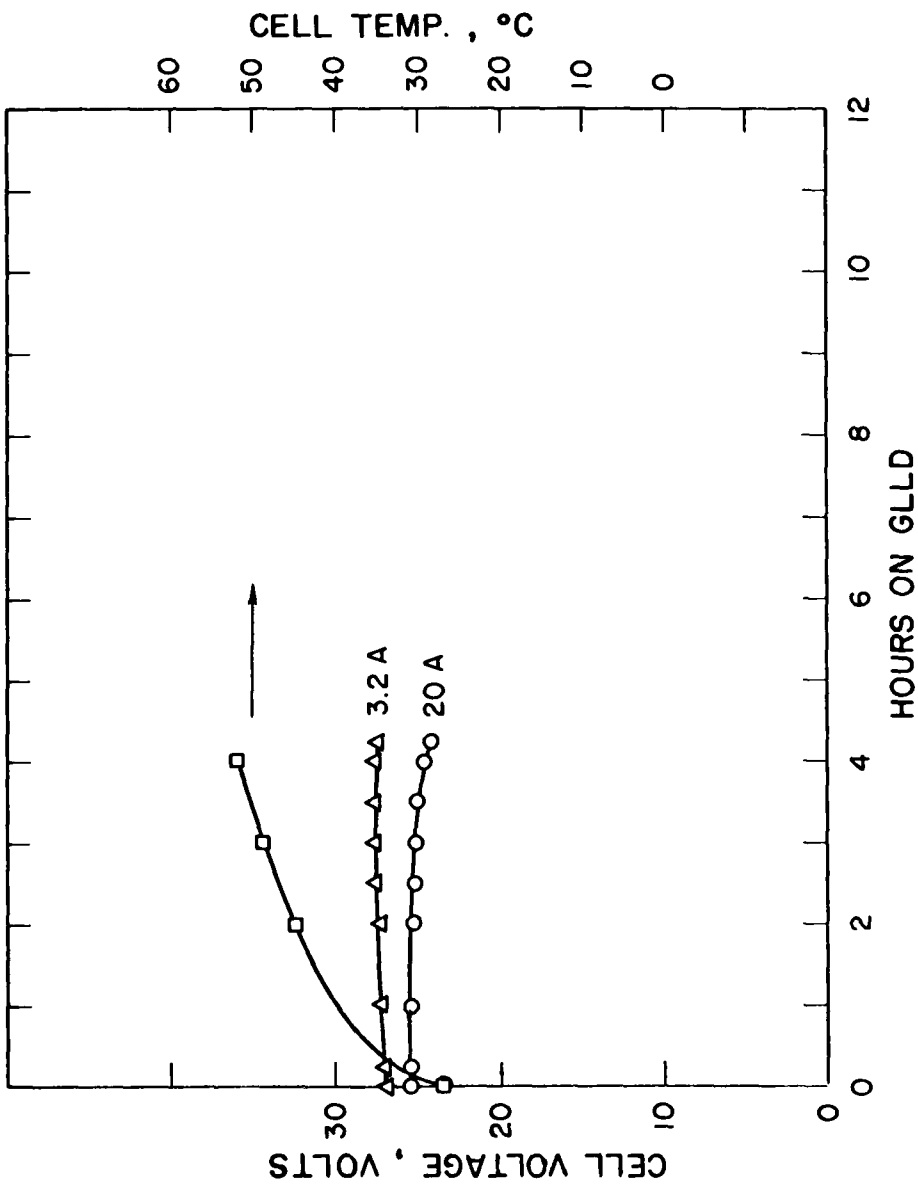


Figure 155. Performance of an 8 cell GLLD battery on the new GLLD duty cycle at 25°C.

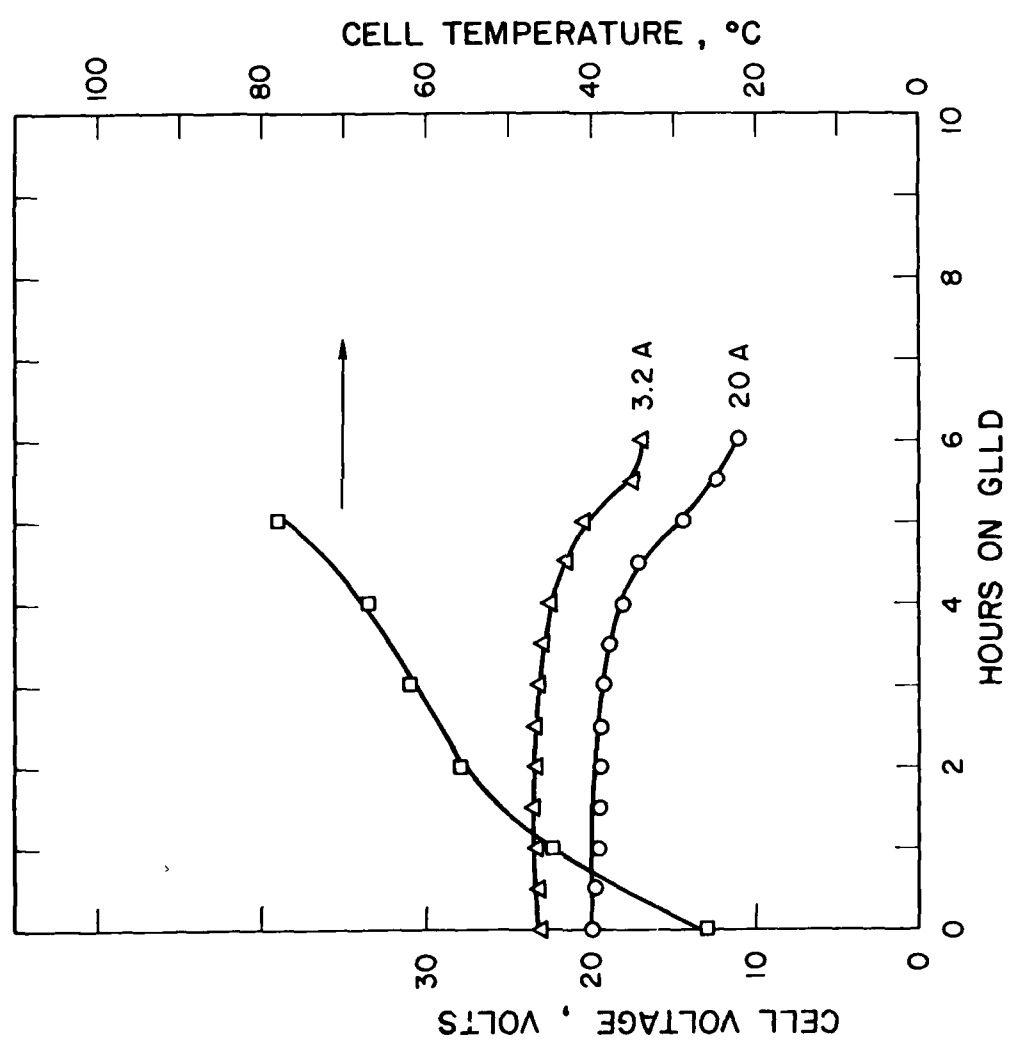


Figure 156. Performance of a 7 cell battery on the GLLD test at 25°C.

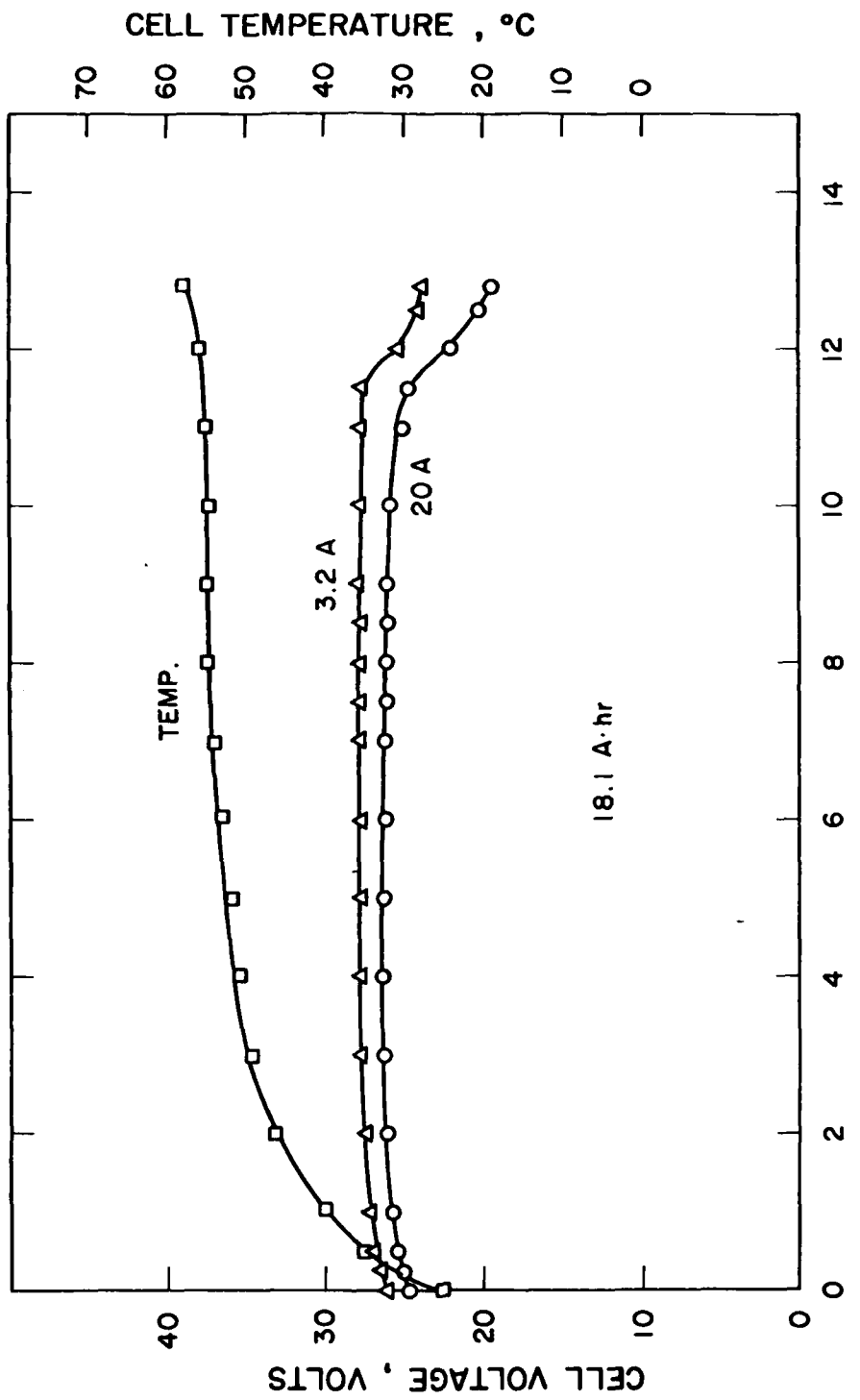


Figure 157. Performance of a GLLD battery on the GLLD test load at 25°C.

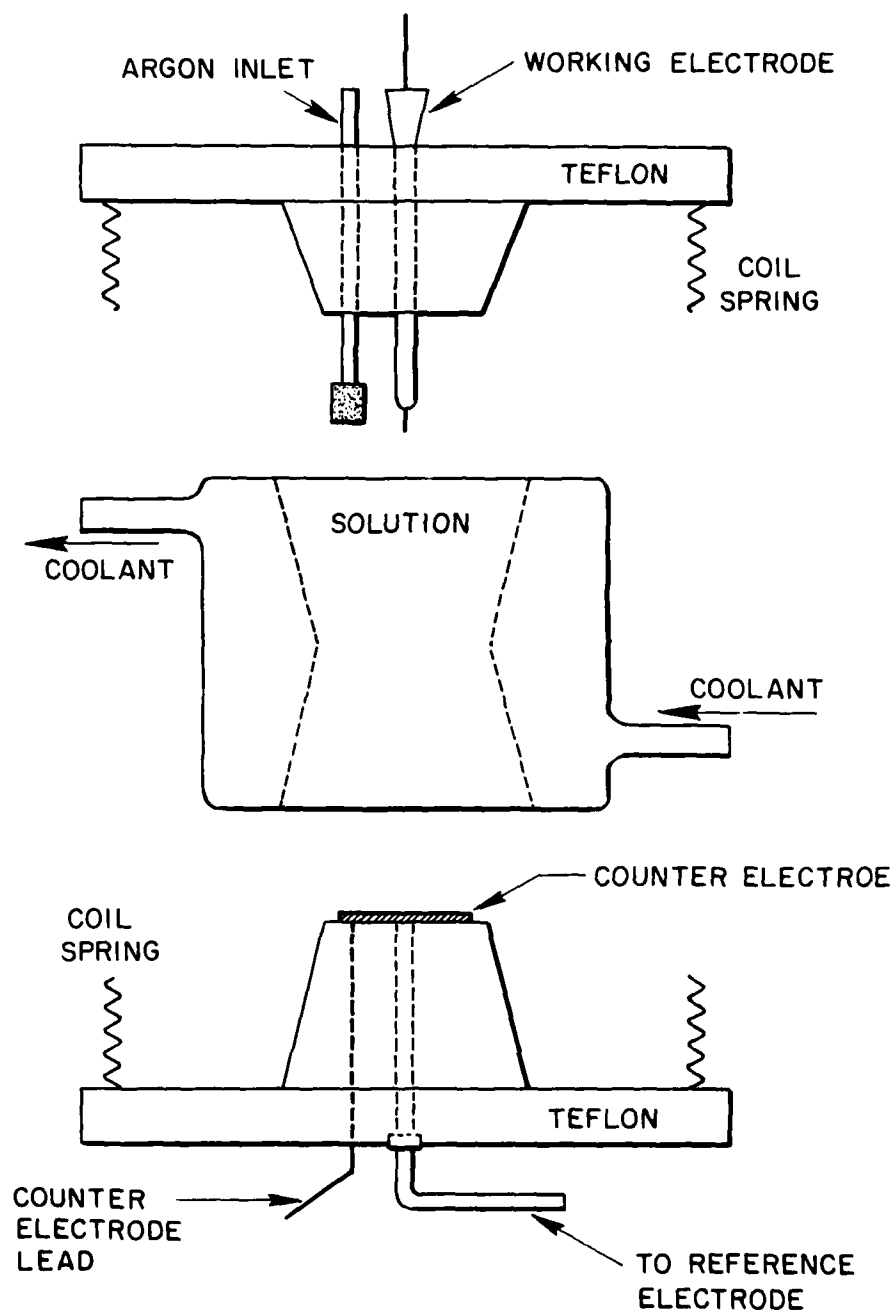


Figure 158. Schematic drawing of the jacketed cell used for cyclic voltammetry at various temperatures.

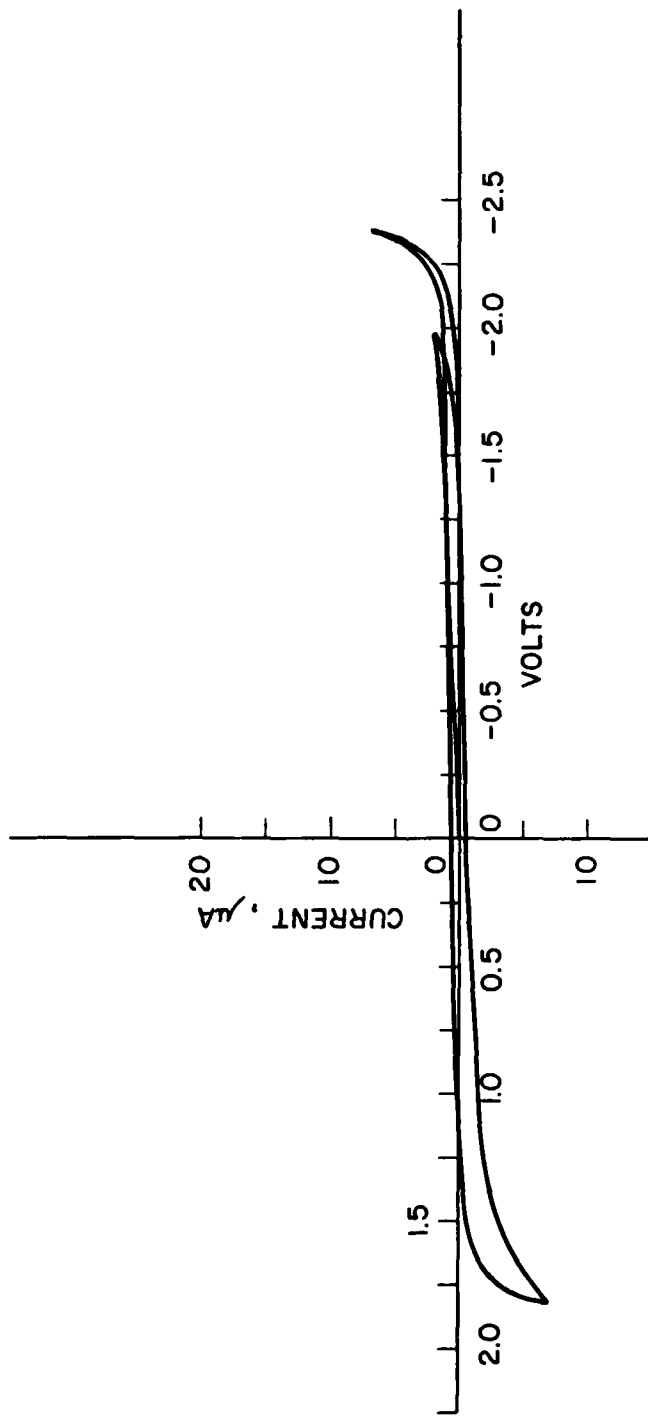


Figure 159. Cyclic voltammograms of tetrabutyl ammonium hexafluorophosphate solution in acetonitrile on Pt electrode, background, scan rate 200 mv/sec.

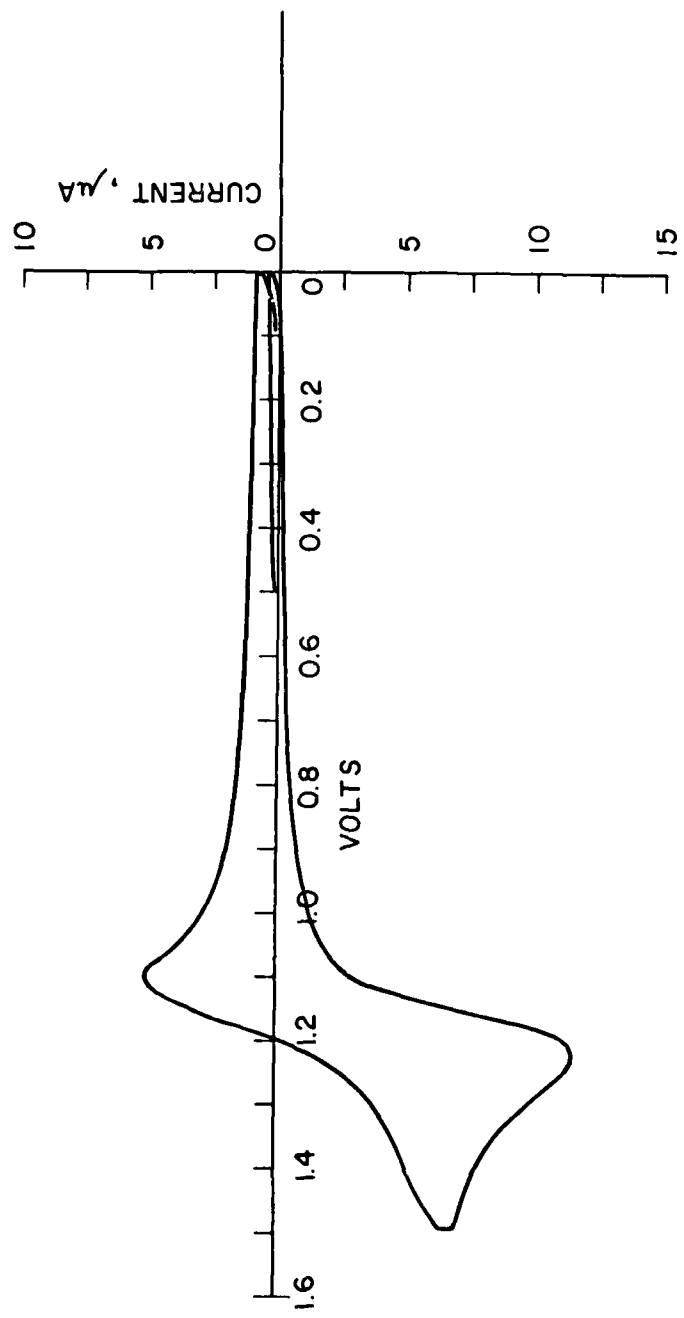


Figure 160. Cyclic voltammogram of tetramethyl ammonium chloride in acetonitrile/tetrabutyl ammonium hexafluorophosphate, scan rate 200 mv/sec.

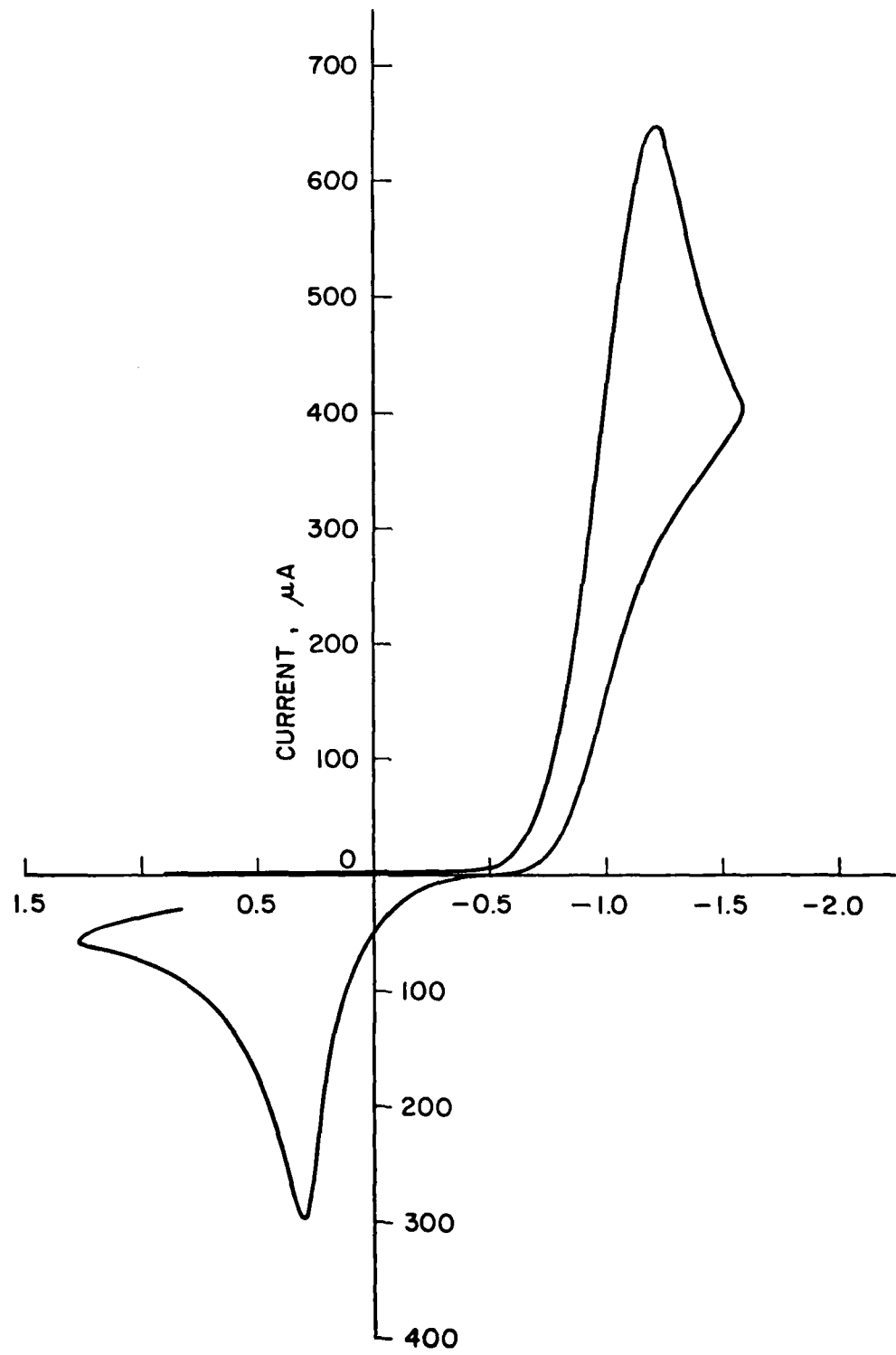


Figure 161. Cyclic voltammogram of  $\text{SO}_2$  in acetonitrile/tetrabutyl ammonium hexafluorophosphate,  
scan rate 1v/sec.

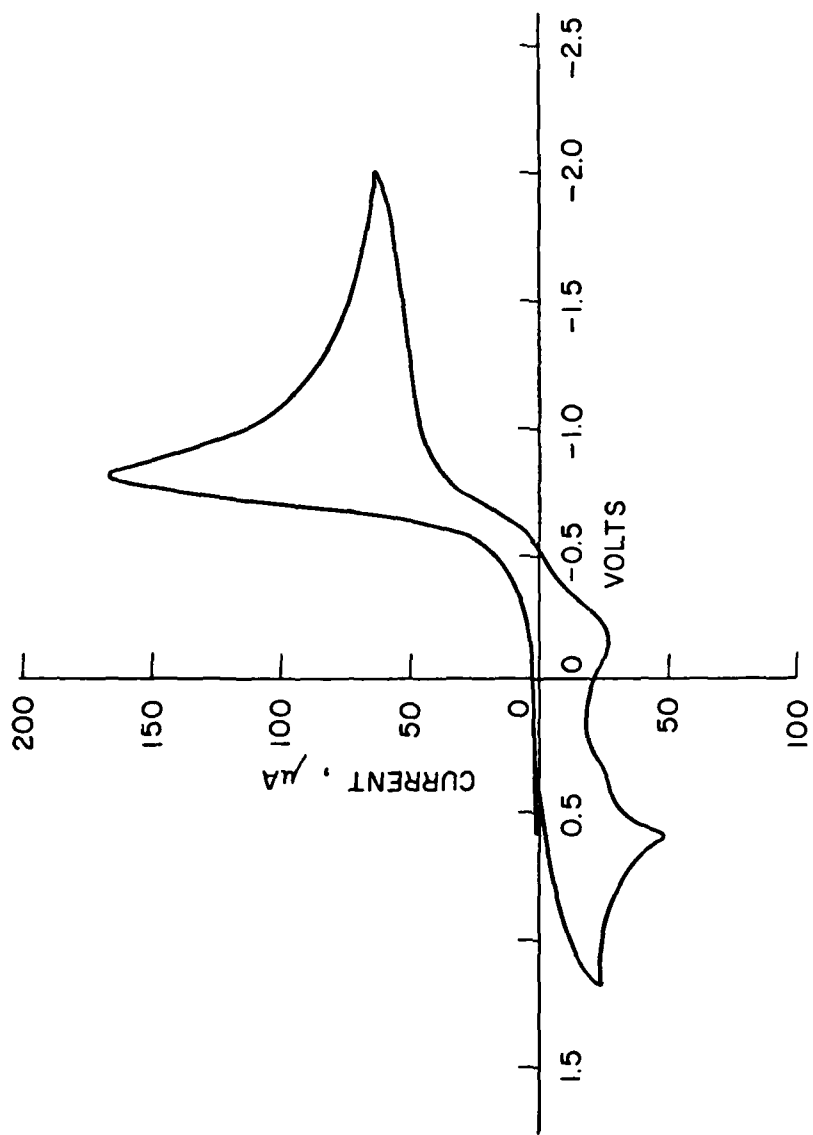


Figure 162. Cyclic voltammogram of  $\text{SO}_2$  in dimethyl formamide (DMF)/tetrabutyl ammonium hexafluorophosphate; scan rate 200 mv/sec.

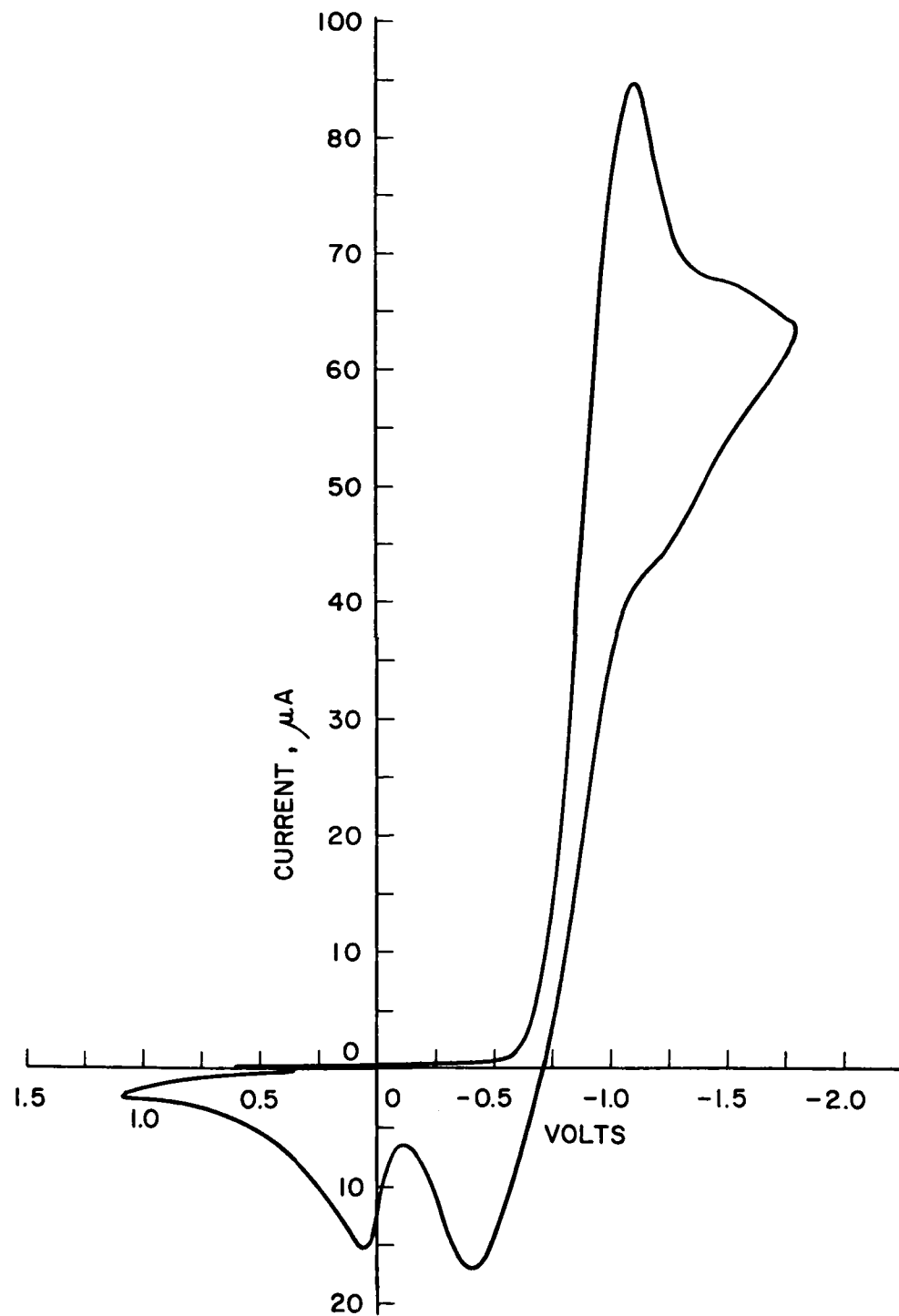


Figure 163. Cyclic voltammogram of  $\text{SO}_2$  in methylene chloride/tetra-butyl ammonium hexafluorophosphate ( $\text{TBAPF}_6$ ), scan rate 100 mv/sec.

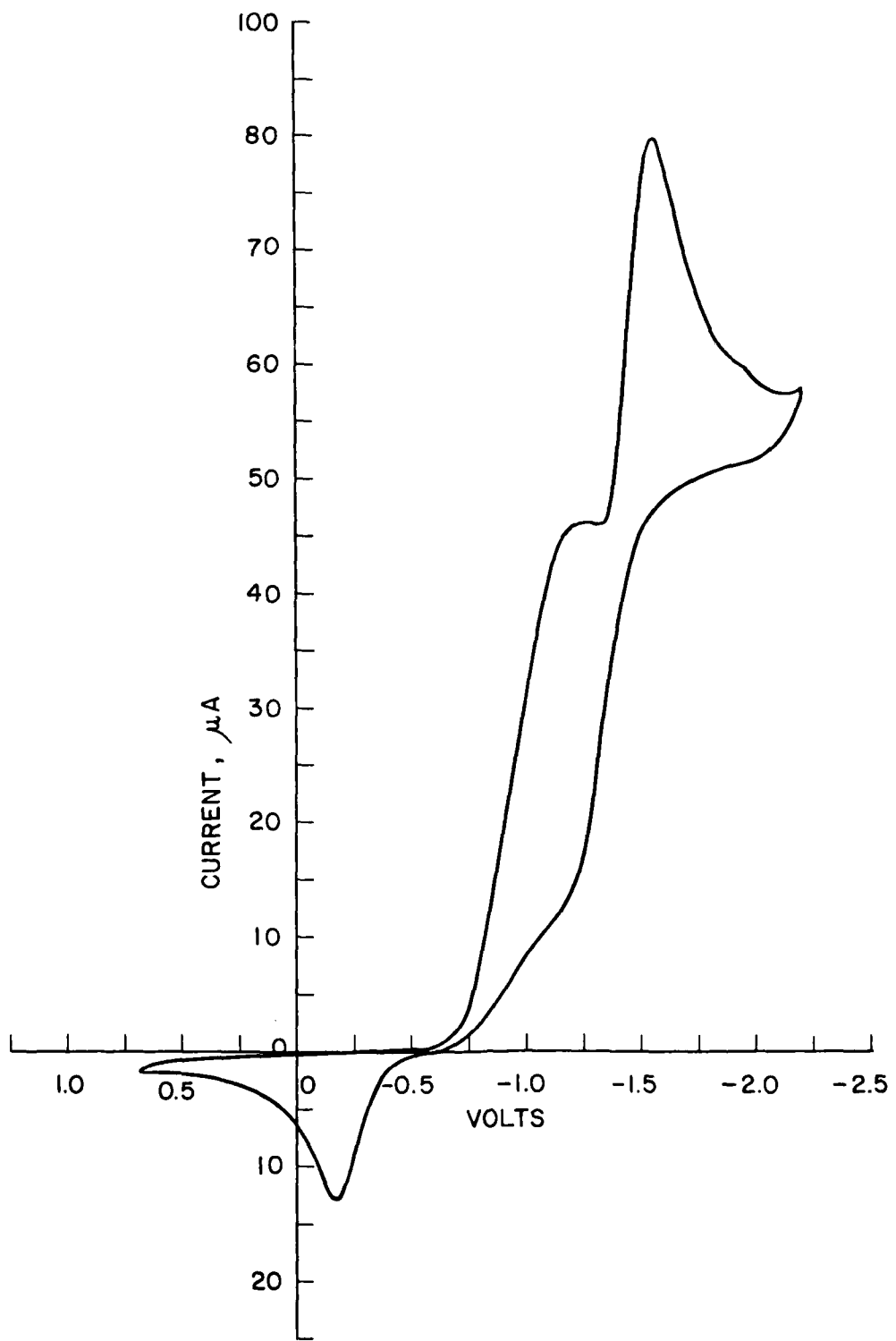


Figure 164. Cyclic voltammogram of S in methylene chloride/TBAPF<sub>6</sub>.  
scan rate 200 mv/sec.

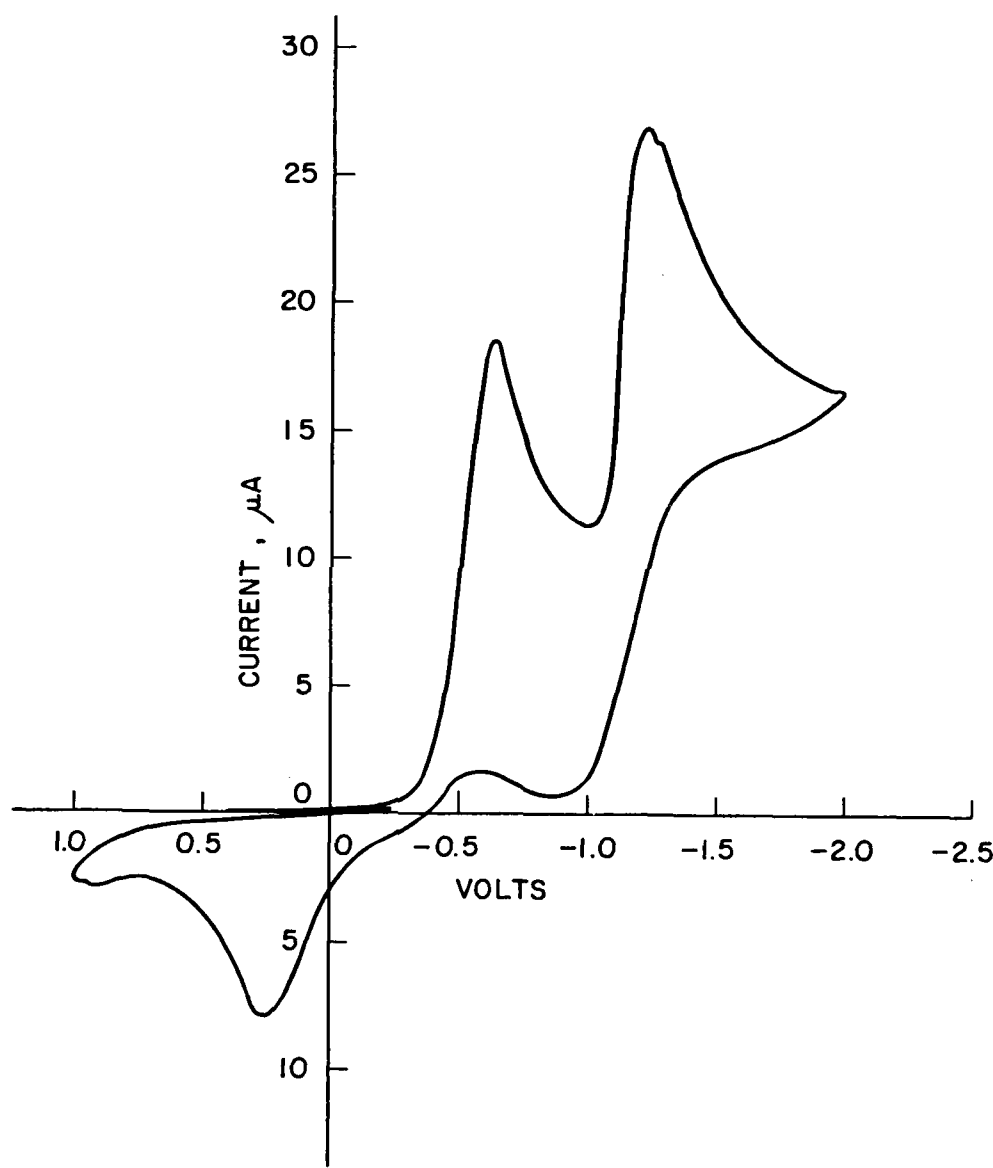


Figure 165. Cyclic voltammogram of S in DMF/TBAPF<sub>6</sub>, scan rate 500 mv/sec.

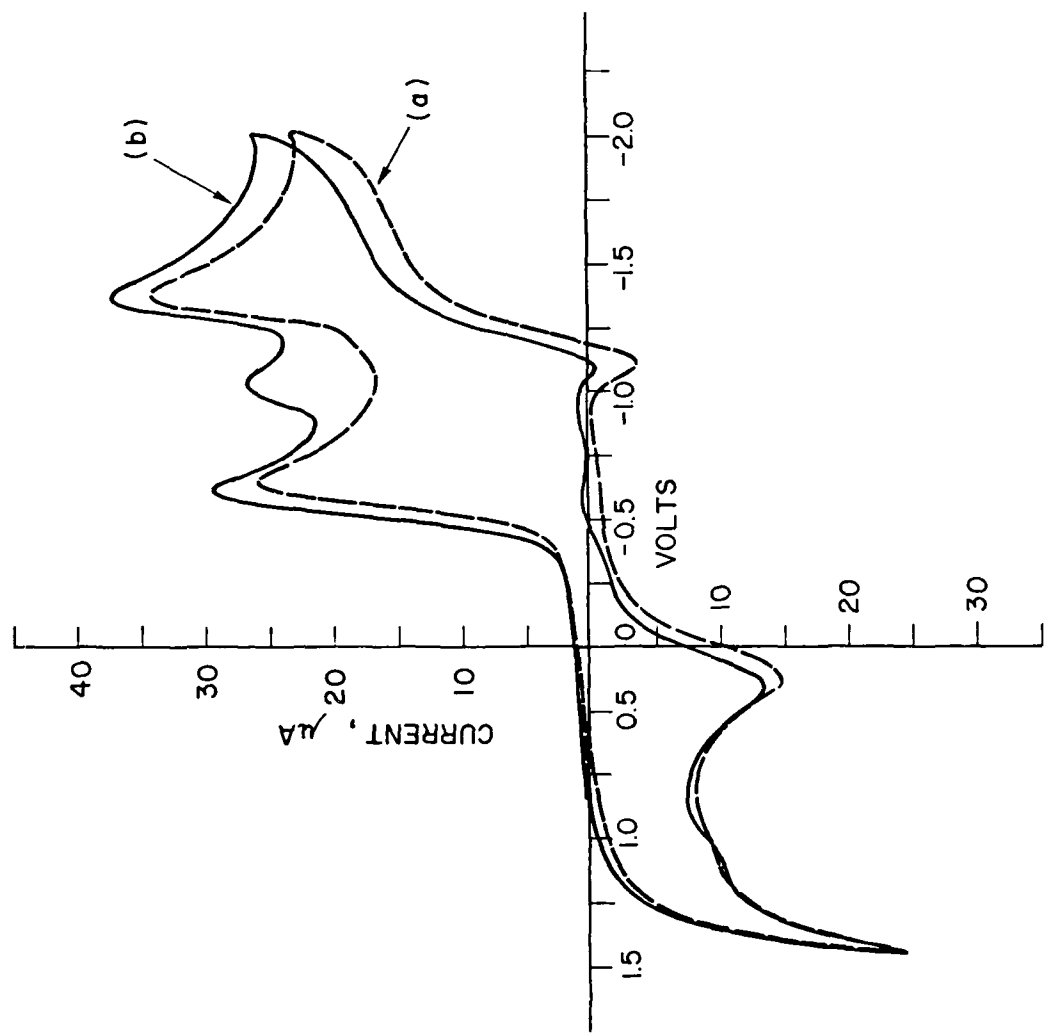


Figure 166. Cyclic voltammograms of (a) S trace  $\text{SO}_2$  in  $\text{DMF}/\text{TBAPF}_6$ , (b) S more  $\text{SO}_2$  in  $\text{DMF}/\text{TBAPF}_6$ , scan rate 200 mV/sec.

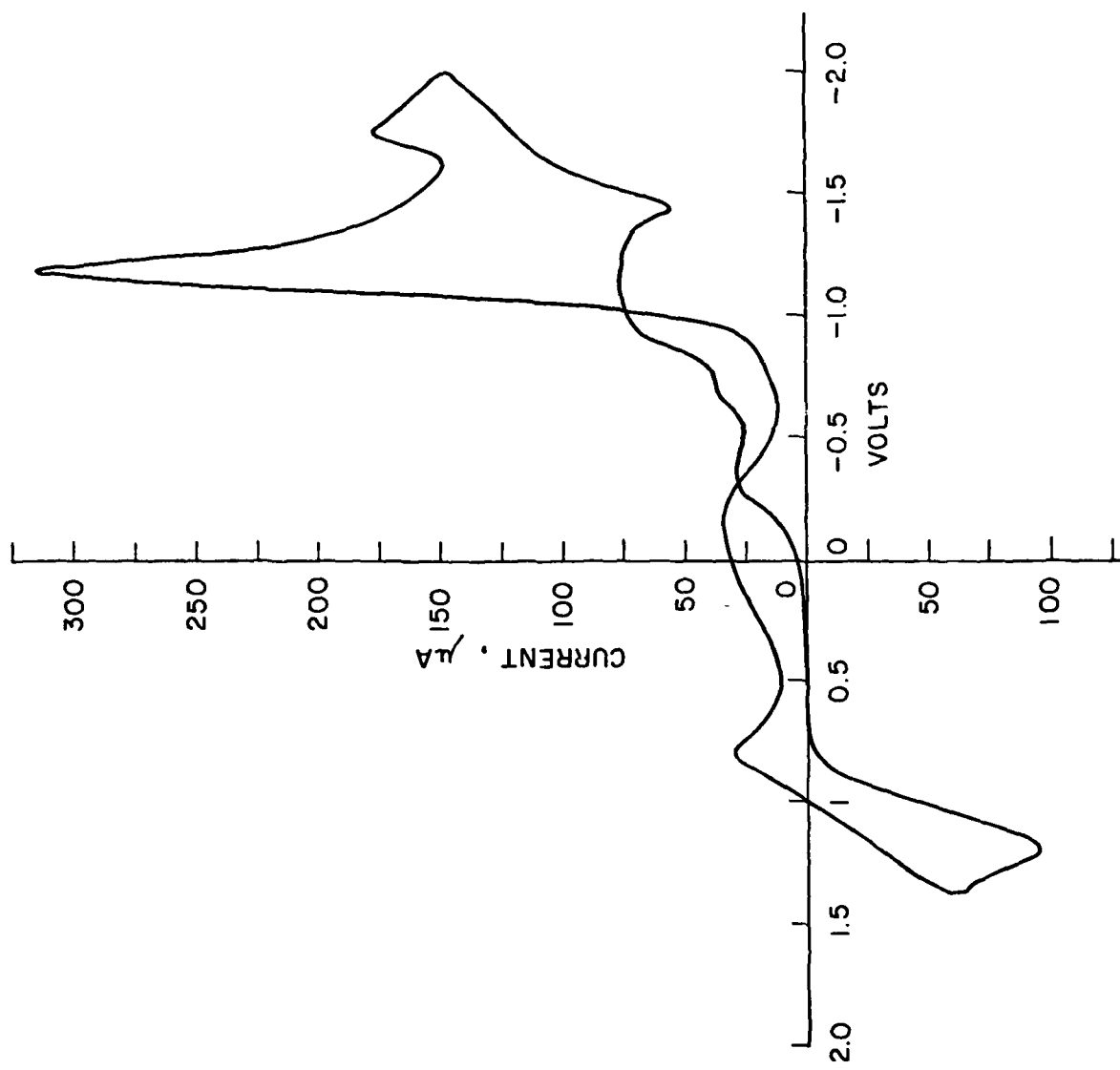


Figure 167. Cyclic voltammogram of  $S_2Cl_2$  in acetonitrile/TBAPF<sub>6</sub>, scan rate 500 mV/sec.

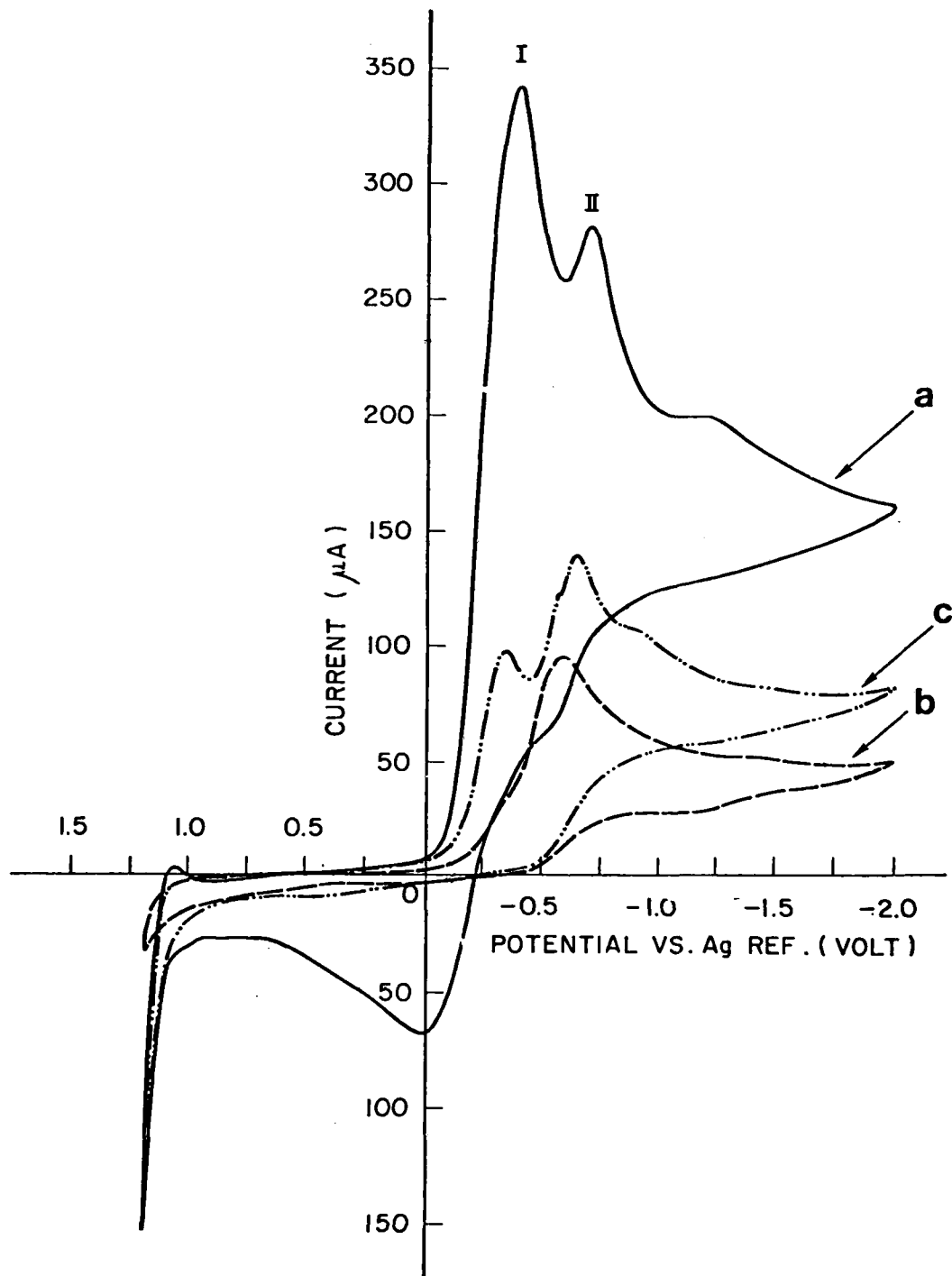


Figure 168. Cyclic voltammograms of  $\text{SOCl}_2$  in  $\text{DMF}/\text{TBAPF}_6$  (a) before the electrolysis, (b) immediately after the exhaustive electrolysis at  $-0.25\text{V}$  vs Ag wire reference, (c) after warming the electrolyzed solution; scan rate 200 mv/sec.

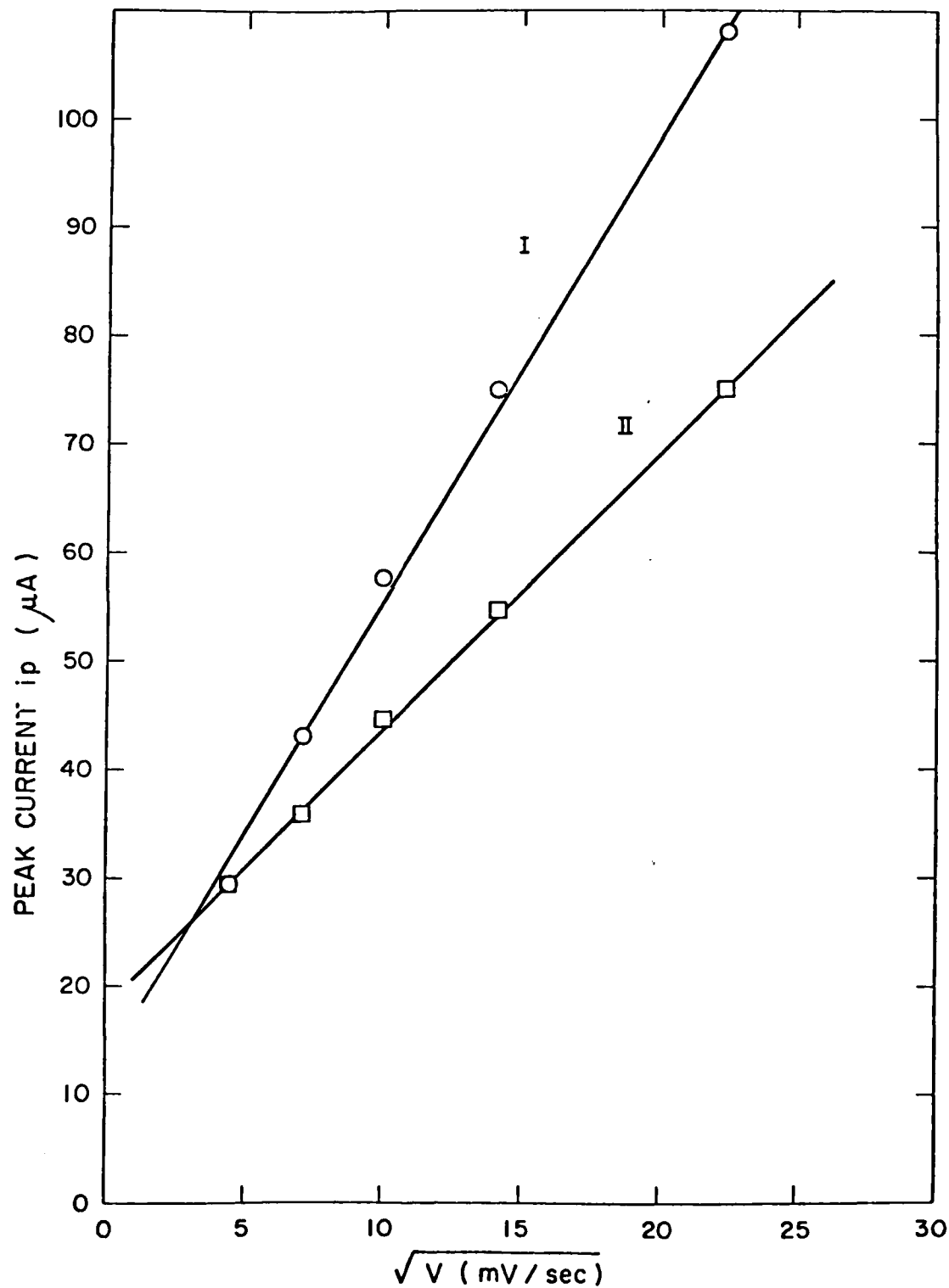
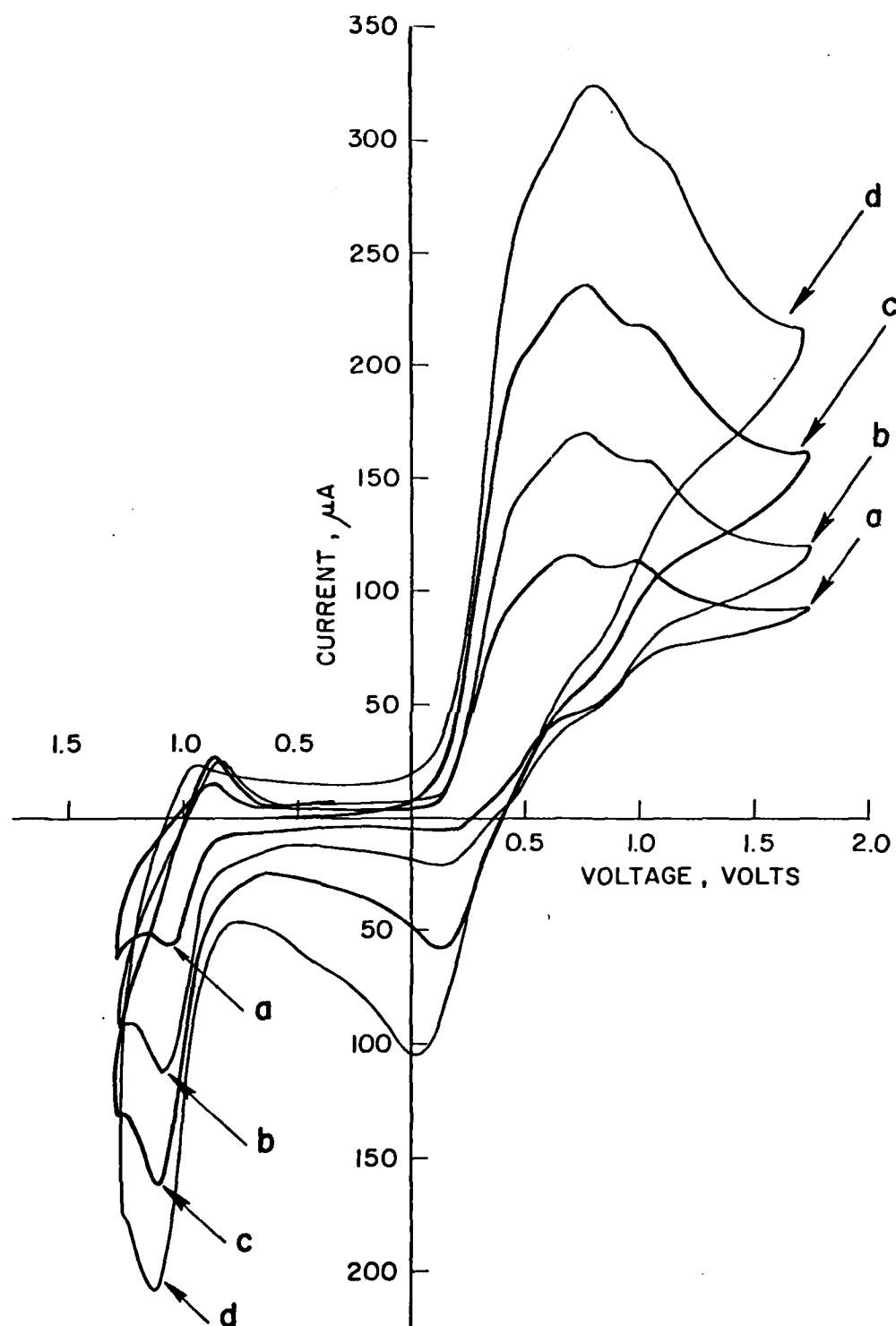
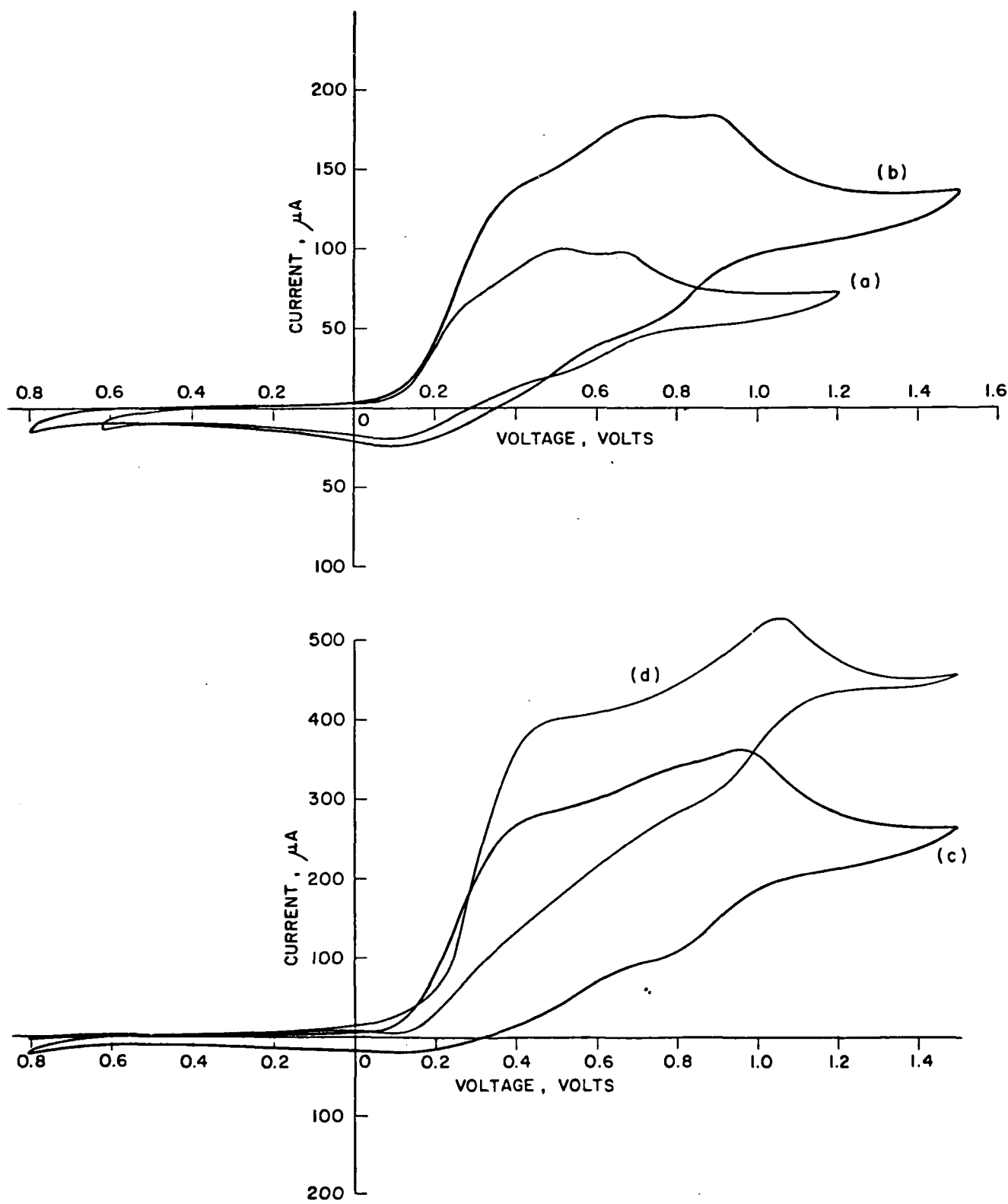


Figure 169. Plot of the peak currents versus the square root of the scan rate ( $V$ ) of the two reduction waves of  $\text{SOCl}_2$  in  $\text{DMF/TBAPF}_6$ .



**Figure 170.** Cyclic voltammogram of  $\text{SOCl}_2$  in  $\text{CH}_3\text{CH}/0.1\text{N N}(\text{C}_4\text{H}_9)_4 \text{PF}_6$  showing the effect of sweep rate at a Pt wire electrode  
 a) 0.20 V/sec b) 0.50 V/sec c) 1.0 V/sec d) 2.0 V/sec

Figure 171. Cyclic voltammograms of  $\text{SOCl}_2$  in  $\text{CH}_3\text{CN}/\text{N}(\text{C}_4\text{H}_9)_4\text{PF}_6$  at various concentrations a)  $25 \mu\text{l } \text{SOCl}_2/75 \text{ ml}$  ( $V 0.50 \text{ V/sec}$ ), b)  $50 \mu\text{l } \text{SOCl}_2/75 \text{ ml}$  ( $V 0.050 \text{ V/sec}$ ), c)  $100 \mu\text{l } \text{SOCl}_2/75 \text{ ml}$  ( $V 0.20 \text{ V/sec}$ ), d)  $200 \mu\text{l } \text{SCCl}_2/75 \text{ ml}$  ( $V 0.20 \text{ V/sec}$ ).



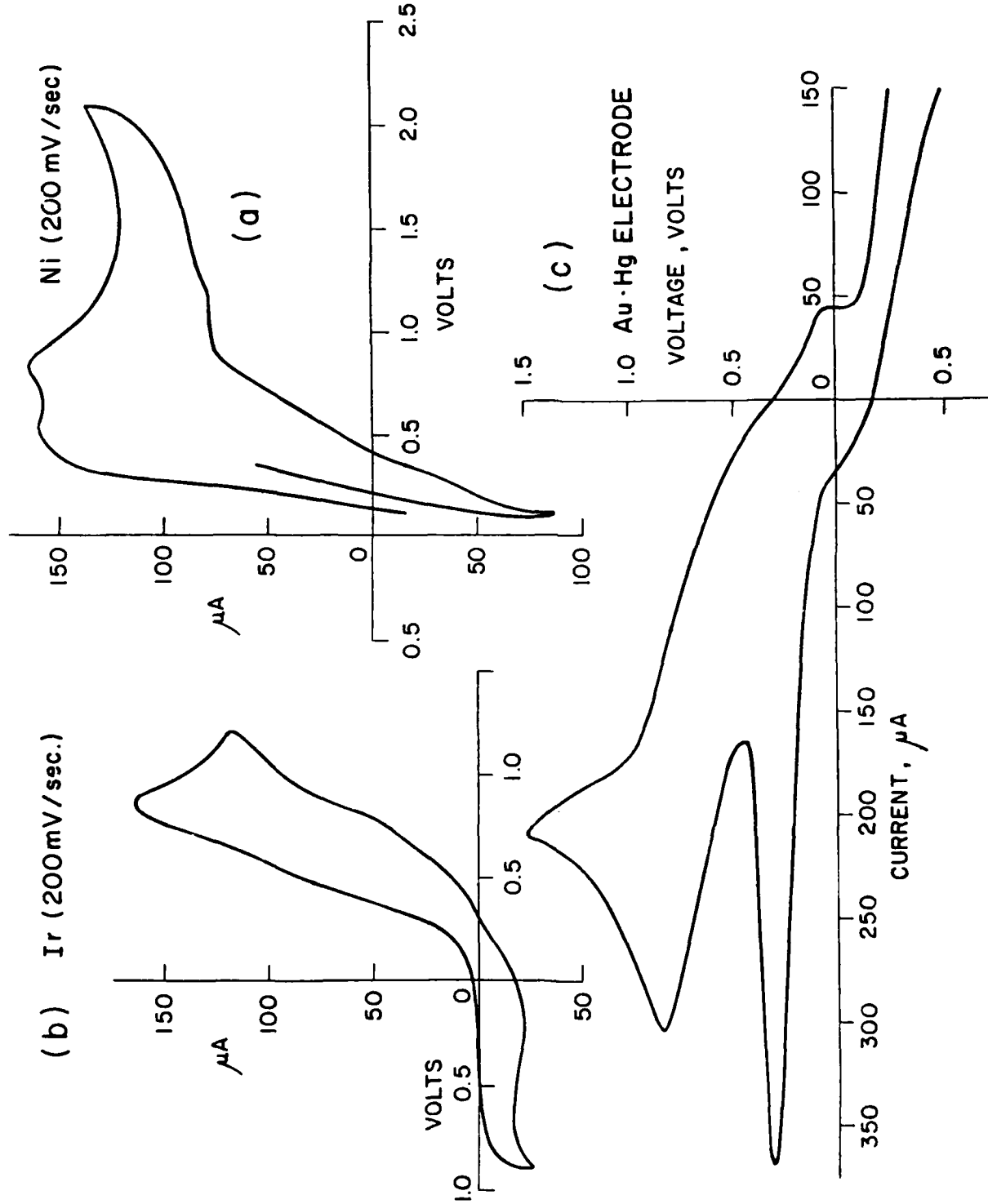


Figure 172. Cyclic voltammograms of  $\text{SOCl}_2$  in  $\text{CH}_3\text{CN}/0.1\text{N}(\text{C}_4\text{H}_9)_4\text{PF}_6$  a) Ni wire electrode,  
b) I<sub>f</sub> wire electrode, c) Au-Hg wire electrode ( $V = .20\text{V/sec}$  in all).

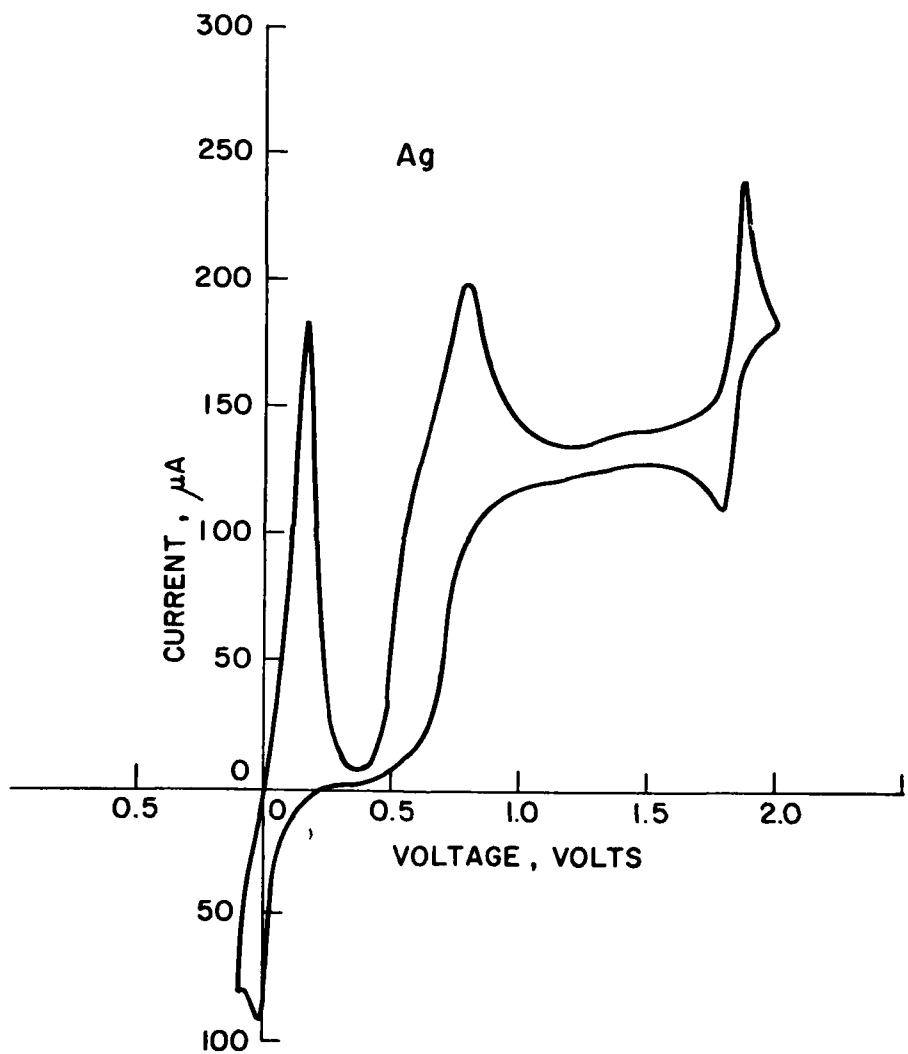


Figure 173. Cyclic voltammogram of  $\text{SOCl}_2$  in  $\text{CH}_3\text{CN}/0.1\text{N } \text{N}(\text{C}_4\text{H}_9)\text{PF}_6$  at a silver wire electrode (0.05V/sec).

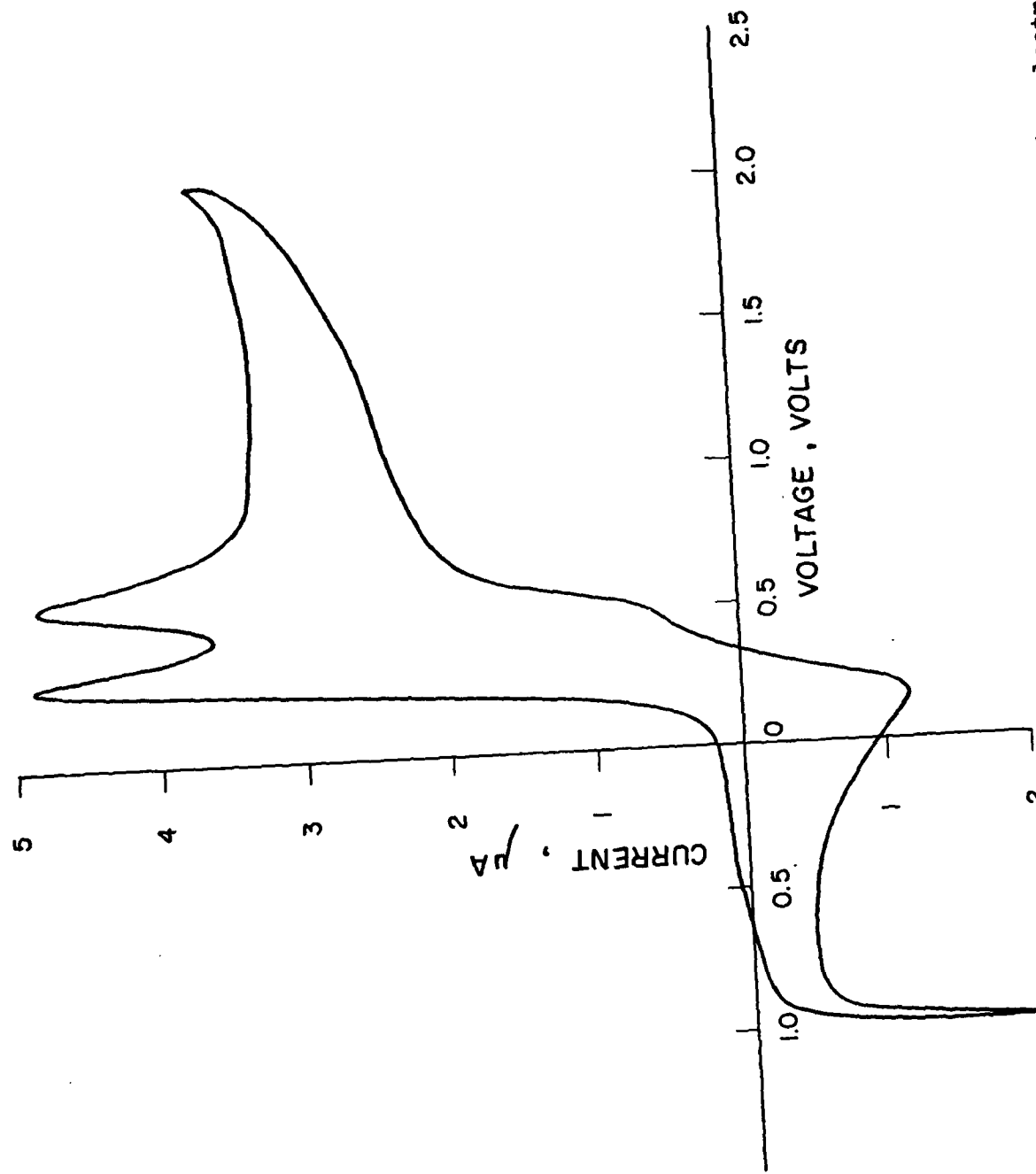


Figure 174. Cyclic voltammogram of  $\text{SOCl}_2$  in  $\text{DMSO}/0.1\text{N } \text{N}(\text{C}_4\text{H}_9)_4 \text{PF}_6$  at a platinum wire electrode  
(0.05 V/sec)

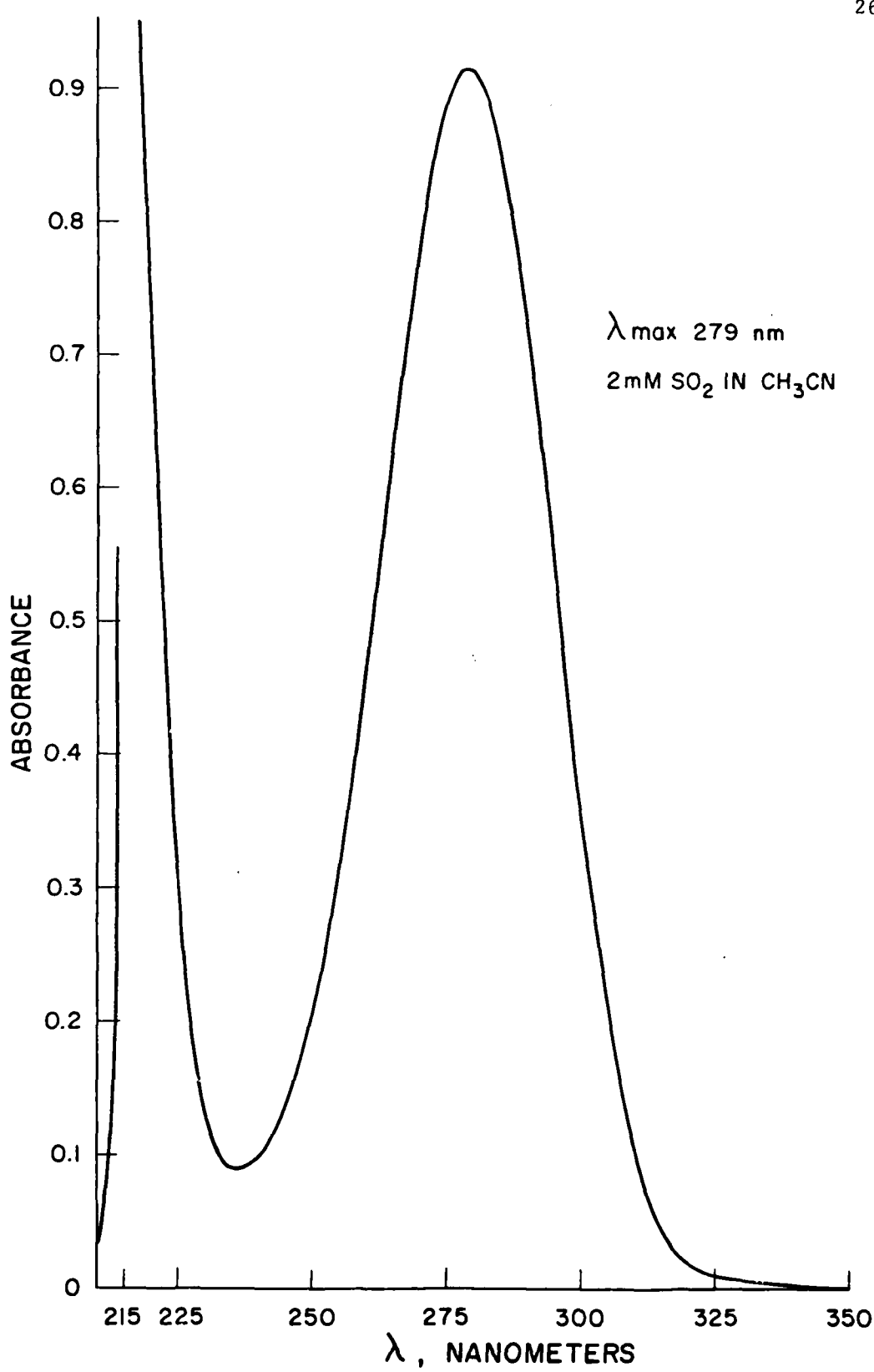


Figure 175. UV-VIS spectrum of 2mM  $\text{SO}_2$  in  $\text{CH}_3\text{CN}$  vs  $\text{CH}_3\text{CN}$  (pathlength 1 cm)

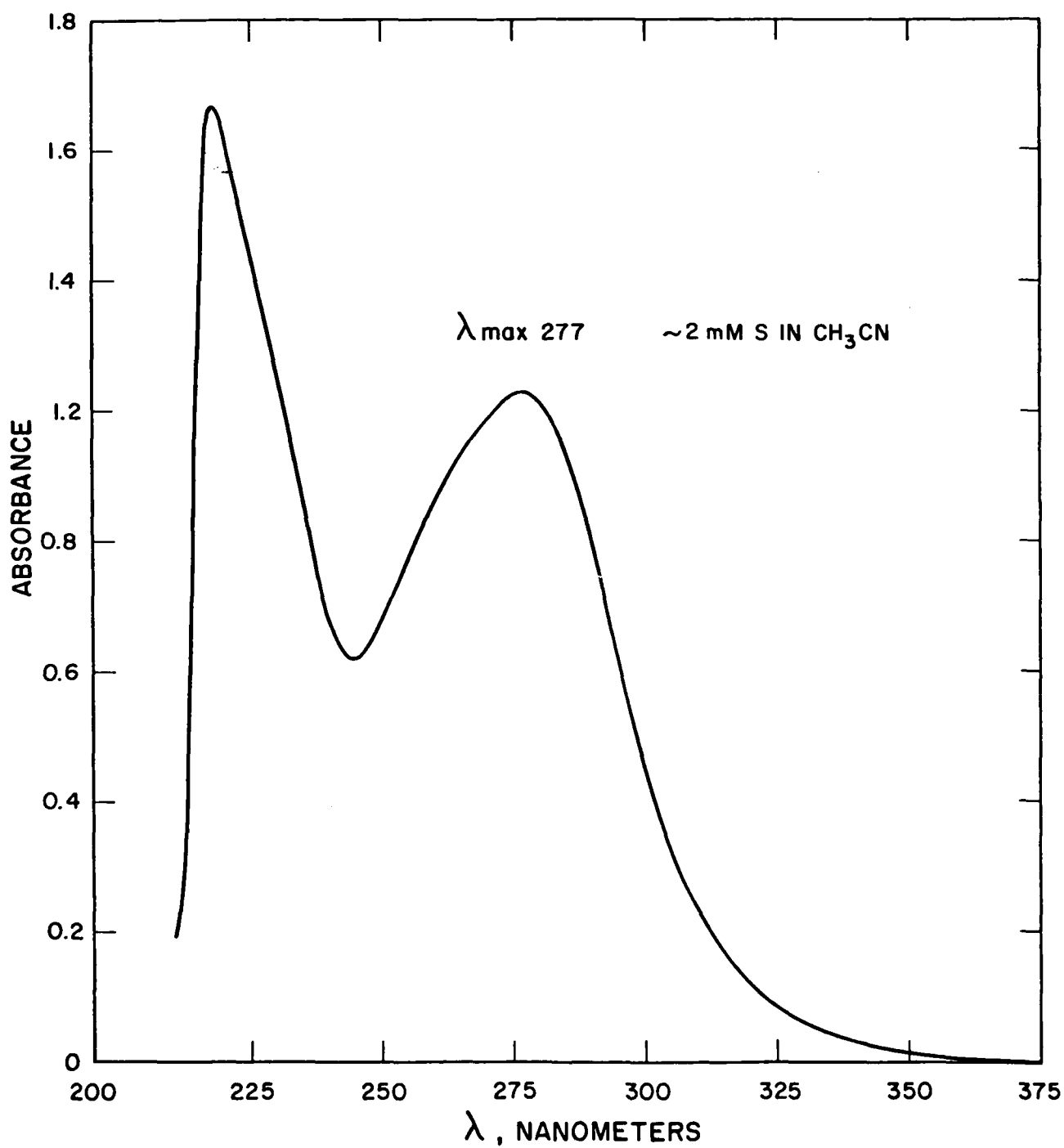


Figure 176. UV-VIS spectrum of 2mM S in  $\text{CH}_3\text{CN}$  vs  $\text{CH}_3\text{CN}$  (pathlength 1 cm).

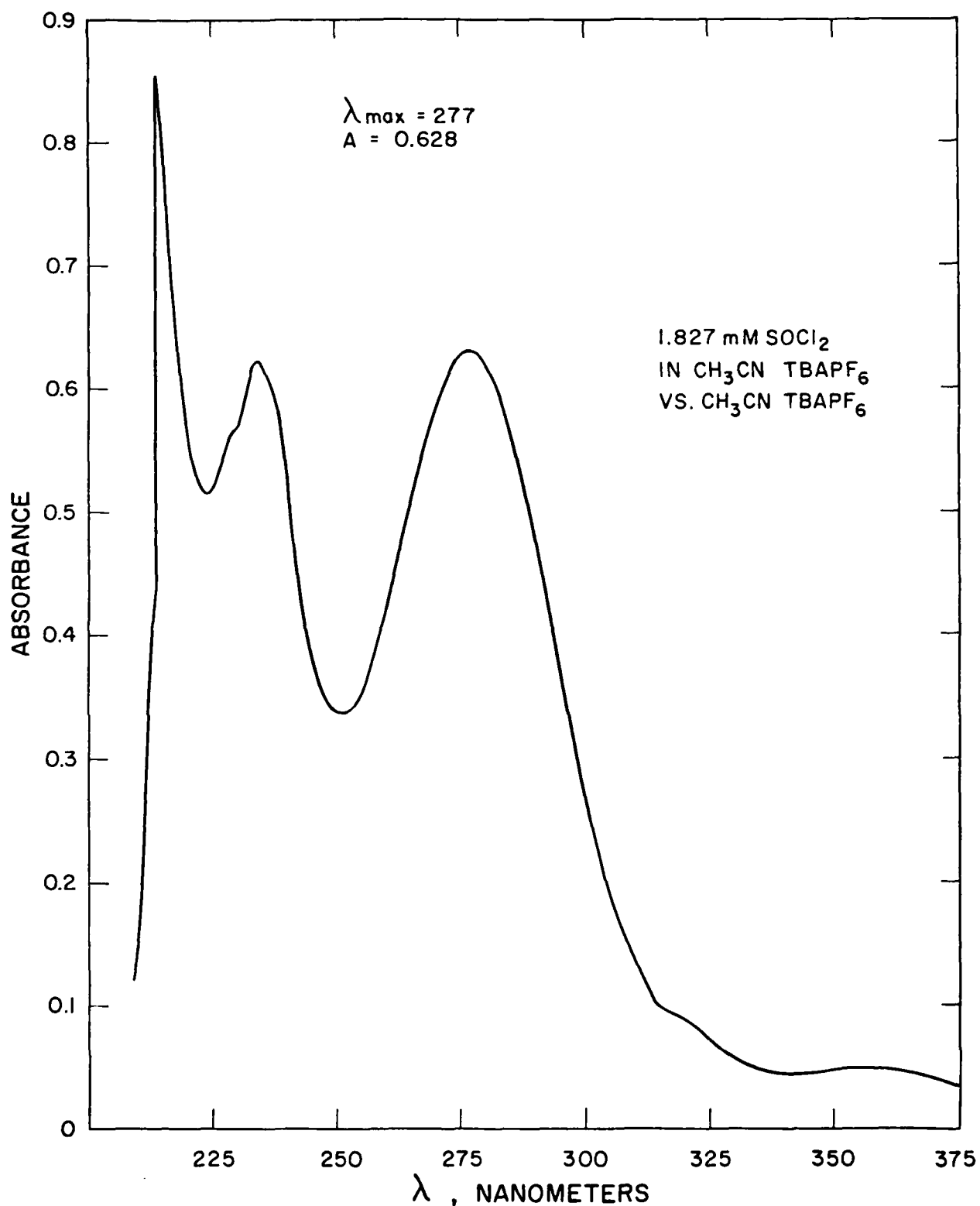
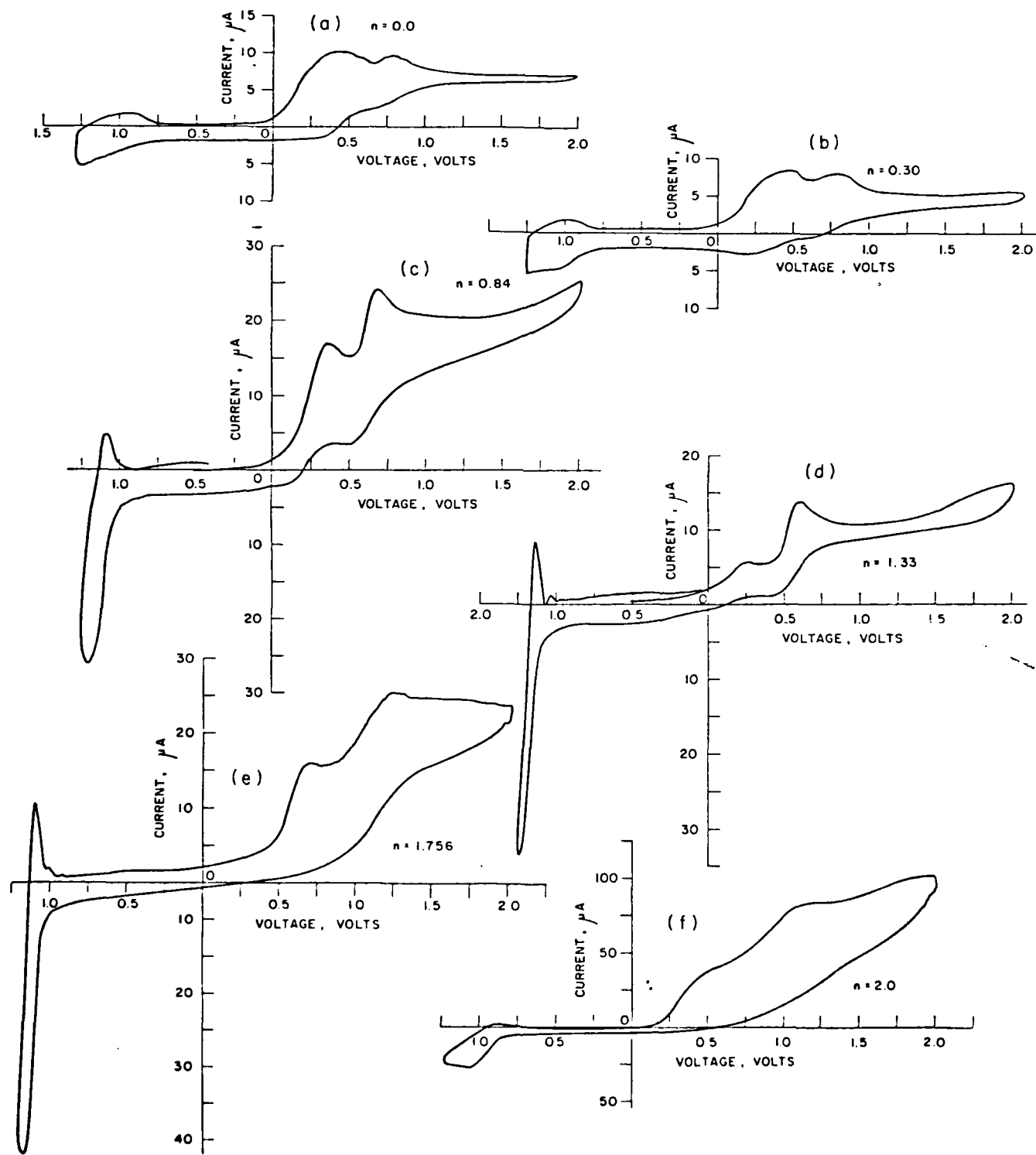
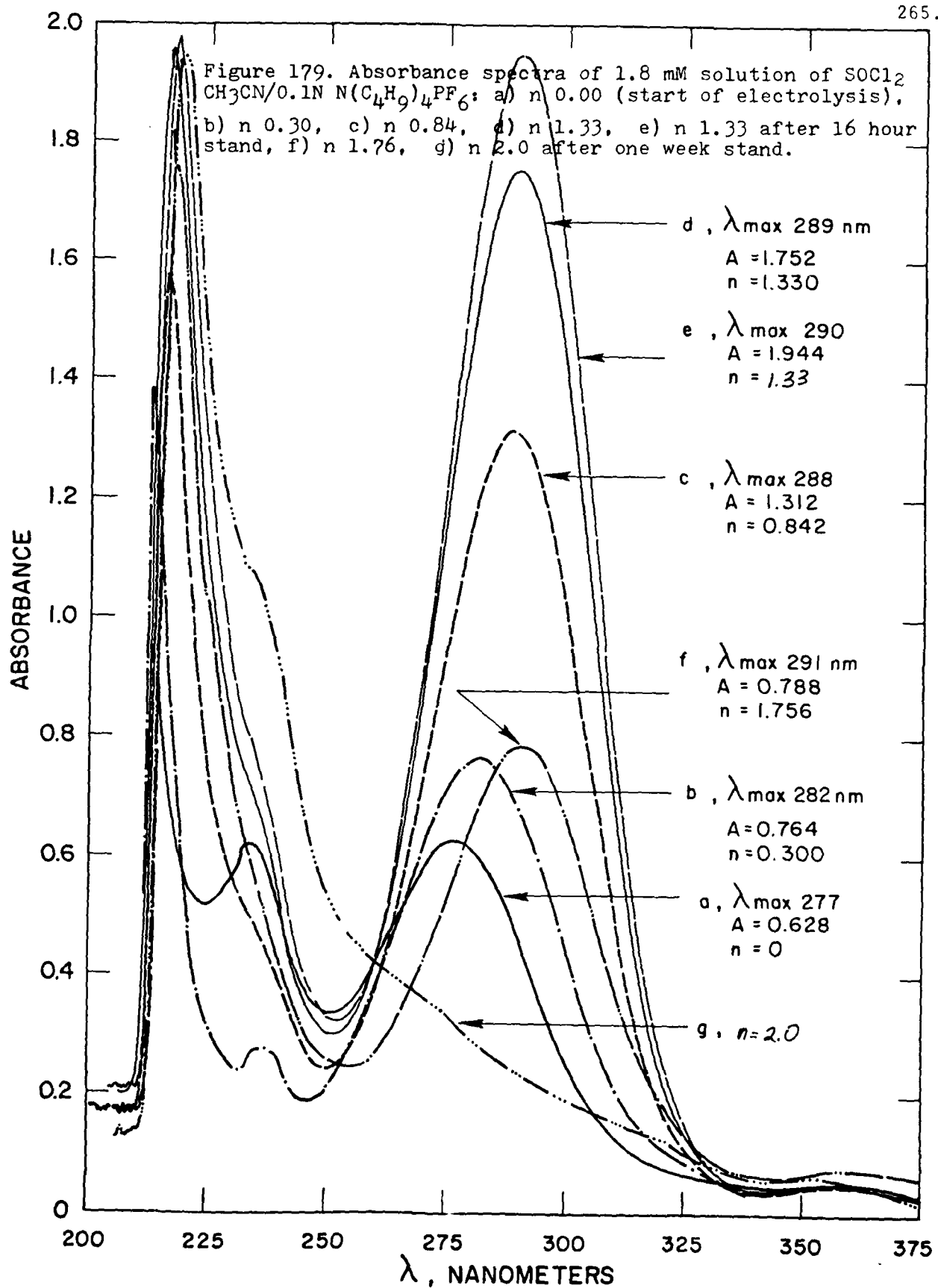


Figure 177. UV-VIS spectrum of 1.8 mM  $\text{SOCl}_2$  in  $\text{CH}_3\text{CN}/0.1\text{N N}(\text{C}_4\text{H}_9)_4 \text{PF}_6$  vs  $\text{CH}_3\text{CN}/0.1\text{N N}(\text{C}_4\text{H}_9)_4 \text{PF}_6$  in a 1 cm pathlength cell.

Figure 178. Cyclic voltammogram of 1.8 mM  $\text{SOCl}_2$  in  $\text{CH}_3\text{CN}/0.1\text{N N}(\text{C}_4\text{H}_9)_4\text{PF}_6$  264.  
 a)  $n = 0.00$ , b)  $n = 0.300$ , c)  $n = 0.84$ , d)  $n = 1.33$ , e)  $n = 1.76$ ,  
 f)  $n = 2.0$  after one week stand.





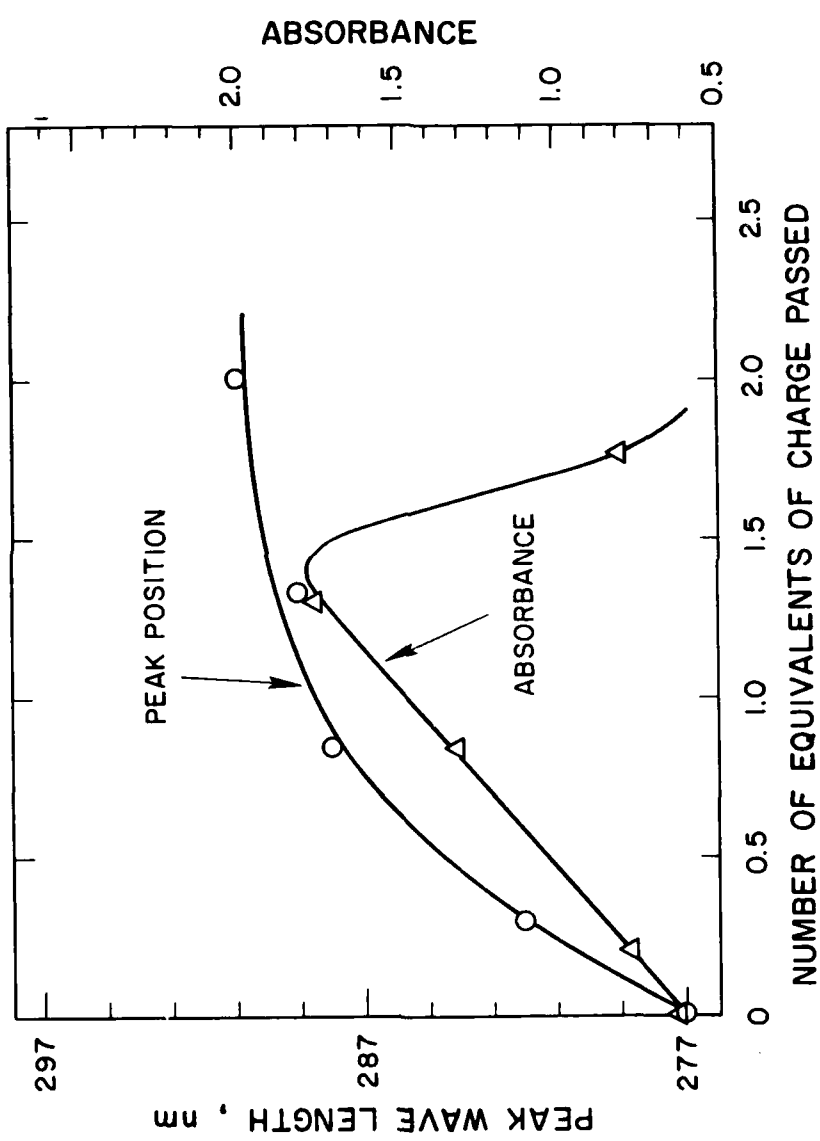


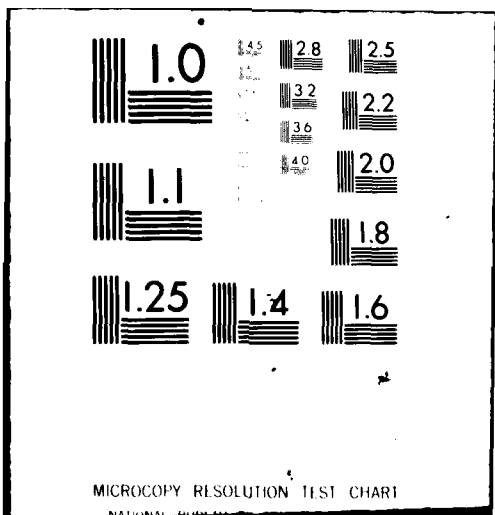
Figure 180. Variation of max and absorbance of  $\text{SOCl}_2$  solution as a function of charge passed during electrolysis.

AD-A098 727 DURACELL INTERNATIONAL INC BURLINGTON MA LAB FOR PHYS--ETC F/6 10/3  
LITHIUM-THIONYL CHLORIDE BATTERY. (U)  
APR 81 D WONG, W BOWDEN, N HAMILTON DAAB07-78-C-0563  
UNCLASSIFIED DELET-TR-78-0563-F NL

4 x 4  
AD 4  
APR 1981



END  
DATE  
FILED  
9-81  
DTIC



13 November 1978

ELECTRONICS TECHNOLOGY AND DEVICES LABORATORY

MANDATORY CONTRACT DISTRIBUTION LIST

101	Defense Technical Information Center ATTN: DTIC-TCA Cameron Station (Bldg 5) Alexandria, VA 22314	579	Cdr, PM Concept Analysis Centers ATTN: DRCPM-CAC Arlington Hall Station Arlington, VA 22212
012		001	
203	GIDEP Engineering & Support Dept TE Section PO Box 398 001 NORCO, CA 91760	602	Cdr, Night Vision & Electro-Optics ERADCOM ATTN: DELNV-D Fort Belvoir, VA 22060
001		001	
205	Director Naval Research Laboratory ATTN: CODE 2627 001 Washington, DC 20375	603	Cdr, Atmospheric Sciences Lab ERADCOM ATTN: DELAS-SY-S White Sands Missile Range, NM 88002
001		001	
301	Rome Air Development Center ATTN: Documents Library (TILD) 001 Griffiss AFB, NY 13441	607	Cdr, Harry Diamond Laboratories ATTN: DELHD-CO, TD (In Turn) 2800 Powder Mill Road Adelphi, MD 20783
001		001	
437	Deputy for Science & Technology Office, Asst Sec Army (R&D) 001 Washington, DC 20310	609	Cdr, ERADCOM ATTN: DRDEL-CG, CD, CS (In Turn) 2800 Powder Mill Road
001		001	Adelphi, MD 20783
438	HQDA (DAMA-ARZ-D/Dr. F. D. Verderame) 001 Washington, DC 20310	612	Cdr, ERADCOM ATTN: DRDEL-CT 2800 Powder Mill Road
001		001	Adelphi, MD 20783
482	Director US Army Materiel Systems Analysis Actv ATTN: DRXSY-T 001 Aberdeen Proving Ground, MD 21005	680	Commander US Army Electronics R&D Command Fort Monmouth, NJ 07703
001		000	1. DELET-P 1. DELEW-D 1. DELET-DD 1. DELSD-L (Tech Library) 2. DELSD-L-S (STII:FO) Originating Office (2) DELET-PR (Gilman)
563	Commander, DARCOM ATTN: DRCD-E 5001 Eisenhower Avenue 001 Alexandria, VA 22333	681	Commander US Army Communications R&D Command ATTN: USCIC-LNO Fort Monmouth, NJ 07703
001		001	
564	Cdr, US Army Signals Warfare Lab ATTN: DELSW-OS Vint Hill Farms Station 001 Warrenton, VA 22186	705	Advisory Group on Electron Devices 201 Varick Street, 9th Floor 002 New York, NY 10014
001		002	

Distribution List - Continued

Electrochimica 2485 Charleston Road Mountain View, CA 94040 ATTN: Dr. Eisenberg	(1)	Energy Conversio: Branch Code 3642 Naval Underwater Systems Center Newport Laboratory Newport, RI 02840 ATTN: Mr. J.R. Moden	(1)
Dr. Hugh Barger P.O. Box 2232 Davidson, NC 28036	(1)	NASA Lewis Research Center Mail Stop 6-1 21000 Brookpark Road Cleveland, OH 44135 ATTN: Dr. Stuart Fordyce	(1)
Energy Storage & Conversion Dept. TRW Systems One Space Park Redondo Beach, CA 90278 ATTN: Dr. H.P. Silverman	(1)	Naval Undersea Center Code 608 San Diego, CA 92132 ATTN: Mr. Joe McCartney	(1)
Sanders Associates, Inc. 24 Simon Street Mail Stop NSI-2208 Nashua, NH 03060 ATTN: J. Marshall	(1)	EIC, Inc. Newton, MA 02158 ATTN: S.B. Brummer	(1)
Power Conversion, Inc. 70 MacQuesten Pkwy Mount Vernon, NY 10550 ATTN: Stuart Chodosh	(1)	Altus Corp. 440 Page Mill Road Palo Alto, CA 94306 ATTN: Douglas Glader	(1)
G207 S.R.I. Menlo Park, CA 94025 ATTN: Dr. Leonard Nanis	(1)	MS 488 NASA Langley Research Center Hampton, VA 23665 ATTN: J. Bene	(1)
Bell Laboratories 600 Mountain Avenue Murray Hill, NJ 07974 ATTN: Dr. J.J. Auborn, Rm 1A-317	(1)	Research and Development Division The Gates Rubber Co. 999 S. Broadway Denver, CO 80217 ATTN: Mr. Eddie T. Seo	(1)
Jet Propulsion Laboratory 4800 Oak Grove Drive Pasadena, CA 91103 ATTN: Mr. Harvey Frank Mail Stop 198-220	(1)	Mail Stop 8C-62 Boeing Aerospace Company P.O. Box 3999 Seattle, WA 98124 ATTN: Mr. Sidney Gross	(1)
Naval Surface Weapons Center White Oak Laboratory, Code R-33 (M/S A026) Silver Spring, MD 20910 ATTN: Dr. D. Ernst	(1)	Honeywell Technology Center 10701 Lyndale Avenue, South Bloomington, MN 55420 ATTN: Dr. H.V. Venkatasetty	(1)
		Jet Propulsion Laboratory-M.S.198-220 4800 Oak Grove Drive Pasadena, CA 91103 ATTN: Mr. Aiji Uchiyama	(1)
		Naval Surface Weapons Center White Oak Laboratory, Code R-33 Silver Spring, MD 20910 ATTN: Dr. Frank Bis	(1)

CMDR, MICO	General Motors Corp.
ATTN: DRCPM-HDE	Research Laboratories
Redstone Arsenal, AL 35809	General Motors Technical Center
	12 Mile and Mounds Roads
	Warren, MI 48090
	ATTN: Dr. J.L. Hartman (1)
Transportation Systems Center	Union Carbide Corporation
Kendall Square	Parma Research Center
Cambridge, MA 02142	P.O. Box 6116
ATTN: Dr. Norman Rosenberg (1)	Cleveland, OH 44101 (1)
Foote Mineral Company	P.R. Mallory & Co., Inc.
Route 100	S. Broadway
Exton, PA 19341	Tarrytown, NY 10591
ATTN: Dr. H. Grady (1)	ATTN: J. Dalfonso (1)
Honeywell, Inc.	North American Rockwell Corp.
104 Rock Road	Atomics Internation Division
Horsham, PA 19044 (1)	Box 309
Sanders Associates, Inc.	Canoga Park, CA 91304
Sonobuoy Division	ATTN: Dr. L. Heredy (1)
95 Canal Street	
Nashua, N.H. 03060 (1)	
Eagle-Picher Industries, Inc.	General Electric Research &
Electronics Division	Development Center
P.O. Box 47	P.O. Box 8
Joplin, Missouri 64801	Schenectady, NY 12301
ATTN: Mr. Robert L. Higgins (1)	ATTN: Dr. Stefan Mitoff (1)
Yardney Electric Company	University of California
82 Mechanic Street	Department of Science & Research
Pawcatuck, CT 06379	Santa Barbara, CA 93100
ATTN: Technical Library (1)	ATTN: Dr. J. Kennedy (1)
Saft Corporation of America	Gulton Industries, Inc.
711-A Industrial Blvd.	Metuchen, NJ 08840
P.O. Box 1284	ATTN: Mr. S. Charlip (1)
Valdosta, GA 31601	
ATTN: Mr. Lou Adams (1)	
Exxon Research & Engineering Co.	INCO Research and Development Center
Corporate Research Laboratory	Sterling Forest
Linden, NJ 07036	Suffern, NY 10901
ATTN: Dr. R. Hamlen (1)	ATTN: Nehemiah Margalit (1)
Argonne National Laboratories	Director
9700 South Cass	Propulsion and Power Division
Argonne, IL 60439	Mail Code EP5
ATTN: Dr. E.C. Gay (1)	NASA-Johnson Space Center
GTE Sylvania, Inc.	Houston, Texas 77058
77 A Street	ATTN: Mr. B.J. Bragg (1)
Needham Heights, MA 02194	
ATTN: Mr. Richard Pabst (1)	
	GTE Laboratories, Inc.
	520 Winter Street
	Waltham, MA 02154
	ATTN: Dr. Ronald McDonald (1)
	Dr. Jerry J. Smith
	ONR Chemical Program
	Arlington, VA 22217 (1)
	Reliability Analysis Center
	Griffiss AFB, NY 13441 (1)

**DATE:  
ILME**